Quantum transport and dynamics of phonons in mesoscopic systems

Thesis by

Deborah H. Santamore

In Partial Fulfillment of the Requirements

for the Degree of

Doctor of Philosophy

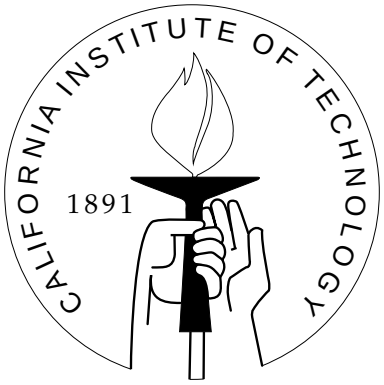

California Institute of Technology

Pasadena, California

2003

(Defended 23 May 2003)

Acknowledgements

Firstly, I would like to thank Mike Cross for giving me the opportunity to work on challenging and interesting research projects. In spite of my many shortcomings, through his guidance, I have successfully picked up some of his research style over the years, which I hope to treasure and safeguard for life. His approach to physics is thorough and his comments always to the core of the problem. He has been truly my research father and he is and will be always the one I look up to.

Looking back on the second part of my PhD work it was rather a challenging project as well as fascinating. I have put one foot in condensed matter physics whilst the other foot in atomic physics/quantum optics, and tried to pull out the best of both fields at the interface. I have also made (sometimes effective and many other times futile) attempts to bridge the gap between the two fields with frequent help from astrophysics for order of approximations and numerical tricks. In course of my PhD research, I have been fortunate to benefit from interactions with several physicists in different branches, who are the leading figures in their respective fields. All of them took an interest in one as small as myself, have taken time from their busy schedule, and kindly helped and guided me. They even agreed to be on my PhD defence committee. Without their help and encouragement, I could not have survived.

I am grateful to Gerard Milburn for allowing me to visit and work with him at the SRC for Quantum Computer Technology at the University of Queensland. During the long stay, I have learnt from him numerous theoretical techniques used in quantum optics and atomic physics.

Many thanks go to Tony Leggett for taking an interest in my project and seriously

listening to a request from a student such as myself. His deep insights in physics have fascinated me from the very first meeting and his physics mind seems to be always filled with ideas. I also thank him for hosting me during my visit. His warm hospitality was superb and nobody could ask for more.

Kip Thorne had supported me on my formative year as a theoretical physicist. He is also famous for caring others and this legend has never failed me. I am grateful for his support and allowing me to attend his group meeting whenever I want to over the years.

I owe thanks to Michael Roukes for financial support in my final year. I also thank him for providing the information about exciting recent experimental developments in his group as well as addressing his great experimental insights.

It was fortunate that I have had an opportunity to interact with Andrew Doherty. He introduced me to a world of quantum dynamics and measurement theory which have eventually brought forth a fruitful collaboration. He has been also very patient listening to my endless moans about the huge gap between quantum optics and condensed matter physics.

My Caltech life started with an interaction with Yuri Levin who had trained me in my infant years as a theoretical physicist until I was weaned. He was very much in favour of Newtonian mechanics and it showed from time to time: I had to unlearn Lagrangian mechanics in order to learn another, but I knew, at the end, his was correct and simpler. I also have enjoyed our collaboration very much.

It was a pleasure to meet Miles Blencowe. He has helped my earlier work by carefully reading manuscripts of my papers and providing useful suggestions as well as inviting me to visit him.

I sincerely express my thanks to Alexei Alexeevich Abrikosov for his kind reply to my e-mail a long time ago, which initiated my quest as a theoretical physicist. I also thank him for sharing some interesting stories about Lev Davidovich Landau.

I must thank Ruben Krasnopolsky abundantly for all his help on coding and LaTeXing, which I have struggled with many times over the years. I also thank both Dustin Laurence and Ruben Kransnopolsky for numerous useful discussions, which,

if outsiders ever have had listened to our conversations, they would have wrongly thought we were fighting.

My heartfelt thanks go to Jonathan Tannenhauser, Ruben Krasnopolsky, and Dustin Laurence for their support, especially in the last few months of my thesis writing. I could not have completed my thesis without their help in proofreading, English grammar, and LaTeX typesetting.

Part I of my PhD research work has been supported by NSF and Part II by DARPA.

Abstract

Recent advances in nanotechnology have shrunk the size of mesoscopic structures. This allows us to investigate the quantum mechanics of mechanical oscillators. In this thesis we focus on two aspects.

In Part I, an individual discrete mode structure of an oscillator and its effect to thermal conductance have been thoroughly examined: Specifically, we investigated the reduction in the thermal conductance in the quantum limit due to phonon scattering by surface roughness, first using scalar waves, then using full three dimensional elasticity theory for an elastic beam with a rectangular cross section. At low frequencies, we find power laws for the scattering coefficients that are strongly mode dependent, and different from the results deriving from Rayleigh scattering of scalar waves, that is often assumed. The scattering gives temperature dependent contributions to the reduction in thermal conductance with the same power laws. At higher frequencies, the scattering coefficient becomes large at the onset frequency of each mode due to the flat dispersion. We use our results to attempt a quantitative understanding of the suppression of the thermal conductance from the universal value observed in experiment.

As individual phonon energy becomes comparable to or greater than the thermal energy, the individual phonon dynamics within each mode can be resolved. In Part II, we examine a possibility of detecting individual quanta of a system: We investigate a scheme that makes a quantum non-demolition measurement of the excitation level of a mesoscopic mechanical oscillator by utilizing the anharmonic coupling between two bending modes of an elastic beam. The non-linear coupling between the two modes shifts the resonant frequency of the readout oscillator proportionate to the excitation

of the system oscillator. This frequency shift may be detected as a phase shift of the readout oscillation when driven on resonance. We show that in an appropriate regime this measurement approaches a quantum non-demolition measurement of the phonon number of the system oscillator. As a result it should be possible to monitor jumps between Fock states caused by the coupling of the system to the thermal reservoirs.

Contents

List of Figures

List of Tables

Part I

Quantum transport of phonons in disordered systems

Chapter 1

Introduction and preliminary calculations

Landauer's formulation of quantum transport showed that when elastic scattering dominates, the electrical conductance can be related to the transmission coefficient of the electron waves [1]. In the ideal case of no scattering, this leads to a universal conductance that is quantized in units of e^2/h at low temperatures, where e is the electron charge and h Planck's constant, with an additional quantum of conductance added as each channel or mode of the conductance pathway opens up. The application of similar ideas to the phonon counterpart, namely, thermal conductance, was recently derived by a number of authors [2, 3, 4], and is now recognized [5] to be related to earlier work on the entropy transport at low temperatures [6]. Rego and Kirczenow have extended the concept of the universality of the thermal conductance to particles of arbitrary statistics (anyons) [7].

The thermal conductance K of a suspended mesoscopic beam connecting two thermal reservoirs has been derived by three groups simultaneously [2, 3, 4] and the expression is

$$K = \frac{\hbar^2}{k_B T^2} \sum_m \frac{1}{2\pi} \int_{\omega_m}^{\infty} \mathcal{T}_m(\omega) \frac{\omega^2 e^{\beta\hbar\omega}}{(e^{\beta\hbar\omega} - 1)^2} d\omega, \tag{1.1}$$

where the integration is over the frequency ω of the modes m propagating in the beam, ω_m is the cutoff frequency of the m-th mode, $\beta = 1/(k_{\rm B}T)$, T is the temperature, $k_{\rm B}$ Boltzmann constant, the factor $(e^{\beta\hbar\omega} - 1)^{-1}$ is the Bose distribution for

$n(\omega)$, and $\mathcal{T}_m(\omega)$ is the transmission coefficient, which equals 1 in the ideal case of no scattering, *i.e.,* $\mathcal{T}_m(\omega) = 1$. Scattering reduces the thermal conductance, and scattering of the lowest modes can reduce the conductance below the universal value, $K_u = (\pi^2/3)k_B^2 T/h$, at low temperatures.

In the case of electrical resistance, the chemical potential or the number of conducting modes can be varied at very low temperatures, giving sharp jumps between various quantized values of the resistance. On the other hand, since thermal transport by phonons necessarily requires nonzero temperatures to populate the modes of the conducting pathway, the width of the Bose distribution function smears out the quantization of the conductance. Only at very low temperatures, where just the modes of the conducting pathway with zero frequency at long wavelengths contribute to the thermal conductance, the quantization of the ideal conductance becomes apparent in a universal thermal conductance $N_0 K_u$ with $K_u = (\pi^2/3)k_B^2 T/h$ the universal conductance per mode, with N_0 the number of modes with zero frequency at long wavelengths, which is four for a freely suspended elastic beam connecting the two thermal reservoirs. Note that this value of the low temperature conductance in the absence of scattering is independent of the dimensions and elastic properties of the thermal pathway.

A low temperature thermal conductance consistent with the predicted universal value was measured by Schwab *et al.* [8] in experiments on a lithographically defined mesoscopic suspended beam of dimensions about 1 μm $\times$ 200 nm $\times$ 60 nm. Whilst their elegant experiment displays the universality of ballistic phonon transport, the experiment also showed a *decrease* in the thermal conductance below the universal value in the temperature range of 0.08 K $< T <$ 0.4 K that cannot be explained by the ballistic theory, since in this theory an increase in the thermal conductance is expected as the temperature is raised and more modes are excited. The decrease in thermal conductance is presumably associated with the scattering of the thermal phonons, and can be understood using the ideas of Landauer in terms of the scattering coefficient of the vibrational waves. This is the topic of the present part of the thesis.

We theoretically investigate a likely cause of the low temperature thermal conduc-

tance decrease. We suggest that the conductance decrease is caused by scattering due to rough surfaces. Recent advanced crystal growth technology guarantees very few impurities in the material during substrate growth, thus eliminating the possibility of impurity scattering. On the other hand, chemical etching can produce surface roughness on a scale of tens of nanometres, large enough to cause significant scattering.

In Part I we examine the surface scattering effect on thermal conductance using two different models. The *scalar model* discussed in Chapter 2 uses scalar waves for the acoustic waves. This model is not only being simple and presents a complete analytical solution to the problem, but also provides much of insight to the nature of rough surface scattering. The *elasticity model* discussed in Chapter 3 expands the scattering concept to a full 3-D elasticity theory and re-examines the scattering effect.

1.1 Ideal thermal conductance

For the rest of this chapter, we consider a mesoscopic beam with rectangular cross section and its dimensions: length L, width W, and depth d.

1.1.1 Analytical method using density of states

To evaluate Eq. (1.1), for small m, we need to evaluate the sum mode by mode, but for large m the modes become closely spaced and we can replace the sum by an integral. The density of states (*i.e.,* the number of mode cutoffs per frequency increment) in a continuous form is

$$\frac{dN}{d\omega} = \frac{Wd}{2\pi}\left(\frac{2}{c_t^2} + \frac{1}{c_l^2}\right)\omega, \tag{1.2}$$

where c_t^2 and c_l^2 are transverse and longitudinal wave speeds, respectively. Let us now evaluate the whole expression using the continuum approximation:

$$K = \frac{\hbar^2}{k_B T^2}\frac{dW}{4\pi^2}\left(\frac{2}{c_t^2} + \frac{1}{c_l^2}\right)\int_0^\infty d\omega_c\,\omega_c \int_{\omega_c}^\infty \frac{\omega^2 e^{\beta\hbar\omega}}{(e^{\beta\hbar\omega}-1)^2}d\omega. \tag{1.3}$$

Changing the order of integration gives

$$K = \frac{\hbar^2}{k_B T^2}\frac{dW}{4\pi^2}\left(\frac{2}{c_t^2} + \frac{1}{c_l^2}\right)\int_0^\infty \frac{\omega^2 e^{\beta\hbar\omega}}{(e^{\beta\hbar\omega}-1)^2}d\omega \int_0^\omega d\omega_c\,\omega_c. \tag{1.4}$$

The ω_c integral is easily done and then introducing the scaled frequency, $y = x\beta\hbar\pi c_t/W$ gives

$$K = \frac{k_B^4 T^3}{\hbar^3}\frac{dW}{8\pi^2}\left(\frac{2}{c_t^2} + \frac{1}{c_l^2}\right)\int_0^\infty \frac{y^4 e^y}{(e^y-1)^2}dy. \tag{1.5}$$

The value of the last integral is 25.976. Note that K has T^3 dependence.

There may be a correction for the discreteness of the mode at small m. This can be estimated by evaluating the sum up to some limit M, and doing the rest as an

integral:

$$K = \frac{\hbar^2}{k_B T^2} \sum_{m=0}^{M} \frac{1}{2\pi} \int_{\omega_m}^{\infty} \frac{\omega^2 e^{\beta\hbar\omega}}{(e^{\beta\hbar\omega}-1)^2} d\omega + \frac{\hbar^2}{k_B T^2} \frac{dW}{4\pi^2} \left(\frac{2}{c_t^2} + \frac{1}{c_l^2} \right) \int_{\omega_M}^{\infty} d\omega_c \, \omega_c \int_{\omega_c}^{\infty} \frac{\omega^2 e^{\beta\hbar\omega}}{(e^{\beta\hbar\omega}-1)^2} d\omega. \tag{1.6}$$

We can evaluate the integral part in the same way to give

$$K = \frac{\hbar^2}{k_B T^2} \sum_{m=0}^{M} \frac{1}{2\pi} \int_{\omega_m}^{\infty} \frac{\omega^2 e^{\beta\hbar\omega}}{(e^{\beta\hbar\omega}-1)^2} d\omega + \frac{k_B^4 T^3}{\hbar^3} \frac{dW}{8\pi^2} \left(\frac{2}{c_t^2} + \frac{1}{c_l^2} \right) \int_{y_M}^{\infty} \frac{y^2 (y^2 - y_M^2) e^y}{(e^y - 1)^2} dy \tag{1.7}$$

with $y_M = \beta\hbar\omega_M$, Convergence can be checked by choosing various values of M.

Scaled with the universal value $K_u = (\pi^2/3)\,(k_B^2 T/h)$

$$\frac{K}{K_u} = \frac{\pi^2}{3} \frac{k_B^2 T}{2\pi\hbar} \frac{\hbar^2}{k_B T^2} \sum_{m=0}^{M} \frac{1}{2\pi} \int_{\omega_m}^{\infty} \frac{\omega^2 e^{\beta\hbar\omega}}{(e^{\beta\hbar\omega}-1)^2} d\omega + \frac{k_B^2 T^2}{\hbar^2} \frac{3dW}{4\pi^3} \left(\frac{2}{c_t^2} + \frac{1}{c_l^2} \right) \int_{y_M}^{\infty} \frac{y^2 (y^2 - y_M^2) e^y}{(e^y - 1)^2} dy. \tag{1.8}$$

This expression can be evaluated numerically. When the temperature is high enough, we can neglect the cutoff frequency and obtain an analytical expression:

$$\frac{K}{K_u} = \frac{k_B^2 T^2}{\hbar^2} \frac{3dW}{4\pi^3} \left(\frac{2}{c_t^2} + \frac{1}{c_l^2} \right) \int_{0}^{\infty} \frac{y^4 e^y}{(e^y - 1)^2} dy. \tag{1.9}$$

1.2 Approximation methods to obtain cutoff frequencies

As seen in Eq. (1.1), the thermal conductance depends on the cutoff frequencies of the modes, thus it is important to calculate cutoff frequencies. Within full elasticity theory, the modes can be obtained only numerically. Below, we examine several approximation methods for obtaining the cutoff frequencies in order to determine the

validity range of these approximations (c.f. Fig. 1.1). We present two approximation methods: a method based on the properties of the bulk modes (§ 1.2.2), and a method based on thin plate theory (§ 1.2.1). Then we compare these methods with the fully numerical solution of the exact method using the "xyz algorithm" that was developed by Nishiguchi, Ando, and Wybourne [9]. This algorithm can calculate the full elastic modes, obtaining the dispersion relation of any geometry.

1.2.1 Thin plate elastic theory method

Whilst the exact solution from the 3-D elasticity theory requires full numerical approach, the thin plate theory allows to obtain some analytical expressions that can be evaluated fairly easily with a lesser programming power. In addition to the computational reason, using the range of modes that can be approximated by the thin elastic theory, we can estimate the temperature range where the thin plate limit is applicable for a given experimental structure. This is essential information to us since our quantitative calculation of the scattering coefficient in Chapter 3 relies on the analytic expressions for the elastic modes available only in the thin plate limit. The cutoff frequencies for each mode can be determined from the dispersion relations. There are a total of four modes in a thin plate: inplane even and odd modes, and flexural even and odd modes. The dispersion relations of these four modes have been derived by Cross and Lifshitz [10]. For inplane modes,

$$(k^2 - \chi_T^2)^2 \tan\frac{\chi_T W}{2} + 4k^2\chi_T\chi_L \tan\frac{\chi_L W}{2} = 0, \tag{1.10}$$

$$4k^2\chi_T\chi_L \tan\frac{\chi_T W}{2} + (k^2 - \chi_T^2)^2 \tan\frac{\chi_L W}{2} = 0, \tag{1.11}$$

and for flexural modes,

$$[\bar{K}^2 + (1-\sigma)k^2]^2\chi_- \tanh(\chi_- W/2) = [\bar{K}^2 - (1-\sigma)k^2]^2\chi_+ \tanh(\chi_+ W/2), \tag{1.12}$$

$$[\bar{K}^2 + (1-\sigma)k^2]^2\chi_- \coth(\chi_- W/2) = [\bar{K}^2 - (1-\sigma)k^2]^2\chi_+ \coth(\chi_+ W/2), \tag{1.13}$$

where

$$\bar{K} = \frac{E}{3(1-2\sigma)}, \quad \mu = \frac{E}{2(1+\sigma)}, \tag{1.14}$$

$$c_l = \sqrt{\frac{E}{\rho(1-\sigma^2)}}, \quad c_t = \sqrt{\frac{E}{2\rho(1+\sigma)}}, \tag{1.15}$$

and E Young's modulus, σ Poisson ratio , ρ the mass density, $\omega^2/c_t^2 = k^2 + \chi_T^2 = r^2(k^2+\chi_L^2)$, and $r = c_l/c_t$, $D = Ed^3/12(1-\sigma^2)$, $\sqrt{\rho d/D}\,\omega = \bar{K}^2$, and $\chi_\pm = \sqrt{k^2 \pm \bar{K}^2}$. The cutoff frequencies can be obtained by solving these transcendental equations.

1.2.2 Bulk mode method

As the wavelength becomes much smaller than the dimensions of the structure, we should be able to treat the waves in terms of separate longitudinal and transverse waves in the bulk of the material, without worrying too much about the complicated standing wave transverse mode structure important for the long wavelength modes. In this regime, which we refer to as the bulk mode limit, the counting of the modes is insensitive to the details of the boundary conditions, and bulk mode approximation becomes valid. This approximation is essentially the discrete case of § 1.1.1.

For the bulk mode calculation, there are three polarizations (one longitudinal and two transverse) with propagation velocities $c_{_{3l}}$ and $c_{\rm t}$, respectively, with $c_{\rm t}$ as in the 2-D thin plate elasticity theory in § 1.2.1, and $c_{_{3l}}$ is according to 3-D elasticity theory

$$c_{3l} = \sqrt{\frac{E\,(1-\sigma)}{\rho\,(1+\sigma)\,(1-2\sigma)}}. \tag{1.16}$$

The precise details of the boundary conditions are unimportant in the mode counting for large mode numbers. If we assume standing waves in the transverse direction corresponding to zero normal derivative boundary conditions on the wave functions, the cutoff frequencies are

$$\omega_{t,mn} = c_t\sqrt{\left(\frac{m\pi}{W}\right)^2 + \left(\frac{n\pi}{d}\right)^2}, \quad \text{(twofold degenerate)} \tag{1.17}$$

for the transverse waves, and

$$\omega_{l,mn} = c_{3l}\sqrt{\left(\frac{m\pi}{W}\right)^2 + \left(\frac{n\pi}{d}\right)^2}, \quad \text{(non degenerate)} \tag{1.18}$$

for the longitudinal waves, with $m, n = 0, 1, 2 \ldots$. As mentioned before, for large m, n we can use the continuous form for the frequency ω_N of the N-th mode.

1.2.3 Comparison of the different methods

Figure 1.1 shows the cutoff frequencies as a function of mode number for the thickness to width ratio $d/W = 0.38$, $\sigma = 0.24$ (the choice of these parameters has been made based on the experimental structure of Schwab *et al.*) The thin plate theory gives a good approximation to the cutoff frequency determined by the exact xyz algorithm at lower frequencies. The accuracy of thin plate theory becomes better as d/W gets smaller. For example, in the case of $d/W = 0.1$ (not shown), the error in the cutoff frequencies of the first 13 modes is less than 3%, whilst the error is as large as 5% for the first 7 modes for the case $d/W = 0.38$ shown in the figure. In terms of the ideal (no-scattering) thermal conductance (Eq. (1.1) with the transmission coefficient set to unity), we find that for $d/W = 0.38$ the error in the thermal conductance is less than 4% up to $T \sim 0.4$ K. Thus the thin plate limit is adequate to examine the scattering effects in this temperature range. At large frequencies, $\omega W/c_t > 30$, the cutoff frequencies calculated from discrete bulk mode method (and its continuum form as well) approach the exact numerical results the continuum. The thin plate approximation clearly fails in this limit, since it predicts $N \propto \omega$ corresponding to a 2-D structure.

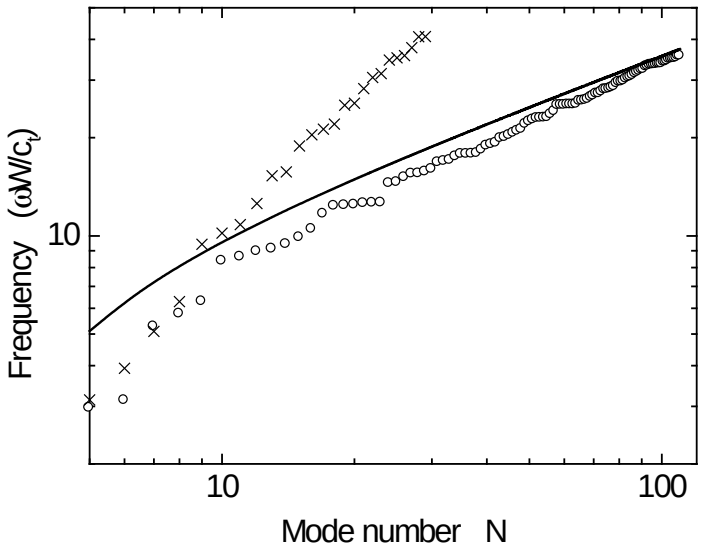

Figure 1.1: Mode cutoff frequency ω_N as a function of mode number N. crosses: thin plate theory; circles: xyz algorithm; solid line: density of states calculation. A thickness to width ratio $d/W = 0.38$ was used. Bulk mode calculation is not shown here.

Chapter 2

Surface scattering of phonons - the scalar model

In this chapter we use a simple scalar model for the elastic waves. The scalar model is a simple and useful tool to obtain analytical solutions, grasps the scattering behaviour, and assesses for our reason for the thermal conductance at low temperatures. This work forms the basis for a published paper [11].

We use a two dimensional approximation for the following reasons: (1) We assume that the important roughness is on the sides of the beam, rather than the top and bottom surfaces, since the horizontal surfaces are MBE grown and have roughness at a scale of a few atomic layers, while the side faces are chemically etched and anisotropic. Thus the roughness is a function of the longitudinal direction but not of the transverse (depth) direction. (2) We assume temperatures low enough that modes with structure across the depth of the beam—the smallest dimension in the experimental geometry—are not excited. We also consider the case of weak scattering.

We refer the reader to Appendix A.1 for a brief introduction to the scattering matrix and the Green function method. In the following, the details of the 2-D scalar model are discussed. Then the calculation of the scattered field using a Green function approach is presented. In § 2.1.6, the scattering probabilities and transmission coefficients are calculated and the latter is incorporated into the modified Landauer formula for thermal conductance. In § 2.2, the thermal conductance is evaluated numerically and compared to the experiments of Schwab *et al.*

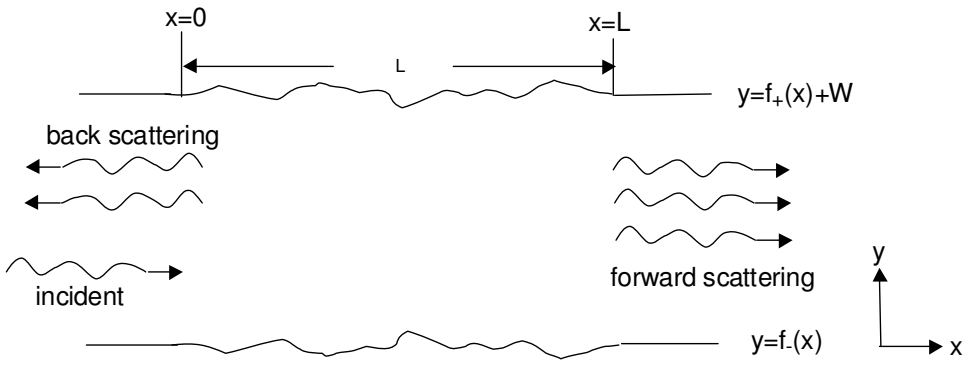

Figure 2.1: 2-D model used for calculation of the scattering of elastic waves by rough surfaces.

2.1 Scattering formalism

2.1.1 The model

The expression for the thermal conductance K of a suspended mesoscopic beam connecting two thermal reservoirs is already given in the previous chapter (Eq. (1.1)). We repeat it here for convenience

$$K = \frac{\hbar^2}{k_B T^2} \sum_m \frac{1}{2\pi} \int_{\omega_m}^{\infty} \mathcal{T}_m(\omega) \frac{\omega^2 e^{\beta\hbar\omega}}{(e^{\beta\hbar\omega} - 1)^2} d\omega. \tag{2.1}$$

and refer the reader to the beginning of § 1.1 for an explanation of the notation used. The change of the thermal conductivity due to the rough surface is obtained by finding the transmission coefficient.

As discussed in the introduction, we use a scalar model for the elastic waves, and model a thin geometry at low temperatures so that a two-dimensional calculation is adequate. Thus we consider a 2-D waveguide-like structure extended in the x-direction and bounded at $y = 0, W$ in the absence of roughness (see Fig. 2.1). The waves satisfy the scalar wave equation, and we assume Neumann boundary conditions at the edges of the wave guide, corresponding to a stress-free boundary condition for the elastic waves. Note that Dirichlet boundaries do not support modes with zero cutoff frequency that are a crucial feature of the elastic problem. We calculate the

scattering process by considering an elastic wave propagating in the waveguide in the $+x$ direction with wave vector k_0 and entering a rough surface region of length L $(0 < x < L)$, where the rough boundaries are at $y = W + f_+(x)$ and $y = f_-(x)$ so that the roughness is characterized by the functions $f_\pm(x)$. We assume that the top and the bottom roughness functions are uncorrelated, and that $f_\pm(x)$ is small and is differentiable. The incident wave Ψ_{in} interacts with the rough surface, is scattered into other modes Ψ_{sc}, and leaves the rough region. The total field Ψ is the sum of the incident field and the scattered field

$$\Psi = \Psi_{in} + \Psi_{sc}. \tag{2.2}$$

Our task is to find an expression for Ψ_{sc} and hence calculate the transmission coefficients. As said before, we do this by using Green functions.

2.1.2 Green function method

2.1.2.1 Scattering amplitude and Green function

In terms of fields, the S-matrix formulation $S = 1+iT$ can be written with an incident field and scattering field. The matrix 1 corresponds to the incident field as explained previously and T matrix corresponds to a scattered field. The easiest and clearest way to obtain the scattered field, Ψ_{sc}, is to use a Green function. The Green function is a solution to the Helmholtz equation with a point source. The description of scattering in terms of scattering amplitudes and that in terms of Green functions are equivalent in a far-field regime [12].

2.1.2.2 Green function

We start with the Helmholtz equation for a scalar wave at frequency ω

$$\nabla^2\Psi(x,y) + K^2\Psi(x,y) = 0, \tag{2.3}$$

where K is ω/c with c the wave speed. Define the Green function as a solution to the point sources

$$\nabla^2 G\left(x,y;x',y'\right)+K^2 G\left(x,y;x',y'\right)=-\delta\left(x-x'\right)\delta(y-y') \tag{2.4}$$

with (x',y') the source coordinates and (x,y) the observation coordinates. It is convenient to define $G\left(x,y;x'y'\right)$ such that it satisfies Neumann boundary conditions at the *smoothed boundaries*, $y=0,W$

$$\partial G/\partial n|_{y=0,W}=0, \tag{2.5}$$

where $\hat{n}$ is the outward-pointing normal to the surface. We then project the physical boundary conditions at the rough surfaces onto the smoothed boundaries to calculate the scattering.

Multiplying Eq. (2.3) by $G(x,y;x',y')$ and Eq. (2.4) by $\Psi(x,y)$ then subtracting one from the other, and integrating over a volume bounded by the position of the smoothed surfaces yields the result of Green's theorem

$$\begin{aligned}\Psi\left(x,y\right)=&\int_{smooth}dx'\frac{\partial\Psi\left(x',y'\right)}{\partial n'}G\left(x',y';x,y\right)\\&\pm\int_{x\to\pm\infty}dy'\left[\frac{\partial\Psi\left(x',y'\right)}{\partial x'}G\left(x',y';x,y\right)-\Psi\left(x',y'\right)\frac{\partial G\left(x',y';x,y\right)}{\partial x'}\right],\end{aligned} \tag{2.6}$$

where the first integral is the integration along the smoothed edges and the second over the distant ends taken at $x\to\pm\infty$, each with its proper sign. We have used the boundary condition Eq. (2.5) for G to eliminate a second term in the first integral.

We now need to calculate the Green function. The Green function $G\left(x,y;x',y'\right)$ satisfies Eq. (2.4). Using the completeness relation, the right hand side can be written

$$-\frac{1}{2\pi}\int_{-\infty}^{\infty}e^{ik(x-x')}dk\sum_n\phi_n(y)\phi_n(y'), \tag{2.7}$$

where ϕ_n is the normalized transverse eigenfunction for smooth boundaries

$$\phi_n = N_n \cos \chi_n y \tag{2.8}$$

with $\chi_n = n\pi/W,\ n = 0, 1, 2, ..,$ and N_n the normalization factor: $N_n = \sqrt{2/W}$ for $n \neq 0$ and $N_n = \sqrt{1/W}$ for $n = 0$. The Green function is then given by Fourier transforming

$$G\left(x, y; x', y'\right) = \frac{1}{2\pi} \int_{-\infty}^{\infty} dk \sum_n \frac{e^{ik(x-x')} \phi_n(y) \phi_n(y')}{k^2 + (n\pi/W)^2 - K^2}. \tag{2.9}$$

The k integral in Eq. (2.9) is now evaluated by contour integration. The poles corresponding to propagating waves at $k = \sqrt{K^2 - (n\pi/W)^2}$ for $K > n\pi/W$ must be given infinitesimal imaginary parts $\pm i\varepsilon$ to yield outgoing waves. We then have

$$G\left(x, y; x', y'\right) = \sum_n \frac{i e^{ik_n |x-x'|} \phi_n(y) \phi_n(y')}{2k_n}, \tag{2.10}$$

where

$$k_n = \begin{cases} \sqrt{K^2 - n^2\pi^2/W^2} & n\pi/W < K \\ i\sqrt{n^2\pi^2/W^2 - K^2} & n\pi/W > K \end{cases}. \tag{2.11}$$

The second term in Eq. (2.6) is just the incoming wave $\Psi_{in}\left(x, y\right)$ as will be discussed below, so that

$$\Psi_{sc}\left(x, y\right) = \int_{smooth} dx' \frac{\partial \Psi\left(x', y'\right)}{\partial n'} G\left(x', y'; x, y\right). \tag{2.12}$$

In Appendix A.2, it is shown that evaluating the second term in Eq. (2.6) results in the incident field.

2.1.3 Boundary perturbation

In the absence of roughness the field Ψ satisfies Neumann boundary conditions at the smooth boundary, and so the scattered field would be identically zero as expected. Correspondingly, for a rough surface with small $f_{\pm}(x)$ we can calculate $\partial\Psi/\partial n$ at

the *smoothed* surface appearing in the integral by expanding about the stress-free rough surface [13]. We will present the calculation for the rough lower surface, and simply double the scattering probabilities assuming uncorrelated roughness on the two surfaces.

Firstly, we express the unit normal vector as

$$\hat{n} = -\hat{y} + f'_{-}(x)\,\hat{x}. \tag{2.13}$$

Then we impose the Neumann boundary condition at $y = f_{-}(x)$

$$\left(-\frac{\partial \Psi(x,y)}{\partial y} + f'_{-}(x)\frac{\partial \Psi(x,y)}{\partial x}\right)\Big|_{y=f_{-}(x)} = 0. \tag{2.14}$$

Now we expand this equation about $y = 0$ in terms of f_{-} and retain only terms that are first order in f and f'. This gives the normal derivative at the smooth surface up to first order in f, f' as

$$\partial_n \Psi(x,y)|_{y=0} = \left[f'_{-}\partial_x \Psi(x,y) - f_{-}\partial_y^2 \Psi(x,y)\right]\big|_{y=0}. \tag{2.15}$$

Thus the scattered field to first order in the roughness amplitude is

$$\Psi_{sc}(x,y) \simeq \int dx' G(x',y';x,y)\left[-f_{-}(x')\,\partial_{y'}^2 \Psi_{in}(x',y') + f'_{-}(x')\,\partial_{x'}\Psi_{in}(x',y')\right]\big|_{y'=0}, \tag{2.16}$$

where we can replace the field appearing in the integral by the incident field Ψ_{in} at this order.

It is now straightforward to insert the explicit expression for the Green function Eq. (2.10) to calculate the scattering from a normalized incident wave entering in the m-th mode $\Psi_{in}(x,y) = \Psi_m(x,y) = N_m \cos(\chi_m y)\, e^{ik_m x}$:

$$\Psi_{sc}(x,y) \simeq \int dx' \sum_n \frac{iN_n^2 N_m}{2k_n}\cos(\chi_n y)\, e^{ik_n|x-x'|}\left[f_{-}(x')\,\chi_m^2 + ik_m f'_{-}(x')\right] e^{ik_m x'}. \tag{2.17}$$

2.1.4 Scattered field

Outside the scattering region, Eq. (2.17) takes the form for the scattered field

$$\begin{aligned}&\Psi_{sc}\left(x\to+\infty,y\right)\\&=\sum_n e^{ik_nx}\cos\left(\chi_ny\right)\int_{-\infty}^{\infty}dx'\frac{iN_n^2N_m}{2k_n}\left[\chi_m^2f_-\left(x'\right)+ik_mf'_-\left(x'\right)\right]e^{i(k_m-k_n)x'},\end{aligned}\tag{2.18}$$

$$\begin{aligned}&\Psi_{sc}\left(x\to-\infty,y\right)\\&=\sum_n e^{-ik_nx}\cos\left(\chi_ny\right)\int_{-\infty}^{\infty}dx'i\frac{iN_n^2N_m}{2k_n}\left[\chi_m^2f_-\left(x'\right)+ik_mf'_-\left(x'\right)\right]e^{i(k_m+k_n)x'},\end{aligned}\tag{2.19}$$

giving the forward scattered field and back scattered fields respectively. The terms in f'_- can be simplified by integration by parts.

$$\int_{-\infty}^{\infty}dx'if'_-\left(x'\right)k_me^{i(k_m\mp k_n)x'}=k_m\left(k_m\mp k_n\right)\tilde{f}_-\left(k_m\mp k_n\right),\tag{2.20}$$

where $\tilde{f}_-$ is the Fourier transform of f_-, *i.e.* $\tilde{f}_-=\int_{-\infty}^{\infty}dx'f_-e^{ikx'}$, and we have used the fact that the roughness is confined to $0<x<L$, so that $f_-(\pm\infty)=0$.

Now using $K=\sqrt{\chi_m^2+k_m^2}$, we get

$$\Psi_{sc}\left(x\to\pm\infty,y\right)=\sum_n\frac{iN_nN_m}{2k_n}\tilde{f}_-\left(k_m\mp k_n\right)\left(K^2\mp k_nk_m\right)\Psi_n\left(x,y\right),\tag{2.21}$$

for the forward and backward scattered waves, expressed as a sum over normalized waves Ψ_n.

2.1.5 Roughness characterisation

Previously we have defined two surface profile functions by $f_\pm$ (c.f. Fig. 2.1) Since they are rough surface functions, we treat them statistically. Then $f_+\left(x\right)$ and $f_-\left(x\right)$ have the same statistical properties and we can drop the subscript and write as $f\left(x\right)$. The first and second moments of the probability distribution function for the roughness

correlation function are

$$\langle f(x)\rangle = 0, \tag{2.22}$$

$$\langle f(x) f(x')\rangle = \delta^2 g(|x-x'|), \tag{2.23}$$

where δ is the root mean square (rms) roughness and $g(|x-x'|)$ is the roughness correlation function, which only depends on the distance between x and x'. $\langle\ \rangle$ denotes an average over the ensemble of realizations of the function. The correlation for Fourier transform of this function $\left\langle \tilde{f}(k)\, \tilde{f}^*(k)\right\rangle$ is

$$\begin{aligned}
\left\langle \tilde{f}(k)\, \tilde{f}^*(k)\right\rangle &= \left\langle \int dx f(x) e^{ikx} \int dx' f(x') e^{-ikx'} \right\rangle \\
&= \int\int dx dx' \langle f(x) f(x')\rangle e^{ik(x-x')} \\
&= \int dx' \int d(x-x')\, \delta^2 g(|x-x'|) e^{ik(x-x')} \\
&= \delta^2 L \int d(x-x')\, g(|x-x'|) e^{ik(x-x')} \\
&= \tilde{g}(k)\, \delta^2 L,
\end{aligned} \tag{2.24}$$

where $\tilde{g}(k)$ is the roughness correlation function in Fourier space and L is the length of the rough surface is the flat surface. Thus the roughness fluctuation is characterised by

$$\left\langle \left| \tilde{f}_-(k) \right|^2 \right\rangle = \delta^2 \tilde{g}(k) L, \tag{2.25}$$

where $\delta^2\tilde{g}(k)$ is the Fourier transform of the surface roughness correlation function with δ the roughness amplitude. As we mentioned before, we have assumed that the roughness function, $\tilde{f}_-$, is stochastic (spatial not temporal) and treat it statistically. We also assume that the correlation function of the roughness function is Gaussian $g(x) = e^{-x^2/a^2}$ with the correlation length a. Since the Fourier transform of a Gaussian is a Gaussian, we obtain

$$\tilde{g}(k) = \sqrt{\pi} a \exp\left[-\frac{a^2k^2}{4}\right]. \tag{2.26}$$

Now we apply this correlation function to calculate the scattering probability using the result from Eq. (2.21). Let $t_{\pm n,m}$ be the scattering amplitude from mode m to $\pm n$, where the plus sign is for forward scattering and the minus sign is for back scattering. Then from Eq. (2.21) we have the scattering amplitude

$$t_{\pm n,m} = \frac{iN_nN_m}{2k_n}\left(K^2 \mp k_nk_m\right)\tilde{f}_-\left(k_m \mp k_n\right). \tag{2.27}$$

To calculate the transmission coefficient appearing in the expression for the thermal conductance we need the energy flux scattering probabilities $\sigma_{\pm n,m}$, given by multiplying $|t_{n,m}|^2$ by the ratio of the group velocities

$$\sigma_{\pm n,m} = \frac{k_n}{k_m}\left\langle |t_{\pm n,m}|^2 \right\rangle. \tag{2.28}$$

The angular brackets denote the average of the rough surface. This finally gives

$$\sigma_{\pm nm} = \frac{N_n^2N_m^2}{4k_nk_m}\left[K^2 \mp k_nk_m\right]^2 \delta^2\tilde{g}(k_m \mp k_n)L\ , \tag{2.29}$$

where $\tilde{g}$ is the correlation function in Fourier space $\tilde{g}(k_m \mp k_n) = \left\langle \left|\tilde{f}_-\left(k_m \mp k_n\right)\right|^2 \right\rangle$.

2.1.6 Thermal conductance

To calculate the thermal conductance we must recognize that not all scattering processes decrease the heat transport. A wave entering in mode m has four possible outcomes: after the scattering events it may stay in mode m propagating forward; it may be converted to mode n also propagating forward; it may stay in mode m but propagating backward (call this mode $-m$); and finally it may be converted to mode n and propagating backward (call this $-n$). The former two cases do not change the heat transport, since each mode at frequency ω contributes the same amount to the conductance. The two back-scattering events do reduce the heat transport, however. Thus the backward scattering rate $\sigma_{-n,m}$ contributes to the reduction of the thermal conductance, while $\sigma_{+n,m}$, the rate for forward scattering, leaves the conductance un-

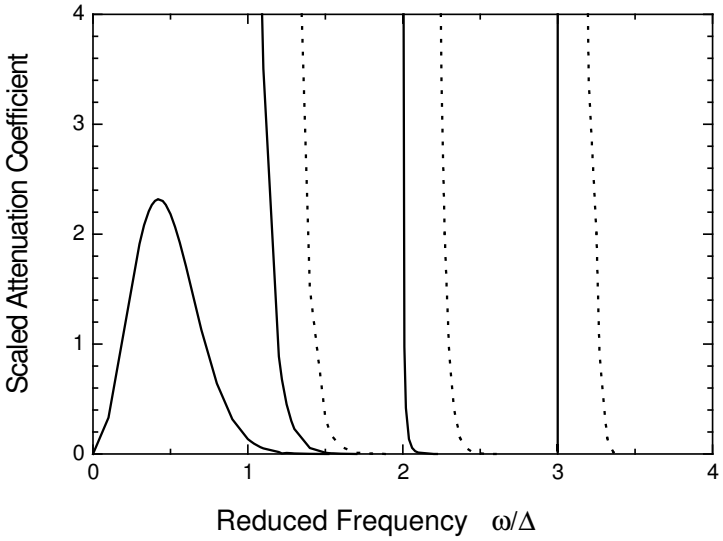

Figure 2.2: Scaled attenuation coefficients $(W^4/\delta^2 aL)\,|\sigma_{-n,m}|^2$ as a function of reduced frequency, ω/Δ where $\Delta = \pi c/W$ with c the velocity of the waves: solid—from mode $m = 0$ to mode $-n$, $n = 0 \ldots 3$ and dashed—mode m to mode $-m$, $m = 1 \ldots 3$. A value of the roughness correlation length $a = 0.75W$ was used.

changed. We therefore define the conductance attenuation coefficient per unit length of the rough surface waveguide as $\gamma_m \equiv (2/L)\sum_n \sigma_{-n,m}$. The factor of two accounts for scattering off the top surface. We have

$$\gamma_m = \sum_n \frac{(K^2 + k_n k_m)^2}{k_n k_m} \frac{\sqrt{\pi} N_n^2 N_m^2 \delta^2 a}{2} e^{-a^2(k_n+k_m)^2/4}. \tag{2.30}$$

The conductance attenuation coefficient γ_m gives the exponential decay rate of the wave in mode m, so that over a length L the transmission is

$$\mathcal{T}_m = e^{-\gamma_m L}. \tag{2.31}$$

To calculate the thermal conductance at a given temperature, we insert Eqs. (2.30,

2.31) into Eq. (2.1):

$$K = \frac{\hbar^2}{k_B T^2} \sum_m \frac{1}{2\pi} \times \int_{\omega_m}^{\infty} d\omega \frac{\omega^2 e^{\beta\hbar\omega}}{(e^{\beta\hbar\omega}-1)^2} \exp[-\sum_n \frac{(K^2+k_n k_m)^2}{k_n k_m} \frac{N_n^2 N_m^2 \sqrt{\pi}\delta^2 a L}{2} e^{-a^2(k_n+k_m)^2/4}]. \tag{2.32}$$

The contributions to the conductance attenuation coefficients per unit length γ_m for the first few modes are shown as a function of the mode frequency in Fig. 2.2. A scattering correlation length of $a/W = 0.75$ was used in the figure. The backscattering amplitude from the lowest mode (mode 0) to its reverse is

$$\gamma_{00}(\omega, a, \delta) = 2\pi^{\frac{1}{2}} \frac{a\delta^2}{W^2} \frac{\omega^2}{c^2} e^{-a^2\omega^2/c^2}. \tag{2.33}$$

This expression is finite for all frequencies. It has a maximum at a frequency $\omega = c/a$ depending on the roughness correlation length, with a peak value of order (δ^2/aW^2). The higher modes have a divergent back-scattering proportional to $(\omega - \omega_m)^{-1}$ at the cutoff frequencies ω_m. In addition each γ_m has a contribution diverging as $(\omega - \omega_n)^{-1/2}$ at the onset of the n-th mode. These divergences are due to the flat spectrum at the mode cutoff frequencies, and will also be found in the full elastic wave calculation.

At low enough temperatures only the lowest mode with $k_0 = \omega/c$ contributes to the thermal conductance, and only the backscattering of this mode given by Eq. (2.33) reduces the conductance below the universal value. This reduction is plotted as a function of the temperature scaled by $k_B T/\hbar\Delta$ in Fig. 2.3. The temperature of maximum reduction depends on the roughness correlation length a, whereas both the roughness amplitude and correlation length change the magnitude of the reduction. For small roughness, we can expand the exponential term in Eq. (2.32). At low temperatures only small ω contributes to the integral so that the Gaussian factor

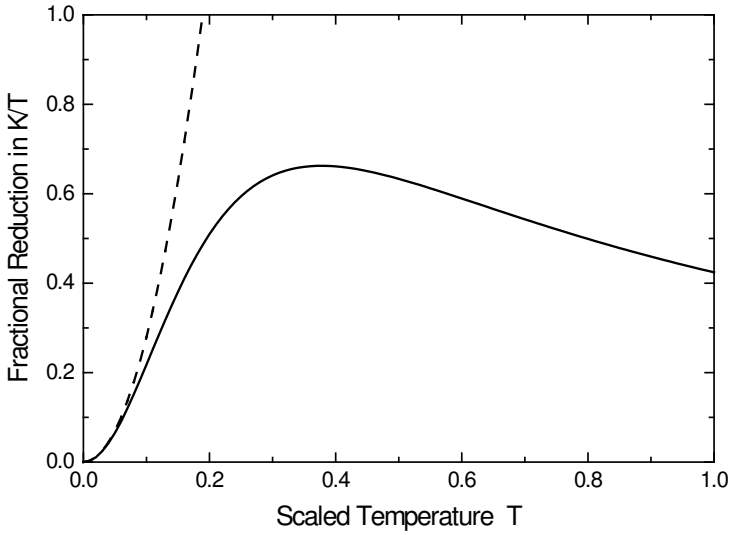

Figure 2.3: Reduction in the thermal conductance divided by temperature due to back scattering of the lowest mode, expressed as the ratio to the universal conductance divided by temperature and then scaled by $aW^2/\delta^2 L$, as a function of temperature scaled by $k_B T/\hbar\Delta$.

may be replaced by unity, $\exp[-a^2\omega^2/c^2] \simeq 1$. This leads to

$$\frac{K}{T} \simeq \frac{\pi^2 k_B^2}{3h}\left[1 - \frac{8\pi^{9/2}}{5}\frac{\delta^2 aL}{W^4}\left(\frac{k_B T}{\hbar\Delta}\right)^2\right], \tag{2.34}$$

where $\Delta = \pi c/W$ is the spacing between the mode cutoff frequencies. Thus at low temperatures, the conductance divided by temperature should show a quadratic temperature decrease with an amplitude depending on the combination of roughness parameters $a\delta^2/W^3$.

2.2 Comparison with the experiment of Schwab *et al.*

To compare with the experiments of Schwab *et al.* [8], we use the following geometry and material parameters. We take a waveguide structure of rectangular cross section

with width $W = 160\,\text{nm}$ and length $L = 1\,\mu\text{m}$. In the experimental geometry the width varied along the length to provide smooth junctions with the reservoirs. This was done to eliminate scattering off abrupt changes in the geometry. We use the width at the narrowest point as our estimate of the size of the structure. For the length we use the length of the central portion over which the width is constant. Since the length only occurs in the combination $\delta^2 L$, changing the value of L used will only change the fitted value of δ. We use a wave propagation speed $c = 8250$ m/s which is the reciprocal average of the velocity of longitudinal and transverse elastic waves in silicon nitride.

The roughness parameters are not known *a priori*. As a first attempt, we might try to estimate the combination $a\delta^2 L/W^4$ from a quadratic fit to the decrease in the thermal conductance data at low temperatures, Eq. (2.34). This would give the value $a\delta^2 L/W^4 \sim 0.05$. However, from Fig. 2.3 we see that the quadratic low temperature fit is only good up to about a quarter of the temperature of the maximum backscattering of the first mode. If we estimate this temperature from the minimum in the measured conductance, we find that the data does not extend to low enough temperatures to provide a reliable fit, and so this value can only be used as an order of magnitude. In fact our "best fit" (see below) over temperatures up to 1 K corresponds to a value $a\delta^2 L/W^4$ about a factor of 4 larger.

It is interesting to use this value of the roughness parameters to estimate the strength of the scattering of the higher modes. For example, for the first mode, with cutoff frequency Δ, and at a wave vector π/W corresponding to a frequency $\sqrt{2}\Delta$, we find for the backscattering into the same mode

$$\gamma_1(k_1 = \pi/W)L \sim 16 \exp\left(-\pi^2 a^2/W^2\right). \tag{2.35}$$

The scattering increases for smaller wave vectors, diverging at onset as shown in Fig. 2.2. Remember that the transmission amplitude is $e^{-\gamma_1 L}$. This means that the scattering of the higher modes is *strong* over the 1 μm length, unless sufficiently reduced by the exponential factor arising from the reduced roughness at short length scales.

To fit the higher temperature data using Eq. (2.32) we will find that we need a value of a comparable to W. Although this strongly reduces the value of $\gamma_1(k_1 = \pi/W)$, there remain frequency ranges where the scattering of this mode and other modes is strong. An interesting consequence is that a significant fraction of the thermally excited phonons at temperatures of order 1 K are predicted to be *localized* in the experiments of Schwab *et al.*, with a localization length less than the length of the bridge. Unfortunately, in this regime the estimate of the contribution to the conductance from these modes predicted by our lowest order scattering calculation, will not be accurate. Kambili *et al.* [14] have used a similar model in a numerical investigation of the effect of surface roughness on the mode propagation. The scattering of scalar waves in waveguides with rough surfaces has been also investigated numerically by other workers [15, 16] in a diffusive region - a transition regime between ballistic regime and localised regime.

From Fig. 2.3 we can suggest two mechanisms that might account for the observed minimum in the dependence of K/T on temperature. The first mechanism ascribes the minimum in K/T to the behaviour of the first mode alone, as plotted in Fig. 2.3. The upturn in K/T arises from the reduced scattering of the lowest mode as the wave vectors of the important modes increase with temperature. The second mechanism supposes that the scattering of the lowest mode is responsible for the decreasing K/T at low temperatures, but that the subsequent increase is from the thermal excitation of the higher modes. For our "best fit" values of a, δ (see below) the results are summarized in Fig. 2.4. The picture is quite complicated, with both the reduced scattering of the lowest mode and the thermal excitation of the higher modes contributing to the rise in K/T with increasing temperature. Furthermore, due to the strong scattering of the higher modes near their cutoff frequencies, these modes become important in the transport at a higher temperature than would be estimated simply from their cutoff frequencies.

In Fig. 2.5 the thermal conductance calculated using Eq. (2.32) is plotted together with the ideal (no-scattering) conductance and the measurements of Schwab *et al.* The conductance is scaled such that the universal conductance appears as unity.

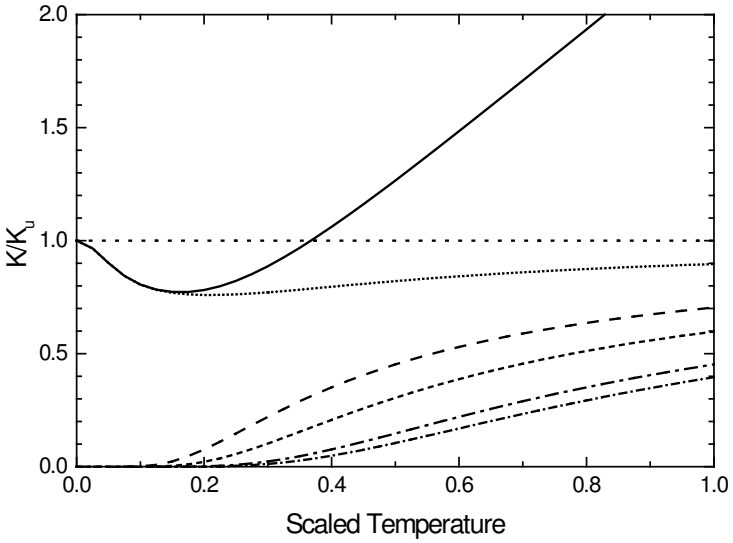

Figure 2.4: Contribution to the thermal conductance K divided by the universal value K_u from the first few modes for the ideal no scattering case, and for the rough case with scattering, as a function of the scaled temperature $k_BT/\hbar\Delta$: solid line—total thermal conductance for the rough surface case; dotted line and short-dotted line—conductance of mode 0 (ideal and rough); dashed line and short-dash-dotted line—conductance of mode 1 (ideal and rough); dashed-dotted line and short-dash-dotted line—conductance of mode 2 (ideal and rough). Values of the roughness parameters were $a/W = 0.75$ and $\delta/W = 0.22$.

The roughness parameters $a/W = 0.75$ and $\delta/W = 0.22$ (so that $a\delta^2 L/W^4 = 0.23$) were used, and yield a reasonable fit to the data. Our 2-D model shows the same trend as the experimental data: a decrease in the thermal conductance below the universal value at low temperatures where only the lowest modes are excited, then a gradually increasing conductance as other modes are excited and the scattering of the lowest mode is reduced. Comparison to the ideal (non-scattering) curve shows that the scattering is important over the whole temperature range examined ($T < 1\,\mathrm{K}$). The values of $\delta = 35\,\mathrm{nm}$ and $a = 120\,\mathrm{nm}$ appear reasonable when one considers the physical process of constructing the mesoscopic bridge structure. For example, a typical chemical etch of silicon nitride can easily produce a few tens of nm in roughness amplitude. Electron micrographs of the actual structure used in the experiment show roughness on scales comparable to the ones we estimate [17].

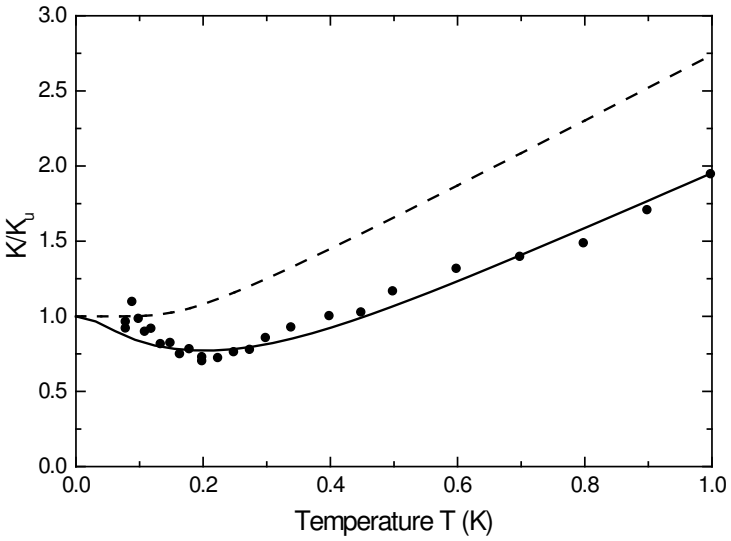

Figure 2.5: Thermal conductance relative to the universal value K_u as a function of temperature for the ideal case (dashed line), the rough surface case (solid line), and the data of Schwab et al. (circles). The roughness parameters used were $a/W = 0.75$, $\delta/W = 0.22$.

There are small but systematic differences at very low temperatures, where the conductance is dominated by the lowest modes, and the theory should be most accurate. The discrepancy suggests that we are overestimating the scattering at long wavelengths. A roughness spectrum $\tilde{g}(k) \sim k^2 e^{-a^2k^2/4}$ with a reduced amplitude at small wave numbers gives a better fit to the data. Such a form might be physically reasonable, since we might expect the roughness to be largest at a scale of order the minimum dimension of the structure, and reduced at larger scales than this. However, since the scalar model does not account for the mode structure of the elastic beam accurately, it is probably unwise to use the discrepancies in Fig. 2.5 to make any firm deductions. Such conclusions require more accurate treatment of the modes within the elasticity theory, which will be the focus in the next chapter.

Chapter 3

Detailed analysis of surface scattering effects - the elastic model

3.1 From a scalar model to an elastic model

In this chapter we again calculate the effect on the low temperature thermal conductance of the scattering of the thermal phonons by surface roughness, but this time, using elastic waves. In the last chapter, we described the scattering in waveguides with rough surfaces via a scalar wave equation. However, this does not accurately capture the low frequency modes of interest at low temperature. For example, the scalar model predicts a linear dispersion at small wave vectors. In fact the dispersion relations of the modes are different, with two of the four modes with zero long-wavelength frequency having a quadratic dispersion at small wave vectors, rather than the linear one given by the simple scalar theory.

To understand the experimental results quantitatively, a more accurate treatment of the vibrational waves is needed. At low temperatures, the wavelengths of the thermally excited modes are large compared with the atomic spacing, and so a treatment based on the equations of macroscopic elasticity theory is appropriate. Blencowe [4, 18] has considered the scattering of elastic waves in a thin plate waveguide with rough surfaces[1], but prior to our work, the scattering of elastic waves confined in a

[1]Blencowe has considered a semi-infinite thin plate. In his case, the out-of-plane mode is a shear-horizontal mode, *i.e.,* the same mode as a bulk mode resulting in no mode coupling for the

beam-like wave guide with rough surfaces has not been considered.

At the end of the last chapter, we noted the apparent discrepancy between the results of the scalar model with a simple assumption for the nature of the surface roughness and the data by Schwab *et al.* [8] below a temperature of 0.1 K: the data seemed to show a delay of the onset of scattering as the temperature increased that was not predicted by the model. However, since the scalar model does not properly account for the properties of the elastic waves, it was not clear whether this discrepancy is due to inadequate modelling of the surface roughness or a flaw in the description of the waves themselves. To resolve this matter, and to obtain a more accurate account of the scattering of the waves by rough surfaces, we develop a theory based on the full elasticity equations, and use this to calculate the thermal conductance at low temperatures. This work forms the basis for three published papers [19, 20, 21].

In § 3.2, the scattering of elastic waves confined to a beam of rectangular cross section with rough surfaces is calculated using the full three dimensional elasticity theory. We use a Green theorem approach, and calculate the scattering coefficient to quadratic order in the amplitude of the surface roughness. These results are quite general, but are rather intractable for further progress, since the structure of the modes in an elastic beam cannot be determined in closed form. Thus in § 3.3 we reduce the expressions to a thin plate limit to provide a closed form for the displacement fields, and to obtain analytical expressions for the scattering behaviour. In § 3.4 the general behaviour of the scattering and the effect on the thermal conductance is analysed in detail, using a simple description of the surface roughness, to investigate the physical consequences of the novel features of the elastic waves. In § 3.5 we use our theory to attempt to fit the data of Schwab *et al.* [8] using more realistic descriptions of the surface roughness. A number of the more difficult issues that arise in the elasticity theory are described in appendices.

Although our main interest is the scattering of thermally excited vibrational waves in mesoscopic systems at low temperatures, the formulation of the surface scattering

---

out-of-plane mode.

is quite general, and can be applied to other situations, such as the scattering of mechanically excited modes in macroscopic samples, for example.

3.2 General formalism

3.2.1 The model

The geometry we consider in this chapter is a 3-D freely suspended elastic beam, which we call the bridge, connecting two thermal reservoirs. We will consider a beam of rectangular cross section of dimensions width W (in the y direction) and depth d (in the z direction). Mesoscopic structures are often produced lithographically from epitaxially grown material. We choose a convention that the depth is the dimension in the growth direction, and the width in the lithographically defined transverse direction. We define the length of the rectangular beam of nominally uniform cross section as L. In practice the bridge may be joined to the reservoirs smoothly, by a portion of continuously growing width, to eliminate or reduce the scattering of the vibration modes off a sharp junction. We will suppose that the scattering by roughness is important only in some narrower portion of length L.

To actually perform the scattering calculation we imbed the rough beam of length L in an infinite beam of the same cross section but with smooth surfaces outside of the region of length L, Fig. 3.1. In the previous chapter, we have defined the rough surface boundaries in y-direction to be $y = f_{-}(x,z)$ and $y = W + f_{+}(x,z)$. In this chapter, we shift the coordinate such that the boundaries in y-direction will be symmetrical about the origin. Thus the mathematical calculation is the scattering of a wave incident from $x = -\infty$ on a rough portion of the beam with surfaces at $y = \pm W/2 \pm f_1(x,z)$ and at $z = \pm d/2 \pm f_2(x,y)$, with the height functions $f_{1,2}$, defining the roughness, nonzero only in a finite region $0 < x < L$. Forward scattering is evaluated from the intensity of waves as $x \to +\infty$, and backward scattering from the intensity of waves as $x \to -\infty$.

To calculate the scattering amplitude, we take a Green function approach similar

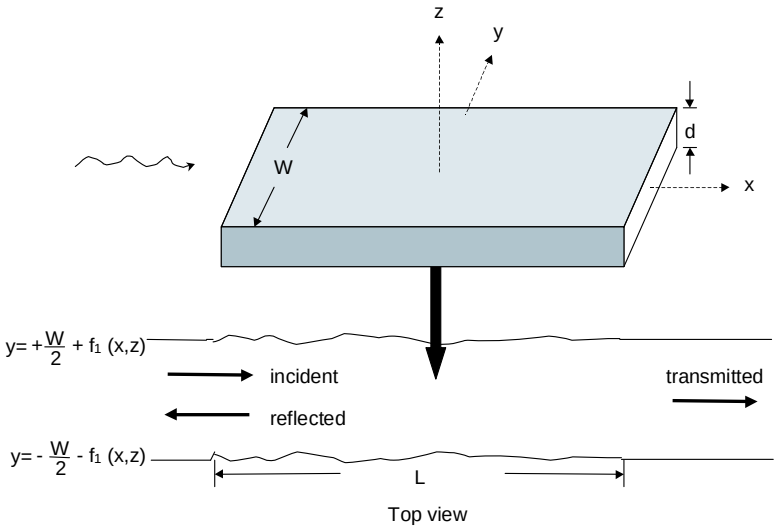

Figure 3.1: Top: Three-dimensional elastic beam with rectangular cross section. The rough surfaces are on the top, bottom, and sides. Bottom: Top view of the mathematical model of the structure actually used for the scattering calculation.

to the one used for the scalar model in the previous chapter.

The displacement field **u** away from any sources satisfies the wave equation:

$$\rho \partial_t^2 u_i = \partial_j T_{ij}, \tag{3.1}$$

where ρ is the mass density, and

$$T_{ij} = C_{ijkl} \partial_k u_l \tag{3.2}$$

is the stress tensor field with C_{ijkl} the elastic modulus tensor. The subscript i runs over the three Cartesian coordinates, we use the symbol ∂_x to denote the derivative $\partial/\partial x$ etc., and repeated indices are to be summed over. The displacement field satisfies stress-free boundary conditions at the surfaces

$$T_{ij} n_j|_S = 0, \tag{3.3}$$

where S denotes the surface boundaries and n_j is normal to the surface. Assuming

harmonic time dependence at frequency ω, Eq. (3.1) becomes

$$\rho\omega^2 u_i + C_{ijkl}\partial_j\partial_k u_l = 0. \tag{3.4}$$

We approximate the material of the system as an isotropic solid. Then the elastic modulus tensor is

$$C_{ijkl} = \lambda\delta_{ij}\delta_{kl} + \mu\left(\delta_{ik}\delta_{jl} + \delta_{il}\delta_{kj}\right), \tag{3.5}$$

where λ and μ are Lamé constants (μ is also the shear modulus)

$$\lambda = E\sigma/(1+\sigma)(1-2\sigma), \quad \mu = E/2\left(1+\sigma\right) \tag{3.6}$$

with E Young's modulus and σ the Poisson ratio.

Even in a rectangular beam geometry the displacement fields in the propagating modes yielded by these equations are complicated, and cannot be found analytically. The modes can be grouped into four classes according to their signature under the parity operations $y \to -y$ and $z \to -z$. Some modes show regions of anomalous dispersion where the group velocity $d\omega/dk$ is negative: these regions require a careful examination of the notions of "forward" and "backward" scattering for the waves. The lowest frequency mode of each class has a frequency that tends to zero at small wave number. These four modes are the only ones excited at low enough temperature, and are the ones contributing to the universal thermal conductance. The structure of these modes at small wave numbers is simple and can be calculated using familiar macroscopic arguments of elasticity theory: they are the compression, torsion, and two orthogonal bending modes.

We define a Green function $G_{iq}(\mathbf{x}, \mathbf{x}'; t, t')$ to satisfy the wave equation with a source term $-\delta_{iq}\delta(\mathbf{x}-\mathbf{x}')\delta(t-t')$, and Γ_{ijq} to be the corresponding stress

$$\Gamma_{ijq} \equiv C_{ijkl}\partial_k G_{lq}. \tag{3.7}$$

It is convenient to introduce the frequency space version of the Green function

$$G_{iq}(\mathbf{x};\mathbf{x}';t,t') = \int \frac{d\omega}{2\pi} G_{iq}(\mathbf{x};\mathbf{x}';\omega) e^{-i\omega(t-t')}, \tag{3.8}$$

with a similar expression defining $\Gamma_{ijq}(\mathbf{x},\mathbf{x}';\omega)$. Inserting G, Γ, and the source term into Eq. (3.4) gives

$$\rho\omega^2 G_{iq}(\mathbf{x},\mathbf{x}';\omega) + \partial_j \Gamma_{ijq}(\mathbf{x},\mathbf{x}';\omega) = -\delta_{iq}\delta\left(\mathbf{x}-\mathbf{x}'\right), \tag{3.9}$$

where $\mathbf{x}$ is the observation coordinate and $\mathbf{x}'$ is the source coordinate.

Equations (3.4) and (3.9) lead to Green's theorem expressing the displacement field at frequency ω in terms of a surface integral

$$u_q(\mathbf{x}) = \int_{S'} \left[n'_j T_{ij}\left(\mathbf{x}'\right) G_{iq}\left(\mathbf{x}',\mathbf{x};\omega\right) - n'_j u_i\left(\mathbf{x}'\right) \Gamma_{ijq}\left(\mathbf{x}',\mathbf{x};\omega\right) \right] dS'. \tag{3.10}$$

We are free to choose any closed integration surface S'. One choice is to use the physical rough surface thereby eliminating the first term in Eq. (3.10) due to the boundary condition Eq. (3.3). However, the resulting integration over the rough surface is not easy. Instead, we integrate over the smoothed surfaces at $y = \pm W/2$ and $z = \pm d/2$ and impose the boundary conditions on the Green function to be stress-free on these smoothed surfaces

$$\Gamma_{ijq} n_j|_S = 0, \tag{3.11}$$

together with cross sections at $x' \to \pm\infty$ to close the surface.

The total field $\mathbf{u}$ can be written as the sum of incident and scattered waves

$$\mathbf{u} = \mathbf{u}^{\text{in}} + \mathbf{u}^{\text{sc}}. \tag{3.12}$$

3.2.2 Incident and scattered fields

Using Green's theorem we have expressed the displacement field at frequency ω in terms of the surface integral

$$u_q(\mathbf{x}) = \int_{S'} \left[n'_j T_{ij}(\mathbf{x}') \, G_{iq}(\mathbf{x}', \mathbf{x}) - n'_j u_i(\mathbf{x}') \, \Gamma_{ijq}(\mathbf{x}', \mathbf{x}) \right] dS'. \tag{3.13}$$

Eq. (3.13) involves the integration over a closed surface S', which we have chosen to be the smooth boundaries together with the cross sections at $x' \to \pm\infty$. We show that the integration over the sections at $\pm\infty$ simply yields the incident field u_q^{in}, and this allows us to deduce the expression for the scattered field as an integration over the side surfaces. To deduce this result, we first need to derive what are known as reciprocity relations for the elastic modes. We follow Auld's approach [22] to derive reciprocity relation. Remember that for $x \to \pm\infty$ the surfaces are smooth, so we are interested in the modes of the ideal beam here.

Let $\mathbf{u}^{(r)}$ and $\mathbf{u}^{(s)}$ be the displacement fields for modes r and s in the ideal beam, and $\mathbf{T}^{(r)}$, $\mathbf{T}^{(s)}$ the corresponding stress tensor fields. The modes satisfy the wave equation at frequency ω, so that

$$\rho\omega^2 u_i^{(r)} + \partial_j T_{ij}^{(r)} = 0. \tag{3.14}$$

Multiply the first equation by $u_i^{(s)*}$ and the complex conjugate of the second by $u_i^{(r)}$, subtract the two equations, integrate over a volume of the beam between $x = x_1$ and $x = x_2$, and finally use the divergence theorem to find

$$\int_S \left[u_i^{(s)*} T_{ij}^{(r)} - u_i^{(r)} T_{ij}^{(s)*} \right] \hat{n}_j dS = 0, \tag{3.15}$$

where the integral is over the surface bounding the volume, consisting of the sides of the beam between x_1 and x_2, and the sections at x_1 and x_2. The integrations over the sides of the beam are zero by the stress-free boundary conditions. For the integration over the sections, introduce the explicit x-dependence $\mathbf{u}^{(r)} = \phi(y, z) e^{ik_r x}$

and $\mathbf{T}^{(r)} = \bar{\mathbf{T}}^{(r)}(y,z)e^{ik_r x}$, with k_r the wave number of mode r at frequency ω, *etc.* Then Eq. (3.15) reduces to

$$\left(1 - e^{i(k_r - k_s)(x_1 - x_2)}\right) \int\int \left[\phi_i^{(s)*} \bar{T}_{ix}^{(r)} - \phi_i^{(r)} \bar{T}_{ix}^{(s)*}\right] dydz = 0, \tag{3.16}$$

and the integral is independent of x. Unless the prefactor is zero, this shows us that the integral over the section must be zero, and so

$$\int\int \left[u_i^{(s)*} T_{ix}^{(r)} - u_i^{(r)} T_{ix}^{(s)*}\right] dydz = 0, \quad k_r \neq k_s. \tag{3.17}$$

This is one version of the reciprocity relations.

For our purposes it is more convenient to express the condition for the reciprocity integral to be zero in terms of the group velocity rather than the wave number. To do so, we need to consider the dispersion curves. The condition for the reciprocity integral to be nonzero, $k_r = k_s$ for modes r, s at the same frequency ω, actually implies r and s are the *same* mode, so that in fact $v_g^{(r)} = v_g^{(s)}$. The only other possibility is that r and s are modes with dispersion curves that cross at frequency ω, $k = k_r = k_s$. However only modes of different y, z parity signatures can cross, and then the integration over the section for these different modes in Eq. (3.17) is again zero. Thus we can rewrite the reciprocity relation as

$$\int\int \left[u_i^{(s)*} T_{ix}^{(r)} - u_i^{(r)} T_{ix}^{(s)*}\right] dydz = 0, \quad v_g^{(r)} \neq v_g^{(s)}. \tag{3.18}$$

If r and s are the same mode, the integral is related to the energy flux and hence to the group velocity (see Eq. (3.25))

$$\int\int dydz \left(u_i^{(r)*} T_{ij}^{(r)} - u_i^{(r)} T_{ij}^{(r)*}\right) = 2i\rho\omega v_g^{(r)}. \tag{3.19}$$

We now use Eqs. (3.18, 3.19) to evaluate the contributions to Eq. (3.13) from the integrations over the sections at $x' \to \pm\infty$.

Let us first consider $x' \to \infty$. According to Eq. (3.24) the x' dependence of the

Green's function pair $\mathbf{G}, \mathbf{\Gamma}$ consist of modes $\mathbf{u}_s(x')^*$ with $v_g^{(s)} < 0$ since here $x' > x$ for any finite x. On the other hand the field pair $\mathbf{u}, \mathbf{T}$ are made up of the incident wave, and waves scattered from the roughness at finite x, and so consist of modes $\mathbf{u}_r(x')$ with $v_g^{(r)} > 0$. The integral in Eq. (3.13) over the section at $x' \to \infty$ is therefore the sum of terms involving $\int\int \left[u_i^{(s)*} T_{ix}^{(r)} - u_r^{(r)} T_{ix}^{(s)*}\right] dydz$ with $v_g^{(r)}$ and $v_g^{(s)}$ of opposite sign. All these terms are zero by Eq. (3.18), and so there is no contribution from the section at $x' \to \infty$.

Similar arguments apply to the section at $x' \to -\infty$. The Green function is made up of modes with $v_g > 0$. The scattered component of the field $\mathbf{u}$ consists of modes with $v_g < 0$, and there is no contribution to the integral over the section from these modes. On the other hand the incident wave $\mathbf{u}^{\text{in}}$ is mode $\mathbf{u}_m$ with $v_g^{(m)} > 0$, and there is the single term with $v_g^{(n)} = v_g^{(m)}$ surviving in the sum over modes in the Green function. Using Eq. (3.19) the integral just gives $u_q^{(m)}(x)$. So the integration over the sections at $x' \to \pm\infty$ on the right-hand side of Eq. (3.10) just gives u_q^{in}. On the other hand, in the integration over the smoothed surfaces at $y = \pm W/2$ and $z = \pm d/2$ the second term in the integrand vanishes due to Eq. (3.11). Thus we find the expression for the scattered field

$$u_q^{\text{sc}}(\mathbf{x}) = \int_{dS} \left[n_j' T_{ij}\left(\mathbf{x}'\right) G_{iq}\left(\mathbf{x}', \mathbf{x}; \omega\right)\right] dS', \tag{3.20}$$

with the surface S the smoothed surfaces $y = \pm W/2$ and $z = \pm d/2$. The stress field T_{ij} on the smoothed surface is evaluated by expanding about its value on the *rough* surfaces, where Eq. (3.3) applies. Writing $\mathbf{u} = \mathbf{u}^{\text{in}} + \mathbf{u}^{\text{sc}}$ then leads to Eq. (3.20).

The remainder of this section proceeds to evaluate Eq. (3.20). Firstly, we find an explicit expression for the Green function with stress-free boundary conditions; then we apply the boundary perturbation method to project the stress at the rough surfaces onto the smooth surfaces by expanding the stress-free boundary terms around the smooth surfaces using the small roughness as the expansion parameter; and finally we evaluate the strength of the scattered waves to give the scattering coefficient.

3.2.3 Green function

We evaluate $G_{iq}(\mathbf{x}, \mathbf{x}'; \omega)$ as an expansion in the complete orthonormal set of normal modes $\mathbf{u}^{(k,m)}(\mathbf{x})$ in the ideal geometry, which satisfy Eq. (3.4) and stress-free boundaries at the smooth surfaces. Here k is the wave number in the x direction, and m labels the branch of the dispersion curve. We define $\omega_m(k)$ as the frequency of the mode m at wave number k in the ideal geometry. The modes satisfy the completeness relation

$$\sum_m \int \frac{dk}{2\pi} u_i^{(k,m)}(\mathbf{x}')^* u_j^{(k,m)}(\mathbf{x}) = \delta_{ij}\delta(\mathbf{x} - \mathbf{x}'). \tag{3.21}$$

Substituting this expression on the right hand side of Eq. (3.9) leads to the expression for the Green function

$$G_{iq}(\mathbf{x}', \mathbf{x}; \omega) = -\sum_m \frac{1}{2\pi} \int_{-\infty}^{\infty} dk \; \frac{\phi_i^{(k,m)}(y', z')^* \phi_q^{(k,m)}(y, z)}{\rho\left[(\omega + i\epsilon)^2 - \omega_m^2(k)\right]} e^{ik(x-x')}, \tag{3.22}$$

where we write

$$u_i^{(k,m)}(\mathbf{x}) = \phi_i^{(k,m)}(y, z) e^{ikx} \tag{3.23}$$

with $\phi_i^{(k,m)}$ giving the transverse dependence of the displacement field. In Eq. (3.22) ϵ is a positive infinitesimal number to incorporate causality, $G_{iq}(\mathbf{x}, \mathbf{x}'; t, t') = 0$ for $t < t'$.

Equation (3.22) can now be evaluated by contour integration. The integrand has poles labelled by an index n near values $k = k_n$ on the real axis which are given by solutions to the dispersion relation $\omega_m(k_n) = \omega$ for all branches m. (We take an incident wave with $\omega > 0$.) Note that for branches with regions of anomalous dispersion there may be more than one solution to this equation for some ω, so that the index n is not identical to the branch index m. The poles are shifted slightly off the real axis by the infinitesimal ε in Eq. (3.22), and are given by expanding about k_n

$$k = k_n + \frac{i\epsilon}{v_g^{(n)}},$$

with $v_g^{(n)}$ the group velocity at the n th pole $d\omega_m/dk|_{k=k_n}$. Notice the poles are in

the upper half plane for $v_g^{(n)} > 0$, and in the lower half plane for $v_g^{(n)} < 0$.

Now we can perform the k integration by complex integration. Consider first the case, $x > x'$. The contour must be closed in the upper half plane so that the contribution from the semicircle at large $|k|$ vanishes. The contour integration then picks up contributions from the poles in the upper half plane, i.e. wave numbers with $v_g^{(n)} > 0$. On the other hand, for $x < x'$ the contour must be closed in the lower half plane and it is poles at wave numbers with $v_g^{(n)} < 0$ that give nonzero residue. Forward scattering or backscattering is thus seen to be determined by the sign of the group velocity $v_g^{(n)}$ rather than by the sign of k_n, as indeed would be expected physically.

Evaluating the residues gives the expression for the Green function:

$$G_{iq}(\mathbf{x}', \mathbf{x}; \omega) = i \sum_n{}' \ \frac{u_i^{(n)}(\mathbf{x}')^* u_q^{(n)}(\mathbf{x})}{2\rho\omega_n \, v_g^{(n)}}, \tag{3.24}$$

where $u_i^{(n)}(\mathbf{x})$ is written for $u_i^{(k,m)}(\mathbf{x})$ at the value of the wave number $k = k_n$ satisfying $\omega_m(k_n) = \omega$. The prime on the sum is used to denote the fact that the sum runs over n with $v_g^{(n)} > 0$ for $x > x'$, and over n with $v_g^{(n)} < 0$ for $x < x'$.

The group velocity $v_g^{(n)}$ does not have an analytical expression for a rectangular beam, and is obtained by differentiating the dispersion curve which must be found numerically. Alternatively, to avoid numerical differentiation, we can rewrite $v_g^{(n)}$ in terms of the average power flow in mode n. Since $u_i^{(n)}$ is normalized, the power P_n in mode n can be written as

$$P_n = \frac{1}{2} \operatorname{Re} \int \int \left(-i\omega T_{ix}^{(n)} u_i^{(n)*} \right) dydz = \frac{1}{2} \rho \omega^2 v_g^{(n)}, \tag{3.25}$$

the first expression of the equality expressing the energy flux in terms of the rate of work done across a section, and the second in terms of the group velocity and the average energy density evaluated as twice the average kinetic energy. Then $v_g^{(n)}$ can

be evaluated in terms of P_n as

$$v_g^{(n)} = 2P_n/\rho\omega^2, \tag{3.26}$$

and P_n has an expression directly in terms of displacement field given by the first equality in Eq. (3.25)

$$P_n = \frac{1}{2}\,\mathrm{Re}\int\int\left(-i\omega T_{ix}^{(n)} u_i^{(n)*}\right) dydz. \tag{3.27}$$

This expression for $v_g^{(n)}$ can also be derived directly from the equations of motion. The details of the derivation is in Appendix A.3.

3.2.4 Boundary perturbation

In this section we show the boundary perturbation technique for the rough surfaces on the sides (*i.e.*, the xz boundary planes). We work out the scattering coefficient explicitly for the surface near $y = W/2$. The surface near $y = -W/2$ will give a similar contribution and, assuming uncorrelated roughness on the two surfaces, is accounted for by multiplying the single-surface scattering rate by 2 at the end of the calculation. The results for the top and bottom surfaces can be obtained by interchanging y and z whenever they occur in the indices in the displacement fields and stress tensors in the calculation below.

In order to calculate the stress on the smooth surface appearing in Eq. (3.20), we expand the stress T_{ij} in a Taylor series about the flat surface, and impose stress-free boundary conditions at the rough surface which is the small distance f_1 away. We also assume f_1 is differentiable.

The unit vector $\hat{n}$ normal to the rough boundaries to first order in f_1 is

$$\hat{n} \simeq \hat{y} - \partial_x f_1(x,z)\,\hat{x} - \partial_z f_1(x,z)\,\hat{z}. \tag{3.28}$$

Then the stress-free surface boundary conditions Eq. (3.3) can be written

$$\left[T_{iy} - \partial_x f_1(x,z)\, T_{ix} - \partial_z f_1(x,z)\, T_{iz}\right]_{y=\frac{W}{2}+f} = 0. \tag{3.29}$$

Now expanding Eq. (3.29) in the neighbourhood of $y = W/2$ and taking only the lowest order in f_1 and f_1', we obtain

$$T_{xy}|_{y=\frac{W}{2}} \simeq \left(\partial_x f_1(x,z)\, T_{xx} + \partial_z f_1(x,z)\, T_{xz} - f_1(x,z)\, \partial_y T_{xy}\right)|_{y=\frac{W}{2}}, \tag{3.30}$$

$$T_{zy}|_{y=\frac{W}{2}} \simeq \left(\partial_x f_1(x,z)\, T_{zx} + \partial_z f_1(x,z)\, T_{zz} - f_1(x,z)\, \partial_y T_{zy}\right)|_{y=\frac{W}{2}}, \tag{3.31}$$

$$T_{yy}|_{y=\frac{W}{2}} \simeq -f_1(x,z)\, \partial_y T_{yy}|_{y=\frac{W}{2}}, \tag{3.32}$$

where the first two expressions for T_{xy} and T_{zy} have been used to simplify T_{yy}. Since the terms on the right hand side of Eqs. (3.30-3.32) are explicitly first order in the small parameter f_1, the stress field T_{ij} on the right hand side can be evaluated at zeroth order, *i.e.* for ideal smooth surfaces. These results are now used in Eq. (3.20).

3.2.5 Scattering coefficient

We now evaluate the expression for the scattered field given by an integration over the beam surfaces Eq. (3.20). To calculate the scattering coefficient, we consider an incident wave of unit amplitude in a single mode m. Again in this section we will outline the calculation for the scattering by the single surface at $y = W/2$, and will include the effects of the other surfaces at the end. We therefore have

$$u_q^{\mathrm{sc}}(\mathbf{x}) = \int\int \left[T_{iy}(\mathbf{x}')\, G_{iq}(\mathbf{x}', \mathbf{x}; \omega)\right]_{y'=\frac{W}{2}} dx' dz'. \tag{3.33}$$

We can now evaluate the forward- and backscattering amplitudes by using Eq. (3.24) for the Green function in Eq. (3.33), and evaluating the scattered wave at

large positive and negative x

$$u_q^{\mathrm{sc}}\left(x\to\infty,y,z\right)\simeq\int_{-\infty}^{x}dx'\int_{-\frac{d}{2}}^{\frac{d}{2}}dz'\sum_{n,v_g^{(n)}>0}\frac{i}{2\rho\omega\,v_g^{(n)}}\left[T_{iy}\left(\mathbf{x}'\right)u_i^{(n)}\left(\mathbf{x}'\right)^*\right]_{y'=\frac{W}{2}}u_q^{(n)}\left(\mathbf{x}\right), \tag{3.34}$$

$$u_q^{\mathrm{sc}}\left(x\to-\infty,y,z\right)\simeq\int_{x}^{\infty}dx'\int_{-\frac{d}{2}}^{\frac{d}{2}}dz'\sum_{n,v_g^{(n)}<0}\frac{i}{2\rho\omega\,v_g^{(n)}}\left[T_{iy}\left(\mathbf{x}'\right)u_i^{(n)}\left(\mathbf{x}'\right)^*\right]_{y'=\frac{W}{2}}u_q^{(n)}\left(\mathbf{x}\right). \tag{3.35}$$

The stress tensor T_{ij} corresponding to the full displacement field of the wave is evaluated from Eqs. (3.30-3.32). Since these expressions explicitly include the small roughness amplitude f_1 on the right hand side, to calculate the scattering at lowest order in the roughness amplitude it is sufficient to replace all T_{ij} on the right hand side by the value $T_{ij}^{(m)}$ in the incident mode m. From Eqs. (3.34, 3.35) we see that $\mathbf{u}^{\mathrm{sc}}(\mathbf{x})$ is expressed as a sum over modes $\mathbf{u}^{(n)}(\mathbf{x})$, and the coefficient of each mode is then the scattering amplitude $t_{n,m}$ from incident mode m into mode n, so that

$$t_{n,m}=\int_{-\infty}^{\infty}dx\int_{-\frac{d}{2}}^{\frac{d}{2}}dz\frac{i}{2\rho\omega\,v_g^{(n)}}\left[T_{iy}^{(m)}\left(\mathbf{x}\right)u_i^{(n)}\left(\mathbf{x}\right)^*\right]_{y=W/2}, \tag{3.36}$$

where we can now extend the integration limit to $\pm\infty$ since f_1, and so the integrand, is zero outside the domain of roughness $0<x<L$. Again mode indices n for which $v_g^{(n)}>0$ represent the forward-scattered waves and those with $v_g^{(n)}<0$ the backward-scattered waves.

Now use the expression for the stress tensor on the smooth surfaces obtained in the previous section Eqs. (3.30-3.32) and integrate the resulting expressions by parts with respect to x or z to rewrite the terms in $\partial_x f_1$ and $\partial_z f_1$ as integrations over f_1. After these manipulations we find $t_{n,m}$ can be written

$$t_{n,m}=-\frac{i}{2\rho\omega v_g^{(n)}}\int_{-\infty}^{\infty}dx\int_{-\frac{d}{2}}^{\frac{d}{2}}dz\,f_1\left(x,z\right)\Gamma^{(m,n)}\left(x,z\right), \tag{3.37}$$

where

$$\begin{aligned}\Gamma^{(m,n)}(x,z) = \big[&\left(\partial_x T^{(m)}_{xx} + \partial_y T^{(m)}_{xy} + \partial_z T^{(m)}_{xz}\right) u^{(n)*}_x \\ &+ \left(\partial_x T^{(m)}_{zx} + \partial_y T^{(m)}_{zy} + \partial_z T^{(m)}_{zz}\right) u^{(n)*}_z \\ &+ \partial_y T^{(m)}_{yy} u^{(n)*}_y + T^{(m)}_{xx}\partial_x u^{(n)*}_x + T^{(m)}_{zz}\partial_z u^{(n)*}_z \\ &+ T^{(m)}_{zx}\left(\partial_x u^{(n)*}_z + \partial_z u^{(n)*}_x\right)\big]_{y=W/2}\,. \end{aligned} \tag{3.38}$$

Applying the equations of motion Eq. (3.4) and remembering $T^{(m)}_{iy}\Big|_{y=W/2} = 0$ for all i and for all x, z leads to the somewhat simpler expression

$$\begin{aligned}\Gamma^{(m,n)}(x,z) = \big[&-\rho\omega^2\left(u^{(m)}_x u^{(n)*}_x + u^{(m)}_y u^{(n)*}_y + u^{(m)}_z u^{(n)*}_z\right) \\ &+ T^{(m)}_{xx}\partial_x u^{(n)*}_x + T^{(m)}_{zz}\partial_z u^{(n)*}_z + T^{(m)}_{xz}\left(\partial_z u^{(n)*}_x + \partial_x u^{(n)*}_z\right)\big]_{y=W/2}\,. \end{aligned} \tag{3.39}$$

Notice that the scattering separates into a kinetic term (the first line) and a stress term (the second line).

The above form for $\Gamma^{(m,n)}$ is still neither instructive nor practical for numerical evaluation. It can be further simplified using the expressions Eqs. (3.2, 3.6) for the stress tensor in terms of the displacements. First we use the boundary condition $T^{(m)}_{yy} = 0$ for the y-stress to give at $y = W/2$

$$\partial_y u^{(m)}_y = -\frac{\sigma}{(1-\sigma)}(\partial_x u^{(m)}_x + \partial_z u^{(m)}_z). \tag{3.40}$$

This can be used to simplify the expressions for the other components of the stress tensors at $y = W/2$

$$T^{(m)}_{xx} = \frac{E}{(1-\sigma^2)}(\partial_x u^{(m)}_x + \sigma\partial_z u^{(m)}_z), \tag{3.41}$$

$$T^{(m)}_{zz} = \frac{E}{(1-\sigma^2)}(\sigma\partial_x u^{(m)}_x + \partial_z u^{(m)}_z), \tag{3.42}$$

$$T^{(m)}_{xz} = \frac{E}{2\,(1+\sigma)}(\partial_x u^{(m)}_z + \partial_z u^{(m)}_x). \tag{3.43}$$

Inverting these gives at $y = W/2$

$$\partial_x u_x^{(m)} = \frac{1}{E}(T_{xx}^{(m)} - \sigma T_{zz}^{(m)}), \tag{3.44}$$

$$\partial_z u_z^{(m)} = \frac{1}{E}(T_{zz}^{(m)} - \sigma T_{xx}^{(m)}), \tag{3.45}$$

$$\partial_x u_z^{(m)} + \partial_z u_x^{(m)} = \frac{2(1+\sigma)}{E} T_{xz}^{(m)}. \tag{3.46}$$

We emphasize that Eqs. (3.40-3.46) are only true on the stress-free boundaries, and are not generally true in the bulk of the material.

Using these results we get

$$t_{n,m} = -\frac{i}{2\rho\omega\, v_g^{(n)}} \int_{-\frac{d}{2}}^{\frac{d}{2}} dz\, \tilde{f}_1\,(k_m - k_n, z)\, \bar{\Gamma}^{(m,n)}(z), \tag{3.47}$$

with

$$\begin{aligned}\bar{\Gamma}^{(m,n)} = \Big\{ & \rho\omega^2(\phi_x^{(m)}\phi_x^{(n)*} + \phi_y^{(m)}\phi_y^{(n)*} + \phi_z^{(m)}\phi_z^{(n)*}) \\ & - \frac{1}{E}\left[(\bar{T}_{xx}^{(m)}\bar{T}_{zz}^{(n)*} + \bar{T}_{zz}^{(m)}\bar{T}_{zz}^{(n)*}) - \sigma(\bar{T}_{zz}^{(m)}\bar{T}_{xx}^{(n)*} + \bar{T}_{xx}^{(m)}\bar{T}_{zz}^{(n)*})\right] \\ & - \frac{1}{\mu}\bar{T}_{xz}^{(m)}\bar{T}_{zx}^{(n)*} \Big\}_{y=W/2},\end{aligned} \tag{3.48}$$

where we have introduced the explicit x dependence of $u_i^{(n)}(\mathbf{x})$ as in Eq. (3.23) and the stress tensor

$$T_{ij}^{(n)}(\mathbf{x}) = \bar{T}_{ij}(y,z)e^{ik_n x}, \tag{3.49}$$

so that the x' integration is just the Fourier transform $\tilde{f}$ of the roughness function, and $\bar{\Gamma}$ is a function of the z coordinate only.

Alternatively, using Eqs. (3.41-3.43) we can derive an expression explicitly in the

displacement fields, which is useful for numerical evaluation,

$$\begin{aligned}\bar{\Gamma}^{(m,n)} = \big\{&\rho\omega^2(\phi_x^{(m)}\phi_x^{(n)*} + \phi_y^{(m)}\phi_y^{(n)*} + \phi_z^{(m)}\phi_z^{(n)*}) \\ &- \frac{2\mu}{(1-\sigma)}\left[(k_m k_n \phi_x^{(m)} u_x^{(n)*} + \partial_z\phi_z^{(m)}\partial_z\phi_z^{(n)*})\right. \\ &\left.+ \sigma(ik_m\phi_x^{(m)}\partial_z\phi_z^{(n)*} - ik_n\partial_z\phi_z^{(m)}\phi_x^{(n)*})\right] \\ &- \mu(ik_m\phi_z^{(m)}\partial_z\phi_x^{(n)*} + k_m k_n\phi_z^{(m)}\phi_z^{(n)*} \\ &+\partial_z\phi_x^{(m)}\partial_z\phi_x^{(n)*} - ik_n\partial_z\phi_x^{(m)}\phi_z^{(n)*})\big\}_{y=W/2}\,. \end{aligned} \tag{3.50}$$

The scattering rate is given by multiplying $|t_{n,m}|^2$ by the ratio of the group velocities in the scattered and incident waves[2]. We also treat the roughness of the surface statistically, and take an ensemble average (denoted by angular brackets) to give the final expression for the scattering rate $\gamma_{n,m}$ from mode m to mode n by the per unit length of single rough surface at $y = W/2$ given by

$$\begin{aligned}\gamma_{n,m}L &= \frac{v_g^{(n)}}{v_g^{(m)}}\left\langle|t_{n,m}|^2\right\rangle \\ &= \frac{1}{4\rho^2\omega^2 v_g^{(m)}v_g^{(n)}}\left\langle\left|\int_{-\frac{d}{2}}^{\frac{d}{2}} dz\tilde{f}_1\left(k_m - k_n, z\right)\bar{\Gamma}^{(m,n)}(z)\right|^2\right\rangle. \end{aligned} \tag{3.51}$$

We are interested in the reduction of the phonon heat transport due to rough surfaces. Only the backscattered waves (those with $v_g^{(n)} < 0$) reduce the amount of heat transmitted. Thus we define γ_m, the thermal attenuation coefficient of mode m per unit length, to be the sum of the scattering rates from the incident mode m to *all* possible backscattered modes, per unit length of rough surface. This can be written

[2]Note that the scattering amplitude normalized by the energy flux $\bar{t}_{n,m} = \sqrt{\left|v_g^{(n)}\right| / \left|v_g^{(m)}\right|}t_{n,m}$ can be seen from Eq. (3.47) to explicitly satisfy the reciprocity relation $\bar{t}_{n,m} = \bar{t}^*_{-m,-n}$. For systems in which energy is conserved, as in our case, reciprocity is equivalent to time-reversal invariance [23].

for scattering off the single rough surface considered so far

$$\begin{aligned}\gamma_m L &= \sum_{\substack{n \\ v_g^{(n)}<0}} \gamma_{n,m} L \\ &= \sum_{\substack{n \\ v_g^{(n)}<0}} \frac{1}{4\rho^2\omega^2 v_g^{(m)} v_g^{(n)}} \left\langle \left| \int_{-\frac{d}{2}}^{\frac{d}{2}} dz \tilde{f}_1 \left(k_m - k_n, z\right) \bar{\Gamma}^{(m,n)}(z) \right|^2 \right\rangle . \end{aligned} \tag{3.52}$$

To include the second rough side surface, assuming uncorrelated roughness, we simply have to multiply the expression for γ_m by a factor of 2. The expression for scattering off the top and bottom surfaces, if these are rough too, can be derived in a similar manner, and the result may be obtained by exchanging y and z in Eq. (3.52). The total scattering rate is the sum of the scattering off all the surfaces.

We have assumed that the amplitude of the surface roughness is small, allowing us to use perturbation theory to derive the above expressions. In this weak scattering limit the transmission coefficient is $\mathcal{T}_m \simeq 1 - \gamma_m L$. When we estimate the size of the surface roughness from the data of Schwab *et al.* [8], we find that the weak scattering approximation is sufficient for all frequencies except near the onset of the higher modes, where the scattering tends to diverge due to the group velocity factors in the denominator of Eq. (3.52) as found in the scalar model. The transmission coefficient becomes small over a narrow range near these onset frequencies, and the simple expression for $\mathcal{T}_m$ is inadequate here. To interpolate to the small transmission for strong scattering, we use the approximation

$$\mathcal{T}_m \simeq \exp\left[-\gamma_m L\right] . \tag{3.53}$$

This expression correctly includes the exponential decay of the wave due to successive scattering out events, but does not include multiple scattering, which may eventually scatter the wave back into the forward direction. However, for the calculation of the thermal conductivity in the temperature range of interest, the effect of the strong scattering regions around the onset of the higher modes is negligible, and

other interpolation expressions between the weak scattering expression valid for most frequencies, and the small transmission near the onset frequencies, give very similar predictions.

3.3 Thin plate limit

Although the expression in the previous section is general and applicable to any rectangular waveguide with rough surfaces, there are no closed-form expressions for the displacement fields in general, and so a direct evaluation of the scattering would have to be done completely numerically. Here, we instead use the *thin plate approximation* $d \ll W$ [10, 25], which yields closed form expressions for the displacement fields of the modes (in terms of dispersion curves $\omega_m(k)$ given by numerical solution of a simple transcendental equation). The thin plate limit captures the important properties of the elastic modes, for example, the quadratic dispersion of the bending modes at small wave numbers, and regions of anomalous dispersion, as well as providing analytical expressions enabling us to do further analysis of the scattering. The thin plate theory is applicable where the thickness of the sample is much less than the width and the wavelengths are much greater than the thickness, which is the case for many mesoscopic systems at low temperatures.

The use of the thin plate limit for mesoscopic structures was proposed in reference [10], where the calculation of the structure of the modes is described in more detail. It is found that the modes can be separated into two classes: *in-plane modes*, where the polarization of the displacement is largely in the xy plane (together with small strains in the z-direction given by the Poisson effect) and the displacement field is completely specified by giving the *vertically averaged horizontal displacement components* $\bar{u}_x(x, y)$ and $\bar{u}_y(x, y)$; and *flexural modes*, where the displacement is primarily in the z direction and is specified by a vertical displacement field $\bar{u}_z(x, y)$. Within each class we can further distinguish the modes by their parity under $y \to -y$. For the in-plane modes we define the mode as even if $\bar{u}_x(x, -y) = \bar{u}_x(x, y)$ and odd if $\bar{u}_x(x, -y) = -\bar{u}_x(x, y)$. Similarly, the even flexural modes have $\bar{u}_z(x, -y) = \bar{u}_z(x, y)$ and the odd modes

have $\bar{u}_z(x,-y) = -\bar{u}_z(x,y)$. As in the general case, there are four branches of the dispersion curves that tend to zero frequency as the wave number goes to zero, corresponding to one mode from each of these classes. The low frequency, even in plane mode corresponds to the compression mode, and the odd mode to a bending mode. The low frequency even, flexural mode corresponds to the second bending mode, and the low frequency odd flexural mode is the torsion mode.

Explicit expressions for the displacement fields can be obtained using the method described in reference [10]. For the in-plane modes we find, up to a normalization factor A_1 that is common to both even and odd parity waves, the even modes

$$\bar{u}_x(x,y) = ikA_1\left[\frac{k^2-\chi_1^2}{2k^2}\cos\left(\frac{\chi_2 W}{2}\right)\cos(\chi_1 y) - \cos(\chi_2 y)\cos\left(\frac{\chi_1 W}{2}\right)\right]e^{ikx}, \tag{3.54}$$

$$\bar{u}_y(x,y) = A_1\left[\frac{k^2-\chi_1^2}{2\chi_1}\cos\left(\frac{\chi_2 W}{2}\right)\sin(\chi_1 y) + \chi_2\cos\left(\frac{\chi_1 W}{2}\right)\sin(\chi_2 y)\right]e^{ikx}, \tag{3.55}$$

and the odd modes

$$\bar{u}_x(x,y) = ikA_1\left[\frac{k^2-\chi_1^2}{2k^2}\sin(\chi_1 y)\sin\left(\frac{\chi_2 W}{2}\right) - \sin\left(\frac{\chi_1 W}{2}\right)\sin(\chi_2 y)\right]e^{ikx}, \tag{3.56}$$

$$\bar{u}_y(x,y) = -A_1\left[\frac{k^2-\chi_1^2}{2\chi_1}\cos(\chi_1 y)\sin\left(\frac{\chi_2 W}{2}\right) + \chi_2\sin\left(\frac{\chi_1 W}{2}\right)\cos(\chi_2 y)\right]e^{ikx}, \tag{3.57}$$

where $\chi_1 = \left(\omega^2/c_t^2 - k^2\right)^{1/2}$ and $\chi_2 = \left(\omega^2/c_l^2 - k^2\right)^{1/2}$, with c_t the transverse sound velocity and c_l the longitudinal velocity *in a large thin plate*

$$c_t = \sqrt{\frac{E}{2\rho(1+\sigma)}}, \quad c_l = \sqrt{\frac{E}{\rho(1-\sigma^2)}}, \tag{3.58}$$

and ω and k related by the dispersion curve which must be found numerically. In the

thin plate limit it is sufficient to take for the in-plane modes

$$u_x(x,y,z) \simeq \bar{u}_x(x,y), \tag{3.59}$$

$$u_y(x,y,z) \simeq \bar{u}_y(x,y), \tag{3.60}$$

$$u_z(x,y,z) \simeq 0. \tag{3.61}$$

Similarly, the vertical displacement field for the even flexural modes is

$$\bar{u}_z(x,y) = A_2 \left[\cosh\left(\frac{\chi_- W}{2}\right) \cosh(\chi_+ y) - \frac{k^2\sigma - \chi_+^2}{k^2\sigma - \chi_-^2} \cosh\left(\frac{\chi_+ W}{2}\right) \cosh(\chi_- y) \right] e^{ikx}, \tag{3.62}$$

and for the odd flexural modes

$$\bar{u}_z(x,y) = A_2 \left[\sinh\left(\frac{\chi_- W}{2}\right) \sinh(\chi_+ y) - \frac{k^2\sigma - \chi_+^2}{k^2\sigma - \chi_-^2} \sinh\left(\frac{\chi_+ W}{2}\right) \sinh(\chi_- y) \right] e^{ikx}, \tag{3.63}$$

where $\chi_\pm$ are defined as $\chi_+ = \left(k^2 + \sqrt{\rho d/D}\omega\right)^2$ and $\chi_- = \left(k^2 - \sqrt{\rho d/D}\omega\right)^2$ with $D = Ed^3/12(1-\sigma^2)$ the flexural rigidity, and ω and k are related by the appropriate dispersion curve. In the classical thin plate theory, the displacement fields are given in terms of $\bar{u}_z$ by the expressions

$$u_x(x,y,z) \simeq -z\partial_x \bar{u}_z(x,y), \tag{3.64}$$

$$u_y(x,y,z) \simeq -z\partial_y \bar{u}_z(x,y), \tag{3.65}$$

$$u_z(x,y,z) \simeq \bar{u}_z(x,y). \tag{3.66}$$

This approximation is adequate for evaluating the surface stress integrals in Eq. (3.52) but turns out not to be sufficiently accurate to evaluate the energy flux expression for the group velocity Eq. (3.27). We discuss this case in § 3.3.2 below.

3.3.1 Attenuation coefficient in the thin plate limit

The thin plate approximation is implemented by noticing that the stress-free boundary conditions imply that the stress components T_{iz} are zero on the top and bottom

surfaces. For small thickness this implies that the components T_{iz} for any i are small everywhere. In most situations these components can be approximated as zero [25]. This simplifies many of the terms appearing in Eq. (3.47). Also, at low temperatures, only modes with no strong dependence on the z coordinate will be excited, so that the mode sum extends over modes with increasing numbers of nodes in the y direction only.

In this section we calculate the scattering of the elastic waves by surface roughness for a thin plate. We assume that the roughness is confined to the sides, since in the experiments theses are prepared lithographically, whereas the top and bottom surfaces are produced by the epitaxial growth process.

For simplicity, we assume the roughness function f_1 has no z dependence. This is probably a reasonable description of the roughness produced by a typical lithographic process of anisotropic chemical etch[3]. Then the Fourier transformed roughness function $\tilde{f}_1(k_m - k_n)$ can be pulled outside of the z integral in Eq. (3.52) and the statistical average over the roughness can be performed to give

$$\left\langle \left| \tilde{f}_1(k) \right|^2 \right\rangle = \tilde{g}(k) L, \tag{3.67}$$

where $\tilde{g}(k)$ is the Fourier transform of the roughness correlation function

$$\tilde{g}(k) = \int dx e^{-ikx} \langle f_1(x) f_1(0) \rangle .$$

Equation (3.52) leads to the back-scattering rate from mode m to mode n

$$\gamma_{n,m} = \frac{\tilde{g}(k_m - k_n)}{2\rho^2 \omega^2 v_g^{(m)} v_g^{(n)}} \left| \int_{-\frac{d}{2}}^{\frac{d}{2}} dz \bar{\Gamma}^{(m,n)}(z) \right|^2 , \tag{3.68}$$

where Eq. (3.52) is multiplied by a factor of 2 to account for the two surfaces at $y = \pm W/2$.

[3]Without this assumption, we would find slightly different z averages of the roughness function $\tilde{f}_1$ involved for the scattering of the in-plane modes and of the flexural modes—in fact a direct average for the inplane modes and an average weighted by z^2 for the flexural modes. In addition there would now be scattering from in-plane to flexural modes, and *vice versa*.

With the closed forms of the displacement fields at hand, we can obtain the analytical expression for the attenuation coefficient. We first evaluate $\bar{\Gamma}^{(m,n)}$ from Eq. (3.48). Since $T_{iz}^{(m)} \simeq 0$, the expression for $\bar{\Gamma}$ reduces to

$$\bar{\Gamma}^{(m,n)} \simeq \left[\rho\omega^2 \left(\phi_x^{(m)}\phi_x^{(n)*} + \phi_y^{(m)}\phi_y^{(n)*} + \phi_z^{(m)}\phi_z^{(n)*}\right) - \frac{1}{E}\left(\bar{T}_{xx}^{(m)}\bar{T}_{xx}^{(n)*}\right)\right]_{y=W/2}. \quad (3.69)$$

In addition, putting $T_{zz}^{(m)}$ in Eq. (3.43) at the stress-free boundary to zero gives

$$\partial_z u_z^{(m)} = -\sigma\partial_x u_x^{(m)}, \quad (3.70)$$

so that $T_{xx}^{(m)}$ from Eq. (3.41) simplifies to

$$T_{xx}^{(m)} = E\partial_x u_x^{(m)}. \quad (3.71)$$

Now Eq. (3.68) can be written as

$$\gamma_{n,m} = \frac{\tilde{g}\left(k_m - k_n\right)}{2\rho^2\omega^2 v_g^{(m)} v_g^{(n)}} \left| \int_{-\frac{d}{2}}^{\frac{d}{2}} dz \left[\rho\omega^2 \phi_i^{(m)}\phi_i^{(n)*} + E k_m k_n \phi_x^{(m)}\phi_x^{(n)*}\right]_{y=\frac{W}{2}} \right|^2, \quad (3.72)$$

where the index i is summed over x, y, z. The scattering in the thin plate limit is seen to have two components: the kinetic term, the first term in the [ ] in Eq. (3.72), which involves all components of the displacement; and the stress term, the second term, which just depends on the longitudinal displacement. Comparing this result with the one in Eq. (2.29) in the scalar model, we notice the same kind of components are contributing the scattering (note that the expression in Eq. (3.72) per unit length in x-direction).

To see how the scattering rate scales with the parameters it is useful to rewrite

Eq. (3.72) as

$$\gamma_{n,m}L = \frac{\tilde{g}\,(k_m - k_n)\,L}{2W^4} \times \frac{W^2\omega^2}{v_g^{(m)}v_g^{(n)}} \times \frac{\left|\int_{-d/2}^{d/2} dz \left[\phi_i^{(m)}\phi_i^{(n)*} + \frac{Ek_sk_n}{\rho\omega^2}\phi_x^{(m)}\phi_x^{(n)*}\right]_{y=\frac{W}{2}}\right|^2}{\left(\int_{-d/2}^{d/2} dz \int_{-W/2}^{W/2} \frac{dy}{W}\phi_i^{(m)}\phi_i^{(m)*}\right)^{1/2}\left(\int_{-d/2}^{d/2} dz \int_{-W/2}^{W/2} \frac{dy}{W}\phi_i^{(n)}\phi_i^{(n)*}\right)^{1/2}}. \quad (3.73)$$

The first factor is a dimensionless measure of the strength of the roughness; the second factor is a dimensionless ratio that depends, through the dispersion relation, only on the geometric ratio d/W and the Poisson ratio σ; and the final factor involves integrals over the displacement fields, where we have introduced the explicit normalization factors in the denominator so that we may evaluate the ratio using convenient unnormalized expressions for the displacements.

3.3.2 Evaluating the group velocity

As we have seen in Eq. (3.26), we can avoid evaluating the group velocity appearing in Eq. (3.72) via numerical differentiating the dispersion curve by instead relating the group velocity to the energy flux in the mode, which in turn can be written as an explicit integral Eq. (3.27). Thus we need to evaluate the expression (we suppress the mode index in this section)

$$P = -\frac{1}{2}\,\mathrm{Re}\left[i\omega \int\int \left(T_{xx}u_x^* + T_{yx}u_y^* + T_{zx}u_z^*\right) dydz\right] \quad (3.74)$$

involving the displacement fields and their derivatives.

In the thin plate limit the z components of the stress are small. If we approximate $T_{zz} = 0$ then expressions Eqs. (3.2, 3.6) can be used to evaluate the z-component of the strain

$$\partial_z u_z = -\frac{\sigma}{(1-\sigma)}\left(\partial_x u_x + \partial_y u_y\right). \quad (3.75)$$

This can be then used to simplify the in-plane components of the stress

$$T_{xx} = \frac{E}{(1-\sigma^2)}(\partial_x u_x + \sigma \partial_y u_y), \tag{3.76}$$

$$T_{yy} = \frac{E}{(1-\sigma^2)}(\sigma \partial_x u_x + \partial_y u_y), \tag{3.77}$$

$$T_{yx} = \frac{E}{2(1+\sigma)}(\partial_x u_y + \partial_y u_x). \tag{3.78}$$

These expression are used to evaluate the first two terms in the integrand in Eq. (3.74). The evaluation of the last term in the integrand turns out to depend on whether we are looking at the in-plane or flexural modes, and we now consider each case in turn.

3.3.2.1 In-plane modes

For the in-plane modes in the thin plate limit it is sufficiently accurate to approximate $T_{zx} \simeq 0$, and we can evaluate the remaining terms in P with the approximations $u_x \simeq \bar{u}_x$, $u_y \simeq \bar{u}_y$ independent of z. This yields

$$P = \mathrm{Re}\left\{ -\frac{i\omega E d}{4\,(1-\sigma^2)} \int dy \left[2(\partial_x \bar{u}_x + \sigma \partial_y \bar{u}_y)\bar{u}_x^* + (1-\sigma)\,(\partial_x \bar{u}_y + \partial_y \bar{u}_x)\,\bar{u}_y^* \right] \right\}. \tag{3.79}$$

3.3.2.2 Flexural modes

For the flexural mode the approximations $T_{zx} \simeq 0$ and $u_z(x,y,z) \simeq \bar{u}_z(x,y)$ independent of z lead to the expressions for the horizontal displacements

$$u_x(x,y,z) \simeq -z \partial_x \bar{u}_z(x,y), \tag{3.80}$$

$$u_y(x,y,z) \simeq -z \partial_y \bar{u}_z(x,y). \tag{3.81}$$

Using these expressions with Eqs. (3.76-3.77) shows that the first two terms in Eq. (3.74) are of order d^3, *i.e.*, *third order* in the expansion parameter of thin plate theory d/W. It turns out that to this order, we *cannot* neglect the last term in T_{zx}, even

though all z-components in the stress tensor are nominally "small". Indeed comparing the group velocity evaluated from Eq. (3.74) neglecting the term in T_{zx} with those given by numerically differentiating the dispersion curve shows a clear discrepancy. This same problem comes up in deriving the wave equation for the flexural waves

$$\rho d\omega^2 \bar{u}_z = D\nabla_\perp^4 \bar{u}_z. \tag{3.82}$$

The term on the left-hand side is the mass per unit area times the vertical acceleration, which is given by the integral over the depth of $\partial_x T_{zx} + \partial_y T_{zy}$. Clearly the components of T_{zi} cannot be neglected completely. Their "smallness" is what leads to the unusual fourth-order derivative appearing in this wave equation, with a coefficient again proportional to d^3.

We have used two methods to arrive at the correct calculation of the energy flux integral for the flexural waves, which is then used to calculate the group velocity for the these waves. The first is to use an improved approximation to the expressions for the in-plane displacements Eqs. (3.76, 3.77) and a nonzero T_{zx} following the approach of Timoshenko [26]. The second evaluates the energy flux in terms of the vertical displacement and an effective vertical force, and in addition the rotational displacement θ and corresponding torque M, as is used in the macroscopic derivation [25] of the wave equation (3.82). Below, we present the energy flux calculations by these two methods and show that these methods give the identical answers (c.f. Eqs. (3.107, 3.113).

In the extended thin plate approximation of Timoshenko the z-dependence of the in-plane displacements is still approximated as linear

$$u_x(x, y, z) \simeq z\psi_x(x, y), \tag{3.83}$$

$$u_y(x, y, z) \simeq z\psi_y(x, y). \tag{3.84}$$

However, the x, y dependence is no longer assumed to be given by the gradient of the

mean vertical displacement $\bar{u}_z(x,y)$, but by the more general expression

$$\psi = -\nabla_\perp \bar{u}_z + \nabla_\perp S + \nabla_\perp \times (\zeta \hat{z}) \tag{3.85}$$

introducing the scalar potential $S(x,y)$ and vector potential $\zeta(x,y)$ defining the corrections to the in-plane strain and rotation. Here $\nabla_\perp = (\partial_x, \partial_y)$ is the horizontal gradient. In addition the vertically averaged stress T_{zx} is taken to be

$$T_{zx} \simeq \kappa^2 \frac{E}{2\,(1+\sigma)} (\partial_x \bar{u}_z + \partial_z u_x) \tag{3.86}$$

(with a similar expression for T_{zy} given by replacing the subscript x with y everywhere). Here the "shear correction factor" κ, a number of order unity, is introduced to take into account deviations of the in-plane displacements from the assumed linear dependence on z [26]. In the usual thin plate approximation T_{zi} are set to zero and $\psi = -\nabla_\perp w$, so that $(u_x, u_y) = -z\nabla_\perp w$.

With the Timoshenko approximations, the equations of motion for the three components of displacement are now investigated.

The equations of motion for the horizontal displacement lead to an equation relating ψ to $\bar{u}_z$ [27]

$$\frac{D}{2} \left\{ (1-\sigma)\nabla^2 \psi + (1+\sigma)\nabla_\perp \nabla_\perp \cdot \psi \right\} - \kappa^2 \mu d\,(\psi + \nabla_\perp \bar{u}_z) = 0 \tag{3.87}$$

(remember $D = Ed^3/12(1-\sigma^2)$, with E Young's modulus, and μ the shear modulus). The inertial terms $\partial_t^2 \psi$ turn out to be negligible in this equation. Using Eqs. (3.85, 3.87) becomes

$$D\nabla_\perp \nabla_\perp^2 (S-w) - \kappa^2 \mu d \nabla_\perp S + \frac{D}{2}(1-\sigma)\nabla_\perp \times (\nabla_\perp^2 \zeta \hat{z}) - \kappa^2 \mu d \nabla_\perp \times (\zeta \hat{z}) = 0. \tag{3.88}$$

Taking the vertical curl of Eq. (3.88) gives

$$\frac{D}{2}(1-\sigma)\nabla_\perp^2 \Omega - \kappa^2 \mu d\,\Omega = 0 \tag{3.89}$$

with $\Omega = \hat{z} \cdot \nabla_\perp \times \psi = -\nabla_\perp^2 \zeta$ the rotation. For a wave disturbance e^{ikx}, this gives an exponential dependence on y, $e^{\pm\lambda y}$ with

$$\lambda^2 \simeq \frac{2\kappa^2 \mu d}{D(1-\sigma)} \sim d^{-2}. \tag{3.90}$$

Since $\lambda^{-1} \sim d \ll W$, the rotation will be large only over a boundary layer region with width of order d near the edges $y = \pm W/2$, where the solution takes the form

$$\Omega(x, y \simeq \pm W/2) \simeq \Omega(\pm W/2) e^{ikx} e^{-\lambda|y \mp W/2|}. \tag{3.91}$$

The vector potential ζ has a similar solution, so that last two terms in Eq. (3.88) cancel. This leaves for the scalar potential S

$$\nabla_\perp \left(D\nabla_\perp^2 (S - \bar{u}_z) - \kappa^2 \mu d S \right) = 0, \tag{3.92}$$

which immediately gives

$$D\nabla_\perp^2 S - \kappa^2 \mu d S = D\nabla_\perp^2 \bar{u}_z. \tag{3.93}$$

(We are only interested in $\nabla_\perp S$ and so do not need to keep track of the arbitrary gradient-free function that could be added to this equation.)

The equation of motion for the vertical displacement is [27]

$$\kappa^2 \mu d \nabla_\perp^2 S = -\rho d \omega^2 \bar{u}_z. \tag{3.94}$$

Together Eqs. (3.93, 3.94) give

$$\rho d \omega^2 (\bar{u}_z - \frac{D}{\kappa^2 \mu d} \nabla_\perp^2 \bar{u}_z) = D\nabla_\perp^4 \bar{u}_z. \tag{3.95}$$

This is the usual fourth order wave equation, with a small correction term of order $(d/W)^2$ (the second term in the brackets on the left hand side). Note that solutions to this equation vary on the long scale of order k^{-1} or W, and not the small scale

$\lambda^{-1} \sim d$, so that to a good approximation we have

$$\rho d\omega^2 \bar{u}_z = D\nabla_\perp^4 \bar{u}_z, \tag{3.96}$$

$$S = -\frac{D}{\kappa^2 \mu d}\nabla_\perp^2 \bar{u}_z. \tag{3.97}$$

The first equation is now the standard fourth order wave equation. The second equation for S shows it to be small compared with $\bar{u}_z$ by of order $(d/W)^2$.

The boundary conditions at the edges are that all stresses are zero, so that in particular at $y = \pm W/2$

$$\int dz T_{zy} = \kappa^2 \mu d(\partial_y \bar{u}_z + \psi_y) = 0. \tag{3.98}$$

Substituting Eq. (3.85) into this gives

$$\partial_y S - \partial_x \zeta = 0. \tag{3.99}$$

Equation (3.99) together with Eq. (3.97) tells us the size of the ζ correction, which at $y = \pm W/2$ takes the value

$$\zeta(x, y = \pm W/2) = -\frac{D}{\kappa^2 \mu d}\frac{1}{ik}\left(\partial_y \nabla_\perp^2 \bar{u}_z\right)\big|_{y=\pm W/2}. \tag{3.100}$$

This expression can be simplified using the boundary condition $T_{yy} = 0$ at $y = \pm W/2$, which from Eq. (3.77) and Eqs. (3.80, 3.81) gives at $y = \pm W/2$

$$\partial_y^2 \bar{u}_z = -\sigma \partial_x^2 \bar{u}_z = \sigma k^2 \bar{u}_z, \tag{3.101}$$

so that

$$\zeta(x, y = \pm W/2) = -\frac{ikD(1-\sigma)}{\kappa^2 \mu d}\left(\partial_y \bar{u}_z\right)\big|_{y=\pm W/2}. \tag{3.102}$$

The potential ζ is only large in the boundary layers near the edges where it takes the form

$$\zeta(x, y \simeq \pm W/2) = -\frac{ikD(1-\sigma)}{\kappa^2 \mu d}\left(\partial_y \bar{u}_z\right)\big|_{y=\pm W/2} e^{-\lambda|y \mp W/2|}. \tag{3.103}$$

Thus finally we have expressions for the horizontal displacement field, Eqs. (3.85, 3.83) together with Eqs. (3.97, 3.103) defining S and ζ, and Eq. (3.86). These can be used to calculate the additional contribution to the energy flux coming from the T_{zx} term in Eq. (3.74). (The corrections to u_x and u_y derived here do not change the contributions from the first two terms in Eq. (3.74) to the order we require, since these terms are already third order in the small parameter d/W.)

We therefore need to evaluate

$$\int\int T_{zx} u_z^* dy dz \simeq \kappa^2 \mu d \int dy (\partial_x S + \partial_y \zeta)\bar{u}_z^*. \tag{3.104}$$

Both terms in the integral give contributions at the same order. The first term, coming from the correction to the in-plane strain Eq. (3.97), is

$$\kappa^2 \mu d \int dy (\partial_x S)\, \bar{u}_z^* = -D \int (\partial_x \nabla_\perp^2 \bar{u}_z)\bar{u}_z^*\, dy. \tag{3.105}$$

The second term in the integrand is only large in the boundary layer region near the edges and from Eq. (3.102) evaluates to the edge contributions

$$\kappa^2 \mu d \int dy\, (\partial_y \zeta)\, \bar{u}_z^* = -ikD(1-\sigma)\, [(\partial_y \bar{u}_z)\bar{u}_z^*]|_{y=-W/2}^{y=W/2}\,. \tag{3.106}$$

Combining these expressions for Eq. (3.104) with Eq. (3.79) together with Eqs. (3.80, 3.81) yields the final expression

$$P \simeq \frac{\omega k D}{2}\,\mathrm{Re}\left\{\int dy \left[2k^2 \bar{u}_z \bar{u}_z^* + (1-\sigma)\,(\partial_y \bar{u}_z)\,(\partial_y \bar{u}_z)^* - (1+\sigma)\left(\partial_y^2 \bar{u}_z\right)\bar{u}_z^*\right] + \left[(1-\sigma)\,(\partial_y \bar{u}_z)\,\bar{u}_z^*\right]_{y=-W/2}^{y=W/2}\right\}, \tag{3.107}$$

which is identical to Eq. (3.113).

An alternative approach to calculate the energy flux is to use the expression for the energy of distortions of the plate evaluated using the lowest order expressions

Eqs. (3.76, 3.77, 3.80, and 3.81) [25]

$$F = \frac{1}{2} D \int \int \left[\left(\nabla_\perp^2 \bar{u}_z \right)^2 + 2(1-\sigma) \left\{ \left(\frac{\partial^2 \bar{u}_z}{\partial x \partial y} \right)^2 - \frac{\partial^2 \bar{u}_z}{\partial x^2} \frac{\partial^2 \bar{u}_z}{\partial y^2} \right\} \right] dxdy. \tag{3.108}$$

It turns out that the higher order corrections discussed above are not needed in this expression, and so we can derive the energy flux without these difficulties. The functional derivative of F with respect to $\bar{u}_z$ yields the vertical force per unit area in the interior of the plate, which can be used to derive the fourth order wave equation, as well as expressions for the energy flux into the plate across the boundaries. The latter expressions give us the result for the energy flux along the beam

$$P = \frac{1}{2} \mathrm{Re} \left\{ -i\omega \left[\int M_x \theta_x^* + V \bar{u}_z^* \, dy + \left(F_c \bar{u}_z^* |_{y=W/2} + F_c \bar{u}_z^* |_{y=-W/2} \right) \right] \right\}, \tag{3.109}$$

where

$$V = -D \partial_x [\partial_x^2 \bar{u}_z + (2-\sigma) \, \partial_y^2 \bar{u}_z] \tag{3.110}$$

is the effective vertical force that couples to the vertical displacement $\bar{u}_z$,

$$M_x = -D \left(\partial_x^2 \bar{u}_z + \sigma \partial_y^2 \bar{u}_z \right) \tag{3.111}$$

is the torque that couples to the angular displacement $\theta_x = \partial \bar{u}_z / \partial x$, and

$$F_c(y = \pm W/2) = \pm \, 2D(1-\sigma) \partial_{xy}^2 \bar{u}_z \big|_{y=\pm W/2} \tag{3.112}$$

is a vertical force localized at the edges of the plate. This force does not appear in a simple elasticity theory and the key equation to the correct calculation.

Substituting Eqs. (3.110-3.112) into Eq. (3.109) gives

$$\begin{aligned} P \simeq \frac{1}{2} \omega D \, \mathrm{Re} \Bigg\{ \int dy \left[2k^3 \bar{u}_z \bar{u}_z^* + k(1-\sigma)(\partial_y \bar{u}_z) \partial_y \bar{u}_z^* - k(1+\sigma)(\partial_y^2 \bar{u}_z) \bar{u}_z^* \right] \\ + Dk \left[(1-\sigma)(\partial_y \bar{u}_z) \bar{u}_z^* \right]_{y=\frac{W}{2}} - Dk \left[(1-\sigma)(\partial_y \bar{u}_z) \bar{u}_z^* \right]_{y=-\frac{W}{2}} \Bigg\}. \end{aligned} \tag{3.113}$$

Evaluating $\partial_x = ik$, and using integration by parts, we again get Eq. (3.107). The comparison of the group velocity derived from Eq. (3.113) and from numerically differentiating the dispersion curve now shows agreement to high accuracy.

3.4 Scattering analysis

The thermal attenuation is calculated from Eq. (3.72) for normalized mode displacement fields or Eq. (3.73) in general. The group velocity for each mode can be accurately evaluated numerically from the equality $v_g = 2P/\rho w^2$, with the energy flux P given by Eq. (3.79) for the in plane modes and Eq. (3.113) for the flexural modes (both expressions are for normalized displacement fields). These are all explicit results in terms of the mode displacements, which are given by Eqs. (3.54-3.57) for the in-plane modes, and Eqs. (3.62, 3.63) for the flexural modes.

Combining the interaction term, the power term, and the attenuation term, we have

$$\gamma_m = \sum_n \frac{\omega^2 \tilde{g}(k_m - k_n)}{8 P_n P_m} \left| \int_{-\frac{d}{2}}^{\frac{d}{2}} dz' \, \Gamma^{(m,n)}\big|_{y=\frac{W}{2}} \right|^2 , \tag{3.114}$$

where

$$\Gamma^{(m,n)}\big|_{y=\frac{W}{2}} = \left[\left(\rho\omega^2 - E k_s k_n \right) u_x^{(s)} u_x^{(n)*} + \rho\omega^2 u_y^{(s)} u_y^{(n)*} + \rho\omega^2 u_z^{(s)} u_z^{(n)*} \right]_{y=\frac{W}{2}} , \tag{3.115}$$

$$\begin{aligned} P_n^{\text{in-plane}} = -i\omega \Bigg[& \int\int dydz \frac{E}{(1-\sigma^2)} \left[\partial_x u_x^{(n)} + \sigma \partial_y u_y^{(n)} \right] u_x^* \\ & + \int\int dydz \frac{E}{2(1+\sigma)} \left(\partial_x u_y^{(n)} u_y^{(n)*} + \partial_y u_x^{(n)} u_y^{(n)*} \right) \Bigg] , \end{aligned} \tag{3.116}$$

$$\begin{aligned} P_n^{\text{flexural}} = \frac{\omega}{2} \Bigg[& D \int dy \left[2k^3 w w^* + k(1-\sigma)(\partial_y w)(\partial_y w)^* - k(1+\sigma)\partial_y^2 w w^* \right] \\ & + Dk \left[(1-\sigma)(\partial_y w) w^* \right]_{y=\frac{W}{2}} \Bigg] . \end{aligned} \tag{3.117}$$

Now the above expressions can be evaluated easily once the displacement field is known, which is followed next.

Before analysing the scattering behaviour, we first need to have a good understanding of the dispersion relation of the modes, since the scattering rates are strongly

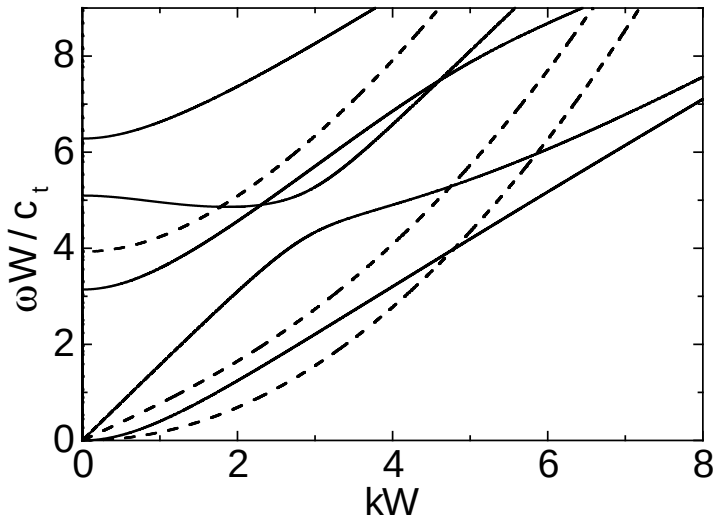

Figure 3.2: Dispersion relation for in-plane modes (solid) and flexural modes (dashed) for a geometry ratio $d/W = 0.375$ and Poisson ration 0.24. The wave numbers are scaled with the width W, and the frequencies by W/c_t with $c_t = \sqrt{\mu/\rho}$.

dependent on this.

3.4.1 Dispersion relation and group velocity

The dispersion relations for a representative case are shown in Fig. 3.2. For this example we have used a Poisson ratio of 0.24, and a depth to width ratio of $d/W = 0.375$, values corresponding to the experimental work of Schwab *et al.* [8]. As we have discussed, the modes fall into four classes, depending on their parity signatures. We label the lowest mode from each class, the one with zero frequency as the wave number goes to zero, as mode 0, and the modes with successively higher cutoff frequencies in each class as mode 1, mode 2, etc., in that class.

Notice that one of the curves in the figure, the one for the in-plane mode with cutoff frequency $\omega W/c_t \simeq 5$, shows anomalous dispersion with the frequency *decreasing* as the wave number increases up to about $3W^{-1}$. (This is actually an even mode, and some higher even and odd modes also show anomalous dispersion.) The dispersion curves for all modes $n > 0$ have zero slope, and so zero group velocity, at onset. As we

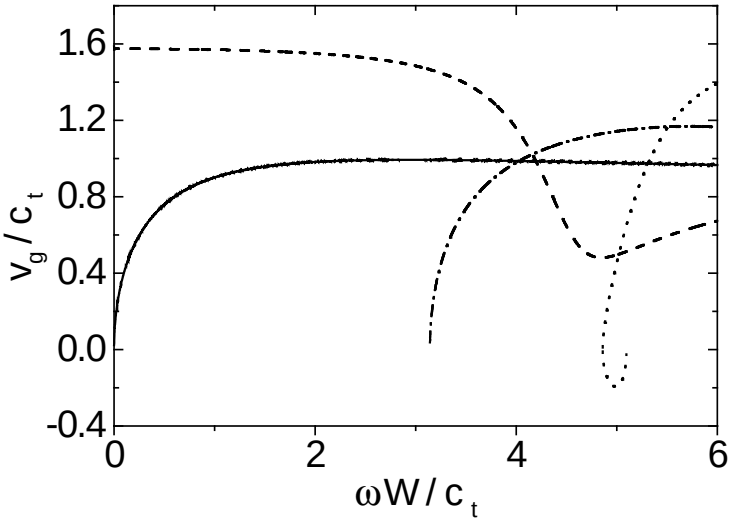

Figure 3.3: Group velocity for in-plane modes for the same parameters as Fig. (3.2): dash dotted line represents in-plane bending mode, solid line represents compression mode. The wave numbers are scaled with the width W, and the group velocities by c_t with $c_t = \sqrt{\mu/\rho}$.

will see later, this results in a diverging scattering rate at each mode onset. For the $n = 0$ modes, as $\omega \to 0$ two of the modes (the compression and torsion modes) have linear dispersion, whilst the other two lowest modes (in-plane and flexural bending modes) exhibit quadratic dispersion. Figure 3.3 shows the group velocities v_g for the four lowest in-plane modes. The group velocity of the bending mode approaches zero as $\omega \to 0$ whilst that of the compression mode becomes constant. The group velocity of the compression mode suddenly drops to $\sim 0.5c_t$ around $\omega W/c_t \sim 4.6$, then gradually recovers and approaches $0.9c_t$. These features of the dispersion curve will be reflected in the behaviour of the scattering of the waves.

3.4.2 Scattering behaviour

We first consider the scattering and reduction of the thermal transport by white noise roughness $\tilde{g}(k) = \tilde{g}(0)$. This allows us to focus on the role of geometry and the unusual mode structure of the elastic waves in the physics.

	$\omega/\sqrt{E/\rho}$	$v_g/\sqrt{E/\rho}$	ϕ_x	ϕ_y	ϕ_z
Extension	k	1	1	$O(ky)$	$O(kz)$
In-plane bend	$(w/\sqrt{12})k^2$	$(w/\sqrt{3})k$	$-iky$	1	$O(kz)$
Torsion	$\sqrt{2/(1+\sigma)}(d/w)k$	$\sqrt{2/(1+\sigma)}(d/w)$	$O(kyz)$	$-z$	y
Flex-bend	$(d/\sqrt{12})k^2$	$(d/\sqrt{3})k$	$-ikz$	$O(k^2yz)$	1

Table 3.1: Dispersion relation, group velocity, and (unnormalized) transverse mode structure for the four modes with zero frequency at zero wave vector.

in-plane			flexural		
cc	bb	bc,cb	tt	bb	tb,bt
$2\bar{\omega}^2$	$\sqrt{3}\bar{\omega}$	$\frac{3^{5/4}}{2^{3/2}}\bar{\omega}^{3/2}$	$\frac{9(1+\sigma)}{4}\left(\frac{W\bar{\omega}}{d}\right)^2$	$\mathrm{O}\left[\left(\frac{W\bar{\omega}}{d}\right)^3\right]$	$\frac{3^{5/4}(1+\sigma)^{1/2}}{4}\left(\frac{W\bar{\omega}}{d}\right)^{3/2}$

Table 3.2: Scattering coefficients for the zero onset frequency modes at low frequencies: c denotes compression, b denotes bend, t denotes torsion, bb denotes bend to bend scattering etc. Values are quoted for $\gamma_m W^4/\tilde{g}(0)$ as a function of scaled frequency $\bar{\omega} = \omega c_E/W$. For the flexural bend to bend scattering (bb) the terms in the braces in Eq. (3.72) cancel to leading order resulting in very small $O(\bar{\omega}^3)$ scattering. There is no scattering between in-plane and flexural modes for the z-independent roughness assumed.

In the low frequency limit the dispersion curve and the spatial dependence of the modes take on the simple analytic forms shown in Table 3.1, allowing us to make analytic predictions for the scattering at low frequencies, and then the thermal conductance at low temperatures. Since only small wave vector scattering is involved in these calculations, the results are true for a general roughness correlation function, providing $\tilde{g}(0)$ is nonzero. The mode structure in Table 3.1 may be calculated from Eqs. (3.54-3.63) taking $k \to 0$ or from arguments of macroscopic elasticity theory.

The contributions to the thermal attenuation coefficient in the low frequency limit ($\omega W/c_t \ll 1$) from the various scattering processes are shown in the Table 3.2 [4]. The expressions take on their simplest form if we introduce the frequency scaled with the velocity of the long wavelength compression mode $\bar{\omega} = \omega c_E/W$ with $c_E = \sqrt{E/\rho} = \sqrt{2(1+\sigma)}c_t$. The power laws can largely be understood from the pre-

[4] A more accurate expression for the scattering between the in-plane compression and bending modes is giving by keeping the next order term in $\bar{\omega}$ which is $O(\bar{\omega}^{1/2})$ for this scattering process. To include this correction multiply the expression in the table by $(1+\sqrt{\bar{\omega}}/12^{1/4})^2$.

factor in Eq. (3.73), $\gamma_{n,m} \propto \omega^2/v_g^{(m)}v_g^{(n)}$. The group velocity v_g becomes a constant at small frequencies for the compression and torsion modes. Thus the torsion-torsion and compression-compression scattering shows the ω^2 dependence corresponding to Rayleigh scattering in one dimension, and as was found for scalar waves with linear dispersion. On the other hand for the bending modes $v_g \propto \omega^{1/2}$. This has the important consequence that the in-plane bend-bend scattering increases more rapidly at low frequencies proportional to ω, and the torsion-bend and compression-bend scattering have an $\omega^{3/2}$ frequency dependence. For the flexural bend-bend scattering the two terms in the braces in Eq. (3.72) cancel to leading order resulting in smaller scattering $O(\omega^3)$ than given by the pre-factor alone. Note that the expressions for the flexural modes involve additional factors of W/d, so that these modes will be scattered more strongly at a given ω in the thin plate limit. This is because these modes are softer, so that the scattering wave vectors are larger for the same frequency.

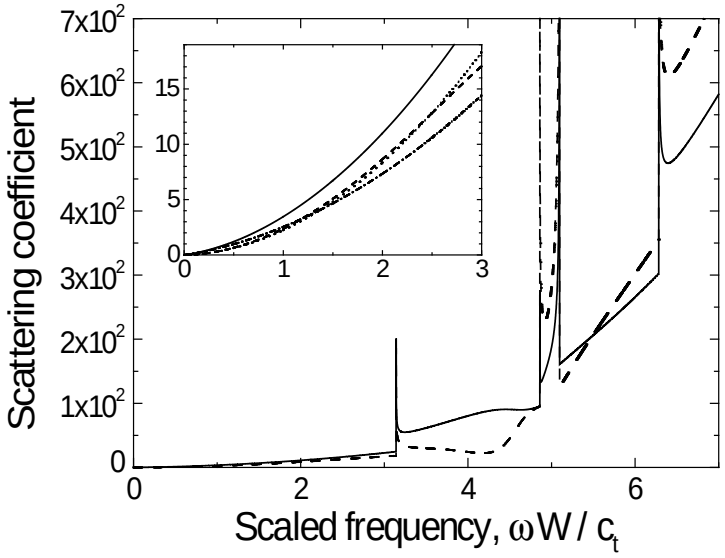

Figure 3.4: Attenuation coefficient $\gamma_m W^4/\tilde{g}(0)$ for scattering from the two lowest $m = 0$ inplane modes to any other mode as a function of scaled frequency $\omega W/c_t$: solid line–inplane bend mode; dashed line–compression mode. The insert shows an enlargement of the low frequency region, and compares with the analytic low frequency expressions from Table 3.2: dotted line–analytic in-plane bend mode; dash-dotted line–analytic compression mode; other lines as in the main figure.

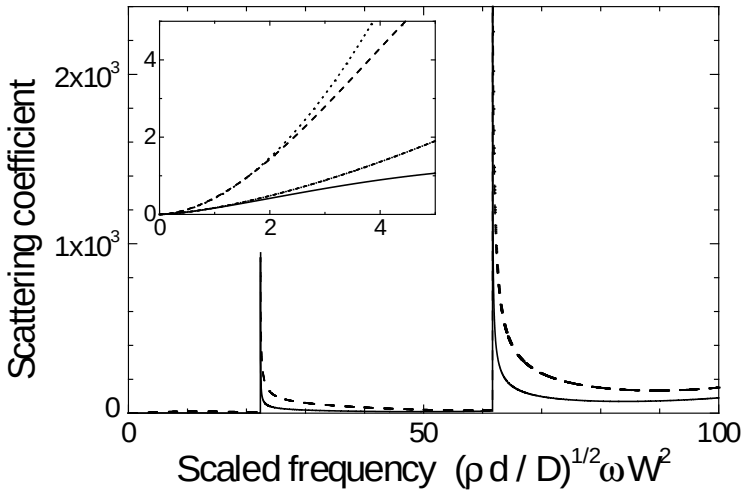

Figure 3.5: Attenuation coefficient $\gamma_m W^4/\tilde{g}(0)$ for scattering from the two lowest $m = 0$ flex modes to any other mode as a function of scaled frequency $\omega\sqrt{12(1-\sigma^2)}(W/d)W/c_E$: solid line–the flex-bend mode; dashed line–torsion mode. The insert shows an enlargement of the low frequency region, and compares with the analytic low frequency expressions from Table 3.2: dotted line–analytic approximation for the flex-bend mode; dash-dotted line–analytic expression for the torsion mode; other lines as in the main figure.

Numerical results for the attenuation coefficient γ_m of the four lowest modes are shown in Fig. 3.4 for the in-plane and Fig. 3.5 for the flexural modes. The plot for the in-plane modes in particular shows interesting structure deriving from the complicated dispersion curves of Fig. 3.2. Much of this structure can be understood from the product of group velocities in the denominator of Eq. (3.72). In particular there is a square root divergence in γ_m at the onset frequency of each mode where the group velocity is zero. In addition, the large scattering around $\omega W/c_t = 5$ derives from the region of anomalous dispersion, since the group velocity is small in this frequency range. The insert to Fig. 3.4 shows an expanded view of the low frequency behaviour, using the results from Table 3.2 together with the next order correction for the compression-bend scattering. The agreement for the compression mode is very good even up to $\omega W/c_t \sim 3$, whereas for the bend mode the correspondence is only good for $\omega W/c_t \lesssim 0.5$. The scattering for the flexural modes shows generally

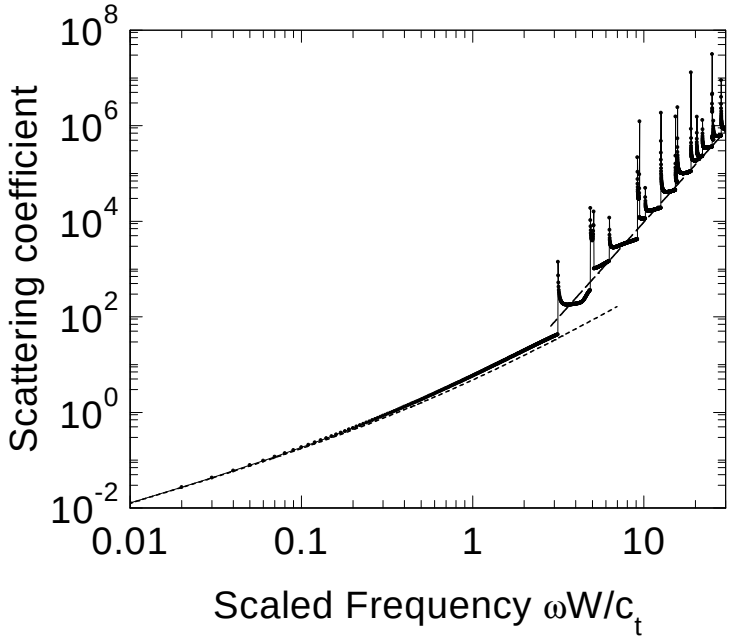

Figure 3.6: Total scattering $\sum_m \gamma_m W^4/\tilde{g}(0)$ for the in-plane modes on a log-log plot. The dotted line shows the low frequency analytic expression from Table 3.2, and the dashed line shows a power law 4. (Note that the heights of the peaks in the plot are not significant, depending on how close the individual points, separated by 0.01 in $\omega W/c_t$, used in constructing the plot are to the mode onset frequencies where the scattering diverges.)

similar results, Fig. 3.5 although the behaviour is simpler corresponding to the rather featureless dispersion curves. At low frequencies, (insert to Fig. 3.5), the scattering of the flexural-bend mode is small, since the intra-mode scattering is reduced by the cancellation discussed above.

Figure 3.6 shows the total scattering $\sum_m \gamma_m$ for the in-plane modes on a log-log plot, again with white noise roughness. At very low frequencies the scattering varies proportional to ω corresponding to the dominant intra-mode scattering of the compression mode at low frequencies (Table 3.2). For frequencies up to $\omega W/c_t \simeq 3.5$, the first nonzero onset frequency of an in-plane mode, the analytic low-frequency expression given by summing the in-scattering expressions from Table 3.2 (cc, cb, bc, and bb), shown as the dotted line in Fig. 3.6, gives a good approximation to the

full results. At higher frequencies the total scattering increases rapidly, following a general trend proportional to ω^4 (dashed line) together with divergent scattering at each mode onset frequency. The ω^4 power law can be understood as the combination of the explicit ω^2 dependence of Eq. (3.72), together with two powers of ω coming from the number of modes available for scattering from and to.

3.4.3 Change in the thermal conductance

In the weak scattering limit the change in thermal conductance at low temperatures can be derived directly from the expressions for the scattering at low frequencies. If we write the thermal attenuation coefficient of mode m as $\gamma_m L = A(\omega/\omega_0)^p$, where p is the power law obtained in the low frequency limit and ω_0 some characteristic frequency, then the corresponding contribution of the suppression of the thermal conductance from this mode is

$$\delta K_m/K_u = AI_p(T/T_E)^p \tag{3.118}$$

with $T_E = \hbar c_E/k_B W$ the corresponding characteristic temperature for the in-plane mode and $K_u = \pi^2 k_B^2 T/3h$ the universal thermal conductance. The constant I_p can be obtained evaluating the integral

$$I_p = \frac{3}{\pi^2}\int_0^\infty dy \frac{y^{p+2}e^y}{(e^y-1)^2}. \tag{3.119}$$

Thus the power law for the temperature dependence of the depression of the thermal conductivity is the same as the one for the low frequency behaviour of the scattering coefficient.

Figures 3.7 and 3.8 show the thermal conductance depression scaled with the universal value K_u as a function of the appropriate scaled temperature for the lowest in-plane and flexural modes, showing the deviation from the low temperature power laws as the temperature is raised. For the in-plane modes we use the characteristic temperature $T_E = \hbar c_E/k_B W$ and for the flexural modes $T_F = \hbar c_E d/k_B W^2$. The

individual plots are then independent of the geometry. To combine the contributions from the in-plane and flexural modes the ratio d/W is needed to relate the two temperature scale factors. In the thin plate limit $T_F = (d/W)T_E \ll T_E$.

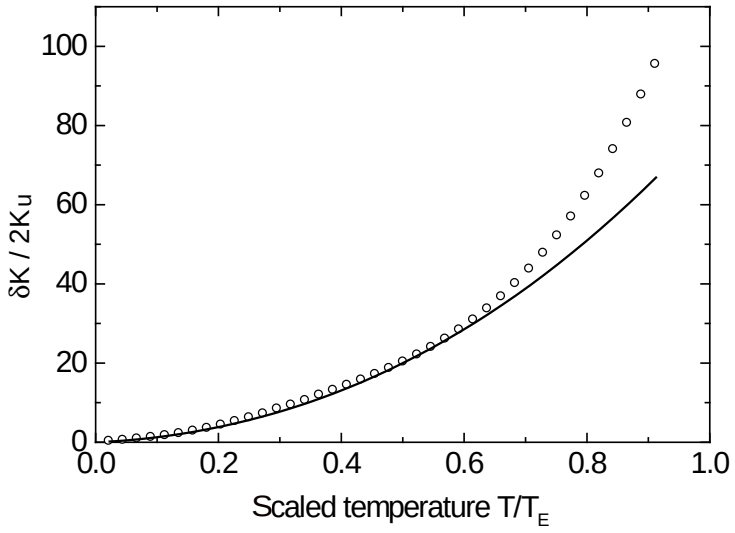

Figure 3.7: Reduction in the thermal conductance scaled with the universal conductance K_u for the lowest in-plane modes as a function of scaled temperature T/T_E with $T_E = \hbar c_E/k_B W$: solid line–low temperature analytical expressions from Table 3.2: points–full expression evaluated numerically. The quantity plotted is $(\delta K_c + \delta K_{ib})/2K_u$ with $\delta K_c, \delta K_{ib}$ the depression of the contributions to the conductance by the scattering for the compression and in-plane bending modes.

3.5 Comparison with the experiment of Schwab *et al.*

3.5.1 Experimental geometry

Based on the SEM micrograph of the experimental structure [24], we set the dimensions of the structure in the following way. In the experimental structure of Schwab *et al.* the thermal pathway was constructed with the shape function $W(x) = W\cosh(Ax)$, so that the beam width becomes large and joins smoothly to the ther-

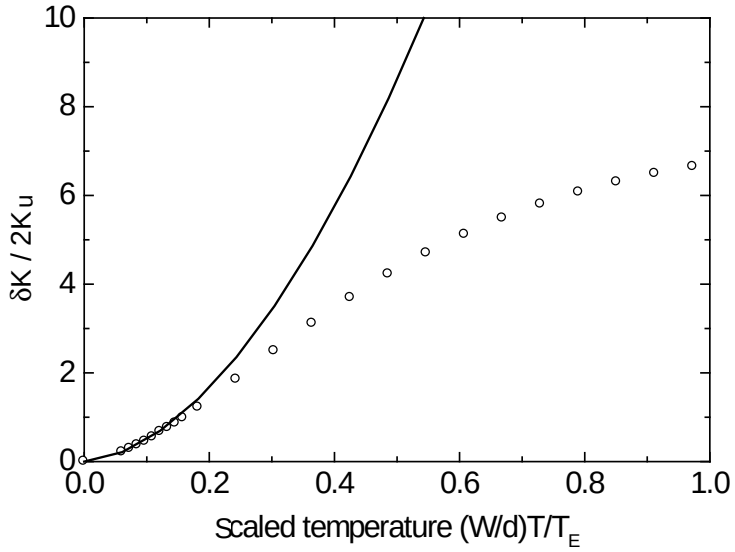

Figure 3.8: Similar to Fig. (3.7), $\delta K/2K_u$ for the lowest flexural modes (torsion and flexural-bending) as a function of the scaled temperature T/T_F with $T_F = \hbar c_E d/k_B W^2$.

mal reservoirs at the ends, reducing the scattering due to the geometric imperfection at these junctions. Unfortunately this makes the calculation of the behaviour of the elastic waves in the beams much harder. However both with and without the scattering off surface roughness, we expect the narrow portion of the beam to dominate the behaviour. Thus we simplify the structure and model it as an elastic beam with rectangular cross section of width W, depth d, and effective length L. We estimate the width as the narrowest width of the structure, $W \simeq 160$ nm, and $L = 1$ μm as the length over which the width is approximately constant. The thickness of the material was $d = 60$ nm. The accuracy of the length estimation is not very critical, since the only length dependence in the scattering rate γ appears in the combination $\delta^2 L$ where δ is the rms roughness which is a parameter of the model, so that any error in the assignment of L will just change the value assigned to δ. The width W on the other hand plays a crucial role, for example determining the frequency cutoffs of the various modes, and so the temperature dependence of the thermal conductivity.

3.5.2 Roughness correlation function

Since the nature of the surface roughness on the experimental structure is not known, to fit the experimental data we need a sensible parametrization of the roughness. As a starting point we choose a Gaussian correlation function for the roughness as we did for the scalar model, leading to the spectral density

$$\tilde{g}\left(k\right) = \sqrt{\pi} a \delta^2 \exp\left[-\frac{a^2}{4}k^2\right]. \tag{3.120}$$

This parametrization of the roughness contains two parameters: δ the rms roughness and a the correlation length.

To analyse the data, we first quantify the amount of scattering by subtracting the data of Schwab *et al.* from the ideal thermal conductance obtained numerically using the "xyz" algorithm [9]. Then we attempt to fit the data by adjusting the two parameters a and $\delta^2 L$.

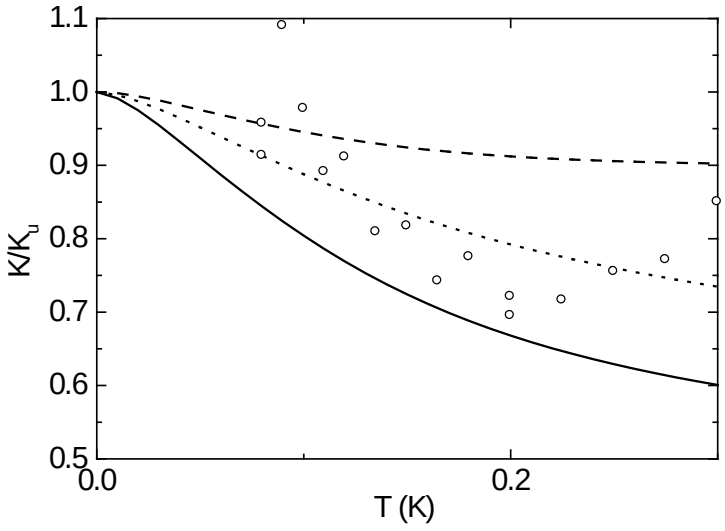

Figure 3.9: Attempts to fit the low temperature data $T \lesssim 0.2$ K using various values of $a\delta^2$: solid line–$\sqrt{\pi}a\delta^2 = 0.1$; dotted line–$\sqrt{\pi}a\delta^2 = 0.05$; dashed line–$\sqrt{\pi}a\delta^2 = 0.02$; open circles–from the experimental data of Schwab *et al.*

The inadequacy of Eq. (3.120) in fitting the experimental data is shown by the

low temperature fits in Fig. 3.9. At these low temperatures only small wave number modes are excited, so that the exponential term in Eq. (3.120) can be approximated as unity and $\tilde{g}(k) \simeq \tilde{g}(0) = \sqrt{\pi} a\delta^2$. Thus the roughness parameters only appear in the combination $a\delta^2$, and this quantity can be varied to attempt to fit the low temperature region. As seen from the figure, increasing $a\delta^2$ causes scattering that is systematically larger than the experimental data at the low temperatures, while decreasing $a\delta^2$ does not provide enough scattering in the range $0.1 < T < 0.2$ K.

Although there is considerable scatter in the data over the range of the fit, the systematic differences between the predictions and the data lead us to propose a modified form of the roughness correlation that reduces the scattering at small wave numbers

$$\tilde{g}(k) = \sqrt{\pi} a\delta^2 \exp\left[-\frac{a^2 (k - k_0)^2}{4}\right]. \tag{3.121}$$

A nonzero value of the parameter k_0 leads to a roughness correlation function that is maximum at a length scale of order k_0^{-1}, and serves to reduce the scattering at long wavelengths. As mentioned before, the same discrepancy (i.e., the overestimation of the scattering at long wavelengths in the theory compared with experiment) was found using the scalar model of the elastic waves [11]. The full elasticity theory considered here actually makes the discrepancy worse, since the scattering at small frequencies now is predicted to increase more rapidly at small frequencies than the ω^2 found in the scalar theory, varying as ω^p with $p < 2$ for most of the scattering processes, see Table 3.2.

To fit the data of Schwab *et al.*, we need to determine three parameters: k_0 , a, and δ. We evaluate the quality of the fit by calculating the mean square deviation of the data from the theory curve over the temperature range up to $0.4K$. At higher temperatures many modes becoming excited, and the scattering of individual modes becomes strong, so that our theory is less reliable. Since the onset frequency of the scattering at low frequencies, and the initial decrease in thermal conductance with increasing temperature near the onset, are mainly determined by k_0, this parameter is the easiest to determine. We find the value $k_0 W = 4.9$, rather insensitive to the

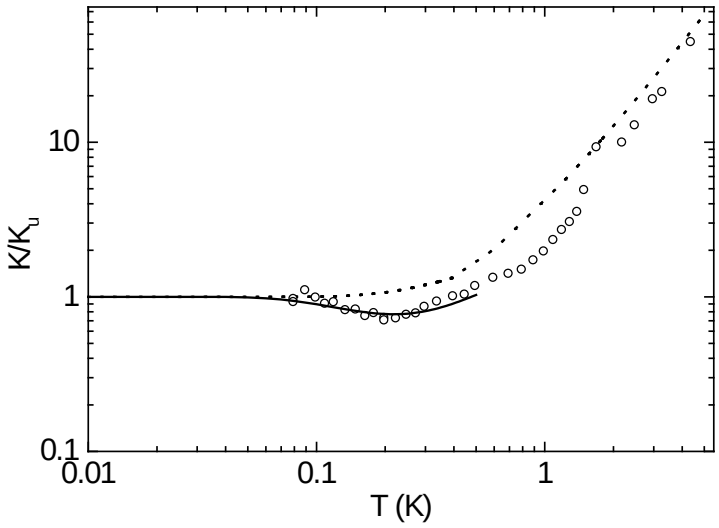

Figure 3.10: Thermal conductance per mode scaled with universal value K_u: solid line–fit using roughness parameters $a/W = 5.5$, $\delta/W = 0.2$, and $k_0 W = 4.9$; circles–data of Schwab *et al.* The dotted line shows the ideal value with no scattering.

values of a and δ.

We have done a systematic investigation of the error. A plot of the error as a function of δ and a shows that the fit parameters δ and a are strongly correlated. This is presumably because an increase in a, which reduces the scattering at small wave numbers and frequencies that is important at low temperatures, can be compensated by an increase in δ. If we fix $k_0 W$ at 4.9, then using the standard χ^2 estimate for the confidence level [28] of the fitted values of δ and a, leads to values of δ, a at a 68.3% confidence level covering ranges as wide as $2 < a/W < 8$ and $0.1 < \delta/W < 0.5$ (and we have not looked at larger values of the parameters). However, as the two fit parameters are correlated, fixing one parameter gives a much tighter constraint on the second one. For example: once δ is fixed at $\delta/W = 0.1$ the 93% confidence limit gives $3 < a/W < 4$; for $\delta/W = 0.25$ gives $5.5 < a/W < 7.6$; and for $\delta/W = 0.4$ gives $6.4 < a/W < 8.4$. Since the values of δ and a are not well determined separately, we use the knowledge of the experimental geometry to constrain the parameters further. The physical roughness due to chemical etch has been estimated [24] from the SEM

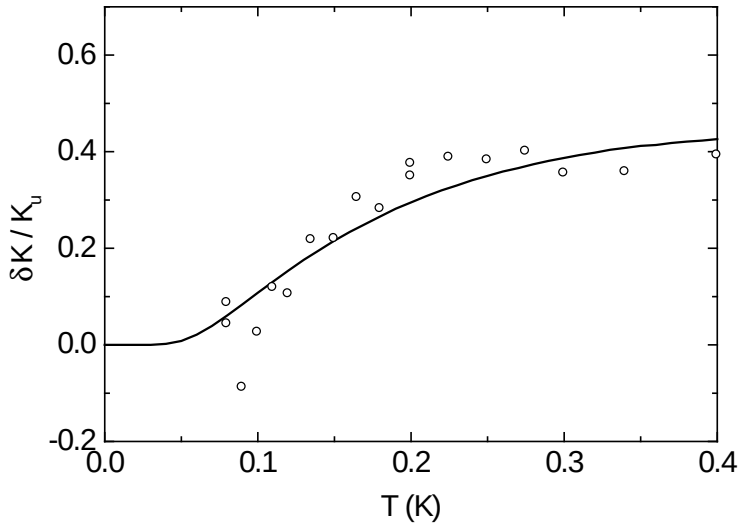

Figure 3.11: Same as in Fig. 3.10 but showing the decrease of K/K_u from the ideal value.

micrograph to be about $\delta/W = 0.2$. The best fit value of a for this value of δ/W is $a/W = 5.5$, and we use these values, together with $k_0 W = 4.9$, to obtain the fit shown in Figs. 3.10 and 3.11. For quantitative estimate of the error in the fit that we are using, we have calculated χ^2 and attempted to optimise the parameters. As a result, the fit is significantly better than the one in Ref. [19] where we have used visual inspection for the fit.

A difficulty of fitting the data is the lack of data points at very low temperatures: it is in this range where only a few modes are involved that we have a very good understanding of the scattering. At higher temperatures many more modes become involved, and the scattering of individual modes becomes strong, so that the second-order approximation used in calculating the scattering will not be good. A full test of the theory explaining the reduction in the thermal conductance in terms of the scattering off surface roughness requires more data below a temperature of about 0.08 K for the type of geometry used by Schwab *et al.*, or systems with smaller geometries where the effects can be measured at higher temperatures.

3.5.3 Individual mode contribution to the thermal conductance

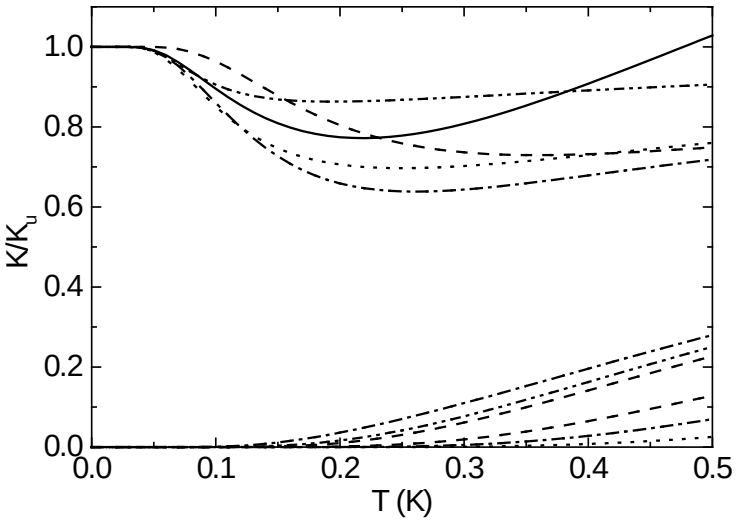

Figure 3.12: Individual mode contribution to the thermal conductance. The lowest two flex modes and lowest three in plane modes are shown. The contributions to K/K_u from the four modes with zero onset frequency tend to unity at low temperatures. The higher modes only contribute at higher temperature. The modes are: dash-dotted–in-plane bending; dashed–compression; dotted–torsion; dashed-dotted-dot–out-of plane bending. The solid line shows the sum of all the mode contributions, reduced by $4K_u$. Values of the roughness parameters used were $a/W = 5.5$, $\delta/W = 0.2$, $k_0W = 4.9$, and $d/W = 0.375$.

It is interesting to investigate the contribution to the total thermal conductance of the individual modes with the roughness parameters used to fit the experimental data. This is shown in Fig. 3.12. The flex-bending mode shows a much smaller contribution to the reduction in K at low temperatures for the reason we have already discussed. The modes with nonzero onset frequencies start to contribute significantly above about $T \simeq 0.2$ K, and this is the predominant cause for the increase in thermal conductivity above this temperature, since the recovery of the thermal conductance for the lowest mode occurs very slowly.

Chapter 4

Conclusion to Part I

We have investigated the effect of surface roughness on the scattering of elastic waves in a rectangular beam or waveguide, and the resulting depression of the thermal conductance in the low temperature quantized limit. We have employed a Green function approach to calculate the reduced transmission of the elastic waves due to surface roughness and then have used Landauer's formula for the thermal conductance.

In Chapter 2 we used a 2-D scalar model and examined the effect of surface roughness on the scattering. At low temperatures, the conductance divided by the temperature is dominated by the lowest mode. The scattering of this mode reduces the conductance below the universal value with a quadratic dependence on temperature for low temperatures with an amplitude proportional to the combination of roughness parameters $a\delta^2$. As the temperature increases, higher modes begin to play a role and the scattering of the lowest modes is reduced, so that the conductance increases. We find that the effect of scattering is always significant, reducing the conductance below the ideal ballistic value over the whole temperature range we investigate $T < 1$ K. Considering the simplicity of our model our results agree well with the experiment of Schwab *et al.* However, there were small differences between the data of Schwab *et al.* data and our theoretical model at very low temperatures. Elastic waves in confined geometries have many unusual features and their dispersion relations are quite different from those for scalar waves. To investigate the scattering at long wavelengths in depth we needed a more accurate model.

Then in Chapter 3 we have moved onto a 3-D elastic model using a full elasticity

theory to analyse the low temperature behaviour of the scattering in detail. Our formulation is quite general, but to obtain concrete results we have specialized to the thin-plate limit, which should be a reasonable approximation for many mesoscopic experiments where the depth of the structures is fixed by the epitaxial growth, whilst the width is determined lithographically. The thin plate limit preserves the peculiar features of the elastic waves in the full elastic theory, namely, quadratic dispersion at long wavelengths for two of the low frequency modes, and regions of negative dispersion in the spectra. A robust result is that the asymptotic dependence of the scattering by unstructured roughness of the low frequency modes important in the low temperature universal thermal conductance depends on the structure of the modes and the dispersion relation, and is *not* the simple ω^2 dependence of Rayleigh scattering as found in the scalar approximation to the modes. We find different power laws for the various mode scattering processes that can be understood largely from the dispersion relations at: ω for intramode scattering for the in-plane bend mode (the flex-bend intramode scattering is anomalous because of a cancellation between leading order terms, and varies as ω^3); $\omega^{3/2}$ for scattering between the bend modes and the modes with linear dispersion (torsion and compression modes); and the usual ω^2 for the intramode scattering of the modes with linear dispersion.

Although the scatter in the data of Schwab *et al.* is considerable at low temperatures, the observations seem to show a delay in the onset of the depression scattering as the temperature is raised, beyond what can be fitted with our predictions for unstructured surface roughness. We tentatively resolve this delay by supposing that the surface roughness has a maximum amplitude at some nonzero length scale, which we parameterize by a shifted Gaussian correlation function. Due to the lack of data at low temperatures, a precise determination of the roughness parameters is not possible. However, we do obtain a fit to the data with parameters that look reasonable when compared with electron micrographs of the actual devices. Recently Yung, Schmit, and Cleland have measured thermal conductance of a mesoscopic rectangular beam at a temperature of 25 mK and found that scattering is important even at this low temperature [29].

Our results are based on second-order perturbation theory, and the thermal conductance is evaluated assuming the scattering over the length of the device is small. This is a good approximation at low temperatures, but the scattering becomes strong at higher temperatures, particularly for the new modes excited as the temperature is raised, which have a diverging scattering at onset due to the flat dispersion relation here. At higher temperatures multiple scattering and perhaps phonon localization will therefore become important. Kambili *et al.* [14] and Sanchez-Gil *et al.* [16] have numerically investigated the these effects in the simplified scalar wave approximation. It might be interesting in the future to consider this phenomenon using the more accurate elasticity treatment.

Part II

Quantum dynamics of phonons

Chapter 5

Introduction

Quantum mechanics tells us that the energy of an oscillator is quantised. However, an observation of quantum limited mechanical motion in macroscopic objects is not possible because the energy associated with individual phonons is much smaller than their thermal energy [30].

Advances in nanotechnology have enabled experimenters to build ever smaller mechanical oscillators with high resonance frequencies and quality factors [31]. As an individual phonon energy becomes comparable to or greater than $k_{\mathrm{B}}T$, quantum effects begin to appear and we can take advantage of the size effects towards the realization of various quantum phenomena.

Here, we are interested in observing quantum transitions amongst the Fock states of a mesoscopic mechanical oscillator. If we had a direct way to measure the energy eigenvalue of the system without influencing the system state transitions, we would see something like Fig. 5.1. However, this is not possible with any conventional measurement scheme. As a consequence, the so-called backaction due to a measurement will add a large error to a subsequent measurement. We propose an indirect measurement scheme which could extract the information of our interest. This is the subject of Part II.

It becomes very important to model the precise way that a quantum system interacts with any measuring apparatus as well as with the environment. Specifically, it is necessary to take into account the measurement backaction and to design the system-readout interaction so as to allow the best possible measurement of the desired

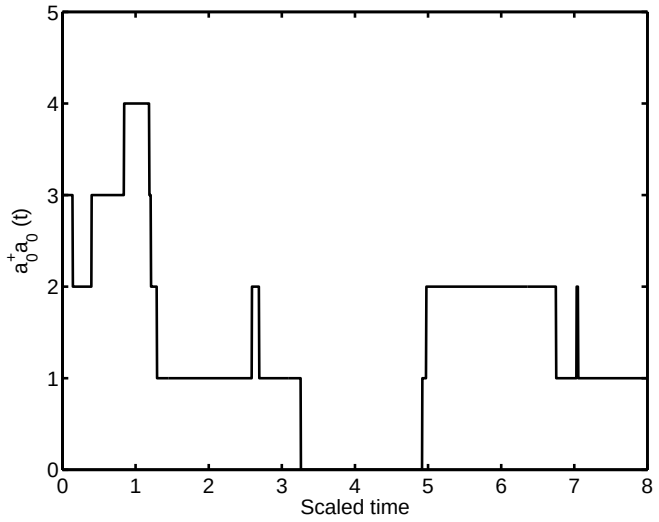

Figure 5.1: A sketch of $\left\langle a_0^\dagger a_0 \right\rangle (t)$ if we were able to observe the transitions of the mechanical oscillator states.

observable. In this part of the thesis we show that it is possible in principle to take advantage of the non-linear interaction between modes of oscillation of an elastic beam or beams to realize a quantum non-demolition measurement of the phonon number of the system oscillator. As a result, it is possible to track the state of the oscillator as it jumps between number states due to its coupling to the surrounding thermal environment.

The rules of quantum mechanics require that, even in the absence of instrumental or thermal noise, every measurement will in some way disturb the state of the measured system. The Hamiltonian interaction between the system and readout means that while information about the measured observable may be read out from the state of the readout, the quantum mechanical uncertainty in the conjugate observable of the readout leads to random changes in a measured observable of the system. This backaction noise on the conjugate observable is an inevitable result of the very interaction with the system that allows the measurement to take place. It has long been recognized that such backaction noise places a fundamental limit on the sensitivity of physical measurements [32]. However, the class of measurements known as quantum non-demolition (QND) measurements partially circumvent this problem by guaran-

teeing that the backaction noise does not affect the results of future measurements. In a QND measurement the interaction Hamiltonian between system and readout commutes with the internal Hamiltonian of the system: an ideal QND measurement is *repeatable* since the backaction noise does not affect the dynamics of the measured observable. In this paper, we are interested in a QND measurement of phonon number. The conjugate observable of number is phase, thus, the measurement backaction in our case will result in diffusion of the phase of the mechanical oscillations (we will see this phase diffusion explicitly when we derive an equation of motion for the system). However, our scheme allows the complete determination of the oscillator excitation level and thus projects the system onto a number state in the ideal limit.

Our proposed scheme for the QND measurement of phonon number uses two anharmonically coupled modes of oscillation of a mesoscopic elastic beam. The resonant frequencies of these two modes are very different. The higher frequency mode is the system to be measured, while the lower frequency serves as the readout system. The key idea of our scheme is that, from the point of view of the readout oscillator, the interaction with the system constitutes a shift in resonance frequency that is proportional to the time-averaged excitation of the system oscillator. This frequency shift may be detected as a change in the phase of the readout oscillation when driven on resonance. We show that our scheme realizes an ideal QND measurement of phonon number in an appropriate limit and discuss the physical readout regime that is necessary to achieve such a measurement.

5.1 A note on our approach

A description of a system interacting the surrounding environment can have four different levels. The first level is the wavefunction defining the whole universe. If such a description is possible, then the state of the universe is pure and we can evolve the Hamiltonian according to a Schrödinger equation of motion and will know everything about its dynamics. However, such a wavefunction is not known and the description of the dynamics at this level is impossible.

The second level is the density matrix description of the part of the universe of interest (this could be called the "whole system") limited by the lack of knowledge of the rest of the universe. At this level it is assumed that the system interacts arbitrarily weakly with the rest of the universe, and thus we could regard this whole system as completely isolated. Then the density matrix evolution is unitary and is given by the internal Hamiltonian. (Note in our case this "whole system" consists of the system of our real interest + secondary system used as a readout purpose + surrounding environment of importance which directly affects our measurement results, which is usually modelled as baths with each bath represents one aspect of the effects to the system).

The third level is integrating out the bath degrees of freedom. In practice, we trace out the bath degrees of freedom to describe the system's behaviour. Since the interaction of the system with the rest of the whole system is not arbitrarily weak, this can only be done in practice with certain approximations - in particular, we will use Markov and rotating wave approximations as well as perturbation and adiabatic elimination techniques. These processes lead to an evolution equation for the system density matrix (the master equation) that is not unitary. The master equation describes an ensemble of systems, *i.e.*, the distribution over the ensemble.

The final level of description introduces the stochastic elements due to measurements. We can describe an ensemble of systems each of which has the same measurement apparatus, *i.e.,* an ensemble of experiments. The stochastic element is introduced when we restrict our attention to a subset of the ensemble with a given measurement sequence and the stochastic terms arise precisely because the value of the measurement outcome is stochastic. The equation that is concerned with the restricted set of elements of the ensemble is called the stochastic master equation. Whilst the master equation describes the distribution over the whole ensemble including all the possible measurement outcomes, the stochastic master equation describes the distribution "conditioned on" the particular measurement outcome.

Based on the concept described above, we proceed our investigation from the third level. In Chapter 6, we introduce our QND measurement scheme and derive a corre-

sponding master equation using a density matrix and tracing out the environment. In Chapter 7 we investigate the time correlations of the measurement signal and the state of the system conditioned on the results of the measurement using the method of stochastic density matrix equations. This allows us to track the quantum jumps of the system as it moves between different Fock states due to the thermal environmental coupling, and we will present numerical evidence for this behaviour. Then we discuss the possibility of tracking the evolution of the system as it jumps between number states due to its interaction with a thermal bath. In Chapter 8, we focus on a damped driven non-linear oscillator and investigate the effect of higher order anharmonic terms.

Chapter 6

Deterministic dynamics - the master equation

6.1 Constructing the Hamiltonian

6.1.1 The model

In this section we introduce our model system and show how the coupling between the system and ancilla approximates a QND coupling in an appropriate limit. We then derive equations of motion that take into account the thermal couplings and the interactions that drive and monitor the oscillations of the readout system.

Consider a mesoscopic beam with rectangular cross section. As already discussed in Part I, there are two orthogonal flexing modes that are not coupled in the linear elasticity theory, but are coupled anharmonically. This coupling exists in nature between the two orthogonal flexing modes of single mechanical beam. However, the coupling can also be controlled and engineered. Such a coupling of two elastic beams has been proposed by Yurke [33]: two mesoscopic elastic beams with rectangular cross section are connected by a series of mechanical coupling devices. These devices have the effect of allowing only one type of strain (the longitudinal stretch) to pass to the other beam. The experimental effort of fabricating such a structure is currently underway by Roukes and his group [31, 34]. Here we focus on the extent to which such a device is able to realize a QND measurement, the eventual sensitivity of the measurement and the constraints this places on the specifications of the device, and

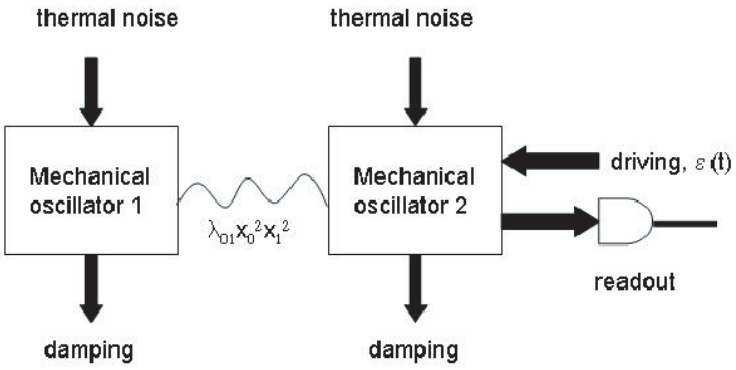

Figure 6.1: Schematics of a QMD measurement using two coupled mechanical oscillators.

the required temperatures. For convenience, we refer to the system of interest as oscillator 0 and the ancilla as oscillator 1, and the corresponding resonant frequencies of the two modes as ω_0 and ω_1, respectively. The ancilla is driven at its resonant frequency, and a measurement apparatus is attached to the ancilla. The whole structure is kept at a low temperature such that $\hbar\omega \sim k_B T$, where $\hbar = h/2\pi$ is Plank's constant, ω is the system beam resonance frequency, T is the temperature, and k_B is Boltzmann's constant. The oscillators and the environment are weakly coupled. Figure 6.1 shows a schematic of our model.

6.1.2 System Hamiltonian

Converting the schematic model in the last section into a realistic mathematical model and obtaining the system dynamics requires some assumptions and simplifications.

Firstly, we focus on the anharmonic coupling and the limit in which it satisfies the QND condition. In linear elasticity theory, two flexing modes, which are perpendicular to each other, propagate independently without interacting. Beyond the linear approximation these modes are coupled. Expansion of the elastic energy with respect to the strain tensor is taken up to second order in the harmonic approximation. The next term, cubic in the elastic energy, gives quadratic terms in the equation of motion [25, 26]. Since the coupling of two flexing modes has a symmetry and they are

not coupled at the linear level, the lowest order coupling is $x_0^2 x_1^2$. So we expand the anharmonic terms up to first order in coupling and obtain

$$H_{\text{anh}} = \hbar \left(\tilde{\lambda}_0 x_0^2 + \tilde{\lambda}_{00} x_0^4 + \tilde{\lambda}_1 x_1^2 + \tilde{\lambda}_{11} x_1^4 \right), \tag{6.1}$$

$$V_{\text{anh}} = \hbar \tilde{\lambda}_{01} x_0^2 x_1^2, \tag{6.2}$$

where $\tilde{\lambda}_{ij}$ is the non-linear coupling constant between the oscillators i and j, and the expansion of anharmonic terms in each potential is up to the same order as the leading anharmonic coupling term, $\hbar \tilde{\lambda}_{01} x_0^2 x_1^2$. In terms of creation and annihilation operators, the Hamiltonian is

$$H = H_0 + H_{\text{anh}} + V_{\text{anh}}, \tag{6.3}$$

$$H_0 = \hbar \omega_0 a_0^\dagger a_0 + \hbar \omega_1 a_1^\dagger a_1, \tag{6.4}$$

$$\begin{aligned} H_{\text{anh}} = {} & \hbar \tilde{\lambda}_0 \left(a_0^\dagger + a_0 \right)^2 + \hbar \left(a_1^\dagger + a_1 \right)^2 \\ & + \hbar \tilde{\lambda}_{00} \left(a_0^\dagger + a_0 \right)^4 + \hbar \tilde{\lambda}_{11} \left(a_1^\dagger + a_1 \right)^4, \end{aligned} \tag{6.5}$$

$$V_{\text{anh}} = \hbar \tilde{\lambda}_{01} \left(a_0^\dagger + a_0 \right)^2 \left(a_1^\dagger + a_1 \right)^2, \tag{6.6}$$

where we have defined the standard raising and lowering operators for the oscillators $a_i = \sqrt{m_i \omega_i / 2\hbar} x_i + i \sqrt{1/2\hbar m_i \omega_i} p_i$ and $a_i^\dagger$ is the Hermitian conjugate of a_i. Elasticity theory also tells us that the anharmonic coefficients are much smaller than the oscillation frequencies, i.e., $\omega_i \gg \tilde{\lambda}_{i,j}$ [35]. So far we have ignored any environmental couplings of the two oscillators so as to focus on the interaction of the two oscillators.

The idea of a QND measurement is widely discussed in the literature (for example, see [32], [36], and [37]) and is nicely summarised by Caves *et al.* [36] as "A measurement which, in principle, can be made time after time on a single system, giving always the same precise result in the absence of external forces (signals). When external forces are present, quantum nondemolition measurements are an ideal tool for monitoring them." Since we want to monitor dynamical changes of $a_0^\dagger a_0$, a QND measurement is what we need. In order to perform a QND measurement of $a_0^\dagger a_0$ the

coupling Hamiltonian between the two oscillators V should satisfy the QND condition

$$[a_0^\dagger a_0, V_{\rm anh}] = 0. \tag{6.7}$$

This condition guarantees that the future dynamics of the measured observable $a_0^\dagger a_0$ are unaffected by the interaction $V_{\rm anh}$ with the ancilla.

At this point, it is useful to move into an interaction picture with respect to H_0 in order to determine the regime that approaches the condition in Eq. (6.7). In the interaction picture with respect to H_0 we find

$$V_{\rm anh}(t) = \hbar\tilde{\lambda}_{01}\left(a_0^\dagger e^{i\omega_0 t} + a_0 e^{-i\omega_0 t}\right)^2\left(a_1^\dagger e^{i\omega_1 t} + a_1 e^{-i\omega_1 t}\right)^2. \tag{6.8}$$

Expanding out the product, there are terms that have the time dependence $\exp(\pm i2\omega_0 t)$, $\exp(\pm i2\omega_1 t)$, or $\exp[\pm i2(\omega_0 \pm \omega_1)t]$. If the frequencies of the two oscillators satisfy $\omega_0 - \omega_1 \gg \tilde{\lambda}_{01}$ and $\omega_i \gg \tilde{\lambda}_{01}$, then all of these time dependences are very fast relative to the interaction picture time dependence of the operators a_0, a_1. In this limit the time-dependent terms in $V_{\rm anh}(t)$ lead to rapid, small amplitude oscillations of a_i that essentially average to zero over the timescales for which the non-linearity $\tilde{\lambda}_{01}$ is relevant. If we admit a time coarse-graining and only consider times longer than a mechanical oscillation period we may disregard these time dependent terms; such an approximation is known as the rotating wave approximation (RWA) and is frequently used in quantum optics. Another intuitive explanation for the rotating wave approximation is that the terms with time dependence in the interaction picture drive energy non-conserving transitions and as long as the condition $\omega_0 - \omega_1 \gg \tilde{\lambda}_{01}$ is satisfied, the differences in energy are large and the associated transitions are strongly suppressed as a result. Thus we disregard the energy non-conserving terms in the Hamiltonian to obtain

$$V_{\rm anh}^{\rm RWA}(t) = \hbar\tilde{\lambda}_{01}\left(1 + 2a_1^\dagger a_1 + 2a_0^\dagger a_0 + 4a_0^\dagger a_0 a_1^\dagger a_1\right). \tag{6.9}$$

Note that having made the rotating wave approximation the anharmonic coupling term now commutes with the observable $a_0^\dagger a_0$, so a QND measurement can be achieved

under the condition $\omega_0 - \omega_1 \gg \tilde{\lambda}_{01}$ [1].

The internal anharmonic terms, $H_{\rm anh}$, can be also treated in a similar manner, which result in

$$\begin{aligned} H_{\rm anh}^{\rm RWA} &= \hbar\left(\omega_0 + 2\tilde{\lambda}_0 + 4\tilde{\lambda}_{00}\right) a_0^\dagger a_0 + 6\hbar\tilde{\lambda}_{00}\left(a_0^\dagger a_0\right)^2 \\ &+ \hbar\left(\omega_1 + 2\tilde{\lambda}_1 + 4\tilde{\lambda}_{11}\right) a_1^\dagger a_1 + 6\hbar\tilde{\lambda}_{11}\left(a_1^\dagger a_1\right)^2 \\ &+ \hbar\left(3\tilde{\lambda}_{11} + 3\tilde{\lambda}_{00} + \tilde{\lambda}_0 + \tilde{\lambda}_1\right). \end{aligned} \tag{6.10}$$

From above, we can see that the anharmonic terms cause both a shift in the oscillator resonant frequency and a non-linear phase shift which depends on intensity (a Kerr non-linearity in optical terminology and it is discussed in detail in Chapter 8). The constant term can be disregarded since it merely provides an overall phase. We assume in the present chapter that the dominant non-linearity is the coupling given by $\tilde{\lambda}_{01}$ and disregard the nonlinearities of the system and ancilla internal Hamiltonians[2]. Returning to the Schrödinger picture the Hamiltonian H now can be written as

$$H^{\rm RWA} = \hbar\omega_0 a_0^\dagger a_0 + \hbar\omega_1 a_1^\dagger a_1 + \hbar\lambda_{01} a_0^\dagger a_0 a_1^\dagger a_1, \tag{6.11}$$

where we have absorbed the corrections to the system and ancilla oscillation frequency into the definition of ω_0 and ω_1 and $\lambda_{01} = 6\tilde{\lambda}_{01}$. This Hamiltonian is an adequate description of the dynamics as long as we are not concerned with short times of the order of a mechanical oscillation period.

In the above rotating wave Hamiltonian the excitation of the system oscillator leads to a frequency shift of the ancilla oscillator. Thus it is necessary to monitor the frequency of the ancilla oscillations in order to determine the system excitation. To achieve this we imagine driving the ancilla oscillations on resonance and detecting

[1] Actually, it is not necessary to make the rotating wave approximation with respect to both oscillators as the interaction $V_{\rm anh}$ becomes QND after the rotating wave approximation made in an interaction picture with respect to $\hbar\omega_0 a_0^\dagger a_0$ only. However, we make the further rotating wave approximation to simplify the later development.

[2] The detailed analysis of non-linearities of the system and ancilla internal Hamiltonian and the correction to the dynamical equation due to these terms will be discussed in Chapter 8.

any shift in phase that is due to the system excitation. There will thus be a driving term on the ancilla that may be written

$$H_{\text{drive}} = 2\hbar E \cos\omega_1 t \left(a_1 + a_1^\dagger\right) \tag{6.12}$$

in the Schrödinger picture. The driving frequency is chosen to resonantly drive oscillations of the ancilla. The phase of the oscillator depends on the frequency of the drive (in-phase below resonance and out-of-phase above resonance). At resonance the phase depends linearly on the driving frequency. If the resonance is shifted due to the system excitation this will be detected as a phase shift between the mechanical oscillations and the drive. In the interaction picture with respect to the ancilla internal Hamiltonian there are again fast oscillating terms that can be neglected in the RWA when $\omega_1 > E$. Then we get

$$H_{\text{drive}} = \hbar E \left(a_1 + a_1^\dagger\right) \tag{6.13}$$

in the interaction picture.

Now we add the coupling of thermal baths to the system and ancilla. We employ a standard technique and model the thermal baths (the surrounding environment) as an infinite number of harmonic oscillators. The thermal baths are linearly coupled to the system (or ancilla) by coordinate-coordinate coupling, *i.e.*, $\sum_j A_j x_i x_j$ where x_i is the system (or ancilla) coordinate, x_j is the coordinate of an oscillator in the bath, and the index j corresponds to different bath oscillators. We will again use the rotating wave approximation for the coupling since the couplings are weak.

The nature of the coupling with the measurement instrument depends on what is to be measured. Here we adapt a magnetomotive detection scheme suggested by Yurke *et al.* [38], which can be summarised as follows (see also Fig. (6.2): The voltage developed depends on

$$V = LB\frac{dx}{dt}, \tag{6.14}$$

where V is the voltage, B is the magnetic field, and x is the displacement of the beam

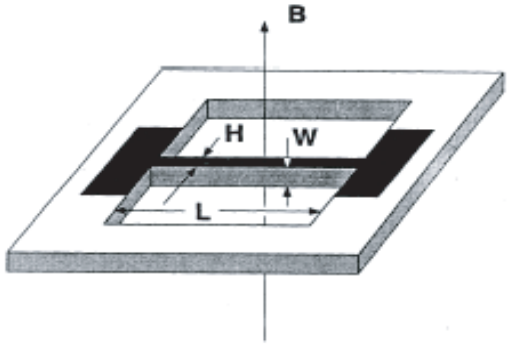

Figure 6.2: A mechanical oscillation measurement scheme proposed by Yurke *et al.* [38]. Adopted from Phys. Rev. A **51** (5), 4211 (1994).

from its equilibrium position. It is then amplified by the amplifier to give the output voltage

$$V_{out} = V(t)\cos(\omega_1 t + \phi(t)), \tag{6.15}$$

where $V(t)$ is the time varying amplitude and $\phi(t)$ is the time varying phase. The current induced by this voltage is monitored by phase lock-in amplifier. An experimenter monitors the amplitude of the current and its phase with respect to the driving current that is set to the resonant frequency. However, we do not focus on technical details of specific measurement schemes at this point and intend to be fairly general, thus similar analysis to the one presented below will hold for variety of measurements where the system is linearly coupled to a measurement current.

The measurement current is given by

$$I(t) = \sqrt{\frac{\hbar\omega_1}{2Lz_0}} \sum_n \left(b_{\mathrm{d},n}(t) + b^\dagger_{\mathrm{d},n}(t) \right), \tag{6.16}$$

where $b_{\mathrm{d},n}(t)$ is the measurement bath operator of mode n, L is the inductance and z_0 is the quantisation length [39]. From here on we use scaled unit $\hbar\omega_1/2Lz_0 = 1$ for convenience.

For a linearly coupled system-bath measurement within the rotating wave approximation, the coupling between the measurement current and ancilla has the form

$i\hbar\left(b_{\mathrm{d},n}^{\dagger}a_1 - b_{\mathrm{d},n}a_1^{\dagger}\right)$, where $b_{\mathrm{d},n}$ is the bosonic bath operator, and thus it has the same mathematical structure as those of thermal baths.

The final Hamiltonian for our model in the interaction picture is

$$H = \hbar\omega_0 a_0^{\dagger}a_0 + \hbar E\left(a_1 + a_1^{\dagger}\right) + \hbar\sum_{\mathrm{s}}\sum_{n}^{\infty}\omega_{\mathrm{s},n}b_{\mathrm{s},n}^{\dagger}b_{\mathrm{s},n} + \hbar\lambda_{01}a_0^{\dagger}a_0a_1^{\dagger}a_1 + i\hbar\left(\Gamma^{\dagger}a_1 - \Gamma a_1^{\dagger}\right) + i\hbar\left(D^{\dagger}a_1 - D\left(t\right)a_1^{\dagger}\right) + i\hbar\left(\Theta^{\dagger}a_0 - \Theta a_0^{\dagger}\right), \tag{6.17}$$

where the index s denotes three different baths: the thermal bath coupled to the system (b0), the thermal bath coupled to the ancilla (b1), and the measurement bath coupled to the ancilla (d). The bath operators and coupling coefficients are defined such that coordinate-coordinate coupling of system-bath will give a factor of $i\hbar$ for later convenience, and

$$\Gamma = \sum_{\mathrm{n}}^{\infty} g_{\mathrm{b1}}\left(\omega_n\right) b_{\mathrm{b1},n} \tag{6.18}$$

$$D = \sum_{\mathrm{n}}^{\infty} g_{\mathrm{d}}\left(\omega_n\right) b_{\mathrm{d},n} \tag{6.19}$$

$$\Theta = \sum_{\mathrm{n}}^{\infty} g_{\mathrm{b0}}\left(\omega_n\right) b_{\mathrm{b0},n}, \tag{6.20}$$

where $g_{\mathrm{s}}\left(\omega_n\right)$ is the coupling coefficient with index n which distinguishes the different modes of frequency ω_n, Since the energy is dissipated among the many modes, there is some coupling to all of the modes. Later, we will derive the relationship between this coefficient and the corresponding damping rate.

We are interested in the dynamics of the system and the performance of the measurement that we have described. The rest of the chapter proceeds in the following sequence. Firstly, we find a master equation that describes the evolution of the system and ancilla alone without explicitly describing the state of the environment. Secondly we further simplify this equation by making use of the difference in time-scales between the system and ancilla to obtain a master equation for the system oscillator alone by means of adiabatic elimination. This allows us to determine the

effect of the QND measurement coupling on the system.

6.2 Dynamics of the system: Master equation and adiabatic elimination

6.2.1 Master equation

In this section we present the evolution equations for the ancilla and system alone, tracing out the environmental couplings. We treat the interaction between the oscillators and the environment in the Markov and rotating wave approximations. This is consistent with our treatment of the internal Hamiltonian and we leave it to future work to consider effects beyond the rotating wave regime. The rotating wave approximation is usually very well satisfied in optical systems where non-linear couplings or loss rates are many orders of magnitude smaller than optical frequencies. The difference of timescales will be smaller in the present case but mechanical oscillators with high Q-factors are becoming realizable in practice and it is in this limit that a QND detection of phonon number will become possible. A master equation can be derived from the Hamiltonian Eq. (6.17).

6.2.1.1 Thermal coupling component of the master equation (Lindblad form)

We consider a thermal bath coupled to a system (The formalism presented here is applicable to all baths). The high temperature system-thermal bath coupling ($T \rightarrow \infty$) has been considered by Caldeira and Leggett [40] while the low temperature case has been examined by Walls and Milburn [37]. We note that, despite of the claims by some, the Caldeira-Leggett formula has a corresponding operator equation derived by themselves (see Eq. (5.12) in [40]) and this equation is in a Lindblad form. Under the RWA, the Caldeira-Leggett operator form at high temperature and the Walls and Milburn Lindblad form at low temperature have very similar expressions, differing only by coefficients.

In the interaction picture, the equation of motion is

$$\frac{d\rho_{\mathrm{SB}}}{dt} = -\frac{i}{\hbar}\left[H_{int}\left(t\right), \rho_{\mathrm{SB}}(t)\right], \tag{6.21}$$

where H_{int} is the interaction Hamiltonian, and ρ_{SB} is the combined system-bath density matrix. The reduced density operator for the system is

$$\rho\left(t\right) = \mathrm{Tr}_{\mathrm{b}}\left\{\rho_{\mathrm{SB}}\left(t\right)\right\}. \tag{6.22}$$

Initially (at $t = 0$), we assume that the system and bath are uncorrelated and the total density matrix is a direct product of the system ρ and bath ρ_{b}

$$\rho_{\mathrm{SB}}\left(0\right) = \rho\left(0\right) \otimes \rho_{\mathrm{b}}. \tag{6.23}$$

Integration of Eq. (6.21) gives

$$\rho_{\mathrm{SB}}(t) = \rho_{\mathrm{SB}}(0) - \frac{i}{\hbar}\int_0^t dt_1 \left[H_{int}\left(t_1\right), \rho_{\mathrm{SB}}(t_1)\right]. \tag{6.24}$$

Iteration of the above equation gives

$$\begin{aligned}\rho_{\mathrm{SB}}(t) = {} & \rho_{\mathrm{SB}}(0) \\ & + \sum_{n=1}^{\infty}\left(-\frac{i}{\hbar}\right)^n \int_0^t dt_1 \int_0^{t_1} dt_2 ... \int_0^{t_{n-1}} dt_n \left[H_{int}\left(t_1\right), ... \left[H_{int}\left(t_n\right), \rho_{\mathrm{SB}}(0)\right]\right].\end{aligned} \tag{6.25}$$

Tracing over the bath results in

$$\rho\left(t\right) = V\left(t\right)\rho\left(0\right), \tag{6.26}$$

where $V\left(t\right)$ is the evolution operator. We now expand $V\left(t\right)$ corresponding to Eq.

(6.25).

$$V(t) = 1 + \sum_{n=1}^{\infty} V_n(t), \tag{6.27}$$

$$V_n(t) = \left(-\frac{i}{\hbar}\right)^n \mathrm{Tr_b}\left\{\int_0^t dt_1 \int_0^{t_1} dt_2 ... \int_0^{t_{n-1}} dt_n \left[H_{int}(t_1), ... \left[H_{int}(t_n), \rho_\mathrm{b} \otimes (.)\right] ...\right]\right\}. \tag{6.28}$$

Multiplying by $V^{-1}(t)$ from left on both side of Eq. (6.26) gives

$$\rho(0) = V^{-1}(t)\,\rho(t). \tag{6.29}$$

Taking the trace, Eq. (6.25) can be written as

$$\begin{aligned}\rho(t) &= \rho(0) + \sum_{n=1}^{\infty}\left(-\frac{i}{\hbar}\right)^n \int_0^t dt_1 \int_0^{t_1} dt_2 ... \int_0^{t_{n-1}} dt_n \mathrm{Tr_b}\left[H_{int}(t_1), ... \left[H_{int}(t_n), \rho_{\mathrm{SB}}(0)\right]\right] \\ &= \rho(0) + \sum_{n=1}^{\infty} V_n(t)\,\rho(0).\end{aligned} \tag{6.30}$$

Using Eq. (6.26) and taking the derivative with respect to t yields

$$\begin{aligned}\frac{d\rho(t)}{dt} &= \frac{d}{dt}\left(V_1(t) + V_2 + ...\right)\rho(0) \\ &= \left(\dot{V}_1(t) + \dot{V}_2 + ...\right) V^{-1}(t)\,\rho(t).\end{aligned} \tag{6.31}$$

If $H_{int}(t)$ is such that

$$\mathrm{Tr_b}\left\{H_{\mathrm{int}}(t)\,\rho_\mathrm{b}\right\} = 0, \tag{6.32}$$

then $V_1(t) = 0$ and the first order term becomes zero. With a series expansion of $V^{-1}(t)$ and keeping terms to second order we obtain

$$\frac{d\rho(t)}{dt} = -\frac{1}{\hbar^2}\int_0^t dt' \mathrm{Tr_b}\left[H_{\mathrm{int}}(t), \left[H_{\mathrm{int}}(t'), \rho_{\mathrm{SB}}(t)\right]\right]. \tag{6.33}$$

The interaction Hamiltonian in the interaction picture is

$$H_{\text{int}}(t) = i\hbar\left[Z^{\dagger}(t)\, a e^{-i\omega_0 t} - Z(t)\, a^{\dagger} e^{i\omega_0 t}\right], \tag{6.34}$$

where $ae^{-i\omega_0 t}$ is the bosonic system operator in the interaction picture, and we define $Z(t)$ as

$$Z(t) \equiv \sum_n g_{\text{b}0}(\omega_n)\, b_n e^{-i\omega_n t}, \tag{6.35}$$

where $g_{\text{b}0}(\omega_n)$ is the coupling coefficient as in Eq. (6.20) and $b_n e^{-i\omega_n t}$ is the bosonic bath operator in the interaction picture. The bath operator satisfies the commutation relation (see B.1):

$$\left[b_n, b_{n'}^{\dagger}\right] = \delta_{n,n'}. \tag{6.36}$$

The commutator of the second order term in the interaction picture is

$$\begin{aligned}
&[H_{int}(t), [H_{int}(t'), \rho(t)\otimes\rho_{\text{b}}]] \\
&= -\hbar^2 \Big\{ aa\rho(t)e^{-i\omega_0(t+t')} \otimes Z^{\dagger}(t) Z^{\dagger}(t')\rho_{\text{b}} - aa^{\dagger}\rho e^{-i\omega_0(t-t')}(t) \otimes Z^{\dagger}(t) Z(t')\rho_{\text{b}} \\
&- a^{\dagger}a\rho(t)e^{i\omega_0(t-t')} \otimes Z(t) Z^{\dagger}(t')\rho_{\text{b}} + a^{\dagger}a^{\dagger}\rho(t)e^{i\omega_0(t+t')} \otimes Z(t) Z(t')\rho_{\text{b}} \\
&- a\rho(t)ae^{-i\omega_0(t+t')} \otimes Z^{\dagger}(t)\rho_{\text{b}}Z^{\dagger}(t') + a\rho(t)a^{\dagger}e^{-i\omega_0(t-t')} \otimes Z^{\dagger}(t)\rho_{\text{b}}Z(t') \\
&+ a^{\dagger}\rho(t)ae^{i\omega_0(t-t')} \otimes Z(t)\rho_{\text{b}}Z^{\dagger}(t') - a^{\dagger}\rho(t)a^{\dagger}e^{i\omega_0(t+t')} \otimes Z(t)\rho_{\text{b}}Z(t') \\
&- a\rho(t)ae^{-i\omega_0(t+t')} \otimes Z^{\dagger}(t')\rho_{\text{b}}Z^{\dagger}(t) + a\rho(t)a^{\dagger}e^{-i\omega_0(t-t')} \otimes Z^{\dagger}(t')\rho_{\text{b}}Z(t) \\
&+ a^{\dagger}\rho(t)ae^{i\omega_0(t-t')} \otimes Z(t')\rho_{\text{b}}Z^{\dagger}(t) + a^{\dagger}\rho(t)a^{\dagger}e^{i\omega_0(t+t')} \otimes Z(t')\rho_{\text{b}}Z(t) \\
&+ \rho(t)aae^{-2i\omega_0 t} \otimes \rho_{\text{b}}Z^{\dagger}(t') Z^{\dagger}(t) - \rho(t)aa^{\dagger}e^{-i\omega_0(t-t')} \otimes \rho_{\text{b}}Z^{\dagger}(t') Z(t) \\
&- \rho(t)a^{\dagger}ae^{i\omega_0(t-t')} \otimes \rho_{\text{b}}Z(t') Z^{\dagger}(t) + \rho(t)a^{\dagger}a^{\dagger}e^{i\omega_0(t+t')} \otimes \rho_{\text{b}}Z(t') Z(t) \Big\}.
\end{aligned} \tag{6.37}$$

Since the dynamical time scale of the system $a(t)$ is after extracting the oscillation at ω_0 much slower than that of the bath, we can pull the system operator outside of

the integral in Eq. (6.33). Taking the trace over the bath, we have

$$
\begin{aligned}
&-\frac{1}{\hbar^2}\int_{t_0}^{t} dt_1 \mathrm{Tr_b}\left[H_{int}\left(t\right),\left[H_{int}\left(t'\right),\rho_{\mathrm{SB}}(t)\right]\right] \\
&= aa\rho(t)\frac{1}{\hbar^2}\int_{t_0}^{t} dt' \left\langle Z^{\dagger}\left(t\right) Z^{\dagger}\left(t'\right)\right\rangle e^{-i\omega_0(t+t')} - aa^{\dagger}\rho(t)\frac{1}{\hbar^2}\int_{t_0}^{t} dt' \left\langle Z^{\dagger}\left(t\right) Z\left(t'\right)\right\rangle e^{-i\omega_0(t-t')} \\
&- a^{\dagger}a\rho(t)\frac{1}{\hbar^2}\int_{t_0}^{t} dt' \left\langle Z\left(t\right) Z^{\dagger}\left(t'\right)\right\rangle e^{i\omega_0(t-t')} + a^{\dagger}a^{\dagger}\rho(t)\frac{1}{\hbar^2}\int_{t_0}^{t} dt' \left\langle Z\left(t\right) Z\left(t'\right)\right\rangle e^{i\omega_0(t+t')} \\
&- a\rho(t)a\frac{1}{\hbar^2}\int_{t_0}^{t} dt' \left\langle Z^{\dagger}\left(t\right) Z^{\dagger}\left(t'\right)\right\rangle e^{-i\omega_0(t+t')} + a\rho(t)a^{\dagger}\frac{1}{\hbar^2}\int_{t_0}^{t} dt' \left\langle Z^{\dagger}\left(t\right) Z\left(t'\right)\right\rangle e^{-i\omega_0(t-t')} \\
&+ a^{\dagger}\rho(t)a\frac{1}{\hbar^2}\int_{t_0}^{t} dt' \left\langle Z\left(t\right) Z^{\dagger}\left(t'\right)\right\rangle e^{i\omega_0(t-t')} - a^{\dagger}\rho(t)a^{\dagger}\frac{1}{\hbar^2}\int_{t_0}^{t} dt' \left\langle Z\left(t\right) Z\left(t'\right)\right\rangle e^{i\omega_0(t+t')} \\
&- a\rho(t)a\frac{1}{\hbar^2}\int_{t_0}^{t} dt' \left\langle Z^{\dagger}\left(t'\right) Z^{\dagger}\left(t\right)\right\rangle e^{-i\omega_0(t+t')} + a\rho(t)a^{\dagger}\frac{1}{\hbar^2}\int_{t_0}^{t} dt' \left\langle Z^{\dagger}\left(t'\right) Z\left(t\right)\right\rangle e^{-i\omega_0(t-t')} \\
&+ a^{\dagger}\rho(t)a\frac{1}{\hbar^2}\int_{t_0}^{t} dt' \left\langle Z\left(t'\right) Z^{\dagger}\left(t\right)\right\rangle e^{i\omega_0(t-t')} + a^{\dagger}\rho(t)a^{\dagger}\frac{1}{\hbar^2}\int_{t_0}^{t} dt' \left\langle Z\left(t'\right) Z\left(t\right)\right\rangle e^{i\omega_0(t+t')} \\
&+ \rho(t)aa\frac{1}{\hbar^2}\int_{t_0}^{t} dt' \left\langle Z^{\dagger}\left(t'\right) Z^{\dagger}\left(t\right)\right\rangle e^{-i\omega_0(t+t')} - \rho(t)aa^{\dagger}\frac{1}{\hbar^2}\int_{t_0}^{t} dt' \left\langle Z^{\dagger}\left(t'\right) Z\left(t\right)\right\rangle e^{-i\omega_0(t-t')} \\
&- \rho(t)a^{\dagger}a\frac{1}{\hbar^2}\int_{t_0}^{t} dt' \left\langle Z\left(t'\right) Z^{\dagger}\left(t\right)\right\rangle e^{i\omega_0(t-t')} + \rho(t)a^{\dagger}a^{\dagger}\frac{1}{\hbar^2}\int_{t_0}^{t} dt' \left\langle Z\left(t'\right) Z\left(t\right)\right\rangle e^{i\omega_0(t+t')}.
\end{aligned}
\tag{6.38}
$$

The bath correlations can be evaluated by firstly Fourier transforming the integral, then assuming that the coupling coefficient is a slowly varying function around the system resonance frequency, and finally evaluating the integral. Since the bath is assumed large the normal modes of the oscillator are very close spaced in frequency, we can approximate the spectrum by a continuum. We have

$$
b_n = \int_{\omega_n - 1/2\rho_{\mathrm{ds}}(\omega_n)}^{\omega_n + 1/2\rho_{\mathrm{ds}}(\omega_n)} A_n b\left(\omega\right) d\omega, \tag{6.39}
$$

where $\rho_{\mathrm{ds}}\left(\omega_n\right)$ is the number of modes of frequency ω_n per unit frequency (the density of states) and A_n is a coefficient to be found such that the commutation rules

$$
\left[b\left(\omega\right), b^{\dagger}\left(\omega'\right)\right] = \delta\left(\omega - \omega'\right) \tag{6.40}
$$

are satisfied. Using Eq. (6.40) and Eq. (6.36) we can write

$$\delta_{n,n'} = \left[b_n, b_{n'}^\dagger\right] = \int_{\omega_n - 1/2\rho_{\rm ds}(\omega_n)}^{\omega_n + 1/2\rho_{\rm ds}(\omega_n)} \int_{\omega_{n'} - 1/2\rho_{\rm ds}(\omega_{n'})}^{\omega_{n'} + 1/2\rho_{\rm ds}(\omega_{n'})} d\omega d\omega' \left[b\left(\omega\right), b^\dagger\left(\omega'\right)\right] A_n A_{n'}, \quad (6.41)$$

and we obtain the coefficient A_n:

$$A_n = \sqrt{\rho_{\rm ds}\left(\omega_n\right)}. \quad (6.42)$$

Thus we can write $\sum_n b_n\left(t\right)$ in the continuum form as

$$\sum_n b_n\left(t\right) = \sum_n \int_{\omega_n - 1/2\rho_{\rm ds}(\omega_n)}^{\omega_n + 1/2\rho_{\rm ds}(\omega_n)} \sqrt{\rho_{\rm ds}\left(\omega_n\right)} b\left(\omega\right) d\omega = \int_0^\infty \sqrt{\rho_{\rm ds}\left(\omega_n\right)} b\left(\omega\right) d\omega. \quad (6.43)$$

The bath correlations are derived in Appendix B.1. Using those results and Eq. (6.40) we have the following correlations

$$\left\langle b\left(\omega\right) b\left(\omega'\right)\right\rangle = \left\langle b^\dagger\left(\omega\right) b^\dagger\left(\omega'\right)\right\rangle = 0, \quad (6.44)$$

$$\left\langle b\left(\omega\right) b^\dagger\left(\omega'\right)\right\rangle = \delta(\omega - \omega')\left(N\left(\omega\right) + 1\right), \quad (6.45)$$

$$\left\langle b^\dagger\left(\omega\right) b\left(\omega'\right)\right\rangle = \delta(\omega - \omega') N\left(\omega\right). \quad (6.46)$$

Here $N\left(\omega\right)$ is the occupation number of the bath at frequency ω given by the Bose-Einstein distribution

$$N\left(\omega\right) = \frac{1}{e^{\hbar\beta\omega} - 1}, \quad (6.47)$$

where $\beta = 1/k_{\rm B}T$ with T the temperature of the bath.

Next, we need to evaluate the integrals. As an example consider the integration

$$I_{ZZ^\dagger} = a^\dagger \rho(t) a \frac{1}{\hbar^2} \int_{t_0}^t dt' \left\langle Z\left(t\right) Z^\dagger\left(t'\right)\right\rangle e^{i\omega_0(t-t')}. \quad (6.48)$$

Writing $Z(t)$ in terms of the continuum Bose operators gives

$$\begin{aligned} I_{ZZ^\dagger} &= \int_{t_0}^{t} dt' \int_0^\infty d\omega \int_0^\infty d\omega' \sqrt{\rho_{\rm ds}(\omega)}\sqrt{\rho_{\rm ds}(\omega')} g_{\rm b0}(\omega)\, g_{\rm b0}^*(\omega') \\ &\quad \times \left\langle b(\omega)\, b^\dagger(\omega') \right\rangle e^{-i(\omega-\omega_0)t} e^{i(\omega'-\omega_0)t'} \\ &= \int_{t_0}^{t} dt' \int_0^\infty d\omega \rho_{\rm ds}(\omega) \left|g_{\rm b0}(\omega)\right|^2 (N(\omega)+1)\, e^{-i(\omega-\omega_0)(t-t')}. \end{aligned} \tag{6.49}$$

Changing the variable from t' to $\tau = t'-t$ and assuming $\rho_{\rm ds}(\omega)$ and $g_{\rm b0}(\omega)$ are slowly varying functions around $\omega = \omega_0$, and setting $\varepsilon = \omega - \omega_0$ and $t_0 \to -\infty$, we get

$$\begin{aligned} I_{ZZ^\dagger} &= \int_0^\infty d\tau \int_{-\infty}^\infty d\varepsilon \rho_{\rm ds}(\varepsilon+\omega_0) \left|g_{\rm b0}(\varepsilon+\omega_0)\right|^2 (N(\varepsilon+\omega_0)+1)\, e^{i\varepsilon\tau} \\ &= \int_{-\infty}^\infty d\varepsilon \rho_{\rm ds}(\varepsilon+\omega_0) \left|g_{\rm b0}(\varepsilon+\omega_0)\right|^2 (N(\varepsilon+\omega_0)+1) \left[\pi\delta(\varepsilon) + i{\rm P}\left(\frac{1}{\varepsilon}\right)\right] \\ &= \pi \rho_{\rm ds}(\omega_0) \left|g_{\rm b0}(\omega_0)\right|^2 (N(\omega_0)+1) \\ &\quad - i{\rm P}\int_{-\infty}^\infty d\varepsilon \frac{1}{\varepsilon} \rho_{\rm ds}(\omega_0+\varepsilon) \left|g_{\rm b0}(\omega_0+\varepsilon)\right|^2 (N(\omega_0)+1), \end{aligned} \tag{6.50}$$

where P denotes a principal value. The second term in Eq. (6.50) is associated with the Lamb shift, which can be absorbed in the definition of oscillator frequency, ω_0. Writing $N(\omega_0) = N_0$, we obtain

$$I_{ZZ^\dagger} \simeq \pi \rho_{\rm ds}(\omega_0) \left|g_{\rm b0}(\omega_0)\right|^2 (N_0+1). \tag{6.51}$$

Other terms in Eq. (6.38) can be evaluated in a similar manner.

Going back to the Schrödinger picture and adding the free Hamiltonian part $H_{\rm S}$, we finally obtain

$$\begin{aligned} \dot\rho(t) &= -\frac{i}{\hbar}[H_{\rm S}, \rho(t)] \\ &\quad + \nu(N_0+1)\left(2a\rho a^\dagger - a^\dagger a\rho - \rho a^\dagger a\right) + \nu N_0 \left(2a^\dagger \rho a - a a^\dagger \rho - \rho a a^\dagger\right), \end{aligned} \tag{6.52}$$

where we have defined

$$\nu \equiv \pi \rho_{\rm ds}(\omega_0) \left|g_{\rm b0}(\omega_0)\right|^2. \tag{6.53}$$

Physically ν gives the damping rate of the amplitude of oscillation.

As explained in § 6.1.1 our model has three baths, and each system (or ancilla) - bath coupling gives the same form of contribution to the master equation as the last two terms in Eq. (6.52). Thus the master equation for the density operator, ρ, describing the state of the system and ancilla in the interaction picture (*i.e.*, the free Hamiltonian terms do not appear explicitly) is

$$\begin{aligned}\frac{d\rho}{dt} = &-\frac{i}{\hbar}\left[\hbar E\left(a_1^\dagger + a_1\right) + \hbar\lambda_{01}a_0^\dagger a_0 a_1^\dagger a_1, \rho\right] \\ &+ \nu(N_0+1)\left(2a_0\rho a_0^\dagger - a_0^\dagger a_0\rho - \rho a_0^\dagger a_0\right) + \nu N_0\left(2a_0^\dagger\rho a_0 - \rho a_0 a_0^\dagger - a_0 a_0^\dagger\rho\right) \\ &+ \mu(N_{\rm d}+1)\left(2a_1\rho a_1^\dagger - a_1^\dagger a_1\rho - \rho a_1^\dagger a_1\right) + \mu N_{\rm d}\left(2a_1^\dagger\rho a_1 - a_1 a_1^\dagger\rho - \rho a_1 a_1^\dagger\right) \\ &+ \eta(N_{\bar{1}}+1)\left(2a_1\rho a_1^\dagger - a_1^\dagger a_1\rho - \rho a_1^\dagger a_1\right) + \eta N_{\bar{1}}\left(2a_1^\dagger\rho a_1 - a_1 a_1^\dagger\rho - \rho a_1 a_1^\dagger\right), \quad (6.54)\end{aligned}$$

where ρ is the system+ancilla density matrix, ν is defined in Eq. (6.53) and η, μ are associated with the damping rates of the amplitudes due to the environmental couplings to the ancilla oscillators,

$$\mu \equiv \pi\rho_{\rm ds}\left(\omega_1\right)\left|g_{\rm d}\left(\omega\right)\right|^2, \quad (6.55)$$

$$\eta \equiv \pi\rho_{\rm ds}\left(\omega_1\right)\left|g_{\rm b1}\left(\omega\right)\right|^2, \quad (6.56)$$

and $N_{\rm i}$ is

$$N_{\rm i} = \frac{1}{e^{\hbar\beta_{\rm i}\omega_{\rm i}} - 1}, \quad (6.57)$$

where $i = 0, \bar{1}$ or d, $\beta_{\rm i}$ is $\left(k_{\rm B}T_i\right)^{-1}$ with T_i the temperature of the bath, and $\omega_{\rm i} = \omega_0$ for $i = 0$ and $\omega_{\rm i} = \omega_1$ for $i = \bar{1}, d$.

The master equation Eq. (6.54) is an evolution equation for the density matrix of the open system formed by the two oscillators. The commutator terms on the first line describe the coherent driving of the ancilla oscillator and the non-linear coupling between the two oscillators in the rotating wave approximation. The remaining terms describe the dissipative interactions with the various baths. The terms contain a form $(N_i + 1)$ describe the emission of phonons into the thermal bath while the ones with

N_i correspond to absorption of phonons from the bath.

Notice that the ancilla is coupled to both the thermal environment and the measurement apparatus and each of these couplings results in analogous emission and absorption terms differing only by coefficients. In principle the environmental and measurement baths can have different temperatures described by $N_{\bar{1}}$ and $N_{\rm d}$, however, the overall width of the ancilla resonance is given by $\kappa = \eta + \mu$, and if uncoupled from the system, the ancilla would reach a steady state consistent with a thermal equilibrium with excitation $N_1 = (\eta N_{\bar{1}} + \mu N_{\rm d})/\kappa$. For the purposes of the evolution of the system-ancilla density matrix we do not need to distinguish between effects arising from the coupling to the thermal bath and those that result from the measurement coupling and we may combine these terms to give

$$\begin{aligned}\frac{d\rho}{dt} = &-\frac{i}{\hbar}\left[\hbar E\left(a_1^\dagger + a_1\right) + \hbar\lambda_{01} a_0^\dagger a_0 a_1^\dagger a_1, \rho\right] \\ &+ \nu(N_0+1)\left(2a_0\rho a_0^\dagger - a_0^\dagger a_0\rho - \rho a_0^\dagger a_0\right) + \nu N_0\left(2a_0^\dagger\rho a_0 - \rho a_0 a_0^\dagger - a_0 a_0^\dagger\rho\right) \\ &+ \kappa(N_1+1)\left(2a_1\rho a_1^\dagger - a_1^\dagger a_1\rho - \rho a_1^\dagger a_1\right) + \kappa N_1\left(2a_1^\dagger\rho a_1 - a_1 a_1^\dagger\rho - \rho a_1 a_1^\dagger\right). \quad (6.58)\end{aligned}$$

The master equation Eq. (6.58) can in principle be numerically integrated. However we will make some further approximations in order to derive a master equation for the system dynamics alone and show that in some limit the readout system coupling results in only the phase diffusion that is required as the backaction for the QND measurement, with no extra noise above this quantum limit. To do this we assume that the ancilla is strongly damped to the measurement apparatus (*i.e.*, $\kappa \simeq \mu \gg \nu$). In this limit the ancilla relaxes rapidly to an oscillating state consistent with the current system state, and as a result its dynamics are slaved to the system oscillator and can in fact be eliminated from the equations of motion. This *adiabatic elimination* is described in the following subsection.

Note that ν, κ are the width of the oscillator vibration amplitude as a function of frequency. The rotating wave (or energy conserving) approximation is only valid if $\omega_0 - \omega_1$ is much greater than the linewidth of the oscillators, *i.e.*, $\omega_0 - \omega_1 \gg \nu, \kappa$. This condition not only allows us to do the rotating approximation but also prevents

tunnelling of phonons between two oscillators.

6.2.2 Adiabatic elimination

For a strongly damped ancilla ($\kappa \gg \nu$) the ancilla state rapidly relaxes to a displaced thermal state, *i.e.*, the thermal state where it is centred at the driven state instead of the vacuum state. So it will be useful to transform the equations of motion in such a way as to make a perturbative expansion around this steady state. The basic idea is to transform the origin of phase space such that the ancilla steady state for the transformed master equation is a thermal state. This transformation will essentially remove the driving term in the master equation. This transformation was utilised by Wiseman and Milburn [41] in their study of a driven harmonic oscillator at zero temperature. Following their approach, we use the displacement operator, $D(\alpha) = \exp\left[\alpha a_1^\dagger - \alpha^* a_1\right]$ with $\alpha = -iE/\kappa$. The transformed system state is $\tilde{\rho} \equiv D(\alpha)\rho D(\alpha)^\dagger$ and we may write the master equation for $\tilde{\rho}$:

$$\begin{aligned}
\dot{\tilde{\rho}} &= D(\alpha)\dot{\rho}D(\alpha)^\dagger \\
&= -i\left|\alpha\right|^2 \lambda_{01}\left[a_0^\dagger a_0, \tilde{\rho}\right] \\
&- i\lambda_{01}\left[a_0^\dagger a_0 a_1^\dagger a_1, \tilde{\rho}\right] - i\lambda_{01}\left[a_0^\dagger a_0\left(\alpha a_1^\dagger + \alpha^* a_1\right), \tilde{\rho}\right] \\
&+ \nu(N_0+1)\left(2a_0\tilde{\rho}a_0^\dagger - a_0^\dagger a_0\tilde{\rho} - \tilde{\rho}a_0^\dagger a_0\right) + \nu N_0\left(2a_0^\dagger\tilde{\rho}a_0 - \tilde{\rho}a_0 a_0^\dagger - a_0 a_0^\dagger\tilde{\rho}\right) \\
&. + \kappa(N_1+1)\left(2a_1\tilde{\rho}a_1^\dagger - a_1^\dagger a_1\tilde{\rho} - \tilde{\rho}a_1^\dagger a_1\right) + \kappa N_1\left(2a_1^\dagger\tilde{\rho}a_1 - a_1 a_1^\dagger\tilde{\rho} - \tilde{\rho}a_1 a_1^\dagger\right). \quad (6.59)
\end{aligned}$$

In this master equation the ancilla oscillator simply damps towards its displaced origin but the excitation of the ancilla oscillations leads to a frequency shift of the system oscillator described by the first three Hamiltonian terms of this equation. The first term is due to the classical mean value of the ancilla oscillator energy and is just a shift in the system oscillation frequency, and thus we may move to an interaction picture at this frequency. This is the most convenient interaction picture in which to perform the adiabatic elimination. The next two terms describe the effect of the fluctuations in the ancilla excitation. The thermal coupling terms (the last two lines)

in the master equation are the same as before.

We extend the techniques of Wiseman and collaborators [41, 42] to the case of a bath at nonzero temperature by expanding the system-ancilla density matrix perturbatively about the ancilla thermal state. The adiabatic elimination will hold when the ancilla is sufficiently strongly damped. These constraints can be understood from our assumption and Eq. (6.59) as the damping rate of the ancilla must be much larger than other terms to have a rapid decay of the ancilla into a steady state. Thus, the adiabatic elimination is valid in a strongly damped regime such that

$$\frac{\lambda_{01}\left|\alpha\right|}{\kappa},\ \frac{\nu}{\kappa}\ \simeq \epsilon \ll 1. \tag{6.60}$$

Note that this means we are assuming that the ancilla oscillator relaxes faster than the system oscillator as well as that the non-linear dynamics are weak compared to the damping of the ancilla oscillator. For the consistency of the following treatment it will also be necessary to have $\lambda_{01}N_1/\kappa \simeq \epsilon^2$. This requirement follows from the second term (non-linear coupling term) in the master equation, and we will explain in detail shortly. This constraint can be achieved consistent with Eq. (6.60), for example, by leaving α finite and choosing $N_1, \lambda_{01}/\kappa \simeq \epsilon$, a regime of low temperature and moderate non-linearity. The approximations are also valid at arbitrary temperature in the limit of strong driving and weak non-linearity such that $\lambda_{01}/\kappa \simeq \epsilon^2$ and $\alpha \simeq \epsilon^{-1}$ hold[3]. Here the scaling of the driving strength is chosen to preserve the measurement sensitivity which will scale with $\lambda_{01}\alpha/\kappa$. In this regime the frequency shift of the system oscillator becomes large.

As mentioned above the readout oscillator is nearly in a thermal state about the shifted position and we expand $\tilde{\rho}$ (with a similar expression for $\dot{\tilde{\rho}}$) in the form

$$\begin{aligned}\tilde{\rho} = \rho_0 \otimes \rho_{N_1} + \rho_1 \otimes a_1^\dagger \rho_{N_1} + \rho_{1^\dagger} \otimes \rho_{N_1} a_1 + \rho_2 \otimes a_1^\dagger \rho_{N_1} a_1 \\ + \rho_{2'} \otimes a_1^{\dagger 2} \rho_{N_1} + \rho_{2'^\dagger} \otimes \rho_{N_1} a_1^2 + O\left(\epsilon^3\right).\end{aligned} \tag{6.61}$$

[3]However, the driving strength is chosen in such a way to avoid the bi-stability region caused by the anharmonicity of the oscillator, see Chapter 8.

where ρ_{N_i} is the thermal density matrix for the ancilla and ρ_i acts on the system oscillator with the subscripts indicating orders of magnitude in ϵ. The scalings of the different parameters with ϵ have been chosen to guarantee the consistency of this expansion. The thermal state of an oscillator in terms of the average excitation number N_1 is

$$\rho_{N_1} = \sum_{n=0} \frac{1}{1+N_1} \left(\frac{N_1}{1+N_1} \right)^n |n\rangle\langle n|. \tag{6.62}$$

Note that we have restricted Eq. (6.61) to normal ordered terms using the following identities:

$$\rho_{N_1} a_1^\dagger = \frac{N_1}{N_1+1} a_1^\dagger \rho_{N_1}, \tag{6.63}$$

$$a_1 \rho_{N_1} = \frac{N_1}{N_1+1} \rho_{N_1} a_1. \tag{6.64}$$

Using these identities, the term that contains $a_1 \rho_{N_1} a_1^\dagger$ and all other anti-normal terms can be expressed in terms of normal ordered terms.

The thermal state in Eq. (6.62) is the steady state solution of the master equation, $\dot{\rho} = \mathcal{L}_{\kappa,N_1}[\rho]$, for an oscillator with lowering operator a_1

$$\begin{aligned} \dot{\rho} = \mathcal{L}_{\kappa,N_1}[\rho] \equiv \kappa(N_1+1) \left(2a_1 \rho a_1^\dagger - a_1^\dagger a_1 \rho - \rho a_1^\dagger a_1 \right) \\ + \kappa N_1 \left(2a_1^\dagger \rho a_1 - a_1 a_1^\dagger \rho - \rho a_1 a_1^\dagger \right). \end{aligned} \tag{6.65}$$

Note that

$$\mathrm{Tr}_1(\rho_{N_1}) = \mathrm{Tr}_1 \left(\sum_n \frac{1}{1+N_1} \left(\frac{N_1}{1+N_1} \right)^n |n\rangle \langle n| \right) = 1,$$

$$\mathrm{Tr}_1(a_1^\dagger \rho_{N_1} a_1) = \mathrm{Tr}_1 \left(\sum_n \frac{1}{1+N_1} \left(\frac{N_1}{1+N_1} \right)^n (n+1) |n+1\rangle \langle n+1| \right) \tag{6.66}$$

$$= N_1 + 1, \tag{6.67}$$

so that the system density matrix after tracing out the ancilla state is

$$\rho_{\rm s} = {\rm Tr}_1\left\{\rho\right\} = \rho_0 + (1+N_1)\rho_2. \tag{6.68}$$

This form actually reduces to the form presented by Wiseman and Milburn [41] in the zero temperature limit $N_1 \to 0$.

Now we start to eliminate the ancilla operators from Eq. (6.59). Firstly we separate the master equation into four parts

$$\dot{\tilde{\rho}} = \dot{\rho}^{\rm P1} + \dot{\rho}^{\rm P2} + \dot{\rho}^{\rm P3} + \dot{\rho}^{\rm P4}, \tag{6.69}$$

where

$$\dot{\rho}^{\rm P1} = \mathcal{L}_{\kappa,N_1}\left[\rho_{N_1}\right], \tag{6.70}$$

$$\dot{\rho}^{\rm P2} = -i\lambda_{01}\left[a_0^\dagger a_0 a_1^\dagger a_1, \tilde{\rho}\right], \tag{6.71}$$

$$\dot{\rho}^{\rm P3} = -i\lambda_{01}\left[a_0^\dagger a_0\left(\alpha a_1^\dagger + \alpha^* a_1\right), \tilde{\rho}\right], \tag{6.72}$$

$$\begin{aligned}\dot{\rho}^{\rm P4} = &-i\left|\alpha\right|^2\lambda_{01}\left[a_0^\dagger a_0, \tilde{\rho}\right] + \nu(N_0+1)\left(2a_0\tilde{\rho}a_0^\dagger - a_0^\dagger a_0\tilde{\rho} - \tilde{\rho}a_0^\dagger a_0\right)\\ &+ \nu N_0\left(2a_0^\dagger\tilde{\rho}a_0 - \tilde{\rho}a_0 a_0^\dagger - a_0 a_0^\dagger\tilde{\rho}\right),\end{aligned} \tag{6.73}$$

and we have defined

$$\begin{aligned}\mathcal{L}_{\kappa,N_i}\left[\rho_{N_i}\right] \equiv\ &\kappa(N_1+1)\left(2a_1\tilde{\rho}a_1^\dagger - a_1^\dagger a_1\tilde{\rho} - \tilde{\rho}a_1^\dagger a_1\right)\\ &+ \kappa N_1\left(2a_1^\dagger\tilde{\rho}a_1 - a_1 a_1^\dagger\tilde{\rho} - \tilde{\rho}a_1 a_1^\dagger\right).\end{aligned} \tag{6.74}$$

Equation (6.73) does not need adiabatic elimination since it is already in a reduced form (*i.e.*, involving the system operators only). We now evaluate each of the remaining three terms.

6.2.2.1 Evaluation of $\dot{\rho}^{\mathrm{P1}}$

We change each term to a normal ordered form by using Eq. (6.64) together with the commutator relation, $\left[a_1, a_1^\dagger\right] = 1$. This will lead to a number of terms that we evaluate in turn. To do this we substitute the expansion form for $\tilde{\rho}$, Eq. (6.61) into Eq. (6.70).

For example, the term $\mathcal{L}_{\kappa,N_1}\left[a_1^\dagger \rho_{N_1} a_1\right]$,

$$\begin{aligned}\mathcal{L}_{\kappa,N_1}\left[a_1^\dagger \rho_{N_1} a_1\right] = \kappa(N_1+1)\left(2a_1 a_1^\dagger \rho_{N_1} a_1 a_1^\dagger - a_1^\dagger a_1 a_1^\dagger \rho_{N_1} a_1 - a_1^\dagger \rho_{N_1} a_1 a_1^\dagger a_1\right) \\ + \kappa N_1\left(2a_1^\dagger a_1^\dagger \rho_{N_1} a_1 a_1 - a_1 a_1^\dagger a_1^\dagger \rho_{N_1} a_1 - a_1^\dagger \rho_{N_1} a_1 a_1 a_1^\dagger\right) \qquad (6.75)\end{aligned}$$

can be transformed into a normal ordered form

$$\mathcal{L}_{\kappa,N_1}\left[a_1^\dagger \rho_{N_1} a_1\right] = -2\kappa a_1^\dagger \rho_{N_1} a_1 + 2\kappa(N_1+1)\rho_{N_1}. \qquad (6.76)$$

For some cases we will need to disregard the off-diagonal terms further away from the diagonal terms than the expansion range of the ancilla state since any state further away from the diagonal decays much faster, at an exponential rate. (We will analyse decoherence in detail in § 6.3).

Similarly, we can derive the following results:

$$\mathcal{L}_{\kappa,N_1}\left[\rho_{N_1}\right] = 0, \qquad (6.77)$$

$$\mathcal{L}_{\kappa,N_1}\left[\rho_{N_1} a_1\right] \simeq -\kappa \rho_{N_1} a_1, \qquad (6.78)$$

$$\mathcal{L}_{\kappa,N_1}\left[a_1^\dagger \rho_{N_1}\right] \simeq -\kappa a_1^\dagger \rho_{N_1}, \qquad (6.79)$$

$$\mathcal{L}_{\kappa,N_1}\left[\rho_{N_1} a_1 a_1\right] \simeq -2\kappa \rho_{N_1} a_1 a_1, \qquad (6.80)$$

$$\mathcal{L}_{\kappa,N_1}\left[a_1^\dagger a_1^\dagger \rho_{N_1}\right] \simeq -2\kappa a_1^\dagger a_1^\dagger \rho_{N_1}. \qquad (6.81)$$

Then from Eq. (6.70) $\dot{\rho}^{\mathrm{P1}}$ is

$$\begin{aligned}\dot{\rho}^{\mathrm{P1}} &= \rho_0 \otimes \mathcal{L}_{\kappa,N_1}\left[\rho_{N_1}\right] + \rho_1 \otimes \mathcal{L}_{\kappa,N_1}\left[a_1^\dagger \rho_{N_1}\right] + \rho_{1^\dagger} \otimes \mathcal{L}_{\kappa,N_1}\left[\rho_{N_1} a_1\right] \\ &+ \rho_2 \otimes \mathcal{L}_{\kappa,N_1}\left[a_1^\dagger \rho_{N_1} a_1\right] + \rho_{2'} \otimes \mathcal{L}_{\kappa,N_1}\left[a_1^\dagger a_1^\dagger \rho_{N_1}\right] + \rho_{2'^\dagger} \otimes \mathcal{L}_{\kappa,N_1}\left[\rho_{N_1} a_1 a_1\right] \\ &\simeq -\kappa\rho_1 a_1^\dagger \rho_{N_1} - \kappa\rho_{1^\dagger}\rho_{N_1} a_1 - 2\kappa\rho_2 a_1^\dagger \rho_{N_1} a_1 + 2\kappa(N_1+1)\rho_2\rho_{N_1} \\ &- 2\kappa\rho_{2'} a_1^\dagger a_1^\dagger \rho_{N_1} - 2\kappa\rho_{2'^\dagger}\rho_{N_1} a_1 a_1 + O\left(\epsilon^3\right). \end{aligned} \tag{6.82}$$

Writing Eq. (6.82) in the form of Eq. (6.61) gives

$$\dot{\rho}_0^{\mathrm{P1}} = 2\kappa(N_1+1)\rho_2\rho_{N_1}, \tag{6.83}$$

$$\dot{\rho}_1^{\mathrm{P1}} = -\kappa\rho_1, \tag{6.84}$$

$$\dot{\rho}_{1^\dagger}^{\mathrm{P1}} = -\kappa\rho_{1^\dagger}, \tag{6.85}$$

$$\dot{\rho}_2^{\mathrm{P1}} = -2\kappa\rho_2, \tag{6.86}$$

$$\dot{\rho}_{2'}^{\mathrm{P1}} = -2\kappa\rho_{2'}, \tag{6.87}$$

$$\dot{\rho}_{2'^\dagger}^{\mathrm{P1}} = -2\kappa\rho_{2'^\dagger}. \tag{6.88}$$

6.2.2.2 Evaluation of $\dot{\rho}^{\mathrm{P2}} = -i\lambda_{01}\left[a_0^\dagger a_0 a_1^\dagger a_1, \rho\right]$

Consider the term of ρ that is the lowest order in ϵ, *i.e.*, $\rho_0 \otimes \rho_{N_1}$. Evaluating the commutator $-i\lambda_{01}\left[a_0^\dagger a_0 a_1^\dagger a_1, \rho\right]$ results in

$$\begin{aligned}-i\lambda_{01}\left[a_0^\dagger a_0 a_1^\dagger a_1, \rho_0 \otimes \rho_{N_1}\right] &= -i\lambda_{01}\left[a_0^\dagger a_0 \rho_0 \otimes a_1^\dagger a_1 \rho_{N_1} - \rho_0 a_0^\dagger a_0 \otimes \rho_{N_1} a_1^\dagger a_1\right] \\ &= -i\lambda_{01}\frac{N_1}{N_1+1}\left[a_0^\dagger a_0 \rho_0 - \rho_0 a_0^\dagger a_0\right] \otimes a_1^\dagger \rho_{N_1} a_1. \end{aligned} \tag{6.89}$$

Since the ancilla operators appearing in this form are $a_1^\dagger \rho_{N_1} a_1$, taking a trace of Eq. (6.89) will result in terms contributing to the evaluation of $\dot{\rho}_2^{\mathrm{P2}}$. Then we can write the expression for $\dot{\rho}_2$ including both $\dot{\rho}^{\mathrm{P2}}$ and also $\dot{\rho}^{\mathrm{P1}}$ from Eq. (6.87)

$$\dot{\rho}_2 = -i\lambda_{01} N_1\left[a_0^\dagger a_0, \rho_0\right] - 2\kappa\rho_2 + \text{ other } \mathcal{O}\left(\epsilon^2\right) \text{ terms}, \tag{6.90}$$

where "other terms" contain $N_1\left[a_0^\dagger a_0, \rho_i\right]$ with ρ_i higher order of ρ components, and terms coming from evaluating $\dot{\rho}_2^{\mathrm{P3}}$. Here we are interested in the lowest order term coming from $-i\lambda_{01}\left[a_0^\dagger a_0 a_1^\dagger a_1, \rho\right]$. In the steady state, ρ_2 would have a solution

$$\rho_2 = -i\frac{\lambda_{01}}{2\kappa}N_1\left[a_0^\dagger a_0, \rho_0\right] + \frac{1}{2\kappa}\text{ other }\mathcal{O}\left(\epsilon^2\right)\text{ terms.} \tag{6.91}$$

Since ρ_2 is, by definition, of order of ϵ^2, we must have $\lambda_{01}N_1/\kappa \simeq \mathcal{O}\left(\epsilon^2\right)$ to be consistent. Thus we can see that the other terms in Eq. (6.90) are actually $\mathcal{O}\left(\epsilon^2\right)$ or higher, so that

$$\dot{\rho}_2^{\mathrm{P2}} \simeq -i\lambda_{01}N_1\left[a_0^\dagger a_0, \rho_0\right]. \tag{6.92}$$

6.2.2.3 Evaluation of $\dot{\rho}^{\mathrm{P3}} = -i\lambda_{01}\left[a_0^\dagger a_0\left(\alpha a_1^\dagger + \alpha^* a_1\right), \rho\right]$

The same reasoning as for the $\dot{\rho}^{\mathrm{P2}}$ evaluation can be applied. Since we have

$$\dot{\rho}_i = -C\kappa\rho_i + \text{ other }\mathcal{O}\left(\epsilon^2\right)\text{ terms,} \tag{6.93}$$

where $C = 2$ for diagonal terms and 1 for off-diagonal terms, the term obtained from the evaluation of $\dot{\rho}^{\mathrm{P3}}$ will lead to components of ρ with the coefficient $\lambda_{01}\alpha/C\kappa$ or $\lambda_{01}\alpha^*/C\kappa$ in steady state, which are $\mathcal{O}\left(\epsilon\right)$. This implies that we need to take terms only up to first order in ρ and can discard the higher order terms to give an expression up to $\mathcal{O}\left(\epsilon^2\right)$.

In order to evaluate $-i\lambda_{01}\left[a_0^\dagger a_0\left(\alpha a_1^\dagger + \alpha^* a_1\right), \rho\right]$, we need to calculate $\alpha a_1^\dagger\tilde{\rho}$, $\alpha^* a_1\tilde{\rho}, \tilde{\rho}\alpha a_1^\dagger$, and $\tilde{\rho}\alpha^* a_1$. The first term

$$\begin{aligned}\alpha a_1^\dagger\tilde{\rho} = {} & \alpha\rho_0 \otimes a_1^\dagger\rho_{N_1} + \alpha\rho_1 \otimes a_1^\dagger a_1^\dagger\rho_{N_1} + \alpha\rho_{1^\dagger} \otimes a_1^\dagger\rho_{N_1}a_1 \\ & + \alpha\rho_2 \otimes a_1^\dagger a_1^\dagger\rho_{N_1}a_1 + \alpha\rho_{2'} \otimes a_1^\dagger a_1^\dagger a_1^\dagger\rho_{N_1} + \alpha\rho_{2'^\dagger} \otimes a_1^\dagger\rho_{N_1}a_1^2\end{aligned} \tag{6.94}$$

is already normal ordered. So removing the off-diagonal terms that are further away

from the expanded range as done in the evaluations of $\dot{\rho}_2^{\mathrm{P1}}$ and $\dot{\rho}_2^{\mathrm{P2}}$, we obtain

$$\alpha a_1^\dagger \tilde{\rho} \simeq \alpha\rho_0 \otimes a_1^\dagger \rho_{N_1} + \alpha\rho_1 \otimes a_1^\dagger a_1^\dagger \rho_{N_1} + \alpha\rho_{1^\dagger} \otimes a_1^\dagger \rho_{N_1} a_1. \tag{6.95}$$

For the term $\alpha^* a_1 \tilde{\rho}$ we have

$$\begin{aligned}\alpha^* a_1 \tilde{\rho} = {} & \alpha^*\rho_0 \otimes a_1\rho_{N_1} + \alpha^*\rho_1 \otimes a_1 a_1^\dagger \rho_{N_1} + \alpha^*\rho_{1^\dagger} \otimes a_1\rho_{N_1}a_1 \\ & + \alpha^*\rho_2 \otimes a_1 a_1^\dagger \rho_{N_1} a_1 + \alpha^*\rho_{2'} \otimes a_1 a_1^\dagger a_1^\dagger \rho_{N_1} + \alpha^*\rho_{2'^\dagger} \otimes a_1\rho_{N_1}a_1^2,\end{aligned} \tag{6.96}$$

which can be manipulated to give a normal ordered form

$$\begin{aligned}\alpha^* a_1 \tilde{\rho} = {} & \alpha^*\rho_1 \otimes \rho_{N_1} + \alpha^*\left[\frac{N_1}{N_1+1}\rho_0 + \rho_2\right]\rho_{N_1}a_1 + 2\alpha^*\rho_{2'} \otimes a_1^\dagger\rho_{N_1} \\ & + \alpha^*\frac{N_1}{N_1+1}\rho_1 \otimes a_1^\dagger \rho_{N_1} a_1 + \alpha^*\frac{N_1}{N_1+1}\rho_{1^\dagger} \otimes \rho_{N_1}a_1a_1.\end{aligned} \tag{6.97}$$

Similarly for $\tilde{\rho}\alpha a_1^\dagger$, we obtain

$$\begin{aligned}\tilde{\rho}\alpha a_1^\dagger = {} & \alpha\rho_{1^\dagger} \otimes \rho_{N_1} + \alpha\left[\frac{N_1}{N_1+1}\rho_0 + \rho_2\right] \otimes a_1^\dagger\rho_{N_1} + 2\alpha\rho_{2'^\dagger} \otimes \rho_{N_1}a_1 \\ & + \alpha\frac{N_1}{N_1+1}\rho_1 \otimes a_1^{\dagger 2}\rho_{N_1} + \alpha\frac{N_1}{N_1+1}\rho_{1^\dagger} \otimes a_1^\dagger\rho_{N_1}a_1.\end{aligned} \tag{6.98}$$

Finally for $\tilde{\rho}\alpha^* a_1$, no manipulation is necessary since it is already normal ordered and we have

$$\tilde{\rho}\alpha^* a_1 = \alpha^*\rho_0 \otimes \rho_{N_1}a_1 + \alpha^*\rho_1 \otimes a_1^\dagger\rho_{N_1}a_1 + \alpha^*\rho_{1^\dagger} \otimes \rho_{N_1}a_1a_1. \tag{6.99}$$

To calculate Eq. (6.72) we need the following combinations

$$\begin{aligned}\alpha a_1^\dagger\tilde{\rho} + \alpha^* a_1\tilde{\rho} = {} & \alpha^*\rho_1 \otimes \rho_{N_1} + [\alpha\rho_0 + 2\alpha^*\rho_{2'}] \otimes a_1^\dagger\rho_{N_1} \\ & + \alpha^*\left[\frac{N_1}{N_1+1}\rho_0 + \rho_2\right]\rho_{N_1}a_1 + \left[\alpha\rho_{1^\dagger} + \alpha^*\frac{N_1}{N_1+1}\rho_1\right] \otimes a_1^\dagger\rho_{N_1}a_1 \\ & + \alpha\rho_1 \otimes a_1^\dagger a_1^\dagger\rho_{N_1} + \alpha^*\frac{N_1}{N_1+1}\rho_{1^\dagger} \otimes \rho_{N_1}a_1a_1,\end{aligned} \tag{6.100}$$

$$\tilde{\rho}\alpha a_1^\dagger + \tilde{\rho}\alpha^* a_1 = \alpha\rho_{1^\dagger}\otimes\rho_{N_1} + \alpha\left[\frac{N_1}{N_1+1}\rho_0+\rho_2\right]\otimes a_1^\dagger\rho_{N_1} + \left[2\alpha\rho_{2'^\dagger}+\alpha^*\rho_0\right]\otimes\rho_{N_1}a_1 + \left[\alpha\frac{N_1}{N_1+1}\rho_{1^\dagger}+\alpha^*\rho_1\right]\otimes a_1^\dagger\rho_{N_1}a_1 + \alpha\frac{N_1}{N_1+1}\rho_1\otimes a_1^{\dagger 2}\rho_{N_1} + \alpha^*\rho_{1^\dagger}\otimes\rho_{N_1}a_1a_1. \tag{6.101}$$

Applying the above results to calculate $\dot{\rho}^{\mathrm{P3}} = -i\lambda_{01}\left[a_0^\dagger a_0\left(\alpha a_1^\dagger+\alpha^* a_1\right),\rho\right]$,

$$\begin{aligned}\dot{\rho}^{\mathrm{P3}} &= -i\lambda_{01}\left[\alpha^* a_0^\dagger a_0\rho_1 - \alpha\rho_{1^\dagger}a_0^\dagger a_0\right]\otimes\rho_{N_1}\\ &- i\lambda_{01}\left[a_0^\dagger a_0\left[\alpha\rho_0+2\alpha^*\rho_{2'}\right]-\alpha\left[\frac{N_1}{N_1+1}\rho_0+\rho_2\right]a_0^\dagger a_0\right]\otimes a_1^\dagger\rho_{N_1}\\ &- i\lambda_{01}\left[\alpha^* a_0^\dagger a_0\left[\frac{N_1}{N_1+1}\rho_0+\rho_2\right]-\left[2\alpha\rho_{2'^\dagger}+\alpha^*\rho_0\right]a_0^\dagger a_0\right]\otimes\rho_{N_1}a_1\\ &- i\lambda_{01}\left[\alpha a_0^\dagger a_0\rho_1-\alpha\frac{N_1}{N_1+1}\rho_1 a_0^\dagger a_0\right]\otimes a_1^\dagger a_1^\dagger\rho_{N_1}\\ &- i\lambda_{01}\left[a_0^\dagger a_0\left[\alpha\rho_{1^\dagger}+\alpha^*\frac{N_1}{N_1+1}\rho_1\right]-\left[\alpha\frac{N_1}{N_1+1}\rho_{1^\dagger}+\alpha^*\rho_1\right]a_0^\dagger a_0\right]\otimes a_1^\dagger\rho_{N_1}a_1\\ &- i\lambda_{01}\left[\alpha^*\frac{N_1}{N_1+1}a_0^\dagger a_0\rho_{1^\dagger}+\alpha^*\rho_{1^\dagger}a_0^\dagger a_0\right]\otimes\rho_{N_1}a_1a_1,\end{aligned} \tag{6.102}$$

which can be separated to have the form of Eq. (6.61)

$$\dot{\rho}_0^{\mathrm{P3}} = -i\lambda_{01}\left[\alpha^* a_0^\dagger a_0\rho_1-\alpha\rho_{1^\dagger}a_0^\dagger a_0\right]+\mathcal{O}\left(\epsilon^3\right), \tag{6.103}$$

$$\dot{\rho}_1^{\mathrm{P3}} = -i\lambda_{01}\left[a_0^\dagger a_0\left[\alpha\rho_0+2\alpha^*\rho_{2'}\right]-\alpha\left[\frac{N_1}{N_1+1}\rho_0+\rho_2\right]a_0^\dagger a_0\right]\otimes a_1^\dagger\rho_{N_1}+\mathcal{O}\left(\epsilon^3\right), \tag{6.104}$$

$$\dot{\rho}_{1^\dagger}^{\mathrm{P3}} = -i\lambda_{01}\left[\alpha^* a_0^\dagger a_0\left[\frac{N_1}{N_1+1}\rho_0+\rho_2\right]-\left[2\alpha\rho_{2'^\dagger}+\alpha^*\rho_0\right]a_0^\dagger a_0\right]+\mathcal{O}\left(\epsilon^3\right), \tag{6.105}$$

$$\dot{\rho}_2^{\mathrm{P3}} = -i\lambda_{01}\left[a_0^\dagger a_0\left[\alpha\rho_{1^\dagger}+\alpha^*\frac{N_1}{N_1+1}\rho_1\right]-\left[\alpha\frac{N_1}{N_1+1}\rho_{1^\dagger}+\alpha^*\rho_1\right]a_0^\dagger a_0\right]+\mathcal{O}\left(\epsilon^3\right), \tag{6.106}$$

$$\dot{\rho}_{2'}^{\mathrm{P3}} = -i\lambda_{01}\alpha\left[a_0^\dagger a_0\rho_1-\frac{N_1}{N_1+1}\rho_1 a_0^\dagger a_0\right]+\mathcal{O}\left(\epsilon^3\right), \tag{6.107}$$

$$\dot{\rho}_{\rho_{2'^\dagger}}^{\mathrm{P3}} = -i\lambda_{01}\alpha^*\left[\frac{N_1}{N_1+1}a_0^\dagger a_0\rho_{1^\dagger}-\rho_{1^\dagger}a_0^\dagger a_0\right]+\mathcal{O}\left(\epsilon^3\right). \tag{6.108}$$

6.2.2.4 Adiabatically eliminating the ancilla operators

Combining $\dot{\rho}^{\mathrm{P1}}, \dot{\rho}^{\mathrm{P2}}$ and $\dot{\rho}^{\mathrm{P3}}$ and defining this partial sum as

$$\dot{\rho}^{\mathrm{P}} = \dot{\rho}^{\mathrm{P1}} + \dot{\rho}^{\mathrm{P2}} + \dot{\rho}^{\mathrm{P3}}, \tag{6.109}$$

we obtain

$$\dot{\rho}_0^{\mathrm{P}} = -i\lambda_{01}\left[\alpha^* a_0^\dagger a_0 \rho_1 - \alpha \rho_{1^\dagger} a_0^\dagger a_0\right] + 2\kappa(N_1+1)\rho_2 + \kappa\mathcal{O}\left(\epsilon^3\right), \tag{6.110}$$

$$\dot{\rho}_1^{\mathrm{P}} = -i\lambda_{01}\left[a_0^\dagger a_0\left[\alpha\rho_0 + 2\alpha^*\rho_{2'}\right] - \alpha\left[\frac{N_1}{N_1+1}\rho_0 + \rho_2\right] a_0^\dagger a_0\right] - \kappa\rho_1 + \kappa\mathcal{O}\left(\epsilon^3\right), \tag{6.111}$$

$$\dot{\rho}_{1^\dagger}^{\mathrm{P}} = -i\lambda_{01}\left[\alpha^* a_0^\dagger a_0\left[\frac{N_1}{N_1+1}\rho_0 + \rho_2\right] - \left[2\alpha\rho_{2'^\dagger} + \alpha^*\rho_0\right] a_0^\dagger a_0\right] - \kappa\rho_{1^\dagger} + \kappa\mathcal{O}\left(\epsilon^3\right), \tag{6.112}$$

$$\begin{aligned}\dot{\rho}_2^{\mathrm{P}} = &-i\lambda_{01}\left[a_0^\dagger a_0\left[\alpha\rho_{1^\dagger} + \alpha^*\frac{N_1}{N_1+1}\rho_1\right] - \left[\alpha\frac{N_1}{N_1+1}\rho_{1^\dagger} + \alpha^*\rho_1\right] a_0^\dagger a_0\right] \\ &- 2\kappa\rho_2 - i\lambda_{01}\frac{N_1}{N_1+1}\left[a_0^\dagger a_0, \rho_0\right] + \kappa\mathcal{O}\left(\epsilon^3\right),\end{aligned} \tag{6.113}$$

$$\dot{\rho}_{2'}^{\mathrm{P}} = -i\lambda_{01}\alpha\left[a_0^\dagger a_0\rho_1 - \frac{N_1}{N_1+1}\rho_1 a_0^\dagger a_0\right] - 2\kappa\rho_{2'} + \kappa\mathcal{O}\left(\epsilon^3\right), \tag{6.114}$$

$$\dot{\rho}_{\rho_{2'^\dagger}}^{\mathrm{P}} = -i\lambda_{01}\alpha^*\left[\frac{N_1}{N_1+1}a_0^\dagger a_0\rho_{1^\dagger} - \rho_{1^\dagger}a_0^\dagger a_0\right] - 2\kappa\rho_{2'^\dagger} + \kappa\mathcal{O}\left(\epsilon^3\right). \tag{6.115}$$

Notice that all off-diagonal terms have the form

$$\dot{\rho}_i^{\mathrm{P}} = \sum_j f\left(\rho_j\right) - C\rho_i, \tag{6.116}$$

where $i = 1, 2'$ and $C = 2\kappa$ for $i = 2'$ and $C = \kappa$ for $i = 1$. When κ is large, the solution to above equation quickly decays to the steady state. So we perform adiabatic elimination by setting $\dot{\rho}_{2'} = \dot{\rho}_{2'^\dagger} = 0$ and obtain the expressions for $\rho_{2'}$ and

$\rho_{2'^\dagger}$:

$$\rho_{2'} = -i\frac{\lambda_{01}\alpha}{2\kappa}\left[a_0^\dagger a_0\rho_1 - \frac{N_1}{N_1+1}\rho_1 a_0^\dagger a_0\right] + \mathcal{O}\left(\epsilon^3\right), \tag{6.117}$$

$$\rho_{2'^\dagger} = -i\frac{\lambda_{01}\alpha^*}{2\kappa}\left[\frac{N_1}{N_1+1}a_0^\dagger a_0\rho_{1^\dagger} - \rho_{1^\dagger}a_0^\dagger a_0\right] + \mathcal{O}\left(\epsilon^3\right). \tag{6.118}$$

Similarly, using Eqs. (6.117, 6.118) and setting $\dot{\rho}_1 = \dot{\rho}_{1^\dagger} = 0$ we find the expressions for ρ_1 and $\rho_{1^\dagger}$.

$$\begin{aligned}\rho_1 &= -i\frac{\lambda_{01}}{\kappa}\left[a_0^\dagger a_0\left[\alpha\rho_0 + 2\alpha^*\rho_{2'}\right] - \alpha\left[\frac{N_1}{N_1+1}\rho_0 + \rho_2\right]a_0^\dagger a_0\right] \\ &= -i\frac{\lambda_{01}}{\kappa}\left[\alpha a_0^\dagger a_0\rho_0 - \alpha\frac{N_1}{N_1+1}\rho_0 a_0^\dagger a_0\right] + \mathcal{O}\left(\epsilon^2\right).\end{aligned} \tag{6.119}$$

$$\begin{aligned}\rho_{1^\dagger} &= -i\frac{\lambda_{01}}{\kappa}\left[\alpha^* a_0^\dagger a_0\left[\frac{N_1}{N_1+1}\rho_0 + \rho_2\right] - \left[2\alpha\rho_{2'^\dagger} + \alpha^*\rho_0\right]a_0^\dagger a_0\right] \\ &= -i\frac{\lambda_{01}}{\kappa}\left[\alpha^* a_0^\dagger a_0\frac{N_1}{N_1+1}\rho_0 - \alpha^*\rho_0 a_0^\dagger a_0\right] + \mathcal{O}\left(\epsilon^2\right).\end{aligned} \tag{6.120}$$

We now evaluate the expression Eq. (6.68) using Eqs. (6.117)-(6.120) together with Eqs. (6.110, 6.113). After manipulating terms, we obtain

$$\mathrm{Tr}_1\left\{\dot{\rho}^{\mathrm{P}}\right\} = -\frac{\lambda_{01}^2\left|\alpha\right|^2(1+2N_1)}{\kappa}\left[a_0^\dagger a_0,\left[a_0^\dagger a_0,\rho\right]\right] - i\tilde{\lambda}_{01}N_1\left[a_0^\dagger a_0,\rho\right] + \kappa\mathcal{O}\left(\epsilon^3\right). \tag{6.121}$$

Adding $\dot{\rho}^{\mathrm{P4}}$, the full expression Eq. (6.109) and replacing ρ_0 with ρ_{s}

$$\begin{aligned}\dot{\rho}_{\mathrm{s}} = &-\frac{\lambda_{01}^2\left|\alpha\right|^2(1+2N_1)}{\kappa}\left[a_0^\dagger a_0,\left[a_0^\dagger a_0,\rho_{\mathrm{s}}\right]\right] \\ &- i\left\{\omega_0 + \lambda_{01}(\left|\alpha\right|^2 + N_1)\right\}\left[a_0^\dagger a_0,\rho_{\mathrm{s}}\right] \\ &+ \nu\left(N_0+1\right)\left(2a_0\rho_{\mathrm{s}}a_0^\dagger - a_0^\dagger a_0\rho_{\mathrm{s}} - \rho_{\mathrm{s}}a_0^\dagger a_0\right) \\ &+ \nu N_0\left(2a_0^\dagger\rho_{\mathrm{s}}a_0 - \rho_{\mathrm{s}}a_0 a_0^\dagger - a_0 a_0^\dagger\rho_{\mathrm{s}}\right).\end{aligned} \tag{6.122}$$

Equation (6.122) is the master equation for the system density matrix. The first

term is associated with the measurement backaction and induces diffusion in the oscillator phase as discussed in the next subsection. Note that our scheme is a QND measurement and the backaction does not cause changes in the system number state. The second term in Eq. (6.122) arises from a harmonic oscillator Hamiltonian for the system oscillator with an energy shift due to the mean excitation of the ancilla. There are two contributions; one from the driving term $E(a_1 + a_1^\dagger)$ and the second from the thermal excitation of the ancilla N_1. This means that the QND measurement counts phonons of the mechanical oscillator with the modified oscillation frequency $\omega_0 + \lambda_{01}^2(|\alpha|^2 + N_1)$. The last two terms in Eq. (6.122) are associated with the system-environment coupling, which may cause transitions between the number states of the system oscillator.

6.3 Analysis of the master equation

We now analyse the first two terms of the following master equation. For convenience, let us disregard the thermal bath - system interaction (*i.e.*, set $\nu = 0$ in Eq. (6.122)) and write the master equation as

$$\frac{d\rho_{\rm s}}{dt} = -i\left(\omega_0 + \Delta\omega\right)\left[a_0^\dagger a_0, \rho_{\rm s}\right] - \Gamma\left[a_0^\dagger a_0, \left[a_0^\dagger a_0, \rho_{\rm s}\right]\right], \tag{6.123}$$

where

$$\Delta\omega \equiv \lambda_{01}(|\alpha|^2 + N_1), \tag{6.124}$$

$$\Gamma \equiv \frac{\lambda_{01}^2 |\alpha|^2 (1 + 2N_1)}{\kappa}. \tag{6.125}$$

The equations of motion for the matrix elements are

$$\begin{aligned}\frac{d\left\langle n\left|\rho_{\mathrm{s}}\right|m\right\rangle}{dt} &= -i\left(\omega_0+\Delta\omega\right)\left\{\left\langle n\right|a_0^{\dagger}a_0\rho v\left|m\right\rangle-\left\langle n\right|\rho_{\mathrm{s}}a_0^{\dagger}a_0\left|m\right\rangle\right\}\\ &\quad+\Gamma\left\{\left\langle n\right|2a_0^{\dagger}a_0\rho_{\mathrm{s}}a_0^{\dagger}a_0\left|m\right\rangle-\left\langle n\right|\left(a_0^{\dagger}a_0\right)^2\rho_{\mathrm{s}}\left|m\right\rangle-\left\langle n\right|\rho_{\mathrm{s}}\left(a_0^{\dagger}a_0\right)^2\left|m\right\rangle\right\}\\ &= \left[-i\left(\omega_0+\Delta\omega\right)\left(n-m\right)-\Gamma\left(n-m\right)^2\right]\left\langle n\right|\rho_{\mathrm{s}}\left|m\right\rangle, \qquad (6.126)\end{aligned}$$

and the solution to the differential equation above is

$$\left\langle n\left|\rho_{\mathrm{s}}\left(t\right)\right|m\right\rangle=\exp\left[-i\left(\omega_0+\Delta\omega\right)\left(n-m\right)t\right]\exp\left[-\Gamma\left(n-m\right)^2t\right]\left\langle n\right|\rho_{\mathrm{s}}\left|m\right\rangle. \quad (6.127)$$

From the equation above, we notice several features: Firstly the second term in Eq. (6.123) produces no change in number state. Secondly, this term causes off-diagonal elements to decay away to zero. This decay of off-diagonal term is known as decoherence. Since the decoherence rate is proportional to $\Gamma\left(n-m\right)^2$, the further a term is from the diagonal, the faster it decays.

Next, we show that the term $\Gamma\left[a_0^{\dagger}a_0,\left[a_0^{\dagger}a_0,\rho_{\mathrm{s}}\right]\right]$ leads to phase diffusion. For simplicity, consider a master equation consisting of just this term:

$$\frac{d\rho_{\mathrm{s}}}{dt}=-\Gamma\left[a_0^{\dagger}a_0,\left[a_0^{\dagger}a_0,\rho_{\mathrm{s}}\right]\right]. \qquad (6.128)$$

To analyse this master equation, it is convenient to change the representation to a coherent state form. Note that any operator can be expressed in the coherent states basis $\left|\alpha\right\rangle$, labelled by the complex number α. In fact it is well-known that because of the overcompleteness every density operator can be uniquely represented in terms of the diagonal elements by just $\varphi\left(\alpha\right)=\left\langle\alpha\left|\rho\right|\alpha\right\rangle$. Here we use the Q-representation which generates a quasi-probability density of the system. The Q function is defined

as

$$Q(\alpha,\alpha^*) \equiv \frac{1}{\pi}\langle\alpha|\rho|\alpha\rangle, \tag{6.129}$$

$$\int d^2\alpha Q(\alpha,\alpha^*) = 1. \tag{6.130}$$

The mapping between $Q(\alpha,\alpha^*)$ and ρ is one to one [43] due to the overcompleteness of the coherent states. To evaluate the commutators in Eq. (6.128) we need to know how the creation and annihilation operators act on a coherent states. First we have

$$a|\alpha\rangle = \alpha|\alpha\rangle, \tag{6.131}$$

$$\langle\alpha|a^\dagger = \alpha^*\langle\alpha|. \tag{6.132}$$

The results for $a^\dagger|\alpha\rangle$ and $\langle\alpha|a$ are not so trivial, and Bergmann states are usually used [43]. They are defined as

$$\|\alpha\rangle \equiv e^{\frac{1}{2}|\alpha|^2}|\alpha\rangle = \sum_{n=0}^{\infty}\frac{\alpha^n}{\sqrt{n!}}|n\rangle, \tag{6.133}$$

so that

$$a^\dagger\|\alpha\rangle = \sum_n \frac{\alpha^n}{\sqrt{n!}}\sqrt{n+1}\,|n+1\rangle = \frac{\partial}{\partial\alpha}\|\alpha\rangle, \tag{6.134}$$

$$\langle\alpha\|a \equiv \frac{\partial}{\partial\alpha^*}\langle\alpha\|. \tag{6.135}$$

In terms of the Bergmann states, the Q function can be written as

$$Q(\alpha) = \langle\alpha|\rho|\alpha\rangle = e^{-|\alpha|^2}\langle\alpha\|\rho\|\alpha\rangle. \tag{6.136}$$

The operator correspondence of α,α^* in terms of Q function are

$$\langle\alpha|\rho a|\alpha\rangle = \alpha\langle\alpha|\rho|\alpha\rangle = \alpha Q, \tag{6.137}$$

$$\langle\alpha\left|a\rho\right|\alpha\rangle = e^{-|\alpha|^2}\frac{\partial}{\partial\alpha^*}\langle\alpha\left\|\rho\right\|\alpha\rangle = \left(\frac{\partial}{\partial\alpha^*}+\alpha\right)Q. \tag{6.138}$$

The Hermitian conjugate terms can be derived in a similar manner. Thus, we obtain the following correspondence:

$$a\rho \leftrightarrow \left(\alpha+\frac{\partial}{\partial\alpha^*}\right)Q\left(\alpha,\alpha^*\right), \tag{6.139}$$

$$a^\dagger\rho \leftrightarrow \alpha^* Q\left(\alpha,\alpha^*\right), \tag{6.140}$$

$$\rho a \leftrightarrow \alpha Q\left(\alpha,\alpha^*\right), \tag{6.141}$$

$$\rho a^\dagger \leftrightarrow \left(\alpha^*+\frac{\partial}{\partial\alpha}\right)Q\left(\alpha,\alpha^*\right). \tag{6.142}$$

Using the above relations, we can derive the following:

$$\left\langle\alpha\left|a^\dagger a\rho\right|\alpha\right\rangle = \left(\alpha^*\frac{\partial}{\partial\alpha^*}+\alpha^*\alpha\right)Q, \tag{6.143}$$

$$\left\langle\alpha\left|\rho a^\dagger a\right|\alpha\right\rangle = \left(\alpha\alpha^*+\alpha\frac{\partial}{\partial\alpha}\right)Q. \tag{6.144}$$

Then Eq. (6.128) can be transformed into

$$\begin{aligned}\frac{\partial Q}{\partial t} &= \Gamma\left[2\left(\alpha^*\frac{\partial}{\partial\alpha^*}\left(\alpha\alpha^*\right)+\alpha^*\frac{\partial}{\partial\alpha^*}\left(\alpha\frac{\partial}{\partial\alpha}\right)+|\alpha|^4+\alpha^*\alpha^2\frac{\partial}{\partial\alpha}\right)\langle\alpha\left|\rho\right|\alpha\rangle\right]\\ &+\Gamma\left[-\left(\alpha^*\frac{\partial}{\partial\alpha^*}+\alpha^*\alpha\right)\langle\alpha\left|\rho\right|\alpha\rangle-\alpha^{*2}\langle\alpha\left|a a\rho\right|\alpha\rangle\right]\\ &+\Gamma\left[-\left(\alpha\alpha^*+\alpha\frac{\partial}{\partial\alpha}\right)\langle\alpha\left|\rho\right|\alpha\rangle-\alpha^2\left\langle\alpha\left|\rho a^\dagger a^\dagger\right|\alpha\right\rangle\right]\\ &= \Gamma\left[-\alpha^*\frac{\partial Q}{\partial\alpha^*}-\alpha\frac{\partial Q}{\partial\alpha}+2|\alpha|^2\frac{\partial^2 Q}{\partial\alpha^*\partial\alpha}-\alpha^{*2}\frac{\partial Q}{\partial\alpha^{*2}}-\alpha^2\frac{\partial Q}{\partial\alpha^2}\right].\end{aligned} \tag{6.145}$$

Now express α in terms of the intensity I and phase θ

$$\alpha\left(I,\theta\right) = \sqrt{I}e^{i\theta}. \tag{6.146}$$

We use the chain rule to write the derivatives in Eq. (6.146) in terms of θ and I,

$$\frac{\partial Q}{\partial \alpha} = \frac{\partial Q}{\partial \theta}\frac{\partial \theta}{\partial \alpha} + \frac{\partial Q}{\partial I}\frac{\partial I}{\partial \alpha} \tag{6.147}$$

$$\frac{\partial^2 Q}{\partial \alpha^2} = \frac{\partial}{\partial \theta}\left(\frac{\partial Q}{\partial \theta}\frac{\partial \theta}{\partial \alpha} + \frac{\partial Q}{\partial I}\frac{\partial I}{\partial \alpha}\right)\frac{\partial \theta}{\partial \alpha} + \frac{\partial}{\partial I}\left(\frac{\partial Q}{\partial \theta}\frac{\partial \theta}{\partial \alpha} + \frac{\partial Q}{\partial I}\frac{\partial I}{\partial \alpha}\right)\frac{\partial I}{\partial \alpha} \tag{6.148}$$

$$...etc. \tag{6.149}$$

The following trick simplifies the evaluation of the derivatives of θ and I with respect to α and α^*

$$\alpha\alpha^* = I \Rightarrow \frac{\partial I}{\partial \alpha} = \alpha^* = \sqrt{I}e^{-i\theta}, \tag{6.150}$$

$$\frac{\alpha}{\alpha^*} = e^{2i\theta} \Rightarrow \ln\left(\frac{\alpha}{\alpha^*}\right) = 2i\theta \Rightarrow \frac{\partial \theta}{\partial \alpha} = \frac{-i}{2\alpha} = \frac{-ie^{-i\theta}}{2\sqrt{I}}. \tag{6.151}$$

The final result is

$$\frac{\partial Q}{\partial t} = \Gamma\frac{\partial^2 Q}{\partial \theta^2}. \tag{6.152}$$

Therefore, the term $-\Gamma\left[a_0^\dagger a_0, \left[a_0^\dagger a_0, \rho\right]\right]$ gives a diffusion process with the diffusion coefficient Γ. The diffusion coefficient is important as the quantity reflects the measurement strength and thus projection time as we will see in the next chapter.

Chapter 7

Measurement statistics and stochastic dynamics - the stochastic master equation

7.1 Measurements and trajectories overview

In an experiment the current will be measured and this signal contains information about the system phonon number because of correlations between the current and the state of the system oscillator. In order to analyse this, it is necessary to have a description of the state of the current that accounts for the interaction with the ancilla oscillator.

Using terminologies taken from the scattering theory discussed in Part I, we calculate the current out-field (after interaction with the ancilla) in terms of the current in-field and the interaction of the in-field with the ancilla. It is then possible to express the correlation functions of the measured current in terms of appropriate correlation functions of the output field, which may by means of the input-output relation be calculated from the correlation functions of the ancilla and the thermal input field. Quantum mechanics also allows us to determine the state of the system *conditioned* on the measured current $I(t)$. The von Neumann projection postulate says that after a measurement a quantum system in some possibly mixed initial state is projected onto the eigenstate corresponding to the measurement outcome. In our system and many others, including those familiar in quantum optics, the projection

is onto states of a large semi-classical measurement apparatus weakly coupled to the quantum system of interest.

The theory of quantum trajectories [44, 45, 46] has been developed to deal with these weak projections and to describe the state of the system at time $t + dt$ given the state at time t and the infinitesimal change in the measurement current $dI = I(t + dt) - I(t)$. The effect on the evolution equation for the system is derived precisely by projecting the output field of the ancilla onto the appropriate current eigenstate.

The measurement process will tend to force the system towards a pure number state and we will be able to determine the number state of the system. The time-scale for this to occur will depend on the coupling of the system to the measurement apparatus, which is in turn connected to the sensitivity of the measurement.

On the other hand, the coupling of the system to a thermal bath will lead it to absorb and emit energy from the bath. So in order to determine which number state the system is in and track its evolution, it must be possible to distinguish between one number state and the next in a time that is short compared to the time-scale over which phonons are absorbed from and emitted into the thermal bath.

7.2 The measurement bath operator description of the current

We now derive an expression for the measurement current. The measurement bath Hamiltonian $H_{\rm bath}$ is undisturbed at $t < t_0$. At time t_0, the interaction with the system is turned on and we calculate the state of the bath at later time.

Consider the ancilla and measurement bath interaction. The Hamiltonian in this case is

$$H = H_{\rm bath} + H_{\rm int}, \tag{7.1}$$

The free Hamiltonian for the measurement bath is from Eq. (6.17)

$$H_{\text{bath}} = \sum_n \hbar\omega_{\text{d},n} b_{\text{d},n}^\dagger b_{\text{d},n}. \tag{7.2}$$

where $b_{\text{d},n}$ is the measurement bath operator and the interaction Hamiltonian is from Eqs. (6.17) and (6.19)

$$H_{\text{int}} = i\hbar \sum_n g_{\text{d}}(\omega_n) \left(b_{\text{d},n}^\dagger a_1 - b_{\text{d},n} a_1^\dagger \right), \tag{7.3}$$

where a_1 is the ancilla oscillator operator and $g_{\text{d}}(\omega_n)$ is the coupling strength as defined in the previous chapter.

Using the Heisenberg equation of motion

$$\frac{d\hat{O}}{dt} = -\frac{i}{\hbar}\left[\hat{O}, H\right], \tag{7.4}$$

for an operator $\hat{O}$, we obtain

$$\begin{aligned} \frac{db_{\text{d},n}}{dt} &= -\frac{i}{\hbar}\sum_{n'}\left[b_{\text{d},n}, \hbar\omega_{\text{d},n'} b_{\text{d},n'}^\dagger b_{\text{d},n'} + i\hbar g(\omega_{n'})\left(b_{\text{d},n'}^\dagger a_1 - b_{\text{d},n'} a_1^\dagger\right)\right] \\ &= -i\omega_n b_{\text{d},n} + g_{\text{d}}(\omega_n)\, a_1(t). \end{aligned} \tag{7.5}$$

Integrating $db_{\text{d},n}/dt$ results in

$$b_{\text{d},n}(t) = C_0 e^{-i\omega_n t} + e^{-i\omega_n t}\int_{t_0}^{t} g_{\text{d}}(\omega_n)\, e^{i\omega_n t'} a_1(t')\, dt', \tag{7.6}$$

and the initial condition $b_{\text{d},n}(t) = b_{\text{d},n}(t_0)$ at $t = t_0$ gives

$$b_{\text{d},n}(t_0) = C_0 e^{-i\omega_n t_0} \Rightarrow C_0 = b_{\text{d},n}(t_0)\, e^{i\omega_n t_0}. \tag{7.7}$$

Thus we can write $\sum_n b_{\text{d},n}(t)$ which appears in the expression for the current Eq.

(6.16) as

$$\sum_n b_{\mathrm{d},n}(t) = \sum_n b_{\mathrm{d},n}(t_0)\, e^{-i\omega_n(t-t_0)} + \int_{t_0}^{t} \sum_n g_{\mathrm{d}}(\omega_n)\, e^{-i\omega_n(t-t')} a_1(t')\, dt'. \tag{7.8}$$

When $g_{\mathrm{d}}(\omega_n)$ varies smoothly around the ancilla oscillation frequency ω_1, we can approximate the discrete frequencies by a continuum. Then the sum can be expressed in integral form in a similar manner to the one presented in Eq. (6.43):

$$\sum_n g_{\mathrm{d}}(\omega_n) = \int_0^{\infty} \rho_{\mathrm{ds}}(\omega)\, g(\omega)\, d\omega, \tag{7.9}$$

where $\rho_{\mathrm{ds}}(\omega)$ is the density of states at frequency ω as before. Writing $a_1(t')$ in the interaction picture $a_1(t')\, e^{-i\omega_1 t'}$, Eq. (7.8) can be written as

$$\begin{aligned}\sum_n b_{\mathrm{d},n}(t) = &\sum_n b_{\mathrm{d},n}(t_0)\, e^{-i\omega_n(t-t_0)} \\ &+ e^{-i\omega_1 t} \int_{t_0}^{t}\int_0^{\infty} \rho_{\mathrm{ds}}(\omega)\, g_{\mathrm{d}}(\omega)\, e^{-i(\omega-\omega_1)(t-t')} a_1(t')\, d\omega dt'.\end{aligned} \tag{7.10}$$

The expression

$$\int_0^{\infty} \rho_{\mathrm{ds}}(\omega)\, g_{\mathrm{d}}(\omega)\, e^{-i(\omega-\omega_1)(t-t')} d\omega = M(t-t') \tag{7.11}$$

is the memory function of the noise since it makes the result at time t depends on the value of $a_1(t')$ for previous times. Because $\rho_{\mathrm{ds}}(\omega)\, g_{\mathrm{d}}(\omega)$ is a slowly varying function of frequency, the memory function goes to zero on a time scale which is much less that the time over which $a_1(t')$ changes in the interaction picture. Then $\sum_n b_{\mathrm{d},n}(t)$ has a short memory, thus we can replace $a_1(t')$ by $a_1(t)$. So we can rewrite Eq. (7.10) as

$$\sum_n b_{\mathrm{d},n}(t) = \sum_n b_{\mathrm{d},n}(t_0)\, e^{-i\omega_n(t-t_0)} + a_1(t)\, e^{-i\omega_1 t} \int_{t_0}^{t} M(t-t')\, dt'. \tag{7.12}$$

If we let $t_0 = -\infty$, then the second term in Eq. (7.12) becomes

$$\begin{aligned} & a_1(t)\, e^{-i\omega_1 t} \int_{t_0}^{t} \int_0^{\infty} dt' d\omega \rho_{\mathrm{ds}}(\omega)\, g_{\mathrm{d}}(\omega)\, e^{-i(\omega-\omega_1)(t-t')} \\ & = a_1(t)\, e^{-i\omega_1 t} \int_0^{\infty} d\tau \int_0^{\infty} d\omega \rho_{\mathrm{ds}}(\omega)\, g_{\mathrm{d}}(\omega)\, e^{i(\omega-\omega_1)\tau}. \end{aligned} \tag{7.13}$$

Then letting $\varepsilon = \omega - \omega_1$ and integrating, we obtain

$$\begin{aligned} & = a_1(t)\, e^{-i\omega_1 t} \int_{-\infty}^{\infty} d\varepsilon \rho_{\mathrm{ds}}(\varepsilon + \omega_1)\, g_{\mathrm{d}}(\varepsilon + \omega_1)\, e^{-i(\varepsilon+\omega_1)t} \left[\pi\delta(\varepsilon) + i\mathrm{P}\left(\frac{1}{\varepsilon}\right)\right] \\ & \simeq a_1(t)\, e^{-i\omega_1 t} \pi \rho_{\mathrm{ds}}(\omega_1)\, g_{\mathrm{d}}(\omega_1), \end{aligned} \tag{7.14}$$

where we have used the same integration technique as in 6.2.1.1. Using

$$\mu \equiv \pi \rho_{\mathrm{ds}}(\omega_1) \left| g_{\mathrm{d}}(\omega_1) \right|^2, \tag{7.15}$$

as in Eq. (6.55) and changing the interaction form of $a_1(t)\, e^{-i\omega_1 t}$ back to the Schrödinger form, Eq. (7.12) becomes

$$\sum_n b_{\mathrm{d},n}(t) = \sum_n b_{\mathrm{d},n}(t_0)\, e^{-i\omega_n(t-t_0)} + \sqrt{\frac{\pi\rho_{\mathrm{ds}}(\omega_1)}{2}} \sqrt{2\mu} a_1(t). \tag{7.16}$$

The measurement current is, from Eqs. (6.16) and (7.16),

$$\begin{aligned} I(t) &= \sum_n \left(b_{\mathrm{d},n}(t) + b_{\mathrm{d},n}^{\dagger}(t) \right) \\ &= \sqrt{\frac{\pi\rho_{\mathrm{ds}}(\omega_1)}{2}} \sqrt{2\mu} \left[a_1(t) + a_1^{\dagger}(t) \right] + \sum_n \left[b_{\mathrm{d},n}(t_0) + b_{\mathrm{d},n}^{\dagger}(t_0) \right] e^{-i\omega_n(t-t_0)}. \end{aligned} \tag{7.17}$$

The second term is the noise which depends only on the initial bath operators with the time evolution $e^{-i\omega_n(t-t_0)}$ and can be more readily calculated from the rms amplitude of the noise than directly calculating from all the combinations of correlations of $b_{\mathrm{d},n}, b_{\mathrm{d},n}^{\dagger}, a_1, a_1^{\dagger}$. We will derive it in the next section. Assuming the bath is initially

in equilibrium and the bath correlation at $t = t_0$ is

$$\langle b_n(t_0)\rangle = \left\langle b_n^\dagger(t_0)\right\rangle = 0, \tag{7.18}$$

the average current is

$$\langle I(t)\rangle = \sqrt{\frac{\pi\rho_{\rm ds}(\omega_1)}{2}}\sqrt{2\mu}\left\langle a_1(t) + a_1^\dagger(t)\right\rangle. \tag{7.19}$$

Before moving onto the next section, we could relate our results just derived to the input-output formalism used in quantum optics: Changing $b_{{\rm d},n}(t)$ to the continuum form using Eq. (6.43), we obtain

$$\int_0^\infty \sqrt{\rho_{\rm ds}(\omega)}b(\omega)\,d\omega = \int_0^\infty \sqrt{\rho_{\rm ds}(\omega)}b(\omega;t_0)\,e^{-i\omega(t-t_0)}d\omega + \sqrt{\frac{\pi\rho_{\rm ds}(\omega_1)}{2}}\sqrt{2\mu}a_1(t) \tag{7.20}$$

Since we are interested in time dependences that are slow, the integral is dominated by ω near ω_1. Thus we may take the slowly varying density of states outside the integral and divided the equation above by $\sqrt{\rho_{\rm ds}(\omega_1)}$. Then

$$\frac{1}{\sqrt{2\pi}}\int_0^\infty b(\omega)\,d\omega = \frac{1}{\sqrt{2\pi}}\int_0^\infty b(\omega;t_0)\,e^{-i\omega(t-t_0)}d\omega + \frac{\sqrt{2\mu}}{2}a_1(t). \tag{7.21}$$

In quantum optics, Eq. (7.21) is known as an alternative form of the quantum Langevin equation using the input-output formalism and has been derived from a different point of view using different language [43].

7.3 Quantum trajectories

7.3.1 Background on quantum trajectories

In order to observe quantum phenomena, we need to connect quantum mechanical microscopic events to a (semi-)classical macroscopic quantity of a measurement apparatus. The model we have described is an indirect measurement of the excitation

of the system oscillator. Both the system and ancilla oscillators are coupled to large thermal environments that lead to irreversible dynamics in the Markov and rotating wave approximations. In the preceding treatment the state of the baths was averaged over (or traced out) to lead to a master equation describing the state of the system oscillator alone.

Quantum trajectories give a method of calculating the state of the system conditioned on the measured current. Specifically if projective measurements are made on the bath, von Neumann projections allow us to calculate the corresponding effect on the system state.

The state of the system prior to the measurement determines the distribution of the values of the current $I = dQ/dt$. So it is possible to perform simulations of the experiment by picking the increment in the charge transported by the measurement current $dQ(t)$ at random from this distribution at each time-step.

The quantum trajectory equations allow us to provide a means of determining the state of the system conditioned on a given set of measurement outcomes. In addition, the quantum trajectory equations allow us to perform a simulation by picking the measurements $I(t)$ with the correct probability distribution and following the corresponding evolution of the system state. This results in a stochastic differential equation for the state evolution and can be used to simulate an ensemble of experiments. The randomness in the measurement results corresponds to a white noise background to the signal arising from intrinsic thermal noise. In addition there maybe apparatus intrinsic noise such as the circuit noise.

It is also interesting to mention that such simulations of idealised measurements are also often performed for numerical reasons in quantum optics since it is possible to calculate the trajectories corresponding to imaginary measurements for which the conditioned state is always pure; then finding mean values from quantum trajectory simulations by averaging over many trajectories. Pure states take less memory to store and less computation to update than the mixed density matrix that appears in the master equation. Thus the trajectory method is often more efficient than the direct integration of the master equation. However, this aspect of trajectories is not

discussed further in this thesis.

7.3.2 Quantum trajectory description of the measurement

7.3.2.1 Unravelling a master equation

The master equation of Eq. (6.122) provides a dynamical description of the system as an evolving probability distribution. This equation provides the average quantities that would be measured over an ensemble of experiments, and we have seen in the previous chapter how each term in the Hamiltonian contributes to the system dynamics. An ensemble of quantum systems is described by a density operator that uniquely satisfies this deterministic differential master equation [51]. However, given a master equation, there is no unique way, without further considering the physical processes, by which one can obtain its corresponding stochastic master equation, which consists of both a deterministic component (the master equation) and a stochastic component. The process of obtaining a stochastic master equation from the master equation is called 'unravelling the master equation'. At present, two unravelling methods have been developed and are commonly used: the quantum diffusion method and the quantum jump method. There are some review/tutorial articles available (see for example, [52] and [53].) and an unravelling for a hetrodyne detection (*i.e.*, measuring both the displacement and momentum of the system at the same time) using the quantum diffusion method is introduced in Appendix B.3.

As long as the objective of a quantum trajectory is to obtain the solution to a master equation, the method used does not matter. However, when a trajectory is used to infer the outcome of an individual experiment, we need to consider the physics associated with the actual measurement. Since our detection scheme uses electrical current, an appropriate unravelling corresponds to projecting the state on current eigenstates. In the rest of this chapter, we unravel the master equation Eq. (6.122), based on our measurement scheme. Firstly, we derive the expression for current $I(t)$ including a stochastic component by calculating the variance of the average current as mentioned in the last section. Then we obtain an expression for

the evolution of the state of the system when the entangled system-bath states are projected onto the current states of the bath modes, *i.e.*, the system state conditioned on the measurements.

7.3.2.2 Measurement current with a stochastic component

In § 6.1.2, we introduced the measurement scheme in which the displacement for the ancilla oscillator mode is monitored through a magneto-motive detection. The current operator in this scheme can be expressed in terms of the modes of the circuit as in Eq. (6.16), where $b_{\mathrm{d},n}$ are Bose operators with the commutation rule $\left[b_{\mathrm{d},m}, b_{\mathrm{d},n}^{\dagger}\right] = \delta_{mn}$. The constant prefactor in the current expression depends on the details of the circuit, which we have set to 1 in the previous chapter. In the absence of the interaction with the ancilla, the free Hamiltonian is given by Eq. (7.2). Since the measurement bath is considered large it is convenient to introduce a continuum form for the bath operators. The description in terms of finally spaced modes of the bath with a smooth density of states can be used to show that the bath has the Markov property of a short memory. To exploit this it is useful to introduce a global bath operator with time-local commutation rules. Consider

$$B\left(t\right) = Ce^{i\omega_1 t}\sum_{n} b_{\mathrm{d},n} = Ce^{i\omega_1 t}\int_0^{\infty}\sqrt{\rho_{\mathrm{ds}}\left(\omega_n\right)}b\left(\omega\right)d\omega. \tag{7.22}$$

Here we have used Eq. (6.43) and extracted the time dependence $e^{i\omega_1 t}$ of the drive and the resonant response of the ancilla since this is the predominant frequency of the operators coupling to the ancilla. We now show, with an appropriate choice of the constant C, that $B\left(t\right)$ has the commutation rule

$$\left[B\left(t\right), B^{\dagger}\left(t\right)\right] = \delta\left(t - t'\right). \tag{7.23}$$

Substituting in the continuum representation, and the time dependence of the $b_{\mathrm{d},n}$ given by the bath free Hamiltonian, we find

$$\begin{aligned}&\left[B\left(t\right),B^{\dagger}\left(t\right)\right]\\&=C^{2}\int_{0}^{\infty}d\omega\int_{0}^{\infty}d\omega'\sqrt{\rho_{\mathrm{ds}}\left(\omega\right)}\sqrt{\rho_{\mathrm{ds}}\left(\omega'\right)}\left[b\left(\omega\right),b^{\dagger}\left(\omega'\right)\right]e^{-i(\omega-\omega_{1})t}e^{i(\omega'-\omega_{1})t'}.\end{aligned}\tag{7.24}$$

Since we are interested in time dependences that are slow, the integral is dominated by ω near ω_1. Thus we may take the slowly varying density of states outside the integral and switch the integration variable to $\varepsilon=\omega-\omega_1$ we get

$$\begin{aligned}\left[B\left(t\right),B^{\dagger}\left(t\right)\right]&=C^{2}\int_{0}^{\infty}d\omega\rho_{\mathrm{ds}}\left(\omega\right)e^{-i(\omega-\omega_{1})(t-t')}\\&=\rho_{\mathrm{ds}}\left(\omega_{1}\right)C^{2}\int_{-\infty}^{\infty}d\varepsilon e^{-i\varepsilon(t-t')}\\&=\rho_{\mathrm{ds}}\left(\omega_{1}\right)C^{2}2\pi\delta\left(t-t'\right),\end{aligned}\tag{7.25}$$

where the lower integration limit $-\omega_1$ has been replaced by $-\infty$. Now using the fact that we want $B\left(t\right)$ to satisfy the commutation rule Eq. (7.23), we find $C=\sqrt{2\pi\rho_{\mathrm{ds}}\left(\omega_{1}\right)}$ and

$$B\left(t\right)=\frac{1}{\sqrt{2\pi\rho_{\mathrm{ds}}\left(\omega_{1}\right)}}e^{i\omega_{1}t}\sum_{n}b_{\mathrm{d},n}.\tag{7.26}$$

Thus the current operator becomes

$$I\left(t\right)=\sum_{n}\left(b_{\mathrm{d},n}\left(t\right)+b_{\mathrm{d},n}^{\dagger}\left(t\right)\right)=\sqrt{2\pi\rho_{\mathrm{ds}}\left(\omega_{1}\right)}\left(B\left(t\right)+B^{\dagger}\left(t\right)\right).\tag{7.27}$$

To formulate the effect of the measurement bath on the ancilla and derive the stochastic component of the system dynamics, we follow Wiseman's discussion (Ref. [47], § 4.4.1) of homodyne detection in quantum optics, which maps onto the same form of Hamiltonian as ours. Note when comparing with Wiseman, the prefactor $\sqrt{2\pi\rho_{\mathrm{ds}}\left(\omega_{1}\right)}$ in our current expression Eq. (7.27) is not included in Wiseman's expression.

The idea of the calculation is to consider the interaction of the ancilla with the

bath at time t, represented by the operator $B(t)$, over a small time interval Δt. It is supposed that each "element" in the time sequence of the bath $B(t)$ is initially described by a thermal state. Over the interval Δt correlations with the ancilla build up, so that the ancilla and bath states become weakly entangled. Measurement of the current (*i.e.*, the bath operator $B(t) + B^{\dagger}(t)$) then finds a value of the current equal to an eigenvalue I of the current operator, with the corresponding eigenstate $|I\rangle$, with a probability distribution $P(I)$ given by the density matrix of the entangled state in the usual way.

$$P(I) = \langle I | \rho(t + \Delta t) | I \rangle . \tag{7.28}$$

The measurement also projects the density matrix onto the eigenstate $|I\rangle$

$$\rho \to \frac{|I\rangle \langle I | \rho(t + \Delta t) | I\rangle \langle I|}{\langle I | \rho(t + \Delta t) | I\rangle}. \tag{7.29}$$

Since the value of the current measured is a stochastic variable, this projection adds a stochastic component to the evolution of the density matrix.

To follow the evolution over a time Δt, where Δt is much shorter the time-scale of $B(t)$, it is useful to introduce the operator

$$dB(t) = \int_{-\Delta t/2}^{\Delta t/2} B(t)\, dt \simeq B(t)\, \Delta t, \tag{7.30}$$

which satisfies the commutation rule

$$\left[dB(t), dB^{\dagger}(t')\right] = \Delta t. \tag{7.31}$$

The stochastic aspects of the density matrix evolution are most easily derived by introducing the normalized operator $d\tilde{B} = dB/\sqrt{\Delta t}$ which has the nice commutation rule,

$$\left[d\tilde{B}(t), d\tilde{B}^{\dagger}(t')\right] = 1. \tag{7.32}$$

With this notation we can now formulate the ancilla-bath entangling and measurement process. At time t the density matrix representing the ancilla and the segment

of the measurement bath represented by $dB(t)$ can be written as a direct product of the system plus ancilla $\rho(t)$ and bath $\rho_{\rm b}(t)$ density matrices

$$\bar{\rho}(t) = \rho(t) \otimes \rho_{\rm b}(t), \tag{7.33}$$

and $\rho_{\rm b}(t)$ is a thermal state. The interaction Hamiltonian in terms of the operators $B(t), B^{\dagger}(t')$ is from Eqs. (7.3) and (7.26),

$$\begin{aligned} H_{\rm int} &= i\hbar\sqrt{2\pi\rho_{\rm ds}(\omega_1)}g_{\rm d}(\omega_1)\left(B^{\dagger}(t)\,a_1 - B(t)\,a_1^{\dagger}\right) \\ &= i\hbar\sqrt{2\mu}\left(B^{\dagger}(t)\,a_1 - B(t)\,a_1^{\dagger}\right), \end{aligned} \tag{7.34}$$

introducing the "damping rate" $\mu \equiv \pi\rho_{\rm ds}(\omega_1)\left|g_{\rm d}(\omega)\right|^2$ as in Eq. (6.53). Then, to lowest order the evolution under the interaction gives

$$\begin{aligned} \bar{\rho}(t+dt) = \rho(t) \otimes \rho_{\rm b}(t) + \sqrt{2\mu}\sqrt{\Delta t}\left[d\tilde{B}^{\dagger}a_1 - a_1^{\dagger}d\tilde{B}, \rho(t) \otimes \rho_{\rm b}(t)\right] \\ + \mathcal{O}(\Delta t). \end{aligned} \tag{7.35}$$

The second term on the right hand side of this equation is the leading order term in the weak entangling of the state, and will lead to the stochastic part of the density matrix evolution. Note that using the $d\tilde{B}$ notation has made the $\mathcal{O}\left(\sqrt{\Delta t}\right)$ size of this term explicitly apparent. To derive the deterministic part of the evolution equation we would need to keep the $\mathcal{O}(\Delta t)$ terms, but since these are already known (the master equation in the Lindblad form) we will not do this here.

The scheme is now to project this density matrix onto an eigenstate of $d\tilde{B} + d\tilde{B}^{\dagger}$ chosen with a probability given by $\bar{\rho}(t+dt)$. Because of the weak coupling of the bath with the system, this will give a small additional contribution (actually proportional to $\sqrt{\Delta t}$) to the system density matrix depending on the value of the current measured. Since the combination of operators $d\tilde{B} + d\tilde{B}^{\dagger}$ is just the "displacement" X of the harmonic oscillator represented by the Bose operator $d\tilde{B}$, this projection is most easily done by writing the density matrix in Wigner form in terms of coherent

states. As mentioned in the previous chapter, writing a density matrix in terms of coherent state is not unique due to the overcompleteness of the coherent state basis. So far, we have introduced two such phase-space distributions (*i.e.*, distribution over real degrees of freedom): the P-function and the Q-function. The moments of the P-function are the normal ordered moments of ρ, whilst the moments of the Q-function are the anti-normal ordered moments of ρ. The Wigner function has symmetrically ordered moments that are the moments of displacement x and momentum p. Since a measurement on the bath is equivalent to projecting the bath state onto the displacement basis, the Wigner function is the most useful representation in this context.

At time t, the bath oscillator $d\tilde{B}$ is in a thermal state and the distribution of $X = d\tilde{B} + d\tilde{B}^\dagger$ is a Gaussian centred at $X = 0$ and with width $2N_\mathrm{d} + 1 = \coth\left(\hbar\omega_1/2k_\mathrm{B}T\right)$. In terms of the Wigner representation, this state can be written as

$$\tilde{W}\left(\alpha, \alpha^*; t\right) = \frac{1}{\pi\left(2N_\mathrm{d}+1\right)/2} \exp\left[-\frac{|\alpha|^2}{\left(2N_\mathrm{d}+1\right)/2}\right], \tag{7.36}$$

where α, α^* are c-numbers corresponding to the bath operators. At time $t + \Delta t$ and to $\mathcal{O}\left(\sqrt{\Delta t}\right)$ the distribution of X after the evolution corresponding to the operation Eq. (7.29) and (7.35) remains Gaussian [47] and with the same width, but now centred around $\sqrt{2\mu}\mathrm{Tr}_{\rho(t)}\left\{a_1 + a_1^\dagger\right\}\Delta t$. This means that the variable $\sqrt{\Delta t}X$ is the Gaussian random variable given by

$$\sqrt{\Delta t}X = \sqrt{2\mu}\left\langle a_1 + a_1^\dagger \right\rangle \Delta t + \sqrt{2N_\mathrm{d}+1}dW, \tag{7.37}$$

with dW a Wiener increment with $dW^2 = \Delta t$. Since the current is $\sqrt{2\pi\rho_\mathrm{ds}\left(\omega_1\right)}X/\sqrt{\Delta t}$ this gives us the first important result, namely, that the measured current is

$$I\left(t\right) = \sqrt{2\pi\rho_\mathrm{ds}\left(\omega_1\right)}\left[\sqrt{2\mu}\left\langle a_1 + a_1^\dagger\right\rangle\left(t\right) + \sqrt{2N_\mathrm{d}+1}\xi\left(t\right)\right], \tag{7.38}$$

where $\xi(t) = dW/dt$ represents delta-function correlated white noise with correlations

$$\langle \xi(t) \rangle = 0, \tag{7.39}$$

$$\langle \xi(t)\, \xi(t') \rangle = \delta(t - t'). \tag{7.40}$$

The second result is for the increment of the system density matrix after evolution through Δt and projection by the measurement (c.f. [47] Eq. (4.113)),

$$\begin{aligned} d\rho^{\mathrm{st}}(t) = \sqrt{\Delta t} X \frac{\sqrt{2\mu}}{2N_{\mathrm{d}}+1} \Big[& (N_{\mathrm{d}}+1)\left(a_1 \rho^{\mathrm{st}} + \rho^{\mathrm{st}} a_1^\dagger\right) - N_{\mathrm{d}}\left(a_1^\dagger \rho^{\mathrm{st}} + \rho^{\mathrm{st}} a_1^\dagger\right) \\ & - \mathrm{Tr}\left\{ a_1 \rho^{\mathrm{st}} + \rho^{\mathrm{st}} a_1^\dagger \right\} \rho^{\mathrm{st}} \Big] + \mathcal{O}(\Delta t). \end{aligned} \tag{7.41}$$

Replacing the stochastic variable X by the expression Eq. (7.37), and retaining only the $\mathcal{O}\left(\sqrt{\Delta t}\right)$ term gives

$$d\rho^{\mathrm{st}} = \sqrt{\frac{2\mu}{1+2N_{\mathrm{d}}}} \Big[(N_{\mathrm{d}}+1)(a_1 \rho^{\mathrm{st}} + \rho^{\mathrm{st}} a_1^\dagger) - N_{\mathrm{d}}(a_1^\dagger \rho^{\mathrm{st}} + \rho^{\mathrm{st}} a_1) - \langle a_1 + a_1^\dagger \rangle \rho^{\mathrm{st}} \Big] dW. \tag{7.42}$$

This is the stochastic term that must be added to the density matrix evolution to give us the stochastic master equation for the density matrix conditioned on the measurement outcome.

7.3.3 Adiabatic elimination of the stochastic master equation

Our objective is to evaluate Eq. (7.42) using Eqs. (6.61, 6.64). The result will lead to Eq. (7.70). In summary, we are able to replace ρ^{st} in Eq. (7.42) by ρ_1 of the deterministic calculations Eq. (6.119).

Since we are dealing with only the stochastic component of the stochastic master equation, we will omit the superscript 'st'. We can use the result from the adiabatic

master equation of Eqs. (6.97, (6.99) to evaluate Eq. (7.42) and obtain

$$
\begin{aligned}
&(N_{\rm d}+1)(a_1\rho+\rho a_1^\dagger)\\
&=(N_{\rm d}+1)\left(\rho_1+\rho_{1\dagger}\right)\otimes\rho_{N_1}\\
&+(N_{\rm d}+1)\left[2\rho_{2'}+\frac{N_1}{N_1+1}\rho_0+\rho_2\right]\otimes a_1^\dagger\rho_{N_1}\\
&+(N_{\rm d}+1)\left[2\rho_{2'\dagger}+\frac{N_1}{N_1+1}\rho_0+\rho_2\right]\rho_{N_1}a_1\\
&+(N_{\rm d}+1)\frac{N_1}{N_1+1}\left[\rho_1+\rho_{1\dagger}\right]\otimes a_1^\dagger\rho_{N_1}a_1\\
&+(N_{\rm d}+1)\frac{N_1}{N_1+1}\rho_1\otimes a_1^\dagger a_1^\dagger\rho_{N_1}+(N_{\rm d}+1)\frac{N_1}{N_1+1}\rho_{1\dagger}\otimes\rho_{N_1}a_1a_1.
\end{aligned}
\tag{7.43}
$$

Similarly, using Eqs. (6.97, 6.95) we can show that

$$
\begin{aligned}
-N_{\rm d}(a_1^\dagger\rho+\rho a_1)=&-N_{\rm d}\rho_0\otimes a_1^\dagger\rho_{N_1}-N_{\rm d}\rho_0\otimes\rho_{N_1}a_1\\
&-N_{\rm d}\left(\rho_1+\rho_{1\dagger}\right)\otimes a_1^\dagger\rho_{N_1}a_1-N_{\rm d}\rho_1\otimes a_1^\dagger a_1^\dagger\rho_{N_1}-N_{\rm d}\rho_{1\dagger}\otimes\rho_{N_1}a_1a_1.
\end{aligned}
\tag{7.44}
$$

Therefore, the last term in Eq. (7.42) can be evaluated by plugging Eq. (6.61) for ρ into $a_1^\dagger\rho+\rho a_1$, then taking the trace results in leaving only the $(\rho_1+\rho_{1\dagger})\otimes a_1^\dagger\rho_{N_1}a_1$ term:

$$
-{\rm Tr}\left[a_1^\dagger\rho+\rho a_1\right]=-\left\langle\rho_{1\dagger}+\rho_1\right\rangle. \tag{7.45}
$$

Thus we obtain

$$
\dot\rho_0=\sqrt{\frac{2\mu}{1+2N_{\rm d}}}\left\{(N_{\rm d}+1)\left(\rho_1+\rho_{1\dagger}\right)-\left\langle\rho_{1\dagger}+\rho_1\right\rangle\rho_0\right\}\xi, \tag{7.46}
$$

$$
\dot\rho_1=\sqrt{\frac{2\mu}{1+2N_{\rm d}}}\left\{(N_{\rm d}+1)\left[2\rho_{2'}+\frac{N_1}{N_1+1}\rho_0+\rho_2\right]-N_{\rm d}\rho_0-\left\langle\rho_1+\rho_{1\dagger}\right\rangle\rho_1\right\}\xi, \tag{7.47}
$$

$$
\dot\rho_{1\dagger}=\sqrt{\frac{2\mu}{1+2N_{\rm d}}}\left\{(N_{\rm d}+1)\left[2\rho_{2'\dagger}+\frac{N_1}{N_1+1}\rho_0+\rho_2\right]-N_{\rm d}\rho_0-\left\langle\rho_1+\rho_{1\dagger}\right\rangle\rho_{1\dagger}\right\}\xi, \tag{7.48}
$$

$$\dot{\rho}_2 = \sqrt{\frac{2\mu}{1+2N_\mathrm{d}}}\left\{\left[(N_\mathrm{d}+1)\frac{N_1}{N_1+1} - N_\mathrm{d}\right](\rho_1+\rho_{1\dagger}) - \langle\rho_1+\rho_{1\dagger}\rangle\,\rho_2\right\}\xi, \tag{7.49}$$

$$\dot{\rho}_{2'} = \sqrt{\frac{2\mu}{1+2N_\mathrm{d}}}\left\{\left[(N_\mathrm{d}+1)\frac{N_1}{N_1+1} - N_\mathrm{d}\right]\rho_1 - \langle\rho_1+\rho_{1\dagger}\rangle\,\rho_{2'}\right\}\xi, \tag{7.50}$$

$$\dot{\rho}_{2'\dagger} = \sqrt{\frac{2\mu}{1+2N_\mathrm{d}}}\left\{\left[(N_\mathrm{d}+1)\frac{N_1}{N_1+1} - N_\mathrm{d}\right]\rho_{1\dagger} - \langle\rho_1+\rho_{1\dagger}\rangle\,\rho_{2'\dagger}\right\}\xi, \tag{7.51}$$

where $\dot{\rho}_i$ means the stochastic component only and $\xi = dW/dt$.

Until now, we have distinguished N_d from N_1. However, for a mesoscopic mechanical beam with current flowing through the surface of the structure, $N_\mathrm{d} = N_1$, so the above differential equations will simplify to

$$\dot{\rho}_0 = \sqrt{\frac{2\mu}{1+2N_1}}\left\{(N_1+1)\,(\rho_1+\rho_{1\dagger}) - \langle\rho_{1\dagger}+\rho_1\rangle\,\rho_0\right\}\xi, \tag{7.52}$$

$$\dot{\rho}_1 = \sqrt{\frac{2\mu}{1+2N_1}}\left\{(N_1+1)\,(2\rho_{2'}+\rho_2) - \langle\rho_1+\rho_{1\dagger}\rangle\,\rho_1\right\}\xi, \tag{7.53}$$

$$\dot{\rho}_{1\dagger} = \sqrt{\frac{2\mu}{1+2N_{1\mathrm{d}}}}\left\{(N_1+1)\,(2\rho_{2'\dagger}+\rho_2) - \langle\rho_1+\rho_{1\dagger}\rangle\,\rho_{1\dagger}\right\}\xi, \tag{7.54}$$

$$\dot{\rho}_2 = \sqrt{\frac{2\mu}{1+2N_1}}\left\{-\langle\rho_1+\rho_{1\dagger}\rangle\,\rho_2\right\}\xi, \tag{7.55}$$

$$\dot{\rho}_{2'} = \sqrt{\frac{2\mu}{1+2N_1}}\left\{-\langle\rho_1+\rho_{1\dagger}\rangle\,\rho_{2'}\right\}\xi, \tag{7.56}$$

$$\dot{\rho}_{2'\dagger} = \sqrt{\frac{2\mu}{1+2N_1}}\left\{-\langle\rho_1+\rho_{1\dagger}\rangle\,\rho_{2'\dagger}\right\}\xi. \tag{7.57}$$

Next we will do the adiabatic elimination as has been done for the master equation. To do the adiabatic elimination, we set off-diagonal terms in $\dot{\rho}_i$ to zero. Since ρ_i is actually stochastically driven as well, this is not exactly correct: strictly speaking, the stochastic terms are fluctuating. Thus in the steady state, ρ_1, ρ_{-1} are not quite constant, as the adiabatic elimination assumes. However, if the fluctuation amplitude is very small (high order in ϵ), we can neglect the fluctuation and approximate these terms with the steady state values. Following Doherty and Jacobs' analysis [48] we calculate the variance of the stochastic term, then integrate it over the time scale of the diagonal term to estimate the amplitude of the fluctuation (*i.e.*, rms of variance).

Suppose $f(t)$ and $g(t)$ are arbitrary continuous functions. Then the variance is

$$\begin{aligned}\sigma &= \left\langle \int_0^{\Delta t} f(t)\, dW(t) \int_0^{\Delta t} g(t')\, dW(t') \right\rangle \\ &= \left\langle \int_0^{\Delta t} f(t)\, \xi(t)\, dt \int_0^{\Delta t} g(t')\, \xi(t')\, dt' \right\rangle \\ &= \int_0^{\Delta t} dt \left\langle f(t)\, g(t) \right\rangle, \end{aligned} \tag{7.58}$$

where we have used $dW(t) = \xi(t)\, dt$ and $\langle \xi(t)\, \xi(t') \rangle = \delta(t - t')$ [43].

Combining Eqs. (6.111) and (7.47) the off-diagonal terms $\mathcal{O}(\epsilon)$ are

$$\begin{aligned} d\rho_1 = &-i\lambda_{01} \left[a_0^\dagger a_0 \left[\alpha \rho_0 + 2\alpha^* \rho_{2'} \right] - \alpha \left[\frac{N_1}{N_1 + 1} \rho_0 + \rho_2 \right] a_0^\dagger a_0 \right] dt - \kappa \rho_1 dt \\ &+ \sqrt{\frac{2\mu}{1 + 2N_1}} \left\{ (N_1 + 1)(2\rho_{2'} + \rho_2) - \langle \rho_1 + \rho_{1^\dagger} \rangle \rho_1 \right\} dW + \mathcal{O}\left(\epsilon^3\right), \end{aligned} \tag{7.59}$$

and Eqs. (6.114) and (7.50) give the $\mathcal{O}(\epsilon^2)$ terms as

$$\begin{aligned} d\rho_{2'} = &-i\lambda_{01}\alpha \left[a_0^\dagger a_0 \rho_1 - \frac{N_1}{N_1 + 1} \rho_1 a_0^\dagger a_0 \right] dt - 2\kappa \rho_{2'} dt \\ &+ \sqrt{\frac{2\mu}{1 + 2N_1}} \left\{ - \langle \rho_1 + \rho_{1^\dagger} \rangle \rho_{2'} \right\} dW. \end{aligned} \tag{7.60}$$

The assumption of adiabatic elimination is that the system dynamics do not vary over the timescale of $1/2\kappa \simeq 1/2\mu$. With $\rho_{1^\dagger}$ and $\rho_{2'^\dagger}$ given by taking the Hermitian conjugate, the fluctuation amplitude can be characterised by the rms amplitude (the square root of variance of the stochastic part of $d\rho_1$ and $d\rho_2$) in the steady state. Thus for $d\rho_2$ the variance is

$$\begin{aligned} \sigma_{2'} &= \frac{2\mu}{1 + 2N_1} \left\langle \int_0^{\Delta t} dW \langle \rho_1 + \rho_{1^\dagger} \rangle \rho_{2'} \int_0^{\Delta t} dW(t') \langle \rho_1 + \rho_{1^\dagger} \rangle \rho_{2'} \right\rangle \\ &= \frac{2\mu}{1 + 2N_1} \int_0^{\Delta t} dt \left\langle \left| \langle \rho_1 + \rho_{1^\dagger} \rangle \rho_{2'} \right|^2 \right\rangle, \end{aligned} \tag{7.61}$$

so that the rms amplitude is

$$\sqrt{\sigma_{2'}} = \sqrt{\frac{2\mu}{1+2N_1}}\,|\langle\rho_1+\rho_{1\dagger}\rangle\,\langle\rho_{2'}\rangle|\,\sqrt{\Delta t}, \tag{7.62}$$

where $\Delta t \sim 1/2\mu$. Since ρ_1 is first order in ϵ, the rms fluctuations about the steady state are of third order in ϵ while the average is the second order. Thus we can ignore the fluctuations to leading order in ϵ. A similar argument holds for $d\rho_1$; we have

$$\begin{aligned}\sigma_1 = &\frac{2\mu}{1+2N_1}\left\langle\int_0^{\Delta t} dW\,(N_1+1)\,(2\rho_{2'}+\rho_2)\int_0^{\Delta t} dW\,(t')\,(N_1+1)\,(2\rho_{2'}+\rho_2)\right\rangle \\ &+\frac{2\mu}{1+2N_1}\left\langle\int_0^{\Delta t} dW\,\langle\rho_1+\rho_{1\dagger}\rangle\,\rho_1\int_0^{\Delta t} dW\,(t')\,\langle\rho_1+\rho_{1\dagger}\rangle\,\rho_1\right\rangle.\end{aligned} \tag{7.63}$$

The rms amplitude is

$$\sqrt{\sigma_1} = \sqrt{\frac{2\mu}{1+2N_1}}\,[(N_1+1)\,|\langle 2\rho_{2'}+\rho_2\rangle| + |\langle\rho_1+\rho_{1\dagger}\rangle\,\langle\rho_1\rangle|]\,\sqrt{\Delta t}, \tag{7.64}$$

and the fluctuation is second order whilst the average is first order. Thus, we find that the contributions from the stochastic terms in $\rho_1, \rho_{1\dagger}$ are insignificant (again, they are not of leading order in ϵ). With this result $d\rho_1$ is just linear multiplicative white noise with the steady-state solution and we set ρ_1 and $\rho_1^\dagger$ to the mean values of their dt terms as in Eqs. (6.119) and (6.120). Then the stochastic part of the diagonal terms are

$$\dot\rho_0 = \text{M.E.} + \sqrt{\frac{2\mu}{1+2N_1}}\,\{(N_1+1)\,(\rho_1+\rho_{1\dagger}) - \langle\rho_{1\dagger}+\rho_1\rangle\,\rho_0\}\,\xi, \tag{7.65}$$

$$\dot\rho_2 = \text{M.E.} + \sqrt{\frac{2\mu}{1+2N_1}}\,\{-\langle\rho_1+\rho_{1\dagger}\rangle\,\rho_2\}\,\xi, \tag{7.66}$$

where M.E. stands for the master equation part. Using Eq. (6.68) we obtain

$$\begin{aligned}
\dot{\rho}_{\rm s} &= \text{M.E.} + \sqrt{\frac{2\mu}{1+2N_1}}\,(N_1+1)\left\{(\rho_1+\rho_{1^\dagger}) - \langle \rho_{1^\dagger}+\rho_1\rangle\,\rho_{\rm s}\right\}\xi \\
&= \sqrt{\frac{2\mu}{1+2N_1}}\,(N_1+1)\left(-i\frac{\lambda_{01}\alpha}{\kappa}\left[a_0^\dagger a_0\rho_0 - \frac{N_1}{N_1+1}\rho_0 a_0^\dagger a_0\right]\right)\xi \\
&+ \sqrt{\frac{2\mu}{1+2N_1}}\,(N_1+1)\left(-i\frac{\lambda_{01}\alpha^*}{\kappa}\left[a_0^\dagger a_0\frac{N_1}{N_1+1}\rho_0 - \rho_0 a_0^\dagger a_0\right]\right)\xi \\
&- \sqrt{\frac{2\mu}{1+2N_1}}\left\langle (N_1+1)\left(-i\frac{\lambda_{01}\alpha}{\kappa}\left[a_0^\dagger a_0\rho_0 - \frac{N_1}{N_1+1}\rho_0 a_0^\dagger a_0\right]\right)\right\rangle \rho_{\rm s}\xi \\
&- \sqrt{\frac{2\mu}{1+2N_1}}\left\langle (N_1+1)\left(-i\frac{\lambda_{01}\alpha^*}{\kappa}\left[a_0^\dagger a_0\frac{N_1}{N_1+1}\rho_0 - \rho_0 a_0^\dagger a_0\right]\right)\right\rangle \rho_{\rm s}\xi. \qquad (7.67)
\end{aligned}$$

Using $i\alpha = -i\alpha^* = |\alpha|$, we can rewrite the above equation

$$\begin{aligned}
\dot{\rho}_{\rm s} &= \text{M.E.} \\
&+ \sqrt{\frac{2\mu}{1+2N_1}}\frac{\lambda_{01}|\alpha|}{\kappa}\left(-(N_1+1)\,a_0^\dagger a_0\rho_0 + N_1\rho_0 a_0^\dagger a_0\right)\xi \\
&+ \sqrt{\frac{2\mu}{1+2N_1}}\frac{\lambda_{01}|\alpha|}{\kappa}\left(N_1 a_0^\dagger a_0\rho_0 - (N_1+1)\,\rho_0 a_0^\dagger a_0\right)\xi \\
&- \sqrt{\frac{2\mu}{1+2N_1}}\frac{\lambda_{01}|\alpha|}{\kappa}\left\langle -(N_1+1)\,a_0^\dagger a_0\rho_0 + N_1\rho_0 a_0^\dagger a_0\right\rangle \rho_{\rm s}\xi \\
&- \sqrt{\frac{2\mu}{1+2N_1}}\frac{\lambda_{01}|\alpha|}{\kappa}\left\langle N_1 a_0^\dagger a_0\rho_0 - (N_1+1)\,\rho_0 a_0^\dagger a_0\right\rangle \rho_{\rm s}\xi, \qquad (7.68)
\end{aligned}$$

which simplifies to

$$\dot{\rho}_{\rm s} = \text{M.E.} - \sqrt{\frac{2\mu}{1+2N_1}}\frac{\lambda_{01}|\alpha|}{\kappa}\left[\left(a_0^\dagger a_0\rho_0 + \rho_0 a_0^\dagger a_0\right) - 2\left\langle a_0^\dagger a_0\right\rangle \rho_{\rm s}\right]\xi. \qquad (7.69)$$

Therefore, we finally obtain the stochastic master equation for the system

$$\begin{aligned} d\rho_{\rm s} = &- \left\{ \frac{\lambda_{01}^2 \left|\alpha\right|^2 (1+2N_1)}{\kappa} \left[a_0^\dagger a_0, \left[a_0^\dagger a_0, \rho_{\rm s}\right]\right] \right\} dt \\ &- i \left\{\omega_0 + \lambda_{01}(|\alpha|^2 + N_1)\right\} \left[a_0^\dagger a_0, \rho_{\rm s}\right] dt \\ &+ \nu \left(N_0 + 1\right) \left(2a_0 \rho_{\rm s} a_0^\dagger - a_0^\dagger a_0 \rho_{\rm s} - \rho_{\rm s} a_0^\dagger a_0\right) dt \\ &+ \nu N_0 \left(2a_0^\dagger \rho_{\rm s} a_0 - \rho_{\rm s} a_0 a_0^\dagger - a_0 a_0^\dagger \rho_{\rm s}\right) dt \\ &- \sqrt{\frac{2\mu}{1+2N_1}} \frac{\lambda_{01}|\alpha|}{\kappa} \left[a_0^\dagger a_0 \rho_{\rm s} + \rho_{\rm s} a_0^\dagger a_0 - 2\langle a_0^\dagger a_0\rangle \rho_{\rm s}\right] dW. \end{aligned} \tag{7.70}$$

Note that the adiabatic elimination gives

$$\langle a_1 + a_1^\dagger \rangle \rightarrow 2 \frac{\lambda_{01}|\alpha|}{\kappa} \langle a_0^\dagger a_0 \rangle. \tag{7.71}$$

This result is important and will be used again in the later section.

As was stated in the previous chapter, the first term in Eq. (7.70) describes the phase diffusion due to the non-linear coupling between the system and ancilla oscillators. The phase diffusion rate required by the measurement sensitivity would be $2k$ from the dW term, where

$$k \equiv \mu \lambda_{01}^2 |\alpha|^2 / \left(1 + 2N_1\right) \kappa^2, \tag{7.72}$$

which is the quantum backaction required by the QND measurement of the phonon number. However, the actual diffusion rate of $\lambda_{01}^2 \left|\alpha\right|^2 (1+2N_1)/\kappa$ could be larger than this due to the thermal motion of the ancilla oscillator that also contributes to the diffusion at non-zero temperature.

Next we consider a case of having initial states that are mixtures of number states, $\rho_s = \sum_n p_n |n\rangle\langle n|$ (such as a thermal state). The stochastic master equation (SME) of Eq. (7.70) leads to the result that system states which are diagonal in the number state basis remain so. The SME for the initially mixed state can be reduced to an

equation for the weights p_n

$$dp_n = -2\nu\left\{(N_0+1)[np_n-(n+1)p_{n+1}]+N_0[(n+1)p_n-np_{n-1}]\right\}dt \\ -2\sqrt{2k}\left(n-\sum n'p_{n'}\right)p_n dW. \tag{7.73}$$

Since such initial states are invariant under changes of phase, neither the phase diffusion term nor the Hamiltonian terms in the stochastic master equation contribute to the evolution of the phonon number distribution. Note that this system of equations describes the evolution of the phonon number distribution $p_n = \langle n|\rho|n\rangle$ for any arbitrary diagonal ρ. The first two terms containing dt describe emission into and absorption from the thermal bath. If the stochastic term (the last term) is absent, the system state eventually reaches equilibrium with the thermal bath and $\left\langle a_0^\dagger a_0\left(t\right)\right\rangle$ approaches the thermal average number at the bath temperature. On the other hand, the stochastic term tends to project the system onto pure number states. We will discuss the competition of these tendencies in the next subsection.

7.3.4 Accumulated projective measurements and thermalisation

There are two components in Eq. (7.73); the term that is proportional to ν and the other that is proportional to $\sqrt{k}$. We now examine the roles of these terms in the dynamics of the system. In the following analysis ν, k, and time t are scaled with some multiple of ω_1 to have dimensionless quantities unless it is noted.

7.3.4.1 The component with dt of Eq. (7.73)

Firstly we turn off the stochastic component and plot the master equation part, which is the average dynamics of the system. Figure 7.1 is a plot for $k = 0$, $\nu = 1$ with the initial state $|1\rangle$ and with the initial state $|2\rangle$. The thermal bath is characterised by the average occupation number $N_0 = 1.62$.

The terms in dt in Eq. (7.73) drive the system toward a mixed (thermal) state,

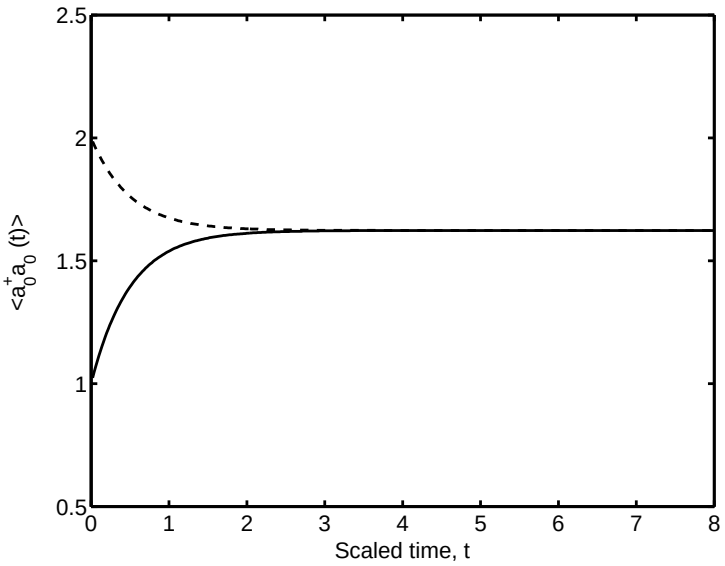

Figure 7.1: A plot of Eq. (7.73) without the stochastic component, $k = 0$, $\nu = 1$ with the intitial state $|1\rangle$ (solid line) and with the intitial state $|2\rangle$ (dashed line).

so that ensemble average of $\left\langle a_0^\dagger a_0 \right\rangle (t)$ gradually reaches the thermal average at the bath temperature. This is true regardless of the initial state. Note that the first term of Eq. (7.73) describes the average over all measurement outcomes. The plot shows the thermalisation effect due to the coupling with the heat bath. The thermalisation time is proportional to $1/\nu$.

7.3.4.2 Dwell time between transitions

The transition rate per unit time can be obtained from the master equation Eq. (6.122). The average dwelling time t_{dwell} between the transitions can be calculated from waiting time distribution of phonon emission/absorption:

$$t_{\text{dwell}} = \frac{1}{2\nu \left[N_0(n+1) + (N_0+1)\, n\right]}, \tag{7.74}$$

where we have assumed the average of the weight function to be $1/e$. Note that the dwell time is dependent only on the states prior to the transition. This is due to the Markovian approximation we have made. The dwell time Eq. (7.74) obtained from

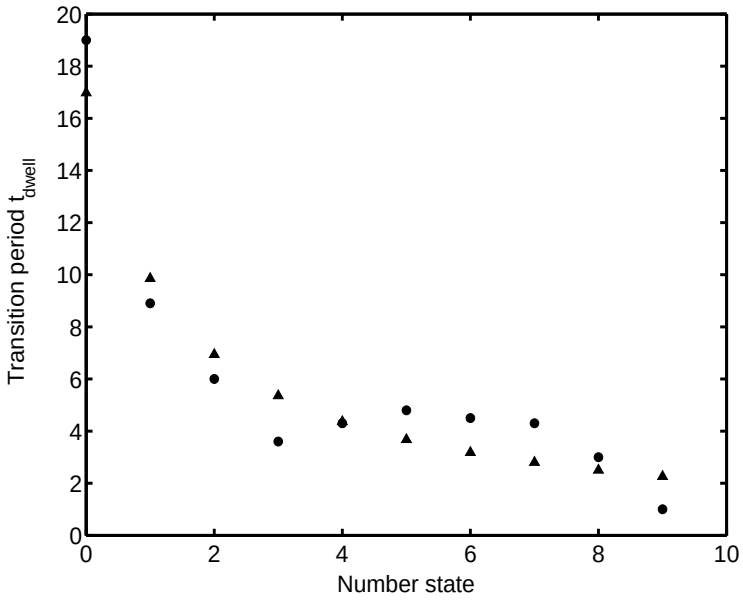

Figure 7.2: Average dwelling time T_{dwell} of each number state between transitions. cross: calculated from Eq. (7.74), circle: simulation results. $\nu = 0.02, k = 10$.

Eq. (7.74) for each state is compared with the one obtained from simulations of Eq. (7.73). For estimating t_{dwell} from the simulations, we ran simulations for a long time ($t > 1000$) using high k/ν ratio ($k/\nu = 500$) to make transitions sharp as well as to minimise the deviations from integral values. Then we round off $\left\langle a_0^\dagger a_0\left(t\right)\right\rangle$ to the nearest integer, and finally evaluate this quantity with a time-step 0.05. Figure 7.2 shows the period between the transitions, t_{dwell} calculated from Eq. (7.2) and the one from the simulation results. The simulated t_{dwell} follows the theoretically calculated t_{dwell} quite well. As the number of the simulations or simulation time t increases the dwell times obtained approach the theoretical values.

7.3.4.3 The component with dW of Eq. (7.73)

Setting $k = 1, \nu = 0$ in Eq. (7.73) results in a projection of the system state onto a pure number state (Fig. 7.3). Since no thermal dissipation or excitation is present, once projected, the state is stationary. Figure 7.4 shows p_n for $n = 0, 1, 2, 3$ with an initial mixed state, which corresponds to the same simulation as in Fig. 7.3. All states

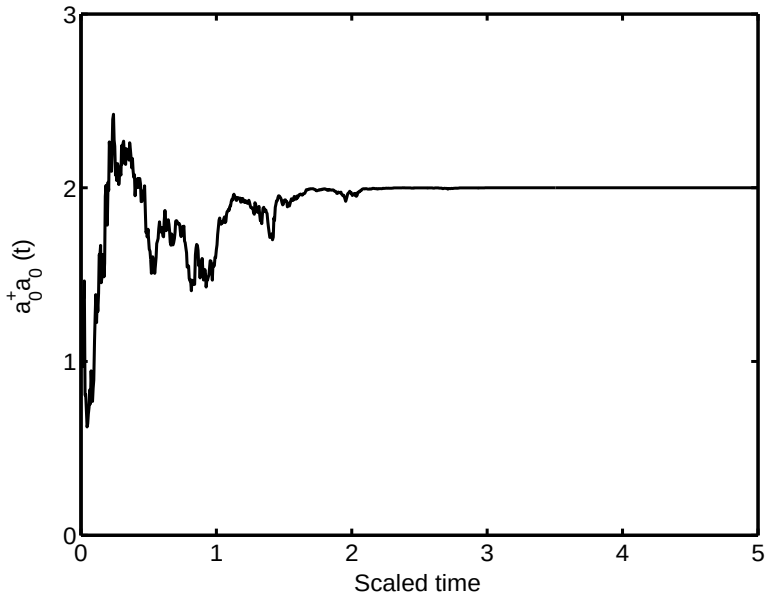

Figure 7.3: A plot of a solution to Eq. (7.73) without the master equation component, $\nu = 0$, $k = 1$ with an intitially thermal state.

are present initially, but eventually the system is projected onto state $|1\rangle$. In other runs with different random numbers for the stochastic term, different final states do result.

Thus given a constant N_0 in Eq. (7.73), we have seen that there are two opposing tendencies: the terms controlled by ν lead to transitions of phonon number and eventually to the thermalization of the distribution p_n, whilst the term controlled by the rate k tends to project the system onto a number state determined by the measurement results.

7.3.4.4 Collapse time, measurement time, and ease of observing transitions

The stochastic part of Eq. (7.73) tells the time which takes the system to be projected onto a pure number state. This time is called the collapse time and is $t_{\text{coll}} \simeq 1/2k$ from Fig. 7.3. (Note that in Fig. 7.3 both t and k are scaled with the same constant. Since we have used $k = 1$, t is scaled with k as well.)

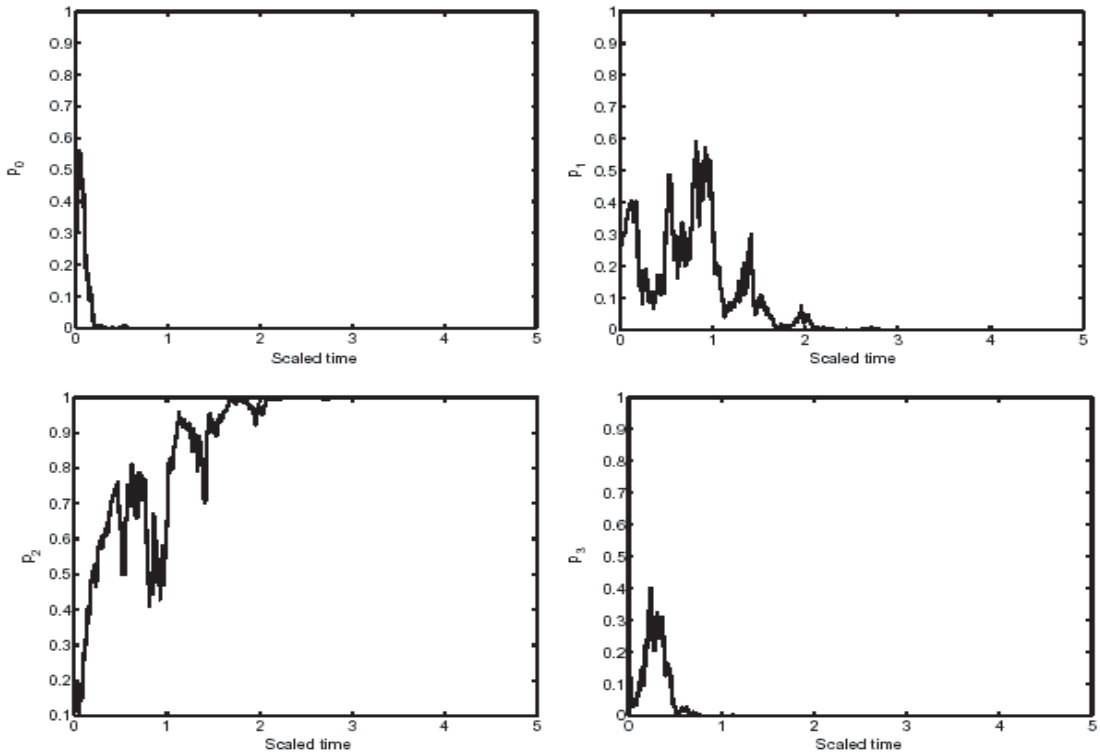

Figure 7.4: p_n plot for a simulation of Eq. (7.73) with $\nu = 0$ for the states $|0\rangle, |1\rangle, |2\rangle, |3\rangle$. The initial state is a mixed state with the average $\langle 1.63 \rangle$. The figures corresponds to Fig. 7.3 (*i.e.*, the same run).

Practically, another important time is the measurement time that is needed for the measurement apparatus to distinguish one state from the next.

In our model, the phase shift of the ancilla is monitored by the current (c.f. § 6.1.2). This is equivalent to monitoring the position of the ancilla oscillator by the current. The current scaled to eliminate unwanted factors has the form (c.f. Eq. (7.38))

$$\begin{aligned}\tilde{I}(t) &= \langle x(t)\rangle + s\xi(t) \\ &= \sqrt{\frac{\hbar}{2m\omega_1}}\langle a_1(t) + a_1^\dagger(t)\rangle + \sqrt{\frac{\hbar}{2m_1\omega_1}}\sqrt{\frac{2N_1+1}{2\mu}}\xi,\end{aligned} \tag{7.75}$$

where we have set $N_1 = N_\mathrm{d}$, $\xi(t)$ a white noise process with correlations $\langle \xi(t)\xi(t+\tau)\rangle = \delta(\tau)$, and s the position sensitivity in units of [length][frequency]$^{-1/2}$. Thus, in our model s is at least $\sqrt{\hbar/2m\omega_1}\sqrt{(2N_1+1)/2\mu}$ but may have extra contributions from other apparatus noise. Using the result in Eq. (7.71) and using the definition of k in Eq. (7.72), $\tilde{I}(t)$ can be written as

$$\tilde{I}(t) = \sqrt{\frac{\hbar}{2m\omega_1}}\sqrt{\frac{2N_1+1}{2\mu}}\left(2\sqrt{2k}\left\langle a_0^\dagger a_0\right\rangle + \xi\right). \tag{7.76}$$

To calculate the measurement time, we need to identify the signal and noise components in the current. It is reasonable to demodulate the measured signal at the ancilla oscillator frequency and to look for the phase shift of the mechanical oscillation since, in reality, we first multiply the signal (information of our interest) by a sinusoidal waveform (called carrier), then send it to the output. This process is called modulation. At the point of reception, the signal is extracted from the modulated carrier, a process we call demodulation. The modulated waveform $y(t)$ will be

$$y(t) = x(t)\cos(\omega_1 t), \tag{7.77}$$

where $x(t)$ is the signal, in our case $x(t) = 2\sqrt{2k}\left\langle a_0^\dagger a_0\right\rangle$. Then the demodulated

waveform $g(t)$ will be

$$\begin{aligned} g(t) &= y(t)\cos(\omega_1 t) = x(t)\cos^2(\omega_1 t) \\ &= \frac{x(t)}{2} + \frac{x(t)}{2}\cos(2\omega_1 t). \end{aligned} \tag{7.78}$$

The function $g(t)$ has two parts. The first is one half the signal, which we are interested. The second part is the product of this signal with a sinusoid having a frequency twice the carrier frequency. If the carrier frequency is much higher than any frequency contained in the signal, $x(t)$, it is easy to separate these two pieces. This is achieved by passing $g(t)$ through a low-pass filter. So that the D.C. component of the demodulated signal is $x(t)/2 = \sqrt{2k}\left\langle a_0^\dagger a_0 \right\rangle$. The measurement time $t_{\rm m}$ can be obtained by equating the signal integrated over an integration $t_{\rm m}$ for $\left\langle a_0^\dagger a_0 \right\rangle = 1$ with the noise integrated over this time, *i.e.*, $S/N = 1$:

$$\frac{S}{N} = 1 = \frac{\left\langle \sqrt{2k} t_{\rm m} \right\rangle^2}{\left\langle \xi \sqrt{t_{\rm m}} \right\rangle^2}, \tag{7.79}$$

$$\Rightarrow t_{\rm m} = \frac{1}{2k} = t_{\rm coll}. \tag{7.80}$$

Notice that the measurement time and the collapse (projection) time are the same. This means that if the experimenter can infer the system number state through the measurement current, then the system is actually projected to that state in the same time-scale. In this sense, the $1/\sqrt{2N_1+1}$ factor in the stochastic term in Eq. (7.69), which, as we have seen, projects the system state onto a number state, can be seen as the inefficiency in the measurement scheme for $N_1 \neq 0$.

7.3.4.5 The measurement time versus the dwell time

When $t_{\rm dwell} \gg t_{\rm m}$, the correlations of the energy eigenstates during a series of subsequent measurements each of duration $t_{\rm m}$ are strong, an experimenter's estimation of the phonon number from the measured current through the relation $\langle I \rangle(t) \propto \left\langle a_0^\dagger a_0 \right\rangle(t)$ should also be able to resolve the jumps in $\left\langle a_0^\dagger a_0 \right\rangle(t)$. Conversely, if

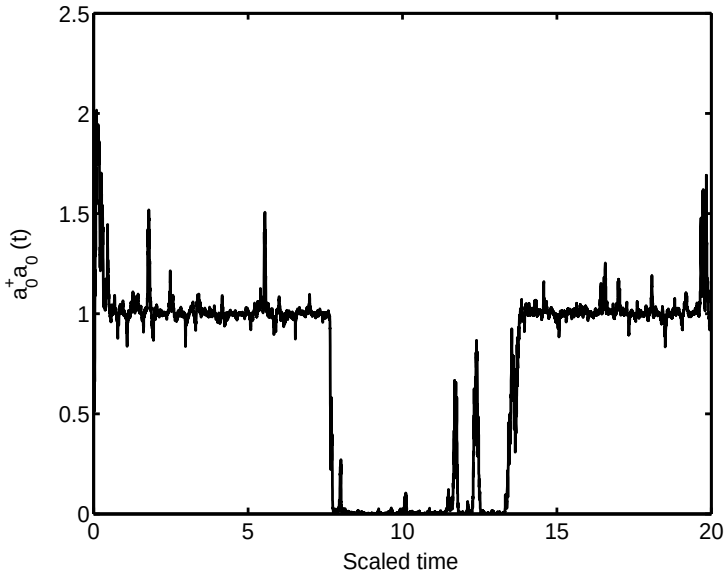

Figure 7.5: A simulation using $N_0 = 1.62$, $\nu = 0.02$, and $k = 5$.

$t_{\text{dwell}} \ll t_{\text{m}}$, transitions of the system state are much faster than the measurement time, so that the discreteness of $\left\langle a_0^\dagger a_0 \right\rangle (t)$ becomes unclear. We have simulated both the $t_{\text{dwell}} \gg t_{\text{m}}$ case and the $t_{\text{dwell}} \ll t_{\text{m}}$ case using fixed parameter: $N_0 = 1.62, \nu = 0.02$, which results in $t_{\text{dwell}} = 15.3$ for $|0\rangle$ and $t_{\text{dwell}} = 4.24$ for $|1\rangle$. We have taken two values of k for the simulations: $k = 5$ which gives $t_{\text{m}} = 0.1$ and $k = 0.1$ which gives $t_{\text{m}} = 5.0$. Figures 7.5 and 7.6 confirm our predictions. The ratio k/ν as discussed in § 7.3.4 determines whether we can see clear transitions. Similarly, as the thermal coupling strength decreases, the transition rate decreases and the time between transitions t_{dwell} becomes longer than t_{m}, the interaction time required for the measurement apparatus and the ancilla. Thus jumps in $\left\langle a_0^\dagger a_0 \right\rangle (t)$ become more apparent.

We can see "jumps" in a qualitative manner by plotting a histogram of $\left\langle a_0^\dagger a_0 \right\rangle (t)$. Figures 7.7, 7.8, and 7.9 show histograms of $\left\langle a_0^\dagger a_0 \right\rangle (t)$ with bin width $\Delta \left\langle a_0^\dagger a_0 \right\rangle = 0.1$ using fixed parameters $k = 1.5$, $N_0 = 1.62$ with these different values of ν: $\nu = 0.01$, 0.1, 0.5, respectively. The clustering of the $\left\langle a_0^\dagger a_0 \right\rangle (t)$ values around integral values is clearly evident for $\nu = 0.01$ ($k/\nu = 150$), is still identifiable for $\nu = 0.1$ ($k/\nu = 15$),

and completely lose the track for $\nu = 0.5$ ($k/\nu = 3$).

A reduction of the discreteness of the jumps with increasing ν can be seen in a more quantitative manner by plotting $\left|\left\langle a_0^\dagger a_0 \right\rangle(t) - \mathrm{Int}\left\langle a_0^\dagger a_0 \right\rangle(t)\right|^2$ with various k/ν (see Fig. 7.10). As $\left\langle a_0^\dagger a_0 \right\rangle(t)$ becomes more discrete due to increasing k/ν, the quantity $\sum_N \left|\left\langle a_0^\dagger a_0 \right\rangle(t) - \mathrm{Int}\left\langle a_0^\dagger a_0 \right\rangle(t)\right|^2 /N$ decreases.

7.3.4.6 Effect of temperature

Since the signal $\langle a_0^\dagger a_0(t)\rangle$ due to the system oscillator is at low frequency, it will generally be necessary to low-pass filter the measured current in order to integrate out the white noise. We have already estimated the time necessary to distinguish the phonon number states, t_m, so we now evaluate the phonon number sensitivity of the measurement in terms of the position sensitivity s. Rescaling $\tilde{I}(t)$ as

$$\bar{I}(t) = \langle a_0^\dagger a_0(t)\rangle + \bar{s}\xi(t), \tag{7.81}$$

where the phonon number sensitivity $\bar{s}$ is $\kappa^2\sqrt{2N_1+1}/\sqrt{8\mu}\lambda_{01}E$. Recall that in order to get a signal to noise of at least one for distinguishing one phonon number from the

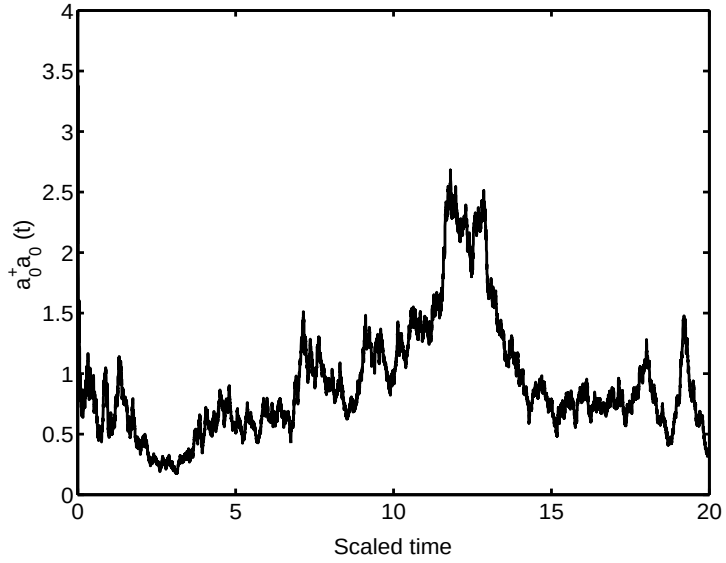

Figure 7.6: A simulation using $N_0 = 1.62$, $\nu = 0.02$, and $k = 0.1$.

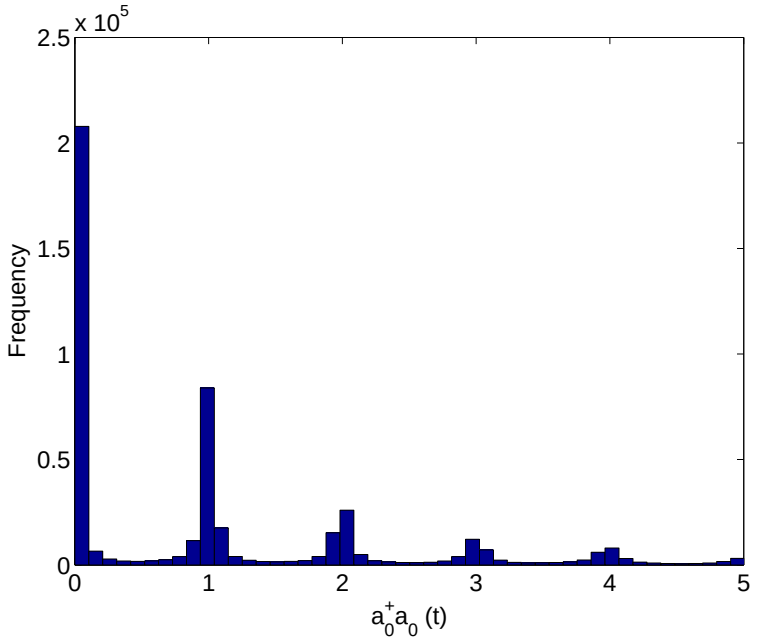

Figure 7.7: A histogram of $\left\langle a_0^\dagger a_0 \right\rangle (t)$ for a simulation $t = 3000$ with $k = 1.5$, $\nu = 0.01$, and $N_0 = 1.62$.

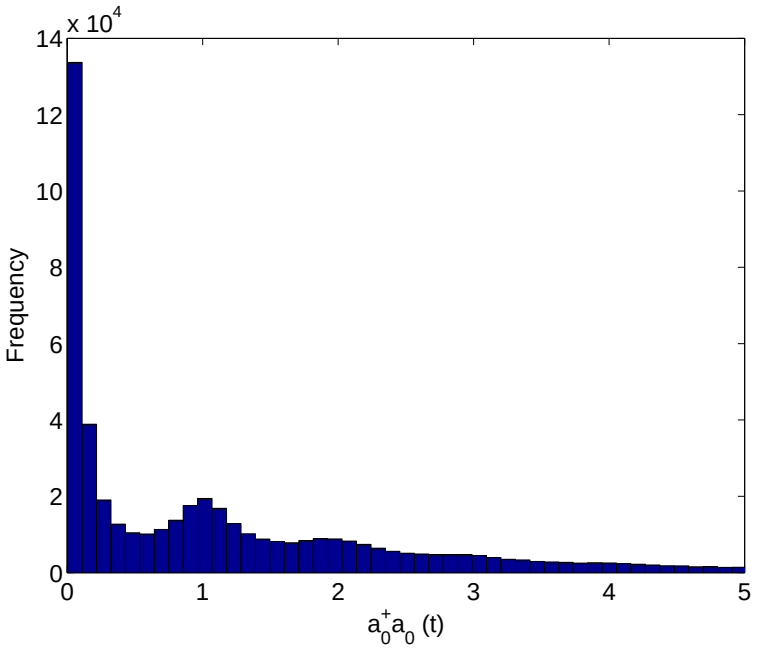

Figure 7.8: A histogram of $\left\langle a_0^\dagger a_0 \right\rangle (t)$ for a simulation $t = 3000$ with $k = 1.5$, $\nu = 0.1$, and $N_0 = 1.62$.

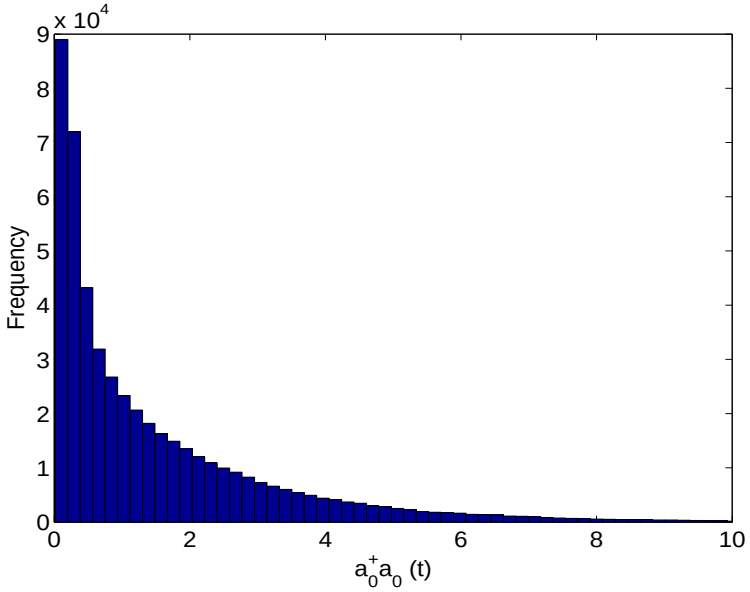

Figure 7.9: A histogram of $\left\langle a_0^\dagger a_0 \right\rangle (t)$ for a simulation $t = 3000$ with $k = 1.5$, $\nu = 0.5$, and $N_0 = 1.62$.

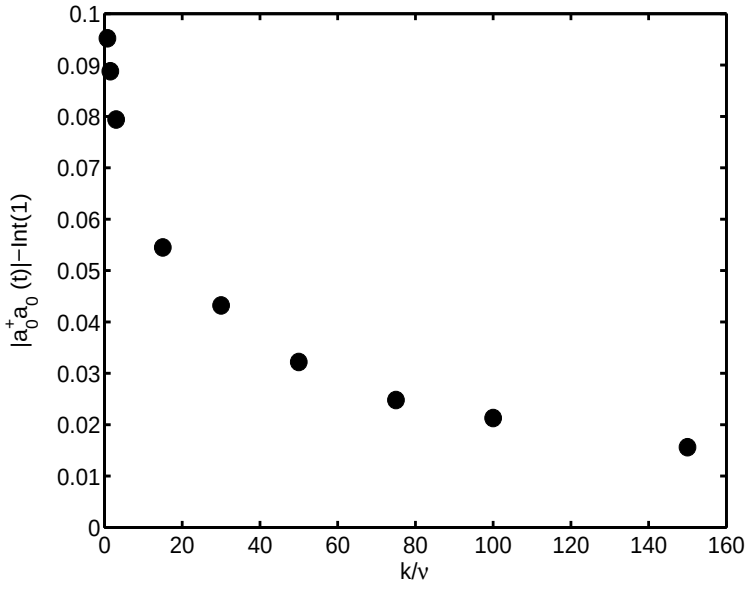

Figure 7.10: The variation of $\left\langle a_0^\dagger a_0 \right\rangle (t)$ from integral numbers is plotted for various k/ν ratio. It is quantified by $\sum_N \left| \left\langle a_0^\dagger a_0 \right\rangle (t) - \mathrm{Int} \left\langle a_0^\dagger a_0 \right\rangle (t) \right|^2 / N$.

next we will need $S/N \geq 1$, but this time we express $t_{\rm m}$ in terms of the sensitivity.

$$\frac{S}{N} \geq \frac{t_{\rm m}^2}{\bar{s}^2 t_{\rm m}} \rightarrow t_{\rm m} \geq \bar{s}^2. \tag{7.82}$$

The transition probability P of the state n during the measurement time $t_{\rm m}$ is given by $P = t_{\rm m}/t_{\rm dwell}$. If it is possible to track the transitions of the system oscillator it should be the case that $P \ll 1$. Calculating for a typical number state $n \simeq N_0$ we get the condition

$$\bar{s}^2 \nu N_0 (N_0 + 1) \ll 1. \tag{7.83}$$

Raising temperature increases N_0, and thus decreases $t_{\rm dwell}$. In order to keep the same resolution for observing clear jumps as the ones at low temperature, k must be increased sufficiently so that $t_{\rm m} < t_{\rm dwell}$ will be kept. This is not an easy task for the experimenters: for example, an oscillator with 1 GHz resonant frequency at $T = 0.1$ K has $N_0 = 1.62$. When the temperature is raised to $T = 1$ K, $N_0 = 20$, so if we keep the same resolution for jumping in both cases, the sensitivity of the measurement at the higher temperature must be increased by a large factor (Note increasing the sensitivity means a smaller value of $\bar{s}$). In addition, the sensitivity itself also contains a temperature factor $\sqrt{2N_1 + 1}$ that further amplifies the temperature effect, which makes it difficult to maintain the condition Eq. (7.83).

From Eq. (6.122) we can see that the transition rate depends on the temperature through the Bose distribution, N_0. Figures 7.11 and 7.12 show $\left\langle a_0^\dagger a_0 \right\rangle (t)$ over time for different temperatures: ($N_0 = 1.62$, $k = 3$, and $\nu = 0.02$) and ($N_0 = 20$, $k = 37$, and $\nu = 0.02$), whilst the product $\nu N_0/k$ has been kept constant at 0.0217 in order to provide the same resolution for the jumps. The plots show that for the higher temperature the transitions occur more frequently. In Fig. 7.12, the transitions occur so fast that it is not easy to see the jumps on the time scale plotted. Also notice from Eq. (7.74) that $t_{\rm dwell}$ decreases with the system state n making it difficult to recognise the discrete jumps when the system state is at higher n.

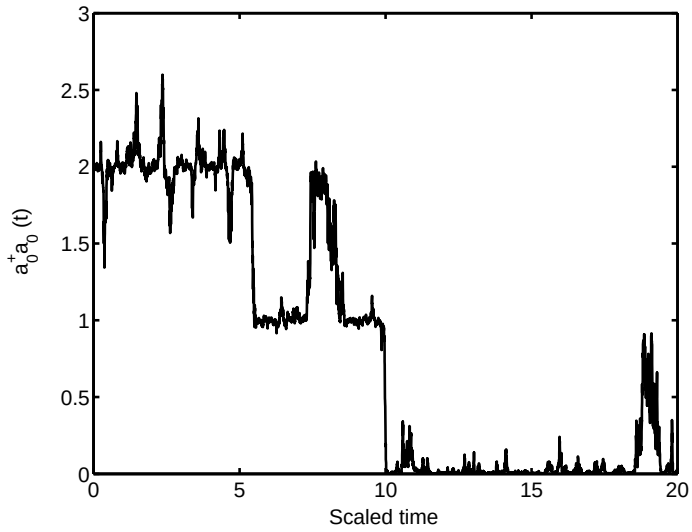

Figure 7.11: $T = 0.1$K, $N_0 = 1.62$, and $\nu N/k = 0.063$ with the initial state $|2\rangle$.

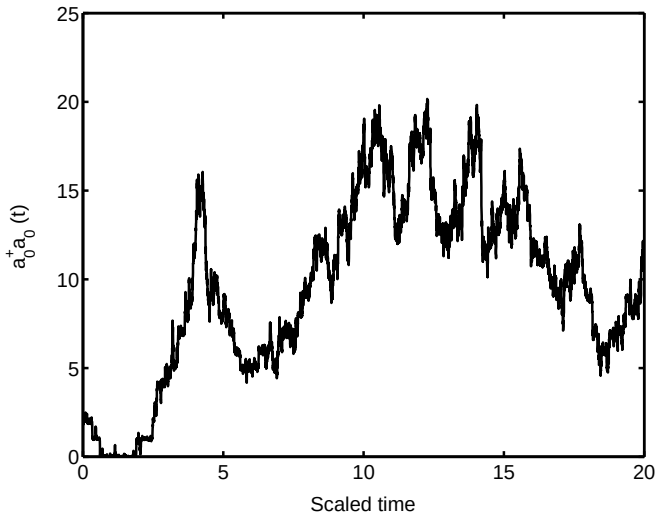

Figure 7.12: $T = 1$ K, $N_0 = 38$, and $\nu N/k = 0.063$ with the initial state $|2\rangle$.

7.4 Trajectories and experimental outcomes

7.4.1 The stochastic master equation and the measured signal

Here we discuss the significance of the stochastic master equation Eq. (7.73) and emphasize the relationship to the experimentally measured signal.

The most important point about the relation between trajectories and experimental outcomes is that, as said before, the quantum trajectory equations not only provide a way to simulate the ensemble average of many runs, but also allow us to perform a simulation by picking the measurements $I(t)$ with the correct probability distribution and following the corresponding evolution of the system state. In other words given the measurement current, one can reconstruct the dynamics of a mixed state of the system given the initial ensemble $\rho_{\rm s}(t_0)$ and $I(t)$. This can be seen more readily if we rewrite Eq. (7.75) as

$$dW = \frac{1}{\sqrt{2N_1+1}} \left\{ I\left(t\right) - 2\sqrt{2k} \left\langle a_0^\dagger a_0 \left(t\right) \right\rangle \right\} dt. \tag{7.84}$$

Our calculation in the previous section shows that in each time-step the probability distribution for $I(t)$ is Gaussian with mean $\left\langle a_0^\dagger a_0 \right\rangle$ and variance $\sqrt{\left(2N_1+1\right)/2k\Delta t}$. In our simulations we draw $I(t)$ at random from this distribution and find the stochastic density matrix $\rho_{\rm s}$ by projecting the output field onto the corresponding current eigenstate. Alternatively $I(t)$ could result from experimental data and the experimenter could propagate Eq. (7.73) using Eq. (7.84) and then estimate the phonon number by $\left\langle a_0^\dagger a_0 \right\rangle = {\rm Tr}\left\{ a_0^\dagger a_0 \rho_{\rm s} \right\}$. This is a kind of low pass filtering process performed by the experimenter using the observed current. We will show how one can extract $\left\langle a_0^\dagger a_0 \right\rangle$ from noisy current by filtering shortly. In this sense, quantum trajectories can be regarded an optimal filter for the current and $\left\langle a_0^\dagger a_0 \right\rangle$ obtained from the trajectories contains the minimal amount of noise due to the measurement apparatus.

From the previous section we have seen that even if there is no thermal coupling for the system oscillator there is a time-scale $t_{\rm m}$ over which it is possible to determine

which number state the system is in. This time $t_{\rm m}$ decreases as the measurement strength k increases. If the energy level transitions due to the thermal coupling of the system oscillator are slow compared to this time, then it should be possible to follow the system as it jumps between number states. There is a characteristic time $t_{\rm dwell}$ that the system will stay in a given number state before absorbing or emitting a phonon into the thermal bath and this depends on the damping rate and the temperature of the bath. In the limit where $t_{\rm dwell} \gg t_{\rm m}$ the distribution p_n given by Eq. (7.73) very closely resembles an energy eigenstate and thus $\left\langle a_0^\dagger a_0 \right\rangle$ becomes nearly a series of integral numbers.

Equation (7.73) gives the probability distribution of number states that are consistent with the measured current $I\left(t\right)$. If the condition $t_{\rm dwell} \gg t_{\rm m}$ does not hold the distribution p_n will have significant support on several number states and $\left\langle a_0^\dagger a_0 \right\rangle$ will resemble Fig. 7.6 with no clear jumps between number states being distinguished.

A simpler but not necessarily optimal procedure for the experimenter is to use a low-pass filter $I\left(t\right)$ with some bandwidth designed to pick out the transitions between number states. We show the results of doing this with time averaging and a Butterworth filter in Fig. 7.13. Note that there is both a significant time delay in detecting transitions between number states in comparison to the Eq. (7.73) and also a significant oscillation about the constant level between number state transitions. We now ask the following question: "what about the cases where $\rho_{\rm s}$ is not a pure number state?" Suppose p_n obtained from Eq. (7.73) results in $p_0 = 1/2$, $p_1 = 1/2$ so that the system state is either 0 or 1. If the condition $t_{\rm dwell} \gg t_{\rm m}$ does not hold, the distribution p_n have to support on a large number of states and $\left\langle a_0^\dagger a_0 \right\rangle \left(t\right)$ will resemble Fig. 7.6 with no clear jumps between number states.

We have simulated a simple filtering process using time average and a Butterworth filter. (see Fig. 7.13) The filtering process introduces a delay of the signal and degrades the signal as well as removing the unwanted noise. Experimenters might actually have much more efficient and clever ways to do low pass filtering than shown here.

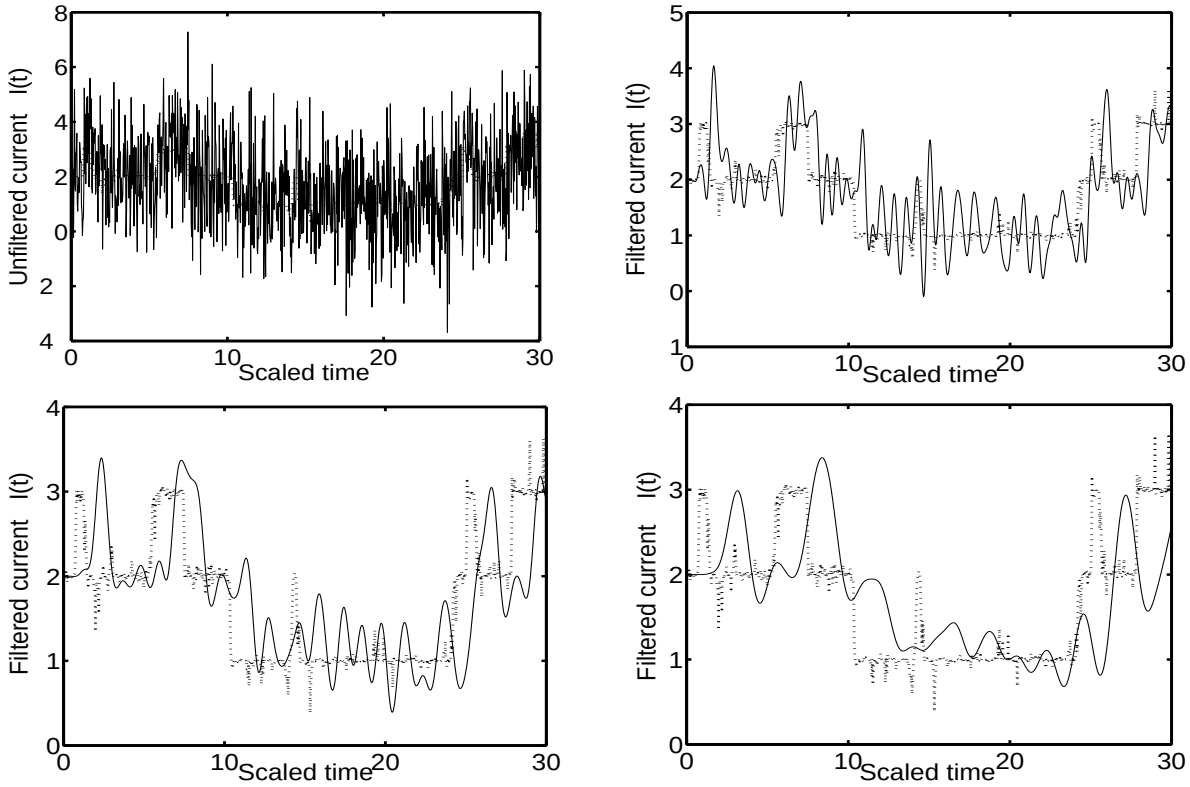

Figure 7.13: Given the measurement current, the above figures show attempts to filter out the noise using a Butterworth filter with various band widths, for parameters $k/\nu = 250$, $N_0 = 1.62$. The dotted line is $\left\langle a_0^\dagger a_0 \right\rangle$ without any noise. The current was first averaged over a time interval of $\Delta t = 0.03$. Left-top current–observed. right top–cutoff frequency $0.17k$; left bottom–cutoff frequency $0.083k$; right bottom–cutoff frequency $0.05k$.

7.4.1.1 Stochastic master equation with an imaginary observer

We have unravelled the master equation with a density matrix. However, it is also possible to unravel using a pure state. We can add another stochastic term to the SME as if the thermal bath that is coupled to the system is measuring the displacement of the system oscillator, and can still obtain the same distribution for the current $I(t)$ and $\left\langle a_0^\dagger a_0 \right\rangle$, yet the system state $\rho_{\rm s}$ will now be pure due to the direct measurement by the thermal bath. This corresponds to imagining that another observer is measuring the thermal bath and projecting the state onto eigenstates. This is a pure state unravelling. The bath is directly interacting with the system, and so the stochastic master equation has the terms of Eq. (7.70) plus another stochastic component similar to Eq. (7.42) with the a_1 operator replaced by a_0, $N_{\rm d}$ by N_0, and μ by ν,

$$\begin{aligned} d\rho_{\rm s} = &-\left\{\frac{\lambda_{01}^2\left|\alpha\right|^2(1+2N_1)}{\kappa}\left[a_0^\dagger a_0,\left[a_0^\dagger a_0,\rho\right]\right]\right\}dt - i\left\{\omega_0+\Delta\omega\right\}\left[a_0^\dagger a_0,\rho\right]dt \\ &+\nu\left(N_0+1\right)\left(2a_0\rho a_0^\dagger - a_0^\dagger a_0\rho - \rho a_0^\dagger a_0\right)dt \\ &+\nu N_0\left(2a_0^\dagger\rho a_0 - \rho a_0 a_0^\dagger - a_0 a_0^\dagger\rho\right)dt \\ &-\sqrt{2k}\left[a_0^\dagger a_0\rho + \rho a_0^\dagger a_0 - 2\langle a_0^\dagger a_0\rangle\rho_{\rm s}\right]dW_{\rm expt} \\ &-\cdot\sqrt{\frac{2\nu}{2N_0+1}}\left[(N_0+1)(a_0\rho+\rho a_0^\dagger) - N_0(a_0^\dagger\rho+\rho a_0) - \langle a_0+a_0^\dagger\rangle\rho_{\rm s}\right]dW_{\rm S.O}, \end{aligned} \tag{7.85}$$

where $\Delta\omega = \lambda_{01}(|\alpha|^2 + N_1)$. In the limit $k \gg \nu$, the system dynamics will have little change from what we already have in Eq. (7.73), but we now can identify the jumping process due to thermal excitation/dissipation by the thermal bath.

For pure state unravelling we can write $\rho_{\rm s}$ in Eq. (7.85) as $\rho_{\rm s} = |\psi\rangle\langle\psi|$, and the equation is now reduced to a Stochastic Schrödinger Equation (SSE). A SSE can be evaluated much more readily than the SME, especially when the initial state is not in diagonal form, and has been commonly used to predict an experimental outcome in the Quantum Optics community. We will not discuss pure state unravelling and its simulation here.

7.4.2 Parameters and constraints

We will now consider achievable values of the physical parameters. In summary we have the following adjustable parameters:

N_1	$1/\left(\exp\left[\hbar\omega_1\beta_1\right]-1\right)$
N_0	$1/\left(\exp\left[\hbar\omega_0\beta_0\right]-1\right)$
λ_{01}	anharmonic coupling coefficient
ν	damping rate for system oscillator
κ	damping rate for ancilla oscillator
$\left\|\alpha\right\|^2$	mean phonon number for the steady state in driven oscillator 1

7.4.2.1 Anharmonic coupling coefficient

The interaction Hamiltonian of the anharmonic coupling together with the free Hamiltonian is

$$\hbar\omega_0 a_0^\dagger a_0 + \hbar\omega_1 a_1^\dagger a_1 + \hbar\lambda_{01} a_0^\dagger a_0 a_1^\dagger a_1 = \hbar\omega_0 a_0^\dagger a_0 + \hbar\left[\omega_1 + \lambda_{01} n\right] a_1^\dagger a_1, \tag{7.86}$$

where the coupling coefficient has units of frequency. The equation above implies that if we find a frequency shift for one quantum ($n = 1$), then, the size of this shift is λ_{01}.

The experimental structure fabricated by Huang *et al.* [31] in Roukes' group transmits the strain of one of two flexing modes of the system to the ancilla oscillator as a longitudinal strain quadratic in the flexing mode amplitude. The strain generated by this flexing motion and the frequency shift associated with this strain have been calculated by Harrington and Roukes [50] and we briefly introduce their results. The longitudinal strain produced by a single quantum in the fundamental flexing motion is

$$\chi \simeq \frac{\hbar}{m_0\omega_0}\frac{1}{L_0^2}, \tag{7.87}$$

where m_0 is the mass and L_0 is the length of the system beam in the small angle

approximation. Then the ancilla frequency shift caused by this strain is [50]

$$\lambda_{01} = \omega_1 \frac{\zeta}{2\pi^2} \chi \frac{L_1^2}{d_1^2}, \tag{7.88}$$

where ζ is a geometric factor ($\zeta = 3$ for clamped beam boundary conditions) and L_1, d_1 are the length and thickness of the ancilla beam, respectively. Introducing a dimensionless quantity,

$$R_i \equiv \frac{\hbar^2}{m_i d_i^2} \frac{1}{\hbar\omega_i}, \tag{7.89}$$

where $i = 0, 1$, then the scaled coupling coefficient can be expressed as

$$\frac{\lambda_{01}}{\omega_1} = \frac{\zeta}{2\pi^2} \frac{L_1^2}{L_0^2} \frac{\hbar}{m_0\omega_0} \frac{1}{d_1^2} = \frac{\zeta}{2\pi^2} \frac{L_1^2}{L_0^2} \frac{d_0^2}{d_1^2} R_0. \tag{7.90}$$

7.4.2.2 Damping rates and k/ν ratio

The coefficient k as we have defined in an earlier section Eq. (7.72) is

$$k = \frac{\mu\lambda_{01}^2 |\alpha|^2}{(1 + 2N_\mathrm{d})\kappa^2}, \tag{7.91}$$

and ν is

$$\nu = \frac{\omega_0}{2Q_0}. \tag{7.92}$$

As seen from the previous section, the ratio k/ν is crucial to be able to observe jumps. We assume that most of the damping of the ancilla comes from the coupling to the measurement device, *i.e.*, $\mu \simeq \kappa$. Then we get

$$\frac{k}{\nu} = \frac{\mu\lambda_{01}^2 |\alpha|^2}{(1 + 2N_\mathrm{d})\kappa^2} \frac{Q_0}{2\omega_0} \simeq 4Q_0 Q_1 \frac{\lambda_{01}^2}{\omega_1\omega_0} |\alpha|^2 \frac{1}{(1 + 2N_\mathrm{d})}. \tag{7.93}$$

7.4.2.3 Driving strength

The driving energy associated with the magnetomotive detection scheme described in § 6.1.2 tells that the driving energy associated with this scheme is

$$\epsilon = BIL_1\sqrt{\frac{\hbar}{2m_1\omega_1}}\left(a_1 + a_1^\dagger\right), \tag{7.94}$$

where B is the magnetic field. Equating the expression of Eq. (7.94) to Eq. (6.13) and together with the relation between E and α

$$|E|^2 = |\alpha|^2 \kappa^2 \tag{7.95}$$

will result in the expression for $|\alpha|$

$$|\alpha| = Q_1\frac{BI_{\text{drive}}L_1}{\hbar\omega_1}\sqrt{\frac{\hbar}{2m_1\omega_1}} = Q_1\frac{BI_{\text{drive}}L_1d_1}{\sqrt{2}\hbar\omega_1}\sqrt{R_1}. \tag{7.96}$$

We then calculate $|\alpha|$ that corresponds to a displacement amplitude of the beam since an experimenter needs to drive the beam strong enough to be able to detect the displacement of the beam. Let the displacement of the beam be x_1. Then the dimensionless displacement scaled with the thickness of the beam d_1 is

$$\frac{x_1}{d_1} = \sqrt{R_1}\,|\alpha|\,. \tag{7.97}$$

With the constraints been already discussed, experimenters will have several adjustable parameters to design a suitable structure for his experimental setup and we will leave the task of seeking appropriate combinations and structure designs to the experimenters who are expert in these fields. Thus, we will conclude this chapter with an example using the parameters that are currently achievable.

At present, oscillators as fast as 1 GHz have been fabricated [31, 49]. So we consider two elastic GaAs beams with resonant frequencies of $\omega_0 = 2$ GHz and $\omega_1 =$ 800 MHz at $T = 0.1$ K. The structural dimensions are 0.63 μm $\times$ 0.2 μm $\times$ 0.1 μm for the system beam and 1.0 μm $\times$ 0.2 μm $\times$ 0.1 μm for the ancilla beam.

The anharmonic coefficient is purely dependent on geometry and materials. Suppose Q-factors of $Q_0 = 5000$ and $Q_1 = 4000$. With these parameters we obtain

$$R_1 = 1.95 \times 10^{-14}. \tag{7.98}$$

Then, for example, to obtain the scaled displacement $x_1/d_1 = 0.1$, we will need $|\alpha| = 10^6$. The magnetic drive with the magnetic field $B = 10$ Tesla and $I_{\text{drive}} = 1$ μA can raise $|\alpha|$ to ~ 580. To have $|\alpha| = 10^6$ using the same magnetic field requires the driving current $I_{\text{drive}} = 2$ mA. With the given beam dimensions, the anharmonic coupling coefficient is $\lambda_{01}/\omega_1 = 4.7 \times 10^{-15}$. These values give clearly $\kappa/\nu \ll 1$ by many orders of magnitude. To obtain $\kappa/\nu \gg 1$ requires a larger coupling coefficient, small m, and thin plate (small d) as well as high frequency oscillators with high Q.

Chapter 8

Anharmonicity - the effect of the nonlinear term

In the measurement scheme we have considered in the previous chapters, non-interacting anharmonic terms are neglected. In this chapter, we remove this restriction and analyse the effect of the non-interacting anharmonic terms, x^4. We show that this nonlinear term, x^4, increases the total phonon number due to both thermal and quantum fluctuations. However, the overall effect of this term can be negligibly small since the nonlinear coefficients are much smaller than the measurement damping.

8.1 The Hamiltonian and master equation

(Note: In this chapter, we change the notation for the system and ancilla operators from a_0, a_1 to a, b, since we will be using the index $0, 1$ to indicate for the steady state and fluctuation components. Note that b is not a bath operator!)

The driving term of the Hamiltonian is similar to Eq. (6.12) but to study detuning effects the ancilla is driven at frequency ω_d, where $\omega_d \neq \omega_1$:

$$H_{\text{drive}} = 2\hbar E \cos\left[\omega_d t\right]\left(b^\dagger + b\right). \tag{8.1}$$

where $\delta\omega$ is the detuning frequency between the ancilla resonant frequency and the driving frequency, $\delta\omega = \omega_1 - \omega_d$ with $\delta\omega \ll \omega_1, \omega_d$. In the interaction picture within

the rotating wave approximation this term becomes

$$H^{\mathrm{I}}_{\mathrm{drive}} = \hbar E \left(b^\dagger e^{+i\delta\omega} + b e^{-i\delta\omega} \right), \tag{8.2}$$

The anharmonic terms are as in Eqs. (6.1) and (6.2)

$$H_{anh} = \hbar \left(\lambda_0 x_0^2 + \lambda_{00} x_0^4 + \lambda_1 x_1^2 + \lambda_{11} x_1^4 \right), \tag{8.3}$$

$$H_I = \hbar \lambda_{01} x_0^2 x_1^2, \tag{8.4}$$

and this time, we will not disregard the x_i^4 terms. In the rotating wave approximation, H_{anh} and H_I become

$$H_{anh} = \hbar \lambda_{00} a^\dagger a a^\dagger a + \hbar \lambda_{11} b^\dagger b b^\dagger b, \tag{8.5}$$

$$H_I = \hbar \lambda_{01} a^\dagger a b^\dagger b. \tag{8.6}$$

The terms $\lambda_0 a^\dagger a$ and $\lambda_1 b^\dagger b$ cause a resonant frequency shift by a constant amount and do not change the dynamics, so we have absorbed these quantities into ω_0 and ω_1. As mentioned in the previous chapter, the terms $\hbar\lambda_{00} a^\dagger a a^\dagger a$ and $\hbar\lambda_{11} b^\dagger b b^\dagger b$ are called Kerr non-linearities. Since these terms commute with $a^\dagger a$ or $b^\dagger b$, they will not change the system state; however, the Kerr effect causes an intensity dependent phase shift. In the case of a coherent state, this effect results in the rotational shear on the phase space plot, whilst for a thermal state, the rotational shear will not occur due to the rotational invarianceThe other terms in the Hamiltonian are the same as in the previous chapter. Thus the master equation for the total density matrix, after tracing out the bath variables, becomes

$$\begin{aligned} \frac{d\rho}{dt} &= -i\omega_0 \left[a^\dagger a, \rho \right] - i\lambda_{00} \left[\left(a^\dagger a \right)^2, \rho \right] \\ &\quad - i\delta\omega \left[b^\dagger b, \rho \right] - i\lambda_{11} \left[\left(b^\dagger b \right)^2, \rho \right] - iE \left[b^\dagger + b, \rho \right] - i\lambda_{01} \left[a^\dagger a b^\dagger b, \rho \right] \\ &\quad + \nu \left(N_0 + 1 \right) \mathcal{D}\left[a \right] \rho + \nu N_0 \mathcal{D}\left[a^\dagger \right] \rho + \kappa \left(N_1 + 1 \right) \mathcal{D}\left[b \right] \rho + \kappa N_1 \mathcal{D}\left[b^\dagger \right] \rho. \end{aligned} \tag{8.7}$$

where ρ is the total state density matrix, and

$$N_0 = \frac{1}{\exp\left[\hbar\omega_0/k_B T_0\right] - 1}, \tag{8.8}$$

$$N_1 = \frac{1}{\exp\left[\hbar\omega_1/k_B T_1\right] - 1}, \tag{8.9}$$

and

$$\mathcal{D}\left[O\right]\rho = 2O\rho O^\dagger - O^\dagger O\rho - \rho O^\dagger O, \tag{8.10}$$

$$\mathcal{D}\left[O^\dagger\right]\rho = 2O^\dagger\rho O - OO^\dagger\rho - \rho OO^\dagger, \tag{8.11}$$

where $O = a, b$. Comparing with the master equation of Eq. (6.58), we now have two extra terms coming from non-interacting anharmonic terms as well as the detuning term.

The ancilla is assumed to be heavily damped due to measurements, *i.e.*, $\kappa \gg \lambda_{ij}, \nu$ where $i, j = 0, 1$. Then the ancilla oscillator in Eq. (8.7) remains near a thermal steady state with the average number N_1. In this case, oscillator 1 will relax very rapidly to its steady state and appear to oscillator 0 as a "bath". Thus, instead of using adiabatic elimination as done in the previous chapter, we will treat the interaction pertubatively and find the correlations of the ancilla operators. This approach is similar to that in § 6.2.1.1; however, unlike the thermal bath which is nearly unchanged by the interaction, the ancilla is changed by the interaction. Thus we need to follow the dynamics on two time-scales. We calculate the relevant steady state average and correlation functions for oscillator 1 in the presence of the anharmonic term $\lambda_{11}\left(b^\dagger b\right)^2$.

To see the consequences of the rapidly decaying oscillator 1 on the dynamics of oscillator 0, we use perturbation theory, expand the interaction Hamiltonian $H_I(t) = \lambda_{01} a^\dagger a b^\dagger b$ up to second order, and trace out the oscillator 1 variables. The master

equation for the density matrix $\rho_{\mathrm{s}}(t)$ for oscillator 0 can be written as

$$\begin{aligned}\frac{d\rho_{\mathrm{s}}(t)}{dt} &= -i\omega_0\left[a^\dagger a, \rho_{\mathrm{s}}(t)\right] - i\lambda_{00}\left[\left(a^\dagger a\right)^2, \rho_{\mathrm{s}}(t)\right] \\ &\quad + \nu\left(N_0+1\right)\mathcal{D}\left[a\right]\rho_{\mathrm{s}}(t) + \nu N_0\mathcal{D}\left[a^\dagger\right]\rho_{\mathrm{s}}(t) \\ &\quad - i\mathrm{Tr}_1\left[H_I\left(t\right), \rho(t)\right] - \int_0^t \mathrm{Tr}_1\left[H_I\left(t\right), \left[H_I\left(t'\right), \rho(t)\right]\right] dt', \end{aligned} \tag{8.12}$$

where ρ is the density matrix for the system and ancilla, $\rho = \rho_{\mathrm{s}} \otimes \rho_{\mathrm{a}}$. Explicitly, the second term of the last line of Eq. (8.12) can be written as

$$\begin{aligned}&\int_0^t \mathrm{Tr}_1\left[H_I\left(t\right), \left[H_I\left(t'\right), \rho(t)\right]\right] dt' \\ &= -\left(\lambda_{01}\right)^2 \int_0^t \mathrm{Tr}_1\left[a^\dagger a\left(t\right) b^\dagger b\left(t\right), \left[a^\dagger a\left(t'\right) b^\dagger b\left(t'\right), \rho(t)\right]\right] dt' \\ &= -\left(\lambda_{01}\right)^2 \int_0^t a^\dagger a\left(t\right) a^\dagger a\left(t'\right) \rho(t) \left\langle b^\dagger b\left(t\right) b^\dagger b\left(t'\right)\right\rangle dt' \\ &+ \left(\lambda_{01}\right)^2 \int_0^t a^\dagger a\left(t\right) \rho(t) a^\dagger a\left(t'\right) \left\langle b^\dagger b\left(t'\right) b^\dagger b\left(t\right)\right\rangle dt' \\ &+ \left(\lambda_{01}\right)^2 \int_0^t a^\dagger a\left(t'\right) \rho(t) a^\dagger a\left(t\right) \left\langle b^\dagger b\left(t\right) b^\dagger b\left(t'\right)\right\rangle dt' \\ &- \left(\lambda_{01}\right)^2 \int_0^t \rho(t) a^\dagger a\left(t'\right) a^\dagger a\left(t\right) \left\langle b^\dagger b\left(t'\right) b^\dagger b\left(t\right)\right\rangle dt'. \end{aligned} \tag{8.13}$$

The exact correlation functions of oscillator 1 are not easy to evaluate due to the presence of the anharmonic, driving, and decay terms. However, one can make an expansion of the mode b around its steady state average value and linearise the fluctuations assuming them to be small [37, 54].

Define the steady-state mean field amplitudes as $\langle b\rangle_\infty = \beta_0$. The operator b can be written, by adding small fluctuations about the steady state, as

$$b\left(t\right) = \beta_0 + b_1\left(t\right). \tag{8.14}$$

Then the interaction Hamiltonian $H_I = \lambda_{01} a^\dagger a b^\dagger b$ becomes, keeping terms up to

quadratic order in $b_1, b_1^\dagger$,

$$H_I = \lambda_{01} a^\dagger a \left[|\beta_0|^2 + \beta_0^* b_1(t) + \beta_0 b_1^\dagger(t) + b_1^\dagger(t) b_1(t) \right]. \tag{8.15}$$

The first term in Eq. (8.15) contributes to a shift in the resonant frequency by a constant amount and can be combined with the free Hamiltonian. Inserting this expression back into the first term of the last line of Eq. (8.12) gives the first order expansion term

$$-i\lambda_{01} \mathrm{Tr}_1 \left[a^\dagger a(t)\, b^\dagger b(t), \rho(t) \right] = -i\lambda_{01} \left[a^\dagger a(t), \rho_\mathrm{s} \right] \left\langle b_1^\dagger b_1(t) \right\rangle, \tag{8.16}$$

where we have used the fact that the averages of fluctuation fields vanish, *i.e.*,

$$\langle b_1 \rangle = \left\langle b_1^\dagger \right\rangle = 0. \tag{8.17}$$

Now we turn our attention to the second order term, Eq. (8.13). Note that since $\kappa \gg \nu$, the phonon number $a^\dagger a(t)$ of oscillator 0 changes on a time-scale much larger than for change of $b^\dagger b(t)$ of oscillator 1. So we can approximate $a^\dagger a(t') \simeq a^\dagger a(t)$ in Eq. (8.13) and pull oscillator 0 terms outside of the integral. Then Eq. (8.13) becomes

$$\begin{aligned}
&\int_0^t \mathrm{Tr}_1 \left[H_I(t), \left[H_I(t'), \rho(t) \right] \right] dt' \\
&= (\lambda_{01})^2 \left\{ a^\dagger a(t)\, \rho(t) a^\dagger a(t) - \left(a^\dagger a(t) \right)^2 \rho(t) \right\} \int_0^t \langle B(t,t') \rangle\, dt' \\
&+ (\lambda_{01})^2 \left\{ a^\dagger a(t)\, \rho(t) a^\dagger a(t) - \rho(t) \left(a^\dagger a(t) \right)^2 \right\} \int_0^t \langle B(t',t) \rangle\, dt',
\end{aligned} \tag{8.18}$$

where

$$\begin{aligned}\langle B(t,t')\rangle &= (\beta_0^*)^2 \langle b_1(t)\, b_1(t')\rangle + |\beta_0|^2 \left\langle b_1(t)\, b_1^\dagger(t')\right\rangle \\ &\quad + |\beta_0|^2 \left\langle b_1^\dagger(t)\, b_1(t')\right\rangle + (\beta_0)^2 \left\langle b_1^\dagger(t)\, b_1^\dagger(t')\right\rangle, \qquad (8.19)\\ \langle B(t',t)\rangle &= (\beta_0^*)^2 \langle b_1(t')\, b_1(t)\rangle + |\beta_0|^2 \left\langle b_1(t')\, b_1^\dagger(t)\right\rangle \\ &\quad + |\beta_0|^2 \left\langle b_1^\dagger(t')\, b_1(t)\right\rangle + (\beta_0)^2 \left\langle b_1^\dagger(t')\, b_1^\dagger(t)\right\rangle, \qquad (8.20)\end{aligned}$$

and higher order fluctuation terms than b_1^2 are ignored. The linearisation transforms the second-order correlation functions of the ancilla operators, $\langle b^\dagger b(t) b^\dagger b(t')\rangle$ and $\left\langle b^\dagger b(t')\, b^\dagger b(t)\right\rangle$, into first order correlation functions of fluctuation fields: $\langle b_1^\dagger(t)\, b_1(t')\rangle$, $\langle b_1^\dagger(t)\, b_1^\dagger(t')\rangle$ $\langle b_1^\dagger(t)\, b_1(t')\rangle$, and $\langle b_1^\dagger(t)\, b_1^\dagger(t')\rangle$.

8.2 A damped driven anharmonic oscillator

8.2.1 One-time correlations

In this section we calculate the one-time and two-time correlation functions of the ancilla. For this purpose, firstly we need to calculate the one-time correlation functions of a single driven anharmonic oscillator. We will follow the method of Drummond and Wall [54] who obtained one-time correlation functions. Then we extend to their method to calculate two-time correlation functions.

The master equation for a driven anharmonic oscillator 1 interacting with the thermal bath is given by

$$\begin{aligned}\frac{d\rho_b(t)}{dt} &= -i\delta\omega\left[b^\dagger b, \rho_b(t)\right] - iE\left[b^\dagger + b, \rho_b(t)\right] - i\lambda_{11}\left[\left(b^\dagger b\right)^2, \rho_b(t)\right] \\ &\quad + \kappa(N_1+1)\,\mathcal{D}[b]\,\rho_b(t) + \kappa N_1 \mathcal{D}\left[b^\dagger\right]\rho_b(t), \qquad (8.21)\end{aligned}$$

where ρ_b is the density matrix of the ancilla oscillator. The exact steady-state one-time correlation functions for a system with master equation Eq. (8.21) at *zero temperature* were given in Refs. [37, 54], in a discussion of optical bistability of a coherently

driven dispersive cavity with a cubic nonlinearity in the polarizability of the internal medium. At finite temperature, there is no exact solution.

Our objective is to derive a stochastic differential equation from the quantum master equation. Representing a density matrix in a coherent state basis is useful in systems described by Bose operators $b^\dagger, b$. We have used the Q-representation (Sec. 6.3) and the Wigner representation (Sec. 7.3.2). The Wigner function simplifies averaging symmetrically ordered operators, but is not convenient for averaging normally ordered operators. On the other hand, the Q-function has the disadvantage that not every positive Q-function corresponds to a positive semidefinite Hermitian density operator [37, 54, 55]. Instead we will use the generalised P-representation introduced by Drummond and Gardiner [55]. This involves an expansion in nondiagonal coherent state projection operators. The generalised P-function is defined as

$$\rho \equiv \int d\mu\left(\alpha,\beta\right) P\left(\alpha,\beta\right) \frac{\left|\alpha\right\rangle \left\langle\beta^*\right|}{\left\langle\beta^*|\alpha\right\rangle}, \tag{8.22}$$

where $d\mu\left(\alpha,\beta\right) = d^2\alpha d^2\beta$. This representation allows (α,β) to vary independently over the whole complex plane. It has been mathematically proved that $P\left(\alpha,\beta\right)$ always exists for a physical density operator and can always be chosen positive [55]. For brevity we write $P\left(\alpha,\beta\right) = P\left(\hat{\beta}\right)$. The following identities hold for the generalised P-representation:

$$b\rho \leftrightarrow \alpha P\left(\hat{\beta}\right), \tag{8.23}$$

$$b^\dagger\rho \leftrightarrow \left(\beta - \frac{\partial}{\partial\alpha}\right) P\left(\hat{\beta}\right), \tag{8.24}$$

$$\rho b \leftrightarrow \left(\alpha - \frac{\partial}{\partial\beta}\right) P\left(\hat{\beta}\right), \tag{8.25}$$

$$\rho b^\dagger \leftrightarrow \beta P\left(\hat{\beta}\right). \tag{8.26}$$

Using the above transformations, the Fokker-Planck equation corresponding to

the master equation Eq. (8.21) can now be written as

$$\begin{aligned}\frac{\partial}{\partial t}P\left(\hat{\beta}\right) = \Bigg\{ & \frac{\partial}{\partial\alpha}\left[\left(\kappa + i\delta\omega\right)\alpha - 2i\lambda_{11}\alpha^2\beta + iE\right] - i\lambda_{11}\frac{\partial^2}{\partial\alpha^2}\alpha^2 \\ & + \frac{\partial}{\partial\beta}\left[\left(\kappa - i\delta\omega\right)\beta - 2i\lambda_{11}\beta^2\alpha - iE\right] \\ & -i\lambda_{11}\frac{\partial^2}{\partial\beta^2}\beta^2 + 2\kappa\bar{n}_1\frac{\partial^2}{\partial\alpha\partial\beta}\Bigg\} P\left(\hat{\beta}\right). \end{aligned} \tag{8.27}$$

Drummond and Gardiner have shown [55] that the Fokker-Planck equation in $\hat{\beta}$ can be transformed to a stochastic differential equation with positive definite diffusion[1]. They found that the stochastic differential equations in the Ito calculus corresponding to Eq. (8.27) are

$$\begin{aligned}\frac{\partial}{\partial t}\begin{bmatrix}\alpha\\ \beta\end{bmatrix} = & \begin{bmatrix}-iE - \alpha\left[\kappa + i\delta\omega + 2i\lambda_{11}\alpha\beta\right]\\ iE - \beta\left[\kappa - i\delta\omega - 2i\lambda_{11}\beta\alpha\right]\end{bmatrix} \\ & + \begin{bmatrix}-2i\lambda_{11}\alpha^2 & 2\kappa\bar{n}_1\\ 2\kappa\bar{n}_1 & 2i\lambda_{11}\beta^2\end{bmatrix}^{1/2}\begin{bmatrix}\xi_1\\ \xi_2\end{bmatrix}, \end{aligned} \tag{8.28}$$

where ξ_1 and ξ_2 are random Gaussian functions so that α and β are complex conjugate in the mean[2]. This stochastic differential equation is non-linear and not solvable as it is. However, it is reasonable to use a small noise expansion and linearise the fluctuations about the steady state of the mean field amplitudes. Thus we write β in terms of the mean amplitude and first order expansion of the fluctuation,

$$\beta\left(t\right) = \beta_0 + \beta_1\left(t\right), \tag{8.29}$$

where β_0 is the mean amplitude of β, and β_1 is the zero mean fluctuation amplitude. We have a similar expression for α. Thus α_0 and β_0 are complex conjugate to each other (i.e., $\alpha_0\beta_0 = \left|\beta_0\right|^2 = \left|\alpha_0\right|^2$). Then the fluctuation amplitude vector $\hat{\beta}_1 =$

[1]Note that their notation is different from ours: their β corresponds to our α and their $\beta^\dagger$ to our β.

[2]The mean of α and β are complex conjugate. However, fluctuation introduces a stochastic component, and so α and β deviate from being complex conjugate.

$(\alpha_1, \beta_1)^T$obeys a stochastic differential equation

$$\frac{\partial}{\partial t}\hat{\beta}_1(t) = -\mathbf{A}\cdot\hat{\beta}_1(t) + \mathbf{D}^{1/2}\left(\hat{\beta}_0\right)\xi(t), \tag{8.30}$$

where $\xi = (\xi_1, \xi_2)^T$ is the noise vector, $\mathbf{A}$ is the linearised drift matrix and $\mathbf{D}$ is the diffusion matrix evaluated at $\hat{\beta} = \hat{\beta}_0$. The matrices $\mathbf{A}$ and $\mathbf{D}$ are

$$\mathbf{A} = \begin{bmatrix} \kappa + i\delta\omega + 4i\lambda_{11}n_0 & 2i\lambda_{11}\alpha_0^2 \\ -2i\lambda_{11}\beta_0^2 & \kappa - i\delta\omega - 4i\lambda_{11}n_0 \end{bmatrix}, \tag{8.31}$$

where $n_0 \equiv \alpha_0\beta_0$, and

$$\mathbf{D} = \begin{bmatrix} -2i\lambda_{11}\alpha_0^2 & 2\kappa\bar{n}_1 \\ 2\kappa\bar{n}_1 & 2i\lambda_{11}\beta_0^2 \end{bmatrix}. \tag{8.32}$$

The one-time correlation matrix is defined as

$$\mathbf{C}(t,t) \equiv \begin{bmatrix} \langle\alpha^2\rangle - \langle\alpha\rangle^2 & \langle\beta\alpha\rangle - |\langle\beta\rangle|\,|\langle\alpha\rangle| \\ \langle\beta\alpha\rangle - |\langle\beta\rangle|\,|\langle\alpha\rangle| & \langle\beta^2\rangle - \langle\beta\rangle^2 \end{bmatrix}. \tag{8.33}$$

Using Eq. (8.29), $\mathbf{C}(t,t)$ becomes

$$\mathbf{C}(t,t) = \begin{bmatrix} \langle\alpha_1^2\rangle & \langle\beta_1\alpha_1\rangle \\ \langle\beta_1\alpha_1\rangle & \langle\beta_1^2\rangle \end{bmatrix}. \tag{8.34}$$

Given Eq. (8.30), Chaturvedi *et. al.* [37, 54, 56, 57] have derived the expression:

$$\mathbf{C}(t,t) = \frac{\mathbf{D}\det(\mathbf{A}) + [\mathbf{A} - \mathbf{I}\mathrm{Tr}(\mathbf{A})]\,\mathbf{D}\,[\mathbf{A} - \mathbf{I}\mathrm{Tr}(\mathbf{A})]^T}{2\mathrm{Tr}(\mathbf{A})\det(\mathbf{A})}. \tag{8.35}$$

Carrying out the calculation we obtain

$$\mathbf{C}(t,t) = \frac{1}{\Lambda}\begin{bmatrix} S & T \\ T & S^* \end{bmatrix}, \tag{8.36}$$

where

$$\Lambda = \kappa^2 + \Lambda_1, \tag{8.37}$$

$$\Lambda_1 = (\delta\omega)^2 + 8(\delta\omega)\lambda_{11}n_0 + 12\lambda_{11}^2 n_0^2, \tag{8.38}$$

$$S = -i\lambda_{11}\alpha_0^2(\kappa - i\delta\omega - 4i\lambda_{11}n_0)(2N_1 + 1), \tag{8.39}$$

$$S^* = i\lambda_{11}\beta_0^2(\kappa + i\delta\omega + 4i\lambda_{11}n_0)(2N_1 + 1), \tag{8.40}$$

$$T = N_1|\kappa + i\delta\omega + 4i\lambda_{11}n_0|^2 + 2\lambda_{11}^2 n_0^2. \tag{8.41}$$

8.2.2 Two-time correlations

Based on the results in Subsection 8.2.1 we now derive an expression for the two-time steady state correlation matrix

$$\mathbf{C}(t,t') = \begin{bmatrix} \langle\alpha_1(t)\alpha_1(t')\rangle & \langle\alpha_1(t)\beta_1(t')\rangle \\ \langle\beta_1(t)\alpha_1(t')\rangle & \langle\beta_1(t)\beta_1(t')\rangle \end{bmatrix}. \tag{8.42}$$

A solution to Eq. (8.30) is

$$\hat{\beta}_1(t) = \exp(-\mathbf{A}t)\hat{\beta}_1(t_0) + \int_{-\infty}^{t} \exp[-\mathbf{A}(t-t')]\mathbf{D}^{1/2}dW, \tag{8.43}$$

where $dW = \xi\sqrt{dt}$. Then the mean of $\hat{\beta}_1(t)$ is zero since the average of the fluctuation is zero, *i.e.*,

$$\left\langle \hat{\beta}_1(t) \right\rangle = \exp(-\mathbf{A}t)\hat{\beta}_1(t_0) = 0. \tag{8.44}$$

and using Eqs. (8.43) and (8.44), two time correlation matrix Eq. (8.42) can be obtained in a form:

$$\mathbf{C}(t,t') = \left\langle \hat{\alpha}_1(t)\hat{\beta}_1(t') \right\rangle = \int_{-\infty}^{\min(t,t')} \exp(-\mathbf{A}(t-t''))\mathbf{D}\exp\left(-\mathbf{A}^T(t'-t'')\right)dt''. \tag{8.45}$$

Thus $\mathbf{C}(t,t')$ for $t > t'$ is

$$\begin{aligned}\mathbf{C}(t,t') &= \exp\left(-\mathbf{A}(t-t')\right) \int_{-\infty}^{t'} \exp\left(-\mathbf{A}(t'-t'')\right) \mathbf{D} \exp\left(-\mathbf{A}^T(t'-t'')\right) dt'' \\ &= \exp\left(-\mathbf{A}(t-t')\right) \mathbf{C}(t,t), \end{aligned} \tag{8.46}$$

and similarly for $t < t'$

$$\mathbf{C}(t,t') = \mathbf{C}(t,t) \exp\left(-\mathbf{A}^T(t'-t)\right). \tag{8.47}$$

Let us define $\mathbf{M}(t,t') \equiv \exp[-\mathbf{A}(t-t')]$. The matrix $\mathbf{M}$ can be calculated as follows. Let the matrix $\mathbf{U} = (u_1, u_2)$ diagonalise $\mathbf{A}$ with eigenvalues $\lambda_\pm$. The eigenvalues for this 2×2 matrix can be found from the characteristic equation:

$$\begin{aligned}\lambda_\pm &= \frac{\mathrm{Tr}(\mathbf{A}) \mp \sqrt{[\mathrm{Tr}(\mathbf{A})]^2 - 4\det(\mathbf{A})}}{2} \\ &= \kappa \mp i\sqrt{\Lambda_1}, \end{aligned} \tag{8.48}$$

where Λ_1 is defined in Eq. (8.38). The eigenvectors are

$$u_1 = \left(-\frac{\delta\omega + 4\lambda_{11}n_0 + \sqrt{\Lambda_1}}{2\alpha^2\lambda_{11}}, 1\right), \tag{8.49}$$

$$u_2 = \left(-\frac{\delta\omega - 4\lambda_{11}n_0 + \sqrt{\Lambda_1}}{2\beta^2\lambda_{11}}, 1\right). \tag{8.50}$$

We can then obtain the matrix $\mathbf{M}$ as

$$\begin{aligned}\mathbf{M}(t,t') &= \mathbf{U} \begin{bmatrix} \exp\left(-\lambda_+(t-t')\right) & 0 \\ 0 & \exp\left(-\lambda_-(t-t')\right) \end{bmatrix} \mathbf{U}^{-1} \\ &= \frac{1}{2\sqrt{\Lambda_1}} \begin{bmatrix} M_{11} & M_{12} \\ M_{21} & M_{22} \end{bmatrix}, \end{aligned} \tag{8.51}$$

where

$$\mathbf{M}_{11} = (\Lambda_1 - c)\, e^{-\lambda_-(t-t')} + (\Lambda_1 + c)\, e^{-\lambda_+(t-t')}, \tag{8.52}$$

$$\mathbf{M}_{12} = 2\lambda_{11}\alpha_0^2 \left[-e^{-\lambda_-(t-t')} + e^{-\lambda_+(t-t')}\right], \tag{8.53}$$

$$\mathbf{M}_{21} = 2\lambda_{11}\beta_0^2 \left[e^{-\lambda_-(t-t')} - e^{-\lambda_+(t-t')}\right], \tag{8.54}$$

$$\mathbf{M}_{22} = (\Lambda_1 + c)\, e^{-\lambda_-(t-t')} + (\Lambda_1 - c)\, e^{-\lambda_+(t-t')}, \tag{8.55}$$

and $c \equiv 4\lambda_{11}n_0 + \delta\omega$. The two-time correlation matrix Eq. (8.42), follows directly from Eqs. (8.46) (8.47) and (8.51), and the fact that $\exp[-\mathbf{A}(t-t')] = \mathbf{M}(t,t')$ and $\exp[-\mathbf{A}^T(t'-t)] = \mathbf{M}^T(t',t)$:

The final results for $\mathbf{C}\,(t,t')$ for $t > t'$ are

$$\begin{aligned}\langle \alpha_1(t)\,\alpha_1(t')\rangle = {} & \frac{1}{2\sqrt{\Lambda_1}}\left\{(\Lambda_1+c)\exp\left[-\lambda_+(t-t')\right] + (\Lambda_1-c)\exp\left[-\lambda_-(t-t')\right]\right\}\left\langle \alpha_1^2\right\rangle \\ & + \frac{\lambda_{11}\alpha_0^2}{\sqrt{\Lambda_1}}\left\{\exp\left[-\lambda_+(t-t')\right] - \exp\left[-\lambda_-(t-t')\right]\right\}\langle \alpha_1\beta_1\rangle,\end{aligned} \tag{8.56}$$

$$\begin{aligned}\langle \beta_1(t)\,\alpha_1(t')\rangle = {} & \frac{1}{2\sqrt{\Lambda_1}}\left\{(\Lambda_1+c)\exp\left[-\lambda_+(t-t')\right] + (\Lambda_1-c)\exp\left[-\lambda_-(t-t')\right]\right\}\langle \beta_1\alpha_1\rangle \\ & + \frac{\lambda_{11}\alpha_0^2}{\sqrt{\Lambda_1}}\left\{\exp\left[-\lambda_+(t-t')\right] - \exp\left[-\lambda_-(t-t')\right]\right\}\left\langle \beta_1^2\right\rangle,\end{aligned} \tag{8.57}$$

$$\begin{aligned}\langle \alpha_1(t)\,\beta_1(t')\rangle = {} & \frac{\Lambda_1 - c^2}{4\lambda_{11}\alpha_0^2\sqrt{\Lambda_1}}\left\{\exp\left[-\lambda_+(t-t')\right] - \exp\left[-\lambda_-(t-t')\right]\right\}\left\langle \alpha_1^2\right\rangle \\ & + \frac{1}{2\sqrt{\Lambda_1}}\left\{(\Lambda_1-c)\exp\left[-\lambda_+(t-t')\right] + (\Lambda_1+c)\exp\left[-\lambda_-(t-t')\right]\right\}\langle \alpha_1\beta_1\rangle,\end{aligned} \tag{8.58}$$

$$\langle \beta_1(t)\,\beta_1(t')\rangle = \frac{\Lambda_1 - c^2}{4\lambda_{11}\alpha_0^2\sqrt{\Lambda_1}}\left\{\exp\left[-\lambda_+(t-t')\right] - \exp\left[-\lambda_-(t-t')\right]\right\}\langle\beta_1\alpha_1\rangle + \frac{1}{2\sqrt{\Lambda_1}}\left\{(\Lambda_1 - c)\exp\left[-\lambda_+(t-t')\right] + (\Lambda_1 + c)\exp\left[-\lambda_-(t-t')\right]\right\}\left\langle\beta_1^2\right\rangle, \tag{8.59}$$

and for $t < t'$ are

$$\langle \alpha_1(t')\,\alpha_1(t)\rangle = \frac{1}{2\sqrt{\Lambda_1}}\left\{(\Lambda_1 + c)\exp\left[-\lambda_+(t-t')\right] + (\Lambda_1 - c)\exp\left[-\lambda_-(t-t')\right]\right\}\left\langle\alpha_1^2\right\rangle + \frac{-(\Lambda_1 - c^2)}{4\lambda_{11}\beta_1^2\sqrt{\Lambda_1}}\left\{\exp\left[-\lambda_+(t-t')\right] - \exp\left[-\lambda_-(t-t')\right]\right\}\langle\beta_1\alpha_1\rangle, \tag{8.60}$$

$$\langle \beta_1(t')\,\alpha_1(t)\rangle = -\frac{\lambda_{11}\alpha_0^2}{\sqrt{\Lambda_1}}\left\{\exp\left[-\lambda_+(t-t')\right] - \exp\left[-\lambda_-(t-t')\right]\right\}\left\langle\alpha_1^2\right\rangle + \frac{1}{2\sqrt{\Lambda_1}}\left\{(\Lambda_1 - c)\exp\left[-\lambda_+(t-t')\right] + (\Lambda_1 + c)\exp\left[-\lambda_-(t-t')\right]\right\}\langle\beta_1\alpha_1\rangle, \tag{8.61}$$

$$\langle \alpha_1(t')\,\beta_1(t)\rangle = \frac{1}{2\sqrt{\Lambda_1}}\left\{(\Lambda_1 + c)\exp\left[-\lambda_+(t-t')\right] + (\Lambda_1 - c)\exp\left[-\lambda_-(t-t')\right]\right\}\langle\alpha_1\beta_1\rangle + \frac{-(\Lambda_1 - c^2)}{4\lambda_{11}\beta_1^2\sqrt{\Lambda_1}}\left\{\exp\left[-\lambda_+(t-t')\right] - \exp\left[-\lambda_-(t-t')\right]\right\}\left\langle\beta_1^2\right\rangle, \tag{8.62}$$

$$\langle \beta_1(t')\,\beta_1(t)\rangle = -\frac{\lambda_{11}\alpha_0^2}{\sqrt{\Lambda_1}}\left\{\exp\left[-\lambda_+(t-t')\right] - \exp\left[-\lambda_-(t-t')\right]\right\}\langle\alpha_1\beta_1\rangle + \frac{1}{2\sqrt{\Lambda_1}}\left\{(\Lambda_1 - c)\exp\left[-\lambda_+(t-t')\right] + (\Lambda_1 + c)\exp\left[-\lambda_-(t-t')\right]\right\}\left\langle\beta_1^2\right\rangle. \tag{8.63}$$

8.2.3 Operator correspondences to c-numbers

Note that in the generalised P-representation, the c-number time correlation function corresponds to a normally ordered time correlation function of the operators. Thus the correlations above do not correspond to all the two-time correlation functions we

need. In general the two-time correlation A and B can be written as $(t > t')$

$$\langle A(t)\, B(t')\rangle = \mathrm{Tr_s}\left\{AV(t,t')\left\{B\rho(t')\right\}\right\}, \tag{8.64}$$

$$\langle A(t')\, B(t)\rangle = \mathrm{Tr_s}\left\{BV(t,t')\left\{\rho(t')\, A\right\}\right\}, \tag{8.65}$$

where $V(t+\tau,t)$ is the evolution operator, which acts as

$$V(t,t')\left\{B\rho(t')\right\} = \mathrm{Tr_s}\left\{\exp\left[-\frac{iH(t-t')}{\hbar}\right] B\rho(t') \exp\left[\frac{iH(t-t')}{\hbar}\right]\right\}. \tag{8.66}$$

Using Eqs. (8.64) and (8.65), we derive the operator correspondence to the two-time correlation matrix $\mathbf{C}(t,t')$ we have just found. For example, using Eq. (8.64) and $\left\langle b_1^\dagger(t)\, b_1(t')\right\rangle$ can be written as

$$\left\langle b_1^\dagger(t)\, b_1(t')\right\rangle = \mathrm{Tr_s}\left\{b_1^\dagger V(t,t')\left\{b_1\rho(t')\right\}\right\}. \tag{8.67}$$

From the identity Eq. (8.23), we evaluate $b_1\rho(t)$:

$$\left\langle b_1^\dagger(t)\, b_1(t')\right\rangle = \mathrm{Tr_s}\left\{b_1^\dagger V(t,t')\int d\mu\left(\hat{\beta}\right)\alpha_1(t')\, P\left(\hat{\beta}\right)\frac{|\alpha\rangle\langle\beta^*|}{\langle\beta^*|\alpha\rangle}\right\}. \tag{8.68}$$

Using the permutation property of the trace, moving $b_1^\dagger$ to the right and evaluating, we obtain

$$\begin{aligned}\left\langle b_1^\dagger(t)\, b_1(t')\right\rangle &= \mathrm{Tr_s}\left\{\alpha_1(t')\left(V(t,t')\int d\mu\left(\hat{\beta}\right)P\left(\hat{\beta}\right)\frac{|\alpha\rangle\langle\beta^*|\, b_1^\dagger}{\langle\beta^*|\alpha\rangle}\right)\right\}\\ &= \mathrm{Tr_s}\left\{\beta_1(t)\,\alpha_1(t')\right\}.\end{aligned} \tag{8.69}$$

This result was to be expected as the P function has a normal ordered operator correspondence. (Note that, by design, for the generalised P-function.$b_1^\dagger$ corresponds to β_1 and b_1 to α_1.)

Similarly evaluating an anti-normal ordered correlation function using Eq. (8.65),

we first obtain

$$\left\langle b_1(t')\, b_1^\dagger(t)\right\rangle = \mathrm{Tr_s}\left\{b_1^\dagger V(t,t')\left\{\rho(t')\, b_1\right\}\right\}, \tag{8.70}$$

$$= \mathrm{Tr_s}\left\{b_1^\dagger V(t,t')\int d\mu\left(\hat{\beta}\right)\left(\alpha_1 - \frac{\partial}{\partial\beta_1(t')}\right) P\left(\hat{\beta}\right)\frac{|\alpha\rangle\langle\beta^*|}{\langle\beta^*|\alpha\rangle}\right\}, \tag{8.71}$$

$$= \mathrm{Tr_s}\left\{b_1^\dagger V(t,t')\int d\mu\left(\hat{\beta}\right)\alpha_1(t)\, P\left(\hat{\beta}\right)\frac{|\alpha\rangle\langle\beta^*|}{\langle\beta^*|\alpha\rangle}\right\}$$

$$- \mathrm{Tr_s}\left\{b_1^\dagger V(t,t')\int d\mu\left(\hat{\beta}\right)\frac{\partial}{\partial\beta_1(t')} P\left(\hat{\beta}\right)\frac{|\alpha\rangle\langle\beta^*|}{\langle\beta^*|\alpha\rangle}\right\}. \tag{8.72}$$

Permuting $b_1^\dagger$ and evaluating the result gives

$$\left\langle b_1(t')\, b_1^\dagger(t)\right\rangle = \mathrm{Tr_s}\left\{\alpha_1(t')\left(V(t,t')\int d\mu\left(\hat{\beta}\right) P\left(\hat{\beta}\right)\frac{|\alpha\rangle\langle\beta^*|\, b_1^\dagger}{\langle\beta^*|\alpha\rangle}\right)\right\}$$

$$- \mathrm{Tr_s}\left\{\left(V(t,t')\int d\mu\left(\hat{\beta}\right)\frac{\partial}{\partial\beta_1(t')} P\left(\hat{\beta}\right)\frac{|\alpha\rangle\langle\beta^*|\, b_1^\dagger}{\langle\beta^*|\alpha\rangle}\right)\right\}, \tag{8.73}$$

$$= \mathrm{Tr_s}\left\{\alpha_1(t')\,\beta_1(t)\right\}$$

$$- \mathrm{Tr_s}\left\{\int d\mu\left(\hat{\beta}\right)\left[\frac{\partial}{\partial\beta_1(t')}\beta_1(t)\right] P\left(\hat{\beta}\right)\frac{|\alpha\rangle\langle\beta^*|}{\langle\beta^*|\alpha\rangle}\right\}. \tag{8.74}$$

where we have used the integration by parts and discarded the surface term. Now we need to evaluate $\partial\beta_1(t)/\partial\beta_1(t')$. Recall that

$$\begin{pmatrix}\alpha_1(t)\\ \beta_1(t)\end{pmatrix} = \exp(-\mathbf{A}\tau)\begin{pmatrix}\alpha_1(t')\\ \beta_1(t')\end{pmatrix} = \mathbf{M}(t,t')\begin{pmatrix}\alpha_1(t')\\ \beta_1(t')\end{pmatrix}. \tag{8.75}$$

Thus we have

$$\beta_1(t) = \mathbf{M}_{21}\alpha_1(t') + \mathbf{M}_{22}\beta_1(t'), \tag{8.76}$$

where $\mathbf{M}_{ij}$ is the element of $\mathbf{M}$. Then

$$\frac{\partial}{\partial\beta_1(t')}\beta_1(t) = \mathbf{M}_{22}. \tag{8.77}$$

Finally, we obtain

$$\left\langle b_1(t')\, b_1^\dagger(t)\right\rangle = \langle\beta_1(t)\,\alpha_1(t')\rangle + \mathbf{M}_{22}. \tag{8.78}$$

Thus, we obtain the following relations.

$$\langle b_1(t)\, b_1(t')\rangle = \langle \beta_1(t)\, \beta_1(t')\rangle, \tag{8.79}$$

$$\left\langle b_1(t)\, b_1^\dagger(t')\right\rangle = \left\langle \beta_1(t)\, \beta_1^\dagger(t')\right\rangle + \mathbf{M}_{11}(t,t'), \tag{8.80}$$

$$\left\langle b_1^\dagger(t)\, b_1(t')\right\rangle = \left\langle \beta_1^\dagger(t)\, \beta_1(t')\right\rangle, \tag{8.81}$$

$$\left\langle b_1^\dagger(t)\, b_1^\dagger(t')\right\rangle = \left\langle \beta_1^\dagger(t)\, \beta_1^\dagger(t')\right\rangle + \mathbf{M}_{21}(t,t'), \tag{8.82}$$

$$\langle b_1(t')\, b_1(t)\rangle = \langle \beta_1(t)\, \beta_1(t')\rangle + \mathbf{M}_{12}(t,t'), \tag{8.83}$$

$$\left\langle b_1(t')\, b_1^\dagger(t)\right\rangle = \left\langle \beta_1^\dagger(t)\, \beta_1(t')\right\rangle + \mathbf{M}_{22}(t,t'), \tag{8.84}$$

$$\left\langle b_1^\dagger(t')\, b_1(t)\right\rangle = \left\langle \beta_1(t)\, \beta_1^\dagger(t')\right\rangle, \tag{8.85}$$

$$\left\langle b_1^\dagger(t')\, b_1^\dagger(t)\right\rangle = \left\langle \beta_1^\dagger(t)\, \beta_1^\dagger(t')\right\rangle, \tag{8.86}$$

where $\mathbf{M}_{ij}(t,t')$ is the matrix elements of the matrix $\boldsymbol{M}(t,t')$.

8.3 The master equation for the reduced density matrix

Having found one-time and two-time correlation functions, we can now evaluate Eqs. (8.16) and (8.18) and obtain the master equation for the reduced density matrix of oscillator 0 as:

$$\begin{aligned}\frac{d\rho_{\mathrm{s}}}{dt} &= -i\left(\omega_0+\Delta\right)\left[a^\dagger a,\rho_{\mathrm{s}}\right] - \Gamma\left[a^\dagger a,\left[a^\dagger a,\rho_{\mathrm{s}}\right]\right] - i\Theta\left[\left(a^\dagger a\right)^2,\rho_{\mathrm{s}}\right] \\ &\quad + \nu\left(N_0+1\right)\mathcal{D}\left[a\right]\rho_{\mathrm{s}} + \nu N_0\mathcal{D}\left[a^\dagger\right]\rho_{\mathrm{s}},\end{aligned} \tag{8.87}$$

where

$$\Delta = \lambda_{01}\left(\frac{N_1}{\Lambda}\left|\kappa + i\delta\omega + 4i\lambda_{11}n_0\right|^2 + \frac{2}{\Lambda}\lambda_{11}^2 n_0^2 + n_0\right), \tag{8.88}$$

$$\Theta = \lambda_{00} - \frac{\lambda_{01}^2 n_0}{\Lambda}\left(\delta\omega + 2\lambda_{11}n_0\right), \tag{8.89}$$

$$\begin{aligned}\Gamma = &-\lambda_{01}^2\frac{4\kappa n_0^2\lambda_{11}}{\Lambda^2}(2N_1+1)\left(\delta\omega + 3\lambda_{11}n_0\right)\\ &+\lambda_{01}^2\left\{\frac{1}{2\Lambda^2}\left[4N_1 n_0\kappa\left|\kappa + i\delta\omega + 4i\lambda_{11}n_0\right|^2 + 8\lambda_{11}^2 n_0^3\kappa\right] + \frac{1}{\Lambda}n_0\right\},\end{aligned} \tag{8.90}$$

with

$$\Lambda = \kappa^2 + \delta\omega^2 + 8\delta\omega\lambda_{11}n_0 + 12\lambda_{11}^2 n_0^2. \tag{8.91}$$

In Eq. (8.87), Δ in the first term is the resonant frequency shift due to anharmonic interactions, and Γ is the phase diffusion coefficient associated with the backaction due to an effective measurement of $a^\dagger a$. The Kerr non-linear phase shift is the third term; its coefficient Θ depends on the anharmonicity of both oscillators λ_{00} and λ_{11} as well as the detuning of the ancilla oscillator. The last two terms drive from the thermal coupling to the system and are responsible for the quantum jumps.

8.3.1 Effects of the anharmonic terms

Firstly, notice that in the case of no detuning and no non-linear uncoupled anharmonic terms (i.e., $\delta\omega = 0$, $\lambda_{00} = \lambda_{11} = 0$), we have

$$\Delta = \lambda_{01}\left(N_1 + n_0\right), \tag{8.92}$$

$$\Theta = 0, \tag{8.93}$$

$$\Gamma = \frac{\lambda_{01}^2 n_0\left(2N_1+1\right)}{\kappa}. \tag{8.94}$$

which agree with the results of adiabatic elimination in the previous chapter.

Secondly, from Eq. (8.87), we see that the condition $\kappa \gg \lambda_{11}$ makes the effect of the non-linear uncoupled anharmonic terms in Δ and Γ very small, which justifies

the assumption of neglecting λ_{11} from the start in Chapter 6. However, the full calculation allows us to make quantitative estimates of the condition $\kappa \gg \lambda_{11}$.

The expressions in Eq. (8.87)-(8.90 depend on the value of n_0 which gives the intensity of the driven motion of the nonlinear oscillator. In the next section we show that there exist parameter values leading to a multiplicity of solutions. This will limit the strength of the driving that can be used in experiment. This issue is also discussed in the next section.

8.3.2 Parameter constraints imposed by the anharmonic terms

We now examine the steady state amplitude β as a function of the driving amplitude E. In the steady state, $\partial\beta/\partial t = 0$ and the mean phonon number of the driven ancilla is $n_0 = \alpha_0\beta_0$, where $|\beta_0| = |\alpha_0|$ is the steady state driving amplitude. Thus, the steady state solutions are given by

$$0 = \frac{\partial}{\partial t}\begin{bmatrix} \alpha \\ \beta \end{bmatrix} = \begin{bmatrix} -iE - \alpha_0\left[\kappa + i\delta\omega + 2i\lambda_{11}\alpha_0\beta_0\right] \\ iE - \beta_0\left[\kappa - i\delta\omega - 2i\lambda_{11}\beta_0\alpha_0\right] \end{bmatrix}, \tag{8.95}$$

i.e., by the solutions of above, we obtain

$$|E|^2 = n_0\left[\kappa^2 + \left(\delta\omega + 2\lambda_{11}n_0\right)^2\right]. \tag{8.96}$$

Equation (8.96) has an analogy to a classical anharmonic oscillator discussed, for example, in Landau and Lifshitz [58]. (The results are sketched in Fig. 8.1.) The resonance frequency shifts with the driving strength. The region between the point C and D (shown as a dotted line) is the instability region. Classically the oscillator will take one or the other of the stable solutions; however, what will happen in the quantum case is not known. As Eq. (7.93) indicates, in order to obtain high k/ν ratio, we want a maximum possible driving strength without getting into the instability region, ideally driving near point B.

The instability points of the solution can be found from the stochastic differential

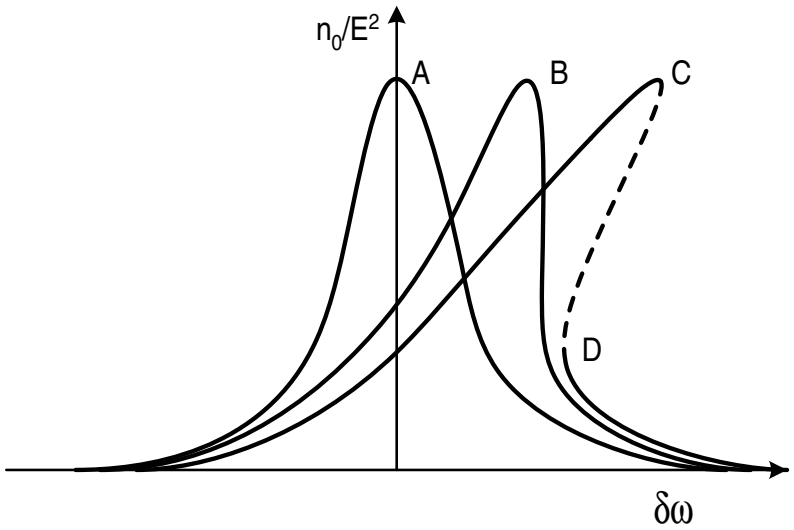

Figure 8.1: A sketch of n_0/E^2 *vs.* $\delta\omega$ with various driving strengths. Curve A shows the linear resonance for small driving. Curves B and C show the effect of increasing driving strength. Notice that B shows the limiting case for no multiplicity of solutions. For case C there are multiple solutions over a range of frequencies. The dotted branch corresponds to unstable solutions.

equation Eq. (8.30) in the steady state, that is, we find the stable solutions for $\mathbf{A}$ in the steady state. Since $\mathbf{A}$ is a 2×2 matrix, its characteristic equation is given by

$$x^2 - x\mathrm{Tr}\left(\mathbf{A}\right) + \det\left(\mathbf{A}\right) = 0. \tag{8.97}$$

Given a system with this characteristic equation and arranged in matrix form,

$$\begin{bmatrix} x^2 & 1 & \det\left(\mathbf{A}\right) \\ x & \mathrm{Tr}\left(\mathbf{A}\right) & .. \\ 1 & \frac{\mathrm{Tr}(\mathbf{A})\det(\mathbf{A})}{\mathrm{Tr}(\mathbf{A})} & .. \end{bmatrix}, \tag{8.98}$$

the Routh-Hurwitz stability criterion states that all coefficients in the second column must be positive or all negative but not a combination of both. From Eq. (8.31), $\mathrm{Tr}\left(\mathbf{A}\right) = 2\kappa > 0$, thus we must have $\det\left(\mathbf{A}\right) > 0$ to have a stable solution. Calculating $\det\left(\mathbf{A}\right)$ gives

$$\det\left(\mathbf{A}\right) = \kappa^2 + \delta\omega^2 + 12\lambda_{11}^2 n_0^2 + 8\delta\omega\lambda_{11} n_0. \tag{8.99}$$

So the instability point is $\det(\mathbf{A}) = 0$,

$$\delta\omega^{\pm} = -4\lambda_{11}n_0 \pm \sqrt{4\lambda_{11}^2 n_0^2 - \kappa^2}. \tag{8.100}$$

Thus the range $\delta\omega^- < \delta\omega < \delta\omega^+$ is the bistability region. Therefore when the ancilla is driven for our QND scheme, the driving strength should be adjusted such that this region will be avoided. Notice that in the absence of nonlinearity ($\lambda_{11} = 0, \delta\omega \neq 0$), bistability does not exit since $\det(\mathbf{A}) > 0$. The same is true in the case where the detuning is zero ($\delta\omega = 0, \lambda_{11} \neq 0$).

The instability points are, from Eq. (8.100)

$$n_0 = \frac{\kappa}{2\lambda_{11}}, \tag{8.101}$$

and

$$\delta\omega = -4\lambda_{11}n_0 = -2\kappa. \tag{8.102}$$

This is the detuning of the point B. The driving amplitude E is from Eq. (8.96)

$$\begin{aligned} |E|^2 &= n_0\left[\kappa^2 + (\delta\omega + 2\lambda_{11}n_0)^2\right] \\ &= \frac{\kappa^3}{2\lambda_{11}}. \end{aligned} \tag{8.103}$$

Carr *et al.* has estimated the anharmonic coefficient for an elastic beam with rectangular cross-section[35], and it is given by

$$\lambda_{11} = \frac{1}{4}\left[3\frac{m_1}{2}\left(\frac{\pi^2}{\sqrt{12}}\sqrt{\frac{E_B}{\rho}}\frac{d_1}{L_1^2}\right)^2\frac{1}{d_1^2}\right]\frac{\hbar}{m_1^2\omega_1^3}\frac{\hbar\omega_1}{\hbar}. \tag{8.104}$$

where E_B is the bulk modulus and ρ is the mass density. Using Eq. (7.95) and the geometry used in Sec. 7.4.2, we obtain $\lambda_{11}/\omega_1 = 1.65 \times 10^{-6}/\omega_1$, and $|\alpha|$

$$|\alpha| = \sqrt{\frac{\kappa}{2\lambda_{11}}} = 4.4 \times 10^5, \tag{8.105}$$

which corresponds to the scaled displacement of the ancilla $x_1/d_1 = 0.06$.

The total phonon number in the oscillator is, from Eqs. (8.36) and (8.41)

$$\begin{aligned} n &= |\alpha_0\beta_0|^2 + \langle \beta_1(t)\,\alpha_1(t')\rangle \\ &= n_0 + \frac{1}{\det(\mathbf{A})}\left[N_1\left|\kappa + i\delta\omega + 4i\lambda_{11}n_0\right|^2 + 2\lambda_{11}^2 n_0^2\right]. \end{aligned} \tag{8.106}$$

If there are no detuning and no nonlinearity, the phonon intensity becomes

$$n = n_0 + N_1, \tag{8.107}$$

that is, the phonon number is just the sum of the driving term contribution and the thermal bath. This is because the driving and the excitation by the thermal bath are uncorrelated and the result is simply a linear superposition. With the presence of nonlinearity, there are additional terms in the intensity. There is a term, $2\lambda_{11}^2 n_0^2$, that is proportional to the intensity n_0^2 even at zero temperature. This is due to the quantum fluctuations in the oscillator and these terms do not exist for the classical oscillator, whereas the terms $N_1\left(i\delta\omega + 4i\lambda_{11}n_0\right)$ will exist in the classical counterpart as well.) When $\det(\mathbf{A})$ is zero, Eq. (8.106) diverges. This is where our linearisation approximation fails and further analysis is required expanding the fluctuation beyond the linear term.

Since this is a calculation of the correlation functions of the ancilla alone, this formalism also lets us calculate the behaviour of a single driven nonlinear oscillator in the quantum regime, including perhaps the tunneling between the two stable classical solutions.

Chapter 9

Conclusion to Part II

We have proposed and analysed a scheme to observe quantum transitions of a mesoscopic mechanical oscillator. The non-linear coupling shifts the frequency of the second (ancilla) oscillator proportionally to the excitation of the first (system) oscillator. This frequency shift may be detected as a phase shift of the ancilla oscillation when driven on resonance. In principle, a QND measurement is possible if the coupling constant λ_{01} is much smaller than the resonance frequencies of the oscillators. We have derived the master equation for the system density matrix, the deterministic part of the dynamical equation, by removing the ancilla operator using the fact that the timescale of the system and ancilla dynamics are quite different. This technique is called the adiabatic elimination. The master equation has three components: phase diffusion as a result of the measurement backaction; a constant energy shift due to the excitation of the ancilla oscillator, and Fock state transitions due to the interaction with the thermal bath (the environment).

Measurements introduce a stochastic component into the system dynamics and we have obtained the stochastic master equation (SME) corresponding to our measurement scheme. This process is called unravelling the master equation. From the SME we identify two competing tendencies that can be characterized by two parameters. One is the coupling strength ν of the system and thermal bath, which is associated with the dwell time $t_{\rm dwell}$ between transitions. The other is the coefficient k, associated with measurements, which includes not only the coupling strength of the system to the bath but also the anharmonic coupling strength between the oscillators, the

driving amplitude, and the sensitivity of the measurement apparatus. This coefficient is related to the measurement time $t_{\rm m}$ that is needed for a measurement to be able to produce an outcome with certainty. To observe clear quantum jumps we would need $t_{\rm dwell} \gg t_{\rm m}$. If this condition is not satisfied, then the experimenter cannot infer the energy eigenstate of the system from the observed current.

We have also shown quantitatively that the neglect of the higher order anharmonic terms is indeed justified. We have also seen that both thermal and quantum fluctuations increase the intensity of phonons.

With the rapid development of higher measurement sensitivity and the ability to control the coupling strengths, there maybe some appropriate experimental parameters that give the condition $t_{\rm dwell} \gg t_{\rm m}$, which might lead to an observation of quantum jumps. Our scheme and theoretical techniques developed here are fairly general, and are not restricted to zero temperature, thus they can be also used for other applications such as a single spin detection, noise analysis for a solid state based quantum computer and phonon counting. Such possibilities might open up a new stage for observing quantum dynamics in mesoscopic systems.

9.1 Future issues

Finally, we would like to address several extensions of the work in this thesis that could be investigated in the near future. Firstly, we have used the rotating wave approximation (RWA) and have discarded the counter-rotating terms. Whilst this approximation is reasonable under the assumptions we have imposed, we have not quantified the counter-rotating terms. Since the RWA is crucial for a QND measurement, it would be of importance to investigate the effect of the counter-rotating terms in depth.

Secondly, we have not considered all couplings that might arise in an actual experimental setup. For example, linear coupling $x_0 x_1$ will not occur theoretically due to the symmetry of flexing motion. However, when an experimental structure is fabricated, this linear term is probably unavoidable due to limitation of the fabrication

techniques. For the two flexing modes of an elastic beam, for example, if the structure is not perfectly symmetric there will be a coupling between the modes, so that the motion of the beam becomes elliptic rather than simple linear bending motion.

Thirdly, we have assumed the efficiency of the measurement apparatus to be 1. In reality, there are no perfect detectors and we need to account for the reduced efficiency.

Finally, in addition to improving our scheme towards more realistic situations, the existence of nonlinear terms itself provides rich dynamics and might lead to interesting phenomena such as the macroscopic tunnelling between two nonlinear states. It is of interest to do a more detailed analysis of the quantum behaviour of driven anharmonic oscillators.

Appendix A

Appendices to Part I

A.1 Optical theorem and S-matrix

The attenuation of a wave in elastic scattering is not due to energy dissipation, but rather to incoherent scattering between different modes. We have taken a Green function approach to calculate the scattering probability. However, it can be calculated using S-matrix theory method as well.

If the incident field does not scatter at all, S is simply the identity operator. We rewrite S as $S = 1 + iT$ to isolate the component due to scattering. The component T due to interactions is called the T-matrix. Since S is unitary and satisfies the reciprocity theorem as a consequence of energy conservation and time reversal invariance, $S^\dagger S = 1$. Thus,

$$S^\dagger S = 1 = \left(1 - iT^\dagger\right)\left(1 + iT\right) \tag{A.1}$$

from which

$$i\left(T^\dagger - T\right) = T^\dagger T. \tag{A.2}$$

Projecting the above onto k_m and using completeness

$$i\left\langle k_m \left|\left(T^\dagger - T\right)\right| k_m\right\rangle = \left\langle k_m \left|T^\dagger T\right| k_m\right\rangle = \sum_{n=\pm 1}^{\max n} \left\langle k_m \left|T^\dagger\right| k_n\right\rangle \left\langle k_n \left|T\right| k_m\right\rangle, \tag{A.3}$$

where k_m is the k-vector of the incident mode m, and k_n is the k-vector of the scattered

mode n (+ is for forward scattering and − is for backscattering). Thus

$$2i \langle k_m |T| k_m \rangle = \sum_{n=\pm 1}^{\max n} |\langle k_n |T| k_m \rangle|^2 . \tag{A.4}$$

This is known as the optical theorem. Eq. (A.4) can be broken down into two components, representing forward and backward scattering.

$$i \langle k_m|T|k_m \rangle = \frac{1}{2} \left(\sum_{n}^{\max n} | \langle k_n|T|k_m \rangle |^2 + \sum_{n}^{\max n} | \langle k_{-n}|T|k_m \rangle |^2 \right). \tag{A.5}$$

Here, $m \rightarrow \pm n$, corresponding to the transition of mode m to mode $\pm n$. Since $i \langle k_m|T|k_m \rangle$ is the coherent scattering field this can be written as $\mathrm{Im} \langle k_m|T|k_m \rangle$ or $\mathrm{Im}[\delta k]|_m$, where δk is the k-vector change between initial and final state of k_m. On the other hand, $\langle k_{\pm n}|T|k_m \rangle$ is the loss due to the incoherent scattering, i.e., the scattering probability amplitude, $\sigma_{\pm n,m}$. Thus,

$$\mathrm{Im}[\delta k]|_m = \sigma_m, \tag{A.6}$$

where

$$\sigma_m = \frac{1}{2} \left(\sum_n \sigma_{-n,m} + \sum_n \sigma_{n,m} \right). \tag{A.7}$$

A.2 The second term of the total field equation

In this appendix, we show that the second term in Eq. (2.6) is the incident field.

Suppose that the incident mode is m. Separating the Green function into its incident and other modes gives

$$\begin{aligned} G(x, y; x', f(x')) = & \frac{\pm i}{W k_m} \cos(\chi_m y) \cos(\chi_m f(x')) e^{ik_m|x-x'|} \\ & + \sum_{\substack{n \\ \chi_n \neq \chi_m}} \frac{\pm i}{W k_n} \cos(\chi_n y) \cos(\chi_n f(x')) e^{ik_n|x-x'|}. \end{aligned} \tag{A.8}$$

We evaluate the second term in Eq. (2.6). Let us define this term as I_{ends} *i.e.*,

$$I_{ends} \equiv \int_{ends} dy' \left[G\left(x', y'; x, y\right) \frac{\partial \Psi\left(x', y'\right)}{\partial x'} - \frac{\partial G\left(x', y'; x, y\right)}{\partial x'} \Psi\left(x', y'\right) \right]. \tag{A.9}$$

This integral is obtained by combining the two integrals, $I_{ends}|_{x'\to\infty}$ and $I_{ends}|_{x'\to-\infty}$, one at each distant end. Due to the change of sign of the outer normal $\hat{n}$, which points in the $+x$ direction for one end, and in the $-x$ direction for the other, we have that the second term of Eq. (2.6) is equal to the difference $I_{ends} = I_{ends}|_{x'\to\infty} - I_{ends}|_{x'\to-\infty}$. Each of these two integrals is of the form

$$\begin{aligned} I_{ends}|_{x'\to\pm\infty} = & \int dy' \frac{\mp i}{W\chi_m} \cos\left(\chi_m y\right) \cos\left(\chi_m y'\right) e^{\mp i k_m (x-x')} \left[\frac{\partial \Psi}{\partial x'} - \left(\pm i k_m\right) \Psi \right] \\ & + \sum_{\substack{n \\ \chi_n \neq \chi_m}} \int dy' \frac{\mp i}{W k_n} \cos\left(\chi_n y\right) \cos\left(\chi_n y'\right) e^{\mp i k_n (x-x')} \left[\frac{\partial \Psi}{\partial x'} - \left(\pm i k_n\right) \Psi \right], \end{aligned} \tag{A.10}$$

where sign is up for $x' \to +\infty$ and down for $x' \to -\infty$. The total field Ψ at $x' \to \infty$ is

$$\Psi\left(x', y'\right) = B_m \cos\left(\chi_m y'\right) e^{i k_m x'} + \sum_{\substack{s \\ \chi_s \neq \chi_m}} B_s \cos\left(\chi_s y'\right) e^{i k_s x'}, \tag{A.11}$$

where B_m, B_s are associated with the transmission coefficient. The first term represents the unscattered field and the second term represents the forward scattered fields. The total field Ψ at $x' \to -\infty$ is

$$\Psi\left(x', y'\right) = \chi_m\left(y'\right) e^{i k_m x'} + A_m \cos\left(\chi_m y'\right) e^{-i k_m x'} + \sum_{\substack{s \\ \chi_s \neq \chi_m}} A_s \cos\left(\chi_s y'\right) e^{-i k_s x'}, \tag{A.12}$$

where A_m, A_s are associated with the reflection coefficient. The first term is the incident field, the second and the third terms are for back scattered fields.

At the boundary $x' \to \infty$, $\hat{n}' = \hat{x}'$. Substituting Eq. (A.11) into Eq. (A.10)

produces

$$
\begin{aligned}
I_{ends}|_{x'\to\infty} = & \sum_{\substack{s \\ \chi_s\neq\chi_m}} \frac{B_s\left(k_s-k_m\right)}{Wk_m}\cos\left(\chi_m y\right)e^{-ik_m(x-x')}e^{+ik_s x'}\int_0^W dy'\cos\left(\chi_m y'\right)\cos\left(\chi_s y'\right) \\
& + \sum_{\substack{n \\ \chi_n\neq\chi_m}} \frac{B_m\left(k_m-k_n\right)}{Wk_n}\cos\left(\chi_n y\right)e^{-ik_n(x-x')}e^{ik_l x'}\int_0^W dy'\cos\left(\chi_n y'\right)\cos\left(\chi_m y'\right) \\
& + \sum_{\substack{n \\ \chi_n\neq\chi_m}}\sum_{\substack{s \\ \chi_s\neq\chi_m}} \frac{B_s\left(k_s-k_n\right)}{Wk_n}\cos\left(\chi_n y\right)e^{-ik_n(x-x')}e^{ik_s x'}\int_0^W dy'\cos\left(\chi_n y'\right)\cos\left(\chi_s y'\right) \\
& = 0. \qquad\qquad (A.13)
\end{aligned}
$$

This is zero by orthogonality since $k_s \neq -k_n$, *i.e.*, all modes are in the same direction.

At $x' \to -\infty$, $\hat{n}' = -\hat{x}'$. substituting Eq. (A.12) into Eq. (A.10) yields

$$
\begin{aligned}
I_{ends}|_{x'\to-\infty} = & \frac{i\left[ik_m+ik_m\right]}{Wk_m}\cos\left(\chi_m y\right)e^{ik_m(x-x')}e^{ik_m x'}\int_0^W dy'\cos^2\left(\chi_m y'\right) \\
& + \sum_{\substack{s \\ \chi_s\neq\chi_m}} \frac{iA_s\left(ik_s+ik_m\right)}{Wk_m}\cos\left(\chi_m y\right)e^{ik_m(x-x')}e^{ik_s x'}\int_0^W dy'\cos\left(\chi_m y'\right)\cos\left(\chi_s y'\right) \\
& + \sum_{\substack{n \\ \chi_n\neq\chi_m}} \frac{iA_m\left(ik_m+ik_n\right)}{Wk_n}\cos\left(\chi_n y\right)e^{ik_n(x-x')}e^{ik_m x'}\int_0^W dy'\cos\left(\chi_n y'\right)\cos\left(\chi_m y'\right) \\
& + \sum_{\substack{n \\ \chi_n\neq\chi_m}}\sum_{\substack{s \\ \chi_s\neq\chi_m}} \frac{iA_s\left(ik_s+ik_n\right)}{Wk_n}\cos\left(\chi_n y\right)e^{ik_n(x-x')}e^{ik_s x'}\int_0^W dy'\cos\left(\chi_n y'\right)\cos\left(\chi_s y'\right). \\
& \qquad\qquad (A.14)
\end{aligned}
$$

This gives a nonzero value only if $k_n = -k_s$. Then

$$
I_{ends}|_{x'\to-\infty} = -\sum_s N_s\cos\left(\chi_s y\right)e^{ik_s x} = -\Psi_{in}. \qquad (A.15)
$$

As discussed above, because $\hat{n}'$ is pointing toward the $-x$ direction at $x' \to -\infty$, the sign of this integral must be changed. Thus, the second term in (2.6) is the incident field Ψ_{in}.

A.3 Group velocity and energy velocity

In this appendix, we derive v_g directly from the equations of motion. When converting the expression containing group velocities to power flows in the main text, we have assumed the energy velocity v_e is equivalent to the group velocity in our case.

The average power P_n flowing in x direction of mode n is

$$P_n \equiv \frac{1}{2}\rho v_e \omega^2 \int_{-d/2}^{d/2}\int_{-W/2}^{W/2} u_{i,n}u_{i,n}^* dy'dz', \tag{A.16}$$

where v_e is the energy velocity. For a waveguide extending in the $x-$direction, the power flow varies with the position of the cross section. So we take an average power flow, and the energy velocity is expressed in terms of an integral over the cross section,

$$\begin{aligned} v_e &= \frac{\text{average Power in the } x\text{-direction}}{\text{Energy per unit length (in the } x\text{-direction)}} = \frac{\int\int dydz\mathcal{P}}{\int\int dydz\,(e)} \\ &= \frac{-\frac{1}{2}\,\text{Re}\int\int (T_{ix}v_i^*)\,dydz}{\frac{1}{2}\int\int \rho\omega^2 u_i u_i^* dydz}, \end{aligned} \tag{A.17}$$

where $\mathcal{P}$ is the Poynting vector and e is the energy density. Thus the power P can be also written as

$$P = \frac{1}{2}\,\text{Re}\int\int (-T_{ix}v_i^*)\,dydz, \tag{A.18}$$

where P is the power. We want to show $v_e = v_g$. The wave equation with harmonic time dependence is Eq. (3.4)

$$\rho\omega^2 u_i + \partial_j\left(C_{ijkl}\partial_k u_l\right) = 0. \tag{A.19}$$

We multiply by u_i^*, integrate over z and y, and rewrite the result as

$$\int\int dydz\rho\omega^2 u_i u_i^* + \int\int dydz\left[\partial_j\left(C_{ijkl}\partial_k u_l\right)u_i^*\right] = 0. \tag{A.20}$$

The second term, after integrating by parts and setting the surface terms to zero by

the stress-free boundary conditions and symmetry, becomes

$$\int\int dydz\left(\partial_j C_{ijkl}\partial_k u_l\right)u_i^* = -C_{ijkl}\int\int dydz\left(\partial_j u_l\right)\partial_k u_i^*. \tag{A.21}$$

Differentiating Eq. (A.20) with respect to the wave vector q gives

$$\begin{aligned}
&2\rho\omega v_g\int\int dydzu_i u_i^* + \int\int dydz\rho\omega^2\frac{\partial u_i}{\partial q}u_i^* + \int\int dydz\rho\omega^2 u_i\frac{\partial u_i^*}{\partial q}\\
&-\int\int dydz\left(\frac{\partial}{\partial q}\partial_j C_{ijkl}u_l\right)\partial_k u_i^* - \int\int dydz\left(\partial_j C_{ijkl}u_l\right)\left(\frac{\partial}{\partial q}\partial_k u_i^*\right)\\
&= 0.
\end{aligned} \tag{A.22}$$

The last two terms on the right hand side can be manipulated in the following way.

In evaluating the q derivative for the second last term in Eq. (A.22), we first separate the x derivative from y and z, take the derivative with respect to q, and regroup the terms with u_l and $\partial_q\bar{u}_l$.

$$\begin{aligned}
&-C_{ijkl}\int\int dydz\left(\frac{\partial}{\partial q}\partial_j u_l\right)\partial_k u_i^*\\
&= -C_{ijkl}\int\int dydz\left[\frac{\partial}{\partial q}\left(iq\delta_{jx}+\partial_j\right)\bar{u}_l\right]e^{ikx}\partial_k\bar{u}_i^* e^{-ikx}\\
&= -C_{ijkl}\int\int dydz\left[i\delta_{jx}u_l + \partial_j\left(e^{ikx}\frac{\partial\bar{u}_l}{\partial q}\right)\right]\partial_k\bar{u}_i^* e^{-ikx}\\
&= -i\delta_{jx}C_{ijkl}\int\int dydzu_l\partial_k u_i^* - C_{ijkl}\int\int dydz\left[\partial_j\left(e^{ikx}\frac{\partial\bar{u}_l}{\partial q}\right)\right]\partial_k\bar{u}_i^*.
\end{aligned} \tag{A.23}$$

Then we rewrite the last term using integration by parts and set the surface terms to zero by the boundary conditions.

$$-C_{ijkl}\int\int dydz\left[\partial_j\left(\frac{du_l}{dq}\right)\right]\partial_k\bar{u}_i^* = \int\int dydz\frac{du_l}{dq}\partial_j C_{ijkl}\partial_k\bar{u}_i^*. \tag{A.24}$$

Thus we have

$$
\begin{aligned}
&-\int\int dydz\left(\frac{d}{dq}\partial_j C_{ijkl}u_l\right)\partial_k u_i^* \\
&=-i\delta_{jx}C_{ijkl}\int\int dydzu_l\partial_k u_i^* + \int\int dydz\frac{du_l}{dq}\left(\partial_j C_{ijkl}\partial_k \bar{u}_i^*\right).
\end{aligned}
\tag{A.25}
$$

We similarly manipulate the last term in Eq. (A.22) to get

$$
\begin{aligned}
&-\int\int dydz\left(\partial_j C_{ijkl}u_l\right)\frac{d}{dq}\left(\partial_k u_i^*\right) \\
&=i\delta_{kx}C_{ijkl}\int\int dydz\left(\partial_j u_l\right)u_i^* - C_{ijkl}\int\int dydz\left(\partial_j u_l\right)\left[\partial_k\left(e^{-ikx}\frac{d\bar{u}_i^*}{dq}\right)\right] \\
&=i\delta_{kx}C_{ijkl}\int\int dydz\left(\partial_j u_l\right)u_i^* + \int\int dydz\left(\partial_j C_{ijkl}\partial_k u_l\right)\frac{d\bar{u}_i^*}{dq}
\end{aligned}
\tag{A.26}
$$

With Eqs. (A.23, A.26), Eq. (A.22) now becomes

$$
\begin{aligned}
&2\rho\omega v_g\int\int dydzu_i u_i^* + \int\int dydz\rho\omega^2\frac{du_i}{dq}u_i^* + \int\int dydz\rho\omega^2 u_i\frac{du_i^*}{dq} \\
&-i\delta_{jx}C_{ijkl}\int\int dydzu_l\partial_k u_i^* + \int\int dydz\frac{du_l}{dq}\left(\partial_j C_{ijkl}\partial_k\bar{u}_i^*\right) \\
&+i\delta_{kx}\int\int dydz\left(C_{ijkl}\partial_j u_l\right)u_i^* + \int\int dydz\left(\partial_j C_{ijkl}\partial_k u_l\right)\frac{d\bar{u}_i^*}{dq} \\
&=0.
\end{aligned}
\tag{A.27}
$$

Rearranging the above and using $v_i = -i\omega u_i$ and $T_{ij} = C_{ijkl}\partial_k u_l$ and recalling $i = l$, we have

$$
\begin{aligned}
&2\rho\omega v_g\int\int dydzu_i u_i^* + \frac{1}{\omega}\int\int dydz\left(v_i T_{ix}^* + T_{ix}v_i^*\right) \\
&+\int\int dydz\frac{du_i}{dq}\left(\rho\omega^2 u_i^* + \partial_j C_{ijkl}\partial_k\bar{u}_i^*\right) + \int\int dydz\left(\rho\omega^2 u_i + \partial_j C_{ijkl}\partial_z u_l\right)\frac{d\bar{u}_i^*}{dq} \\
&=0.
\end{aligned}
\tag{A.28}
$$

But by Eq. (3.4), the third and the fourth term are zero. Thus Eq. (A.22) is

$$2\rho\omega v_g \int\int dydz u_i u_i^* + \frac{1}{\omega}\int\int dydz\,(v_i T_{ix}^* + T_{ix} v_i^*) = 0, \tag{A.29}$$

so that

$$v_g = \frac{-\frac{1}{\omega}\int\int dydz\,(v_i T_{ix}^* + T_{ix} v_i^*)}{2\rho\omega v_g \int\int dydz u_i u_i^*} = \frac{-\frac{2}{\omega}\,\mathrm{Re}\int\int dydz\,(T_{ix} v_i^*)}{2\rho\omega v_g \int\int dydz u_i u_i^*} = v_e. \tag{A.30}$$

From Eq. (A.16)

$$P \equiv \frac{1}{2}\rho v_g \omega^2 \int_{-d/2}^{d/2}\int_{-W/2}^{W/2} |\bar{u}_i|^2 dy' dz'. \tag{A.31}$$

With u_i being normalized, we get $v_g = 2P/\rho\omega^2$. Now we have an analytical expression for the group velocity expressed in terms of the displacement and stress fields.

Appendix B

Appendices to Part II

B.1 Thermal bath correlations

In this appendix, we derive the bath correlation relations. The free Hamiltonian for the bath is

$$H_B = \sum_i \hbar\omega_i b_i^\dagger b_i, \tag{B.1}$$

where b_i is a Bose operator. Choose a canonical ensemble in which the density operator is

$$\rho_b(\omega) = \frac{\exp\left[-\frac{H_B}{k_\mathrm{B}T}\right]}{\mathrm{Tr}\left\{\exp\left[-\frac{H_B}{k_\mathrm{B}T}\right]\right\}}, \tag{B.2}$$

where the density operator for the bath ρ_b commutes with the bath Hamiltonian. The density operator can be written as

$$\rho_b = \prod_i \rho_i = \prod_i \frac{\exp\left[-\frac{\hbar\omega_i}{k_\mathrm{B}T}\left(b_i^\dagger b_i\right)\right]}{Z_i}, \tag{B.3}$$

and

$$Z_i = \mathrm{Tr}\left\{\exp\left[-\frac{\hbar\omega_i}{k_\mathrm{B}T}\left(b_i^\dagger b_i\right)\right]\right\} = \sum_n \exp\left[-\frac{\hbar\omega_i(n)}{k_\mathrm{B}T}\right]. \tag{B.4}$$

The mean occupation number is

$$\langle n_i\rangle = \left\langle b_i^\dagger b_i\right\rangle = \sum_n \exp\left[-\frac{\hbar\omega_i(n)}{k_\mathrm{B}T}\right]\frac{1}{Z_i} = \frac{1}{\exp\left[-\frac{\hbar\omega_i}{k_\mathrm{B}T}\right]-1}, \tag{B.5}$$

$$\left\langle b_i^\dagger b_j \right\rangle = \frac{\mathrm{Tr}\left\{\exp\left[-\frac{\hbar\omega_i}{k_\mathrm{B}T} b_i^\dagger b_i\right]\right\}}{\mathrm{Tr}\left\{\exp\left[-\frac{H_B}{k_\mathrm{B}T}\right]\right\}} = \sum_{i,j} \langle n_i| \langle n_j| b_i^\dagger b_i |n_i\rangle |n_j\rangle = N\delta_{ij}, \tag{B.6}$$

$$\left\langle b_i {b^\dagger}_j \right\rangle = \left\langle 1 + {b^\dagger}_i b_j \right\rangle = (N+1)\,\delta_{ij}, \tag{B.7}$$

$$\langle b_i b_j \rangle = \left\langle b_i^\dagger b_i^\dagger \right\rangle = 0, \tag{B.8}$$

where

$$N = \frac{1}{\exp\left[\beta\hbar\omega\right] - 1}. \tag{B.9}$$

B.2 Wiener process

The Wiener process is described by the Fokker-Planck equation with zero drift and unit diffusion.

$$\frac{\partial P\left(w_t, t|w_0, 0\right)}{\partial t} = \frac{1}{2}\frac{\partial^2}{\partial t^2} P\left(w_t, t|w_0, 0\right), \tag{B.10}$$

where

$$P\left(w_t, t|w_0, 0\right) = \frac{1}{\sqrt{2\pi t}} \exp\left[-\frac{1}{2}\frac{1\left(w_t - w_0\right)^2}{t}\right]. \tag{B.11}$$

The initial delta-function evolves with constant and a variance increasing linearly in time

$$\langle W_t \rangle = w_0, \tag{B.12}$$

$$\left\langle \left(W_t - w_0\right)^2 \right\rangle = t. \tag{B.13}$$

Random variables $\{W_0, W_1, ..., W_n\}$ corresponding to the times $t_0 = 0, t_1, ..., t_n$ separated by Δt. Wiener process when the $w_i, i = 1, ...n$ are chosen from a series of Gaussian distributions, each conditioned on the value taken by the random variable one step earlier in time. Then the probability density for a sequence $\{w_0, w_1, ..., w_n\}$ is

$$P\left(w_0, w_1, ..., w_n, t_n|w_0, 0\right) = \frac{1}{\sqrt{\left(2\pi\Delta t\right)^n}} \prod_{i=1}^{n} \exp\left[-\frac{1}{2}\frac{1\left(w_i - w_{i-1}\right)^2}{\Delta t}\right]. \tag{B.14}$$

We have assumed a Markovian process (note that the Fokker-Planck equations describe Markov processes) and each component W_i has the following correlations:

$$\langle W_i \rangle = w_0, \tag{B.15}$$

$$\left\langle (W_i - w_0)^2 \right\rangle = i\Delta t = t, \tag{B.16}$$

$$\langle (W_j - w_0)(W_i - w_0) \rangle = \min(j,i)\,\Delta t = \min(t_j, t_i). \tag{B.17}$$

Discrete trajectories generate in this way describe the Wiener process at reduced resolution, but do not reduce accuracy, and thus is good for a numerical evaluation/

Write an equation of motion for a random variable ρ_t driven by both deterministic forces and a fluctuating force derived from $\dot{W}_t$.

$$d\rho_t = A(\rho_t)\,dt + B(\rho_t)\,dW_t \tag{B.18}$$

$$\Rightarrow \rho_t = \int_0^t A(\rho_t)\,dt' + \int_0^t B(\rho_t)\,dW_t. \tag{B.19}$$

Wiener increments between t_i and t_{i-1} provides the source of fluctuations. When the strength of the fluctuating force depends on the random variable X_t it is called multiplicative noise (not additive). However, a linearised analysis is performed using the system size expansion, the multiplicative noise is approximated by an additive noise, with ρ_t replace by $\rho(t)$ to determine the noise strength B.

A standard Wiener process (often called Brownian motion) on the interval $[0, T]$ is a random variable $W(t)$ that depends continuously on $t \in [0, T]$ and satisfies the following:

$$W(0) = 0, \tag{B.20}$$

for $0 < s < t < T$,

$$W(t) - W(s) \sim \sqrt{t-s}\xi, \tag{B.21}$$

where ξ is the random variable $\xi = N(0,1)$ with the normal distribution with zero mean and unit variance. Because the normal distribution is used, the process is often referred to as Gaussian.

For $0 < s < t < u < v < T$, $W(t) - W(s)$ and $W(v) - W(u)$ is independent. For use on a computer, we discretize the Wiener process with a timestep dt as

$$dW = \sqrt{dt}\xi(t). \tag{B.22}$$

B.3 Unravelling of a master equation for a heterodyne detection

A master equation provides a dynamical description in terms of an evolving probability distribution which determines the average quantities that would be measured over an ensemble of experiments. Alternatively, one can obtain the averages by finding a set of equations whose solutions generate trajectories in phase space, which is a representative of what would be observed in a single experiment. The Langevin equation has an stochastic component that are not observed in microscopic detail, but manifest themselves macroscopically as sources of noise and fluctuations.

Here we show the master equation in Lindblad form

$$\begin{aligned}\dot{\rho}(t) = &-\frac{i}{\hbar}[H,\rho] + \gamma(n+1)\sum_m \left(2O_m\rho O_m^\dagger - O_m^\dagger O_m\rho - \rho O_m^\dagger O_m\right) \\ &+ \gamma n\sum_m \left(2O_m^\dagger\rho O_m - O_m O_m^\dagger\rho - \rho O_m O_m^\dagger\right)\end{aligned} \tag{B.23}$$

will lead to the stochastic Schrödinger equation

$$\begin{aligned}d|\psi\rangle = \Bigg[&-\frac{i}{\hbar}Hdt + \gamma(n+1)\sum_m \left(2\left\langle O_m^\dagger\right\rangle O_m - O_m^\dagger O_m - \left\langle O_m^\dagger\right\rangle\langle O_m\rangle\right)dt \\ &+ \gamma n\sum_m \left(2\langle O_m\rangle O_m^\dagger - O_m O_m^\dagger - \langle O_m\rangle\left\langle O_m^\dagger\right\rangle\right)dt \\ &+ \sum_m \left[\sqrt{\gamma}\left(O_m - \langle O_m\rangle\right)d\xi_m + \sqrt{\gamma}\left(O_m^\dagger - \left\langle O_m^\dagger\right\rangle\right)d\xi_m^\dagger\right]\Bigg]|\psi\rangle.\end{aligned} \tag{B.24}$$

This form has both real and complex noise, *i.e.*, a heterodyne detection form.

B.3.1 Derivation

The following derivation is based on Percival [51]. We want to find is differential equations for $|\psi\rangle$ so that $d\rho/dt$ is determined by a differential equation such as Eq. (B.23). Even at $t = 0$ starts with a pure state, the state evolves into a mixed state, so there is no general deterministic equation for the pure states $|\psi\rangle$. But there are stochastic equations since the system-environment coupling has a probabilistic nature. Write $d|\psi\rangle$ in the Ito stochastic form

$$d|\psi\rangle = |v\rangle\, dt + \sum_j |u_j\rangle\, d\xi_j, \tag{B.25}$$

where the first term is drift term and the second term is differential stochastic fluctuations and $d\xi_j$ is Wiener process. Each fluctuation has mean 0 and variance $\sqrt{dt}$ and

$$M\left[d\xi_j\right] = 0, \tag{B.26a}$$

$$M\left[d\xi_j d\xi_i\right] = 0, \tag{B.26b}$$

$$M\left[d\xi_j^* d\xi_i\right] = 2\bar{n}\delta_{ij}dt, \tag{B.26c}$$

$$M\left[d\xi_i d\xi_j^*\right] = 2\left(\bar{n}+1\right)\delta_{ij}dt. \tag{B.26d}$$

To preserve the normalisation of the state vector, the fluctuation in the state must be orthogonal to that state, *i.e.*,

$$\langle\psi|u_j\rangle = 0. \tag{B.27}$$

Taking mean over $|d\psi\rangle$ and $|d\psi\rangle\langle d\psi|$. Using Eq. (B.25),

$$M|d\psi\rangle = M|v\rangle\, dt + M\sum_j |u_j\rangle\, d\xi_j = |v\rangle\, dt, \tag{B.28}$$

$$
\begin{aligned}
M\left|d\psi\right\rangle\left\langle d\psi\right| &= M\left(\left|v\right\rangle dt+\sum_j\left|u_j\right\rangle d\xi_j\right)\left(\left\langle v\right| dt+\sum_j\left\langle u_j\right| d\xi_j^*\right)\\
&= M\left|v\right\rangle\left\langle v\right|(dt)^2+\sum_j\left|v\right\rangle\left\langle u_j\right| dtMd\xi_j^*+\left|u_j\right\rangle\left\langle v\right| Md\xi_j dt\\
&+\sum_j\left|u_j\right\rangle\left\langle u_j\right| Md\xi_j d\xi_j^*\\
&= M\left|v\right\rangle\left\langle v\right|(dt)^2+2\sum_j\left|u_j\right\rangle\left\langle u_j\right| dt\\
&\simeq 2\sum_j\left|u_j\right\rangle\left\langle u_j\right| dt. \qquad \text{(B.29)}
\end{aligned}
$$

For a pure state, a density operator ρ can be expressed as

$$\rho=\left|\psi\right\rangle\left\langle\psi\right|. \qquad \text{(B.30)}$$

Since $d\rho/dt$ gives the average of change for all possible states, the differential form of the state is $M\left|d\psi\right\rangle$, where M is the mean over a distribution of normalised pure-state projection operators. Then the change in ρ is, using Ito calculus rule and the means obtained above gives the relation between $d\rho/dt$ and Ito stochastic form.

$$
\begin{aligned}
d\rho &= \left|\psi\right\rangle M\left\langle d\psi\right|+M\left|d\psi\right\rangle\left\langle\psi\right|+M\left|d\psi\right\rangle\left\langle d\psi\right|\\
&= \left|\psi\right\rangle\left\langle v\right| dt+\left|v\right\rangle\left\langle\psi\right| dt+2\sum_j\left|u_j\right\rangle\left\langle u_j\right| dt\\
&\Rightarrow \dot\rho=\left|\psi\right\rangle\left\langle v\right|+\left|v\right\rangle\left\langle\psi\right|+2\sum_j\left|u_j\right\rangle\left\langle u_j\right|. \qquad \text{(B.31)}
\end{aligned}
$$

We want to express $\left|v\right\rangle$ and $\sum_j\left|u_j\right\rangle\left\langle u_j\right|$ in terms of $d\rho/dt$. Consider $\dot\rho\left|\psi\right\rangle$,

$$
\begin{aligned}
\dot\rho\left|\psi\right\rangle &= \left|\psi\right\rangle\left\langle v|\psi\right\rangle+\left|v\right\rangle\left\langle\psi|\psi\right\rangle+2\sum_j\left|u_j\right\rangle\left\langle u_j|\psi\right\rangle\\
&= \left|\psi\right\rangle\left\langle v|\psi\right\rangle+\left|v\right\rangle, \qquad \text{(B.32)}
\end{aligned}
$$

where the fluctuating terms (sums) is zero due to orthogonality Eq. (B.27). Notice

that

$$\langle\psi\,|\dot{\rho}|\,\psi\rangle = \langle\psi|\psi\rangle\,\langle v|\psi\rangle + \langle\psi|v\rangle = 2\,\mathrm{Re}\,\langle v|\psi\rangle\,, \tag{B.33}$$

so

$$|v\rangle = \dot{\rho}\,|\psi\rangle - \frac{1}{2}\,\langle\psi\,|\dot{\rho}|\,\psi\rangle\,. \tag{B.34}$$

Next $d\rho/dt$ expression orthogonal to ψ is the stochastic terms

$$2\sum_j |u_j\rangle\,\langle u_j| = (I-\rho)\,\dot{\rho}\,(I-\rho)\,. \tag{B.35}$$

Therefore, the stochastic equation can be expresses as

$$d\,|\psi\rangle = \left[\dot{\rho}\,|\psi\rangle - \frac{1}{2}\,\langle\psi\,|\dot{\rho}|\,\psi\rangle\right]dt + (I-\rho)\,\dot{\rho}\,(I-\rho)\,d\xi_j. \tag{B.36}$$

Now consider Eq. (B.23). We get

$$\begin{aligned}
\dot{\rho}\,|\psi\rangle &= -\frac{i}{\hbar}\,(H\,|\psi\rangle\,\langle\psi|\psi\rangle - |\psi\rangle\,\langle\psi|\,H\,|\psi\rangle) \\
&\quad + \gamma\,(n+1)\sum_m \left(2O_m\,|\psi\rangle\,\langle\psi|\,O_m^\dagger\,|\psi\rangle - O_m^\dagger O_m\,|\psi\rangle\,\langle\psi|\psi\rangle - |\psi\rangle\,\langle\psi|\,O_m^\dagger O_m\,|\psi\rangle\right) \\
&\quad + \gamma n\sum_m \left(2O_m^\dagger\,|\psi\rangle\,\langle\psi|\,O_m\,|\psi\rangle - O_m O_m^\dagger\,|\psi\rangle\,\langle\psi|\psi\rangle - |\psi\rangle\,\langle\psi|\,O_m O_m^\dagger\,|\psi\rangle\right) \\
&= -\frac{i}{\hbar}\,(H\,|\psi\rangle - |\psi\rangle\,\langle\psi|\,H\,|\psi\rangle) \\
&\quad + \gamma\,(n+1)\sum_m \left(2O_m\,|\psi\rangle\,\left\langle O_m^\dagger\right\rangle - O_m^\dagger O_m\,|\psi\rangle - |\psi\rangle\,\left\langle O_m^\dagger\right\rangle\langle O_m\rangle\right) \\
&\quad + \gamma n\sum_m \left(2O_m^\dagger\,|\psi\rangle\,\langle O_m\rangle - O_m O_m^\dagger\,|\psi\rangle - |\psi\rangle\,\langle O_m\rangle\left\langle O_m^\dagger\right\rangle\right),
\end{aligned} \tag{B.37}$$

and

$$
\begin{aligned}
-\frac{1}{2}\left\langle\psi\left|\dot{\rho}\right|\psi\right\rangle &= -\frac{1}{2}\left(\left\langle\psi\right|H\left|\psi\right\rangle\left\langle\psi|\psi\right\rangle - \left\langle\psi|\psi\right\rangle\left\langle\psi\right|H\left|\psi\right\rangle\right) \\
&\quad - \frac{1}{2}\gamma\left(n+1\right)\sum_m \left\langle\psi\left|\left(2O_m\left|\psi\right\rangle\left\langle\psi\right|O_m^\dagger - O_m^\dagger O_m\left|\psi\right\rangle\left\langle\psi\right| - \left|\psi\right\rangle\left\langle\psi\right|O_m^\dagger O_m\right)\right|\psi\right\rangle \\
&\quad - \frac{1}{2}\gamma n\sum_m \left\langle\psi\left|\left(2O_m^\dagger\left|\psi\right\rangle\left\langle\psi\right|O_m - O_m O_m^\dagger\left|\psi\right\rangle\left\langle\psi\right| - \left|\psi\right\rangle\left\langle\psi\right|O_m O_m^\dagger\right)\right|\psi\right\rangle \\
&= 0, \qquad \text{(B.38)}
\end{aligned}
$$

so that $\left|v\right\rangle$ is

$$
\begin{aligned}
\left|v\right\rangle &= -\frac{i}{\hbar}\left(H\left|\psi\right\rangle - \left|\psi\right\rangle\left\langle\psi\right|H\left|\psi\right\rangle\right) \\
&\quad + \gamma\left(n+1\right)\sum_m \left(2O_m\left|\psi\right\rangle\left\langle O_m^\dagger\right\rangle - O_m^\dagger O_m\left|\psi\right\rangle - \left|\psi\right\rangle\left\langle O_m^\dagger\right\rangle\left\langle O_m\right\rangle\right) \\
&\quad + \gamma n\sum_m \left(2O_m^\dagger\left|\psi\right\rangle\left\langle O_m\right\rangle - O_m O_m^\dagger\left|\psi\right\rangle - \left|\psi\right\rangle\left\langle O_m\right\rangle\left\langle O_m^\dagger\right\rangle\right). \qquad \text{(B.39)}
\end{aligned}
$$

The stochastic terms are

$$
\begin{aligned}
&\left(I-\rho\right)\dot{\rho}\left(I-\rho\right) \\
&= -\frac{i}{\hbar}\left(I - \left|\psi\right\rangle\left\langle\psi\right|\right)\left(\left[H\left|\psi\right\rangle\left\langle\psi\right| - \left|\psi\right\rangle\left\langle\psi\right|H\right]\right)\left(I - \left|\psi\right\rangle\left\langle\psi\right|\right) \\
&+ \gamma\left(n+1\right)\sum_m \left(I - \left|\psi\right\rangle\left\langle\psi\right|\right)\left(2O_m\left|\psi\right\rangle\left\langle\psi\right|O_m^\dagger - O_m^\dagger O_m\left|\psi\right\rangle\left\langle\psi\right| - \left|\psi\right\rangle\left\langle\psi\right|O_m^\dagger O_m\right)\left(I-\rho\right) \\
&+ \gamma n\sum_m \left(I-\rho\right)\left(2O_m^\dagger\left|\psi\right\rangle\left\langle\psi\right|O_m - O_m O_m^\dagger\left|\psi\right\rangle\left\langle\psi\right| - \left|\psi\right\rangle\left\langle\psi\right|O_m O_m^\dagger\right)\left(I-\rho\right) \qquad \text{(B.40)}
\end{aligned}
$$

$$
\begin{aligned}
&- \left(I-\rho\right)O^\dagger O\rho\left(I-\rho\right) \\
&= -\left(I-\rho\right)O^\dagger O\rho + \left(I-\rho\right)O^\dagger O\rho\rho \\
&= -O^\dagger O\left|\psi\right\rangle\left\langle\psi\right| + \left\langle O_m^\dagger\right\rangle\left\langle O_m\right\rangle\left|\psi\right\rangle\left\langle\psi\right| + O^\dagger O\left|\psi\right\rangle\left\langle\psi\right| - \left|\psi\right\rangle\left\langle O_m^\dagger\right\rangle\left\langle O_m\right\rangle\left\langle\psi\right| \\
&= 0, \qquad \text{(B.41)}
\end{aligned}
$$

which gives

$$2\sum_j |u_j\rangle\langle u_j| = \gamma\left[O_m|\psi\rangle\langle\psi|O_m^\dagger - \langle O_m\rangle|\psi\rangle\langle\psi|O_m^\dagger\right] + \gamma\left[-\langle O_m^\dagger\rangle O_m|\psi\rangle\langle\psi| + \langle O_m\rangle\langle O_m^\dagger\rangle|\psi\rangle\langle\psi|\right] \tag{B.42}$$

$$2\sum_j |u_j^*\rangle\langle u_j^*| = \gamma\left[O_m^\dagger|\psi\rangle\langle\psi|O_m - \langle O_m^\dagger\rangle|\psi\rangle\langle\psi|O_m\right] + \gamma\left[-\langle O_m\rangle O_m^\dagger|\psi\rangle\langle\psi| + \langle O_m^\dagger\rangle\langle O_m\rangle|\psi\rangle\langle\psi|\right]. \tag{B.43}$$

They are satisfied by

$$|u_m\rangle = \sqrt{\gamma}\left(O_m - \langle O_m\rangle\right)|\psi\rangle, \tag{B.44}$$

$$|u_m^*\rangle = \sqrt{\gamma}\left(O_m^\dagger - \langle O_m^\dagger\rangle\right)|\psi\rangle. \tag{B.45}$$

Therefore, $d|\psi\rangle$ is, after combining all the terms,

$$d|\psi\rangle = \Bigg[-\frac{i}{\hbar}Hdt + \gamma(n+1)\frac{1}{2}\sum_m\left(2\langle O_m^\dagger\rangle O_m - O_m^\dagger O_m - \langle O_m^\dagger\rangle\langle O_m\rangle\right)dt + \gamma n\sum_m\left(2\langle O_m\rangle O_m^\dagger - O_m O_m^\dagger - \langle O_m\rangle\langle O_m^\dagger\rangle\right)dt + \sum_m\left[\sqrt{\gamma}\left(O_m - \langle O_m\rangle\right)d\xi_m + \sqrt{\gamma}\left(O_m^\dagger - \langle O_m^\dagger\rangle\right)d\xi_m^\dagger\right]\Bigg]|\psi\rangle. \tag{B.46}$$

Bibliography

[1] R. Landauer, IBM J. Res. Dev. **1**, 223 (1957).

[2] D. E. Angelescu, M. C. Cross, and M. L. Roukes, Superlattice and Microstructure, **23**, 673 (1998).

[3] L.C. Rego and G. Kirczenow, Phys. Rev. Lett. **81**, 232 (1998).

[4] M. P. Blencowe, Phys. Rev. B **59**, 4992 (1999).

[5] M. P. Blencowe and V. Vitelli, Phys. Rev. A **62**, 52104 (2000).

[6] J. B. Pendry, J. Phys. A **16**, 2161 (1983).

[7] L. G. C. Rego and G. Kirczenow, Phys. Rev. B **59** (20) 13080 (1999).

[8] K. Schwab, E. A. Henriksen, J. M. Worlock, M. L. Roukes, Nature **404**, 974, (2000).

[9] N. Nishiguchi, Y. Ando, M. N. Wybourne, J. Phys. Condens. Matter **9**, 5751 (1997).

[10] M. C. Cross and R. Lifshitz, Phys. Rev. B **64**, 085324 (2001).

[11] D. H. Santamore and M. C. Cross, Phys. Rev. B **63**, 4306 (2001).

[12] A. G. Voronovich, *Wave Scattering from Rough Surfaces*, Springer-Verlag, Berlin (1993).

[13] S. V. Biryukov, Yu. B. Gulyaev, V. V. Krylov, V. P. Plessky, *Surface Acoustic Waves in Inhomogeneous Media*, Springer-Verlag, Berlin (1995).

[14] A. Kambili, G. Fagas, V. I. Fal'ko, and C. J. Lambert, Phys. Rev. B **60**, 15593 (1999).

[15] M. Spivack, J. Acoust. Soc. Am. **101** (3), 1250 (1997).

[16] J.A. Sanchez-Gil, V. Freilikher, A.A. Maradudin, I.V. Yurkevich, Phys. Rev. B **59**, 5915 (1999).

[17] Schwab, K., Private communication.

[18] M. P. Blencowe, J. of Phys. Cond. Mat. **7** (27) 5177 (1995).

[19] D. H. Santamore and M. C. Cross, Phys. Rev. Lett. **87**, 115502 (2001).

[20] D. H. Santamore and M. C. Cross, Phys. Rev. B **66**, 144302 (2002).

[21] D. H. Santamore and M. C. Cross, Physica B, **316-317C**, 389 (2002).

[22] B. A. Auld, *Acoustic Fields and Waves in Solids* Vol. 2, Robert E. Krieger Publishing, Malabar (1990).

[23] Y. Pomeau, Phil. Mag. B, **78** (2), 235 (1998).

[24] K. Schwab (private communication)

[25] L. D. Landau and E. M. Lifshitz, *Theory of Elasticity*, Butterworth-Heinemann, Oxford (1986).

[26] S. Timoshenko, *Theory of Elastic Stability*, McGraw-Hill, New York (1991).

[27] K. Graff, *Wave Motion in Elastic Solids*, Dover, New York (1991).

[28] W. H. Press, S. A. Teukolsky, W. T. Vetterling, B. P. Flannery, *Numerical Recipes for FORTRAN*, Cambridge University Press, Cambridge (1992).

[29] C. S. Yung, D. R. Schmidt, and A. N. Cleland, Appl. Phys. Lett., **81** (1), 31 (2002).

[30] Adrian Cho, Science, **299**, 36 (2003).

[31] X. M. H. Huang, C. A. Zorman, M. Mehregany and M. L. Roukes, Nature, **421** (6922), 495 (2003).

[32] V. B. Braginsky and F. Ya. Khalili, *Quantum Measurement*, Cambridge University Press, Cambridge (1995).

[33] B. Yurke, Personal Communication.

[34] M. L. Roukes and X. M. H. Huang Personal Communication.

[35] S. M. Carr, W. E. Lawrence, and M. N. Wybourne, Physica B, **316**, 464 (2002).

[36] C. M. Caves, K. S. Thorne, R. W. P. Drever, V. D. Sandberg, and M. Zimmermann, Rev. Mod. Phys. **52** (2), 341 (1980).

[37] D. F. Walls and G. J. Milburn, *Quantum Optics*, Springer-Verlag, Berlin 2nd Ed. (1995).

[38] B. Yurke, D. S. Greywall, A. N. Pargellis, and P. A. Busch, Phys. Rev. A **51** (5), 4211 (1994).

[39] R. E. S. Polkinghorne and G. J. Milburn, Phys. Rev. A **64**, 042318 (2001).

[40] A. O. Caldeira and A. J. Leggett, Physica **121A**, 587 (1983).

[41] H. M. Wiseman and G. J. Milburn, Phys. Rev. A **47** (1), 642 (1993).

[42] P. Warszawski and H. M. Wiseman, Phys Rev. A **63**(1) 013803 (2001).

[43] C. W. Gardiner, *Qauntum Noise*, Springer-Verlag, Berlin 2nd Ed. (2000).

[44] A. Barchielli, Phys. Rev. A 34, 1642 (1986).

[45] A. Barchielli, J. Phys. A 20, 6341 (1987).

[46] A. Barchielli and V. P. Belavkin, J. Phys. A 24, 1495 (1991).

[47] H. M. Wiseman, PhD Thesis, University of Queensland, St. Lucia (1994).

[48] A. C. Doherty and K. Jacobs, Phys. Rev A **60** (4) 2700 (1999).

[49] R. Knobel and A. N. Cleland, Appl. Phys. Lett. **81** (12), 2258 (2002).

[50] D. A. Harrington and M. L. Roukes, Caltech Technical Report CMP-106 (1994).

[51] I. Percical, *Quantum State Diffusion*, Cambridge University Press, Cambridge (1998).

[52] M. B. Plenio and P. L. Knight, Rev. Mod. Phys., **70**, 101 (1998).

[53] T. A. Brun, quant-ph 0108132 (2001).

[54] P. D. Drummond and D. F. Walls, J. Phys. A: Math.Gen., **13**, 725 (1980).

[55] P. D. Drummond and C. W. Gardiner, J. Phys. A: Math.Gen., **13**, 2353 (1980).

[56] S. Chaturvedi, C. W. Gardiner, I. Matheson and D.F. Walls, J. Stat. Phys. **17**, 649 (1977).

[57] C. W. Gardiner, *Handbook of Stochastic Methods*, 2nd. ed., Springer-Verlag, Berlin (1985).

[58] L. D. Landau and E. M. Lifshitz, *Mechanics*, Butterworth-Heinemann, Oxford (1993).